Faculty of Science and Engineering
Department of Chemistry

The Development of a Rigorous Nanocharacterization Scheme for Electrochemical Systems

Jean-Pierre M Veder

This thesis is presented for the Degree of
Doctor of Philosophy
of
Curtin University

September 2010

Declaration

To the best of my knowledge and belief this thesis contains no material previously published by any other person except where due acknowledgment has been made.

This thesis contains no material which has been accepted for the award of any other degree or diploma in any university.

Jean-Pierre Marcel Veder

September 20th 2010

Abstract

This thesis reports on a methodology for the nanocharacterization of complex electrochemical systems. A series of powerful techniques have been adapted and applied to studies of two scientifically important electrochemical systems; namely polymer membrane solid-state ion-selective electrodes (ISEs) and electrochemically generated tetracyanoquinodimethane (TCNQ) charge-transfer materials. These studies have mainly encompassed the use of neutron reflectometry (NR), electrochemical impedance spectroscopy (EIS), secondary ion mass spectrometry (SIMS), small angle neutron scattering (SANS), synchrotron radiation / Fourier transform-infrared microspectroscopy (SR / FT-IRM), synchrotron radiation / X-ray photoelectron spectroscopy (SR / XPS) and synchrotron radiation / grazing incidence X-ray diffraction (SR / GIXRD). Significantly, an NR technique has been specially developed to enable simultaneous EIS measurements through the development and refinement of a novel electrochemical / reflectometry cell. Furthermore, the development of a versatile electrochemical cell that is capable of allowing SR / GIXRD measurements to be made in practically any conceivable electrochemical problem has also been of great significance.

The investigation of polymer membrane solid-state ISEs focused on the problem of water layer formation at the buried polymer interface after prolonged exposure to an analyte. Initially, a rigorous surface and materials characterization scheme was developed and applied to plasticized poly(vinylchloride) (PVC) coated wire electrodes (CWEs) that are known to be adversely affected by water layer formation. It was determined that water and the associated ions from the sample analyte were transported through the PVC membrane. This resulted in the formation of a water layer (approximately 120 Å thick) at the substrate / ion-selective membrane interface. The results of the study suggested that this event occurred after 3 to 20 hours of constant

exposure to solution. Moreover, the water layer at the buried interface was found to contain traces of plasticizer, whilst nanodroplets of water were also found in the membrane. The former is evidence for the exudation of plasticizer from the PVC membrane into the water layer at the buried interface.

Further investigations on a solid-state ISE utilizing a hydrophobic poly(methylmethacrylate) / poly(decylmethacrylate) (PMMA / PDMA) copolymer as the ion-selective membrane revealed that water was transported through the membrane at a far slower rate than that of plasticized PVC ISEs. In fact, a regular ISE of this type severely restricted water accumulation at the buried interface, with such an event occurring after 460 hours. In addition, water was restricted to accumulation as droplets at the buried interface, as opposed to continuous water layers. A negligible amount of water was found in the bulk of this hydrophobic polymer membrane.

Given CWEs are susceptible to forming water at the buried interface, it is customary to employ solid-contact (SC) underlayers. The primary function of the SC is to provide an appropriate mechanism for ion-to-electron transduction. Certain SCs are also theorized to discourage the formation of water layers. The results of this thesis revealed that a hydrophobic poly(3-octylthiophene-2,5-diyl) (POT) SC can prevent the formation of a water layer in SC ISEs altogether. This is not only achieved through the hydrophobic nature of POT, but also through the fact that the underlayer of POT is able to cover any imperfections at the buried interface, which water can use as a site for accumulation. By contrast, a hydrophilic polymer SC, known as poly(3,4-ethylenedioxythiophene): poly(styrenesulfonate) (PEDOT:PSS), was found to scavenge available traces of water at the buried interface. Instead of forming a well defined water layer or even water-droplets at the buried interface, the PEDOT:PSS SC system was found to soak up all traces of water transported through the ion-selective membrane to the buried interface. Water was detected in the PEDOT:PSS

underlayer in a miscible state and not as a separate phase as observed with the CWE systems.

The mechanism for ion-to-electron transduction in electroactive polymer SCs was also investigated. The study was performed in order to address the extent to which charger-transfer events occur throughout the underlying polymer SC. By studying the electrochemical doping of POT with [3,5-bis(triflouro-methyl)phenyl]borate ($TFPB^-$) ions it was shown that the ion-to-electron transduction process is surface confined. This outcome demonstrates that the performance of various SCs does not depend on the thickness of the polymer film. In fact, it is proposed that the sparing use of the SC material may possibly achieve better charge-transfer performance. Such a hypothesis is based on the reduced electron path through the SC, hence reducing the probability that electrons are hindered by impurities and film imperfections. The suggestion of surface confined charge-transfer events also supports previous notions that the effectiveness of SCs is based on the capacitive nature of the material.

The final part of the thesis deals with the characterization of the structure and morphology of TCNQ-based charge-transfer materials. Due to the lack of prior research on the electrochemical syntheses and structures of these materials, $Cd(TCNQ)_2$ and $Zn(TCNQ)_2$ were studied. By using SR / GIXRD together with synchrotron powder diffraction, the electrochemically synthesized $Cd(TCNQ)_2$ was found to be crystallographically similar to the powder sample. Subtle differences between the two materials were evident; however, it was found that the major phase of non-hydrated $Cd(TCNQ)_2$ phase was present in both samples. Notably, this phase was found to have a tetragonal unit cell, with cell parameters: a = 16.78Å and c = 8.83Å.

Finally, a potential-dependant voltammetric study was carried out on a $Zn(TCNQ)_2$ system. This was done in order to investigate the effects of electrodepositing $Zn(TCNQ)_2$ under different electrochemical conditions. It was

found that the material electrocrystallized prior to, or at, the peak potential for reduction of TCNQ to $TCNQ^-$ comprised two layers. The upper layer was shown to consist of a densely packed and highly amorphous layer of $Zn(TCNQ)_2$, while the lower layer was a crystalline phase of $Zn(TCNQ)_2$. The material deposited at a potential after the peak suggested that only the crystalline phase of $Zn(TCNQ)_2$ was present. This finding is significant for two reasons. First, in electrochemistry, it demonstrates that the *in situ* SR / GIXRD technique can be used to interrogate electrode reaction products under different voltammetric conditions. Next, it is important in the manufacture of electrocrystallized materials, where it demonstrates that complete control of the morphology and major phases is possible and that SR / GIXRD is a useful research tool to study the process.

Acknowledgements

Over the past several years since the commencement of my doctoral candidature I have been privileged to have had the help and support of many colleagues, friends and family members. Although I will attempt to acknowledge all of these people for their assistance, I apologize from the outset for any omissions that have been made. Rest assured that all your efforts were greatly appreciated.

The Australian Research Council (ARC), the National Institute of Health and the Swiss National Foundation are acknowledged for financial support of the project. I am particularly grateful to the Australian Government for providing me with an Australian Postgraduate Award (APA), as well as the Australian Institute of Nuclear Science and Engineering (AINSE) for a Postgraduate Research Award (PGRA). Curtin University, the Nanochemistry Research Institute and the Department of Chemistry are not only acknowledged for providing me with a top-up scholarship but also for providing me with the support and facilities to make my research possible.

I am sincerely grateful for all of the help and guidance provided to me from my project supervisor, Prof. Roland De Marco. I am glad to have had such an approachable supervisor who I have been able to learn a great deal from. Roland has worked tirelessly to keep me focussed and ensure that the years of my doctoral candidature have been successful. Furthermore, I cannot thank him enough for providing me with the many opportunities to travel the world to carry out some great research and to meet many gifted international researchers. I look to Roland as not only a supervisor and a mentor, but also a friend with a great sense of humour.

Many people have provided me with scientific and technical advice over the years, and this has been invaluable to the progression of my research. In particular, I owe a great deal to Graeme Clarke for all of his help throughout my PhD project. I cannot begin to describe how much help he has provided me with from the time I began my postgraduate research. I am sure he knows how appreciative I am. Graeme is also a very good friend who has provided some great entertainment from the very beginning of my candidature. My AINSE co-supervisor Prof. Michael James, Prof. Eric Bakker, Prof. Ernö Pretsch, Dr. Ryan, Chester, Dr. Pengchao Si, Kunal Patel, Ross Williams, William Rickard and Dave Walton are all also acknowledged for their valuable assistance at various stages throughout the project.

I could not possibly forget the many friends that have kept me sane through some very stressful years. I would specifically like to thank Andrew Ng and Laurence Dyer for the many antics that have made me laugh uncontrollably whilst at work. Anthony Nguyen, John Dinh and Vince Martino are also thanked for being great friends and providing respite from the stress of research when needed the most.

I cannot stress enough how much help and support my partner, Caitlin, has provided me with over the toughest few years of my life. Although she may not realise it, she has carried me through the most difficult times of my life. I also cannot forget the many sacrifices that Caitlin has made for me over the time we have known each other and I am forever grateful. I will always appreciate the ineffable love and continued support that Caitlin has provided me with over the years. I am a better person for having known her.

I would also like to acknowledge my siblings, Orietta, Anthony and Andre, who have had a big impact in shaping me to be the person that I am. I am thankful that we have such a close family because I have been privileged to have learnt so much from them. I have grown up in admiration of my three

siblings and am always inspired by their nature and the paths that they have carved out for themselves.

Finally, I would like to thank my parents, George and Francoise, for everything they have done for me. From working several jobs each to put food on the table and pay for our education to the late nights spent helping us with our homework and assignments the night before it was due, they have always worked extremely hard to provide us with everything needed for us to flourish, both socially and academically. We have certainly had all of the love and support that we could ever possibly ask for. Unfortunately my father is no longer here to bear witness to the fruits of his labour, but I truly hope that I have done my best to make him and my mother proud.

Jean-Pierre Veder
September 2010

Primary Publications

This thesis is assembled by publications, either published, in press, in review, or to be submitted. The publications form the individual chapters and are listed below.

Chapter 2

De Marco, R., and **Veder, J.-P.** *In Situ* Structural Characterization of Electrochemical Systems Using Synchrotron - Radiation Techniques, *Trends in Analytical Chemistry* **29**, 538-537 (2010).

Chapter 3

De Marco, R., **Veder, J.-P.**, Clarke, G., Nelson, A., Prince, K., Pretsch, E. and Bakker, E. Evidence of a Water Layer in Solid-Contact Polymeric Ion Sensors, *Physical Chemistry Chemical Physics* **10**, 73-76 (2008).

Chapter 4

Veder, J.-P., De Marco, R., Clarke, G., Chester, R., Nelson, A., Prince, K., Pretsch, E. and Bakker, E. Elimination of Undesirable Water layers in Solid-Contact Polymeric Ion-Selective Electrodes, *Analytical Chemistry* **80**, 6731-6740 (2008).

Chapter 5

Veder, J.-P., De Marco, R., Connell, B., Dalgliesh, R., Pretsch, E. and Bakker, E. Water Uptake in the Hydrophilic Solid-Contact of Polymeric Ion-Selective Electrodes, *The Analyst* **In Preparation** (2010).

Chapter 6

Veder, J.-P., Patel, K., Clarke, G., Grygolowicz-Pawlak, E., Silvester, D., De Marco, R., Pretsch, E. and Bakker, E. A Synchrotron Radiation / Fourier Transform – Infrared Microspectroscopy Study of Undesirable Water Inclusions in Polymeric Solid-Contact Ion-Selective Electrodes, *Analytical Chemistry* **82**, 6203-6207 (2010).

Chapter 7

Veder, J.-P., De Marco, R., Patel, K., Si, P., Grygolowicz-Pawlak, E., Pretsch, E. and Bakker, E. Studying the Depth of Ion-to-Electron Transduction in Solid-Contact Ion-Selective Electrodes, *Analytical Chemistry* **In Preparation** (2010).

Chapter 8

Veder, J.-P., Nafady, A., Clarke, G., Williams, R., De Marco, R. and Bond, A. A Flow Cell for Transient Voltammetry and its Application to *In Situ* GIXRD Characterization of Electrocrystallized $Cd(TCNQ)_2$, *Electrochimica Acta* **56**, 1546-1553 (2010).

Chapter 9

Veder, J.-P., Nafady, A., Clarke, G., De Marco, R. and Bond, A. A Combined Voltammetric / GIXRD Study of the Electrocrystallization of Zinc Tetracyano-quinodimethane, *Physical Chemistry Chemical Physics* **In Preparation** (2010).

Contribution of Others

The work presented in this thesis was primarily designed, executed, interpreted and written by the author, however contributions by colleagues are duly acknowledged and described here.

Chapter 2

Jean-Pierre Veder and Roland De Marco planned the structure of the review. The article was written by Jean-Pierre Veder and subsequently edited by Roland De Marco.

Chapter 3

Jean-Pierre Veder, Roland De Marco and Graeme Clarke designed and performed the experiments. Jean-Pierre Veder interpreted results and co-wrote the paper with Roland De Marco. Andrew Nelson and Kathryn Prince provided assistance with operating the instruments housed at the Australian Nuclear Science and Technology Organisation (ANSTO) in Lucas Heights, New South Wales. Ernö Pretsch and Eric Bakker provided intellectual input relating to the planning of experiments and the interpretation of results.

Chapter 4

Jean-Pierre Veder, Roland De Marco, Graeme Clarke and Ryan Chester designed and performed the experiments. Jean-Pierre Veder interpreted results and wrote the paper. Andrew Nelson and Kathryn Prince provided assistance with operating the instruments housed at ANSTO. Ernö Pretsch and Eric Bakker are acknowledged for their scientific discussions pertaining to the planning of experiments and the interpretation of results.

Chapter 5

Jean-Pierre Veder planned and executed the experiments, interpreted results and wrote the paper. Roland De Marco and Benjamin Connell also provided assistance with carrying out the experiments. Robert Dalgliesh assisted with the operation of the neutron reflectometer housed at the ISIS pulsed neutron and muon source in the Rutherford Appleton Laboratory, Oxfordshire, United Kingdom. Ernö Pretsch and Eric Bakker provided intellectual input pertaining to the planning of experiments and the interpretation of results.

Chapter 6

Jean-Pierre Veder designed and performed experiments, interpreted results and wrote the paper. Graeme Clarke, Kunal Patel, Ewa Grygolowicz-Pawlak, Debbie S. Silvester also assisted in executing the experiments at the Australian Synchrotron (AS) in Victoria, Australia. Kunal Patel is also acknowledged for contributions through scientific discussion and assistance in writing the paper. Roland De Marco, Ernö Pretsch and Eric Bakker provided intellectual input relating to the planning of experiments and the interpretation of results.

Chapter 7

Jean-Pierre Veder designed and performed experiments, interpreted results and wrote the paper. Roland De Marco, Kunal Patel, Pengchao Si and Ewa Grygolowicz-Pawlak also assisted in executing the experiments at the AS. Roland De Marco, Ernö Pretsch and Eric Bakker provided intellectual input.

Chapter 8

Jean-Pierre Veder planned and carried out experiments, interpreted results and wrote the paper. Roland De Marco and Ayman Nafady also aided in

the planning and execution of experiments at the Photon Factory (PF) in Tsukuba, Japan. Alan Bond provided intellectual input through scientific discussions on the design of experiments and interpretation of results.

Chapter 9

Jean-Pierre Veder planned and carried out experiments, interpreted results and wrote the paper. Roland De Marco and Graeme Clarke also assisted with carrying out experiments at the PF. Alan Bond, Ayman Nafady and Roland De Marco provided intellectual input through scientific discussions on the design of experiments and interpretation of results.

Secondary Publications

A list of manuscripts and abstracts based on research that was conducted during the preparation of this thesis, but not included in the thesis, is provided below.

Peer-reviewed

Veder, J.-P., De Marco, R., Clarke, G., Chester, R., James, M., Pretsch, E. and Bakker, E., Tuning electrochemical devices using quantum effects **In Preparation**.

Abstracts

Veder, J.-P., De Marco, R., Clarke, G., Nelson, A., Pretsch, E. and Bakker, E., Tuning electrochemical sensors using thin film confinement effects. *Proc. Matrafured 2008 – International Conference on Electrochemical Sensors*, Dobogoko, Hungary, 2008. Oral presentation.

Veder, J.-P., De Marco, R., Clarke, G., Nafady, A. and Bond, A., Tuning the Electrocrystallization Parameters of Semiconducting Metal(II)-Tetracyanoquinodimethane phases - An In-situ Synchrotron Radiation Grazing Incidence X-Ray Diffraction Study. *Proc. Australian X-ray Analytical Association,* Melbourne, Victoria, 2008. Poster presentation.

Veder, J.-P., De Marco, R., Clarke, G., Chester, R., Nelson, A., Pretsch, E. and Bakker, E., Tuning electrochemical devices using quantum confinement effects. *Proc. 59th Pittsburgh Conference on Analytical Chemistry and Applied Spectroscopy,* New Orleans, Louisiana, USA, 2008. Poster presentation.

Veder, J.-P., De Marco, R., Prince, K., Pretsch, E. and Bakker, E., A Spectroscopic Study of Water Layers in Coated-Wire and Solid-Contact Polymeric Ion-Selective Electrodes (ISEs). *Proc. 58th Pittsburgh Conference on Analytical Chemistry and Applied Spectroscopy,* Chicago, Illinois, USA., 2007. Poster Presentation.

Veder, J.-P., De Marco, R., Clarke, G., Nelson, A., Pretsch, E. and Bakker, E., A Combined X-ray Reflectometry / Neutron Reflectometry Study of Water Layers in Solid-Contact Polymeric Ion-Selective Electrodes (ISEs). *Proc. INTERACT*, Perth W.A., 2006. Poster Presentation.

Table of Contents

Chapter Four

Chapter Five

Chapter One

1 Introduction and Overview

Electrochemical Systems

It is widely acknowledged that an electrochemical system is underpinned by chemical reactions at the interface of a conductive substrate (either an electron conductor or an ionic conductor). In the simplest case, electrons are driven across the electrode (i.e. the electron conductor) and electrolyte (i.e. the ionic conductor) interface resulting in, or as a result of, a chemical reaction of some type.

Whilst the general theory behind electrochemistry may at first appear simplistic, the reality is that electrochemical systems are often extremely difficult to comprehend due to the complexity of the chemical and physical interactions taking place at electrode / electrolyte interfaces. It is often the case that these systems are the cause of great anguish to scientists due to the fact that the electrochemistry can be unpredictable at the best of times. As a result, electrochemical systems may be misconstrued as being temperamental; however, this unpredictability is merely due to a lack of understanding of such systems.

Arguably, the most significant complexity exists at the electrode boundary layer where charge-transfer processes occur at depths of up to several hundred Ångstroms on either side of the electrode surface. The molecular structure of both phases in this boundary region (commonly referred to as the interphase) can differ considerably from those of the bulk structures (1). These structural properties can have a significant effect on the behaviour of the electrochemical reactions occurring at the interface. A phenomenon known as the electrical

double layer bears testament to the difference in molecular structure and reinforces the complexity of the interphase. Essentially, an electrical double layer is established when a charged surface is exposed to an electrolyte solution. A net charge at the surface of an object affects the distribution of ions in the surrounding region. This results in an increased concentration of counter ions close to the objects surface (as depicted in ***Figure 1-1***). Incidentally, the electrical double layer can be highly influential in the electrochemical behaviour of electrodes.

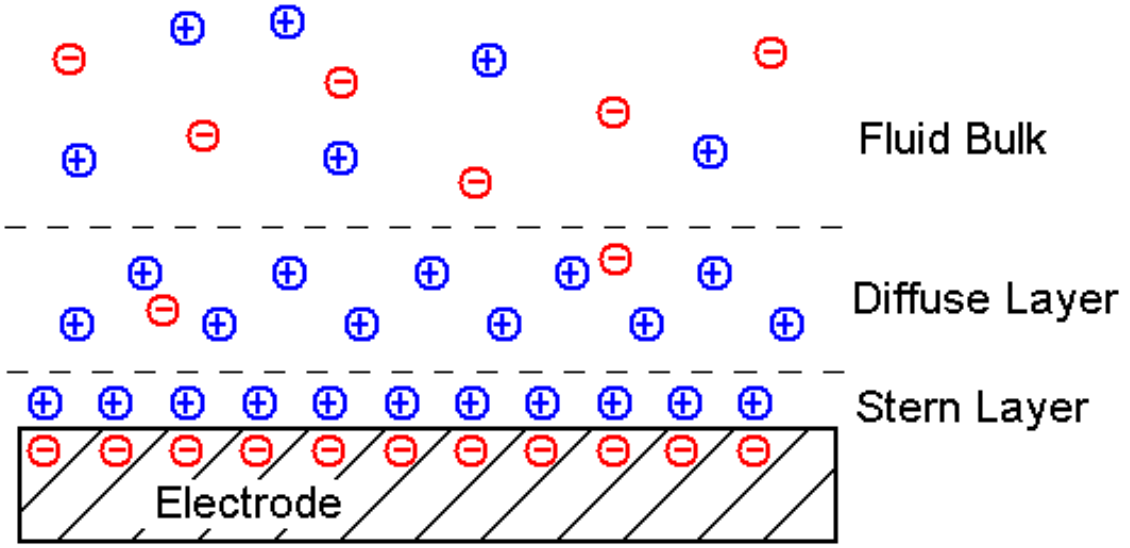

Figure 1-1 *Schematic representation of the electrical double layer formed at a negatively charged surface.*

The complexity associated with the characterization of the interphase arises from the fact that it is essentially a “buried interface.” Early research into this field could only speculate about the material properties of the interphase due to the absence of effective methods for characterizing this buried region. This hampered efforts to obtain a true understanding of the underlying reaction mechanisms. As research has advanced, a range of suitable surface sensitive techniques became available that opened up new avenues for studying the physical and chemical properties of the interphase. Although providing a significant boost in current knowledge, these methods of analysis are often

carried out *ex situ* due to the limitations of the instrumental techniques. By and large, *ex situ* studies provide valuable insights into certain properties of different systems; however, there is always a nagging doubt about the effect of removing the electrodes from their natural electrochemical environment (2-4). In some cases, exposure of electrochemically treated surfaces to ambient air - containing not only oxygen but also other reactive components like carbon dioxide - results in uncontrollable structural changes (4). To exacerbate this problem, electrochemical surfaces are likely to undergo physical transformations simply due to the switching off of the applied electrode potential, as well as the loss of surface water when the electrode is removed from its native electrochemical environment. These difficulties demonstrate that *ex situ* surface analysis can sometimes lead to misleading and unrepresentative information about the electrochemical interphase. Accordingly, the prospect of examining the interphase *in situ* is very attractive to contemporary electrochemical researchers. *In situ* surface analysis techniques have not displaced *ex situ* ones as it is often necessary to use multiple techniques capable of providing complementary information. Hence, a combination of *in situ* and *ex situ* methods can be much more effective in providing solutions to interphase problems in electrochemistry. In this context, the studies presented in this thesis are focused on the utilization of modern *in situ* techniques in combination with well established *ex situ* techniques in order to obtain a well-rounded representation of the studied electrochemical system.

It must be stressed that the scope of this thesis is not to carry out exhaustive characterizations of every known electrochemical system. The intention is rather to demonstrate, by application to two complex electrochemical systems, that new and existing characterization techniques can be applied in innovative ways to solve longstanding problems in electrochemistry. Specifically, this thesis will focus on solid-state polymeric ion-selective electrodes (ISEs) and the effect that long-term exposure to solution has on the physical and electrochemical properties of the electrodes. In order to demonstrate that the

same methodology (i.e. using new and existing techniques in innovative ways) can be implemented to other systems, the thesis also details the investigation of, albeit to a lesser extent, electrodeposited tetracyanoquinodimethane (TCNQ) charge-transfer materials. These two systems of interest are profoundly different in nature and have required vastly different surface characterization approaches. Collectively, the studied systems are representative of a raft of electrochemical systems and, as such, many of the nanocharacterization techniques described herein may be applied generally to any electrochemical system.

Significantly, a review article is presented in ***Chapter 2*** which focuses on the use of various *in situ* synchrotron techniques in the characterization of electrochemical systems. This article was written in response to an invitation to contribute based on the experience and knowledge gathered by the authors throughout this research. In the context of this thesis, the review serves to provide an introduction into the power of synchrotron radiation (which will be relied heavily upon in the later stages of the thesis) to elucidate various problems facing electrochemists. In addition, ***Chapter 2*** reaffirms the complexities that exist in electrochemical systems (as established in this chapter).

Polymeric Solid-State ISEs

Solid-state ISEs utilizing polymeric ion-selective membranes have shown great promise for use in mainstream analytical chemistry. They have been used for many years as a means of providing reliable methods for the determination of analytes in most aqueous media (5-7). In many applications requiring urgent measurements of ionic activity, ISEs have replaced even the most advanced methods due to their rapid response times and comparable ion selectivities. As a result of these activities, solid-state ISEs have become the centre of considerable attention across many disciplines of science. Potential applications of modern solid-state ISEs in clinical, environmental and forensic analyses (6,

8-12) have been the driving force for the recent growth in research activity, and this attention has further intensified through innovations such as the batch fabrication of sensor arrays using screen printing technologies (13). Of particular relevance to today's booming nano- and micro-technology sector, the general trend towards miniaturization has opened up possibilities for the creation of micro-electrodes capable of mechanically robust intracellular measurements (14).

A polymeric solid-state ISE is a polymer membrane electrode that responds selectively to certain ions in the presence of other ions. The ISEs of interest in this thesis are a breed of chemical sensors known as "potentiometric" sensors. These sensors work on the basic principle of the galvanic cell whereby the electric potential generated across a membrane by "selected" ions is measured against a reference electrode under zero current conditions (8, 15). A net potential is determined which is related to the concentration of the selected ion according to the well-known Nernst equation (16):

$$E_{cell} = E_o + \frac{RT}{zF} \ln a_i \qquad \textbf{Equation 1-1}$$

where E_{cell} is the cell potential and E_o is the standard cell potential at the measuring temperature. R is the universal gas constant (8.314 JK^{-1} mol^{-1}), T is the absolute temperature, z is the number of moles of electrons transferred and F is the Faraday constant (9.648 x 10^4 C mol^{-1}). Importantly, a_i is the ion activity of the primary ion, which is related to the concentration of the primary ion.

The beginnings of the solid-state polymeric ISE came from the invention of the coated wire electrode (CWE) (***Figure 1-2 (a)***) almost 40 years ago (17). Although popular for its simplistic design, the ion-to-electron transduction process at the interface between the ionically conducting ion-selective membrane and the electron transferring metallic electrode was not well defined in CWEs (18), which resulted in a significant instability in the measured

potential (19). In the years that followed, the Finnish group of Ivaska (20) showed that the incorporation of an intermediate layer with suitable redox and ion-exchanging properties between the ion-selective membrane and the metallic substrate eliminated electrode instability (19, 21). The addition of the intermediate layer, or solid-contact (SC), signalled the birth of modern solid-state ISEs (***Figure 1-2 (b)***).

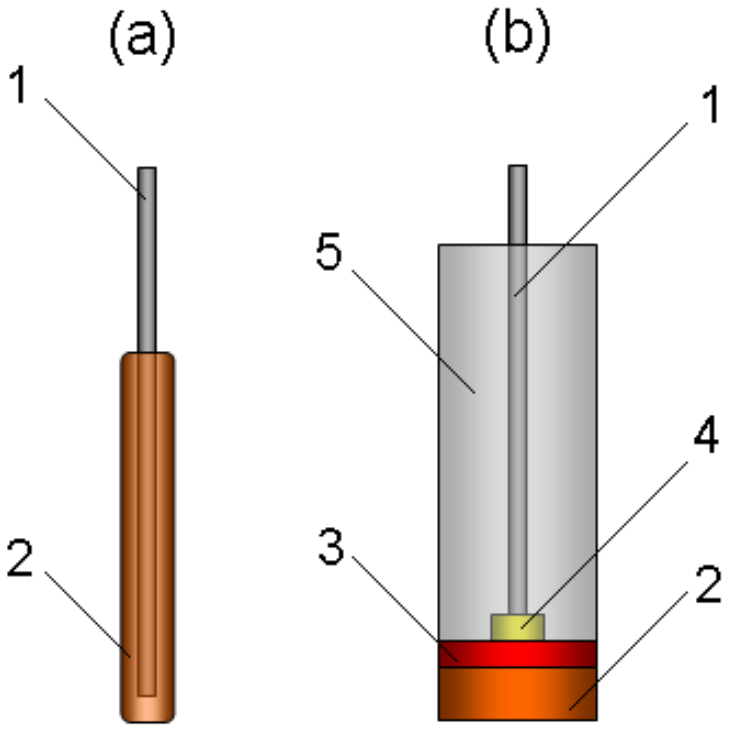

Figure 1-2 *Two variations of ion-selective electrodes (ISE). (a) Coated wire electrode (CWE), (b) Modern day solid-contact ISE. 1) Metallic electrode, 2) ion-sensing membrane, 3) conducting polymer under-layer, 4) electronic conductor with a high work function, 5) electrically insulating and chemically inert electrode body.*

A typical SC ISE comprises a conductive polymer SC which is applied to an inert electrically conductive support. The SC is, in turn, coated with an ion-selective polymer matrix incorporating an ionophore and a lipophilic ion-exchanger. In some instances, the ion-selective polymer support may require

the addition of lipophilic salts (not to be confused with lipophilic ion-exchange salts) to lower the resistance of the membrane without significantly affecting the primary ion response of the membrane (22). These salts can also play a role in influencing the selectivity of the ISE by increasing the ionic strength of the membrane (23).

Conducting polymer SCs are electroactive materials of mixed electronic and ionic conductivity. This property gives them the unique ability to convert ionic signals into electronic signals (24). In the conventional Ag / AgCl reference electrode, the ion-to-electron transduction process takes place at the internal reference electrode that is immersed in an electrolyte solution containing Cl^- ions, viz.:

$$Ag + Cl^- \leftrightarrow Ag^+Cl^- + e^- \qquad \textbf{Equation 1-2}$$

For a neutral conducting polymer SC, the ion-to-electron transduction process is accompanied by anion insertion as shown below:

$$P + A^- \rightarrow P^+A^- + e^- \qquad \textbf{Equation 1-3}$$

where P is the neutral conducting polymer phase and A^- is an anion. Electron transfer coupled to the anion leads to anion dependent electron transfer that can be fixed by a constant level of anion supply.

Several polymers have all of the necessary features of a conducting polymer. These include doped conjugated polymers, redox polymers, polymer composites and polymer electrolytes (19). The present research will focus on conjugated polymers that can be made electrically conductive by partial oxidation (p-doping). In particular, the hydrophobic poly(3-octylthiophene-2,5-diyl) (POT) (***Figure 1-3 (a)***) will be assessed in terms of its suitability for application in solid-state ISEs and compared with the largely hydrophilic polymer

mixture of poly(3,4-ethylenedioxythiophene):poly(styrenesulfonate) (PEDOT: PSS) (***Figure 1-3 (b)***).

The electroactivity evidenced in these poly alkylthiophene polymers is due to the highly conjugated backbone. The overlapping p_z orbitals, which arise as a result of the alternating single (σ) and double bonds (π), allow for the transportation of electrons, which result in current flows when there is either an excess or deficiency of π-electrons along the chain.

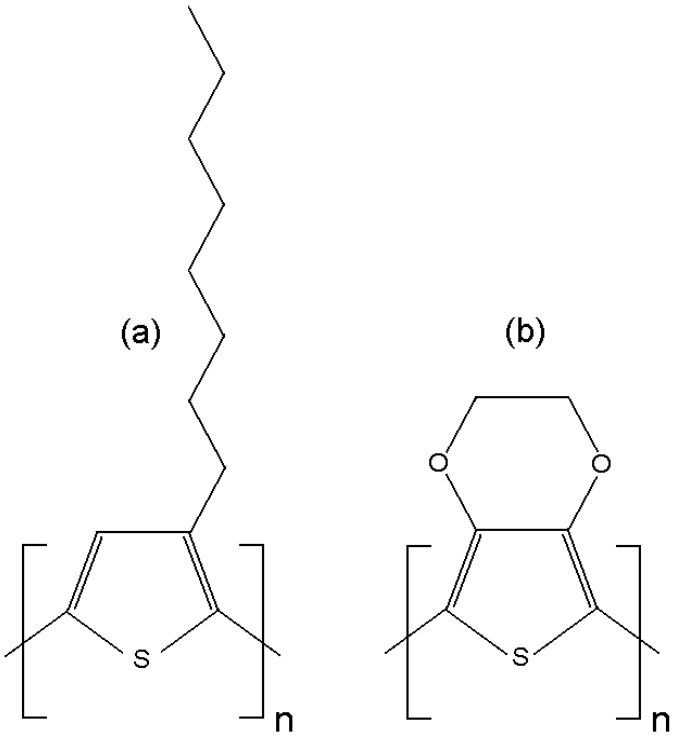

Figure 1-3 *Two conducting polymers used in this research. (a) poly(3-octylthiophene-2,5-diyl) (POT), (b) poly(3,4-ethylenedioxythiophene) (PEDOT). Note: the hydrophilic poly(styrenesulfonate) component used to stabilize PEDOT in water is not shown here.*

Ideally, any polymer employed as an ion-selective membrane should have a glass transition temperature (T_g) lower than room temperature. When this requirement is met, the membrane is sufficiently fluid under ambient conditions to allow for reasonable ionic conductivities and diffusion of membrane

components. For this reason, an appropriate polymer support in an ion-selective membrane matrix can be regarded simplistically as a hydrophobic solvent of high viscosity (25). An important addition to these requirements is that an ideal polymer support should essentially be inert and unable to perturb the electrode response in any way. In this study, two polymers with different attributes will be utilized to identify which best suits such an application.

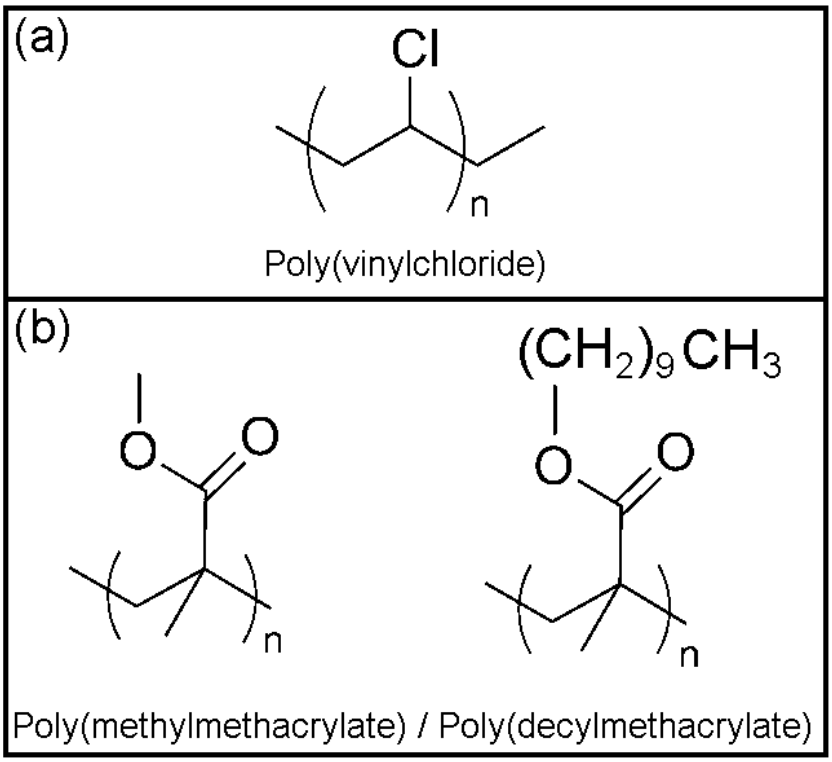

Figure 1-4 *The ion-selective polymer membranes investigated in this thesis. (a) Poly(vinylchloride) (PVC) and (b) poly(methylmethacrylate) / poly(decylmethacrylate) copolymer.*

Plasticized poly(vinylchloride) (PVC) (***Figure 1-4 (a)***) is arguably the most popular polymer support in polymeric ISEs, and will be one of the polymers investigated in this study. Although it has been used successfully for over 40 years (26), ***Chapter 3*** will demonstrate that PVC has a number of drawbacks associated with its use in long-term sensing applications. Significantly, whilst the use of the plasticizer is imperative in reducing the T_g of the PVC matrix, such a

component has been known to be the cause of potential drift in the sensor's response. This is due to exudation or leaching of the plasticizer from the membrane into the sample solution (27). An effect such as this is highly undesirable due to the danger posed by sample contamination, especially in the context of clinical and biological applications. Nevertheless, any attempts to reduce the plasticizer content causes significant decreases in the diffusion coefficient of the PVC membrane which can lead to ionophore inactivity and a substantial slowing of the membrane response (28). ***Chapter 4*** will demonstrate that the use of methacrylate copolymers (***Figure 1-4 (b)***) in place of plasticized PVC can eliminate these problems. Specifically, the combination of poly(methylmethacrylate) (PMMA) (T_g = 105°C) together with poly(decylmethacrylate) (PDMA) (T_g = -30°C) negates the requirement for plasticizers altogether. A polymer with a T_g well below room temperature can be tailored by mixing the appropriate quantities of each monomer according to the Fox equation shown below:

$$\frac{1}{T_g(co)} = \frac{F_A}{T_g(A)} + \frac{F_B}{T_g(B)} \qquad \textbf{Equation 1-4}$$

where $T_g(A)$ and $T_g(B)$ are the glass transition temperatures of the homopolymers and $T_g(co)$ is the glass transition temperature of the copolymer in Kelvin. F_A and F_B are the weight fractions of the monomers. The resultant polymer possesses greater durability and much better adhesion properties than its plasticized PVC counterpart. Furthermore, toxicity concerns are defeated due to the absence of plasticizers.

The incorporation of the ionophore into the ISE membrane is imperative for the appropriate functioning of the sensor as it accounts for the sensor's selectivity (refer to ***Figure 1-5 (a)*** for the structure of a commonly used ionophore). Essentially, this is achieved through the ionophore's ability to target a specific ion and form reversible complexes with it, whilst forming only weak

complexes, if at all, with interfering ions. Although it is desirable for the targeted ion to form strong complexes with the ionophore, the binding should not be so strong as to hinder the complexation / decomplexation kinetics. Such a property would cause slow response times and deviations from Nernstian response (29).

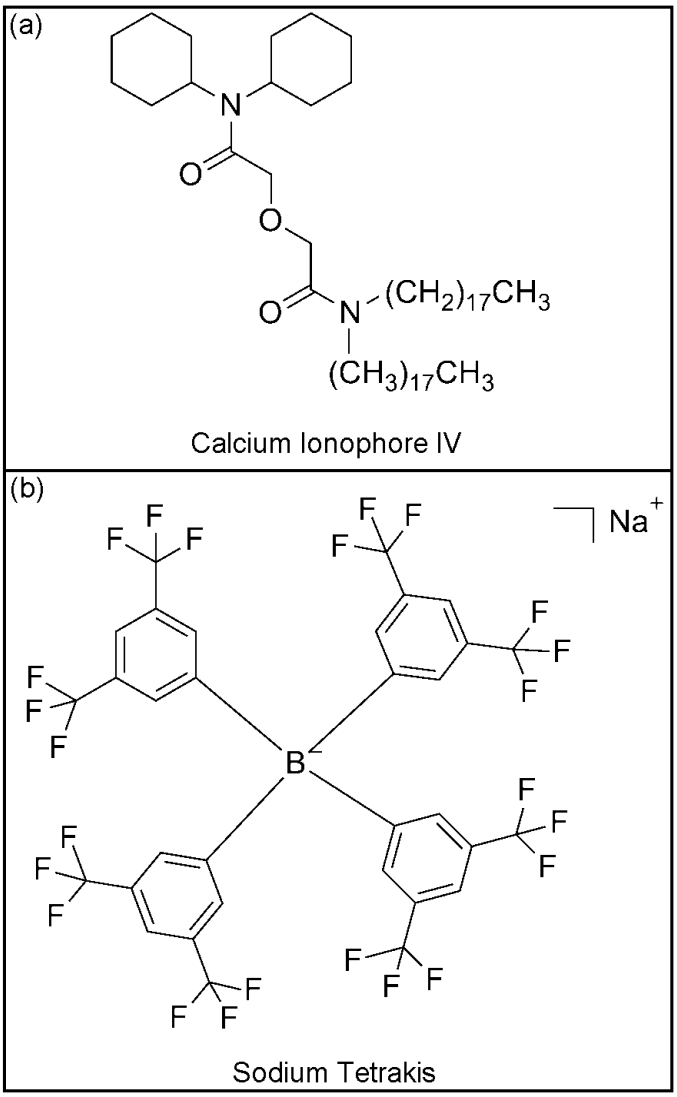

Figure 1-5 *The doping salts used in the polymer membrane to facilitate ion-selectivity. (a) N,N-dicyclohexyl-N',N'-dioctadecyl-3-oxapentanediamide (Calcium ionophore IV) and (b) sodium* [3,5-bis(triflouromethyl)phenyl]borate (sodium tetrakis).

Importantly, whilst the ionophore is largely responsible for the ISE's selectivity, a Nernstian slope cannot, and should not, be observed unless the final component, an ion-exchanger, is added to the matrix (30, 31). The ion-exchanger is essentially a large salt (see ***Figure 1-5 (b)***) that, when incorporated into an ion-selective membrane, significantly reduces the co-extraction of the target ion's counter-ion into the membrane phase. This concept is often referred to as permselectivity. A significant property of the ion-exchange additive is that it must be sufficiently lipophilic to remain solely in the organic membrane phase when in contact with aqueous solution.

Although thousands of combinations exist for the components used in ion-selective membranes, this project will be focused toward cationic selective electrodes, namely Ca^{2+}. As such, the membranes utilized in this study in almost all instances incorporate the calcium ionophore IV (***Figure 1-5 (a)***) and sodium tetrakis (***Figure 1-5 (b)***) as the ion-selective membrane components, unless otherwise specified.

Although SC ISEs have been around for decades, the technology has been hindered by a lack of understanding of the chemistry occurring at the buried interface between the SC and the ion sensing polymer. In general, these sensors have lacked the long-term stability for use in robust sensor applications and have sometimes possessed mediocre detection limits when compared to other electrochemical sensors (32). Recent suggestions ascribe the degradation in sensor response to the existence of a water layer between the polymer membrane and the electrode substrate (see ***Figure 1-6***). Such a water layer often results in spurious ISE potentials by acting as a reservoir, allowing the transportation of H_2O, O_2 and CO_2 molecules along with ions into and out of the water layer underneath the membrane (19, 32-35). As a result of these significant concerns, this thesis will focus on the buried interfaces in solid-state ISEs to determine the effects that prolonged exposure to aqueous analytes have on the sensor's functionality. Accordingly, this investigation sets out to achieve

an enhanced understanding of the physical and chemical factors influencing the buried interfaces of these electrodes.

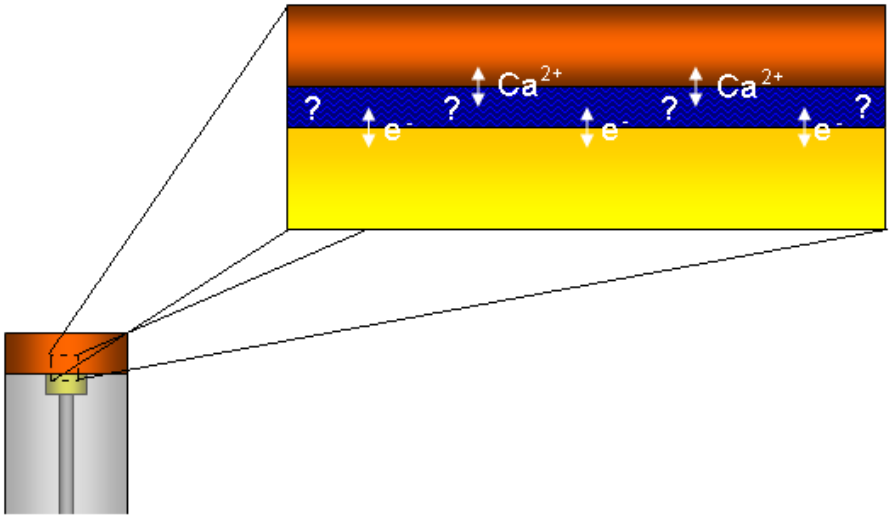

Figure 1-6 *Expanded schematic of a solid-contact ion-selective electrode affected by an undesirable water layer. The formation of a water layer at the buried interface causes unpredictability in the chemistry and physics occurring at the interface.*

A Nanocharacterization Scheme for Solid-State Ion-Selective Electrodes

Importantly, it is by no means the intention of this thesis to provide comprehensive accounts of the concepts associated with each experimental technique used in this research, as well as research pertaining to metal TCNQ compounds and polymeric ion sensors, but rather to demonstrate the effective use of these techniques in the characterization of electrochemical systems. The reader is instead referred to ***Appendix I*** for further descriptions of some of the more complex or less known techniques introduced in this Chapter.

Undoubtedly, the most attractive approach to characterising SC ISE systems subjected to prolonged exposure to water is electrochemical impedance spectroscopy (EIS). EIS is a powerful tool in an electrochemist's armoury due to the fact that it is extremely sensitive to nanoscale non-

uniformities at electrode interfaces (36). The technique differs from other electrochemical characterization techniques (i.e. cyclic voltammetry, scanning electrochemical microscopy, etc.) that may probe the buried interfaces by using large perturbations that drive reactions to conditions far from steady-state. Instead, EIS is a steady-state technique that provides non-destructive *in situ* information on relaxation times over large frequency ranges by using an AC potential of small amplitude. As a consequence, EIS ensures that the kinetic information pertaining to the buried interfaces is close to near zero current conditions, which are prevalent with ISEs in potentiometry. As will be shown in ***Chapters 3 - 5***, the specific application of EIS to solid-state ISEs can reveal important information about the nature of the buried interfaces, along with data about the dielectric properties of the material. In particular, the ability of EIS to monitor the bulk impedance of the ISE membrane has enabled the search for water layer formations at the buried interface. It is hypothesised that a significant reduction in bulk membrane impedance will signal the evolution of water due to the fact that the water acts as a low-resistance shunt at this buried interface.

Although EIS is a useful tool when used solely to study electrochemical systems, ***Chapters 3 - 5*** also demonstrate that the real power of EIS is its suitability for use in conjunction with other structural measurements such as neutron reflectometry (NR). Reflectometry is a technique which probes the structural parameters of thin films, i.e. thickness, density and roughness. This structural information can be investigated as a function of time and related to the electrode kinetic information obtained by EIS which is also measured simultaneously. Moreover, neutrons scatter differently off isotopes of an element, thus opening up the possibility of studying the materials under different isotope contrasts. This can be achieved by mixing the electrolyte in different amounts of water and heavy water (i.e. H_2O and D_2O). Henceforth, an investigator has the ability to selectively highlight or conceal certain components of the system to probe different perspectives of the system under investigation (refer to ***Appendix I*** for further information).

From an electrochemical perspective, neutron reflectometry can be configured so as to probe electrolyte / thin film interfaces, as well as buried interfaces down to the substrate. ***Chapter 3*** introduces a specially designed neutron reflectometry cell that is capable of probing solid / liquid interfaces with neutrons and also measuring EIS simultaneously. On the other hand, ***Chapter 5*** introduces an evolved version of the cell that is capable of more versatile electrochemical measurements. Significantly, NR is able to resolve water layers formed as a consequence of electrolyte penetration. Due to the sample prerequisite of atomically smooth layers for reliable neutron reflectivity, water droplets or inhomogeneities at the buried interface are expressed as a significant roughening of the interface.

By contrast, X-ray reflectometry (XR) is not easily adapted to electrochemical systems due to the fact that X-rays are significantly attenuated by the electrolyte. Whilst the techniques are almost conceptually identical, the difference in the medium used as the characterization probe (i.e. X-rays as opposed to neutrons) accounts for such an effect. In a laboratory based X-ray reflectometer, such as that used throughout the course of the project, this attenuation results in a low signal to noise ratio which tends to obscure valuable structural information pertaining to the system of interest. As a consequence, all XR measurements in this study are carried out *ex situ* at a solid / air interface.

Generally, NR and XR studies work under the assumption that the polymer layers are homogenous throughout the sublayers of the ISE. Whilst the two reflectometry techniques are extremely powerful tools to study the effects of water uptake on prolonged exposure to analytes, they are unable to provide insights into any nano-inclusions that may exist in the polymer. In such a case, small angle neutron scattering (SANS) can be used to study the internal structure of the polymer at length scales from approximately 10 to 1000 Å (37). Essentially, such a technique involves the elastic scattering of neutrons from a

sample resulting in a scattering pattern which is analysed to provide information on the size, shape and orientation of certain components of the system (38).

Chapter 4 introduces SANS as a technique that is capable of assessing the formation of water within the membrane, as opposed to at the interfaces. Such a technique is imperative to this study due to the fact that it will be used to identify any water formed within the membrane that is not homogenous in nature, i.e. undetectable by NR, and provide information relating to the size and distribution of the inhomogeneities. Accordingly, SANS has also been used to provide insights into the effects of using a plasticizer.

Although the information that can be obtained from a combination of reflectivity, SANS and EIS is extremely valuable, these techniques fall short of providing meaningful compositional information for the materials under investigation. With reference to the uptake and formation of water at the interfaces of SC ISEs, these techniques are unable to provide insights into the ion content of the transported water (i.e. water transported in a pure or electrolytic form). The usefulness of secondary ion mass spectrometry (SIMS) is demonstrated in this instance, where trace ion concentrations of transported ions at the buried interface can be determined with excellent sensitivity. ***Chapters 3 – 5*** demonstrate the use of SIMS in such a manner.

In this research, SIMS analyses are carried out after removing ISEs from solution and exposing the buried interfaces by manually peeling away various polymer layers. In theory, peeling away the polymer layer should lead to an almost immediate evaporation of any water whilst leaving behind salt residues from the electrolyte that can be analysed by SIMS. Whilst such a methodology will give an indication of the existence of water and the transported ions at the interface, ***Chapters 5*** and ***6*** demonstrate that the use of synchrotron radiation / Fourier transform-infrared micro-spectroscopy (SR / FT-IRM), although still an *ex situ* technique, negates the requirement to remove polymers from the ISE's

conductive support. In addition, SR/FT-IRM allows a visual depiction of water inclusions formed at the buried interface. Nevertheless, whilst the two techniques share similar experimental approaches (i.e. both techniques require the *ex situ* analysis of the ISEs following membrane hydration), the information that each technique is able to provide is inherently different. As such, these techniques can be used in conjunction with each other to provide valuable and complementary information.

The study of solid-state polymeric ISEs is concluded by a preliminary examination of the ion-to-electron transduction process occurring in the SC sublayer. ***Chapter 7*** serves as a preface to such a study which will inevitably form a significant component of the future direction of this research. Given that the research pertaining to this thesis has focussed on characterizing and subsequently eliminating the problem of the water layer through use of polymer SCs, it follows that future research should be focussed on the chemical and electrochemical mechanisms at work in these materials. Synchrotron radiation / X-ray photoelectron spectroscopy (SR / XPS) is presented as an ideal approach for studying the charge transfer processes occurring at the ion-selective membrane / SC interface. In contrast to SIMS, the ability of SR / XPS to provide information pertaining to the oxidation states of atoms opens up avenues to study the electrochemical doping of the SC. In this respect, the extent that the ion-to-electron process occurs in the SC can be examined in the poly alkylthiophenes by exploring for the existence of oxidized sulfur throughout the material. NR is also presented as a tool to study these charge transfer processes by monitoring changes in the neutron scattering length density (SLD) of the SC after forcibly doping it with lipophilic ion-exchanger anions.

Metal – Tetracyanoquinodimethane Molecules

Charge-transfer materials based on tetracyanoquinodimethane (TCNQ) (see ***Figure 1-7***), have been used in many contexts over several decades (39-

41). Often, the $M^{x+}[TCNQ]^{-}_{x}$ (where M = transition metal) derivatives exhibit interesting conducting and magnetic properties that make them useful in applications such as data storage and novel sensor materials (42). In particular, the prospect of using these compounds as molecular on / off switches (i.e. alternating from a high to a low impedance state upon the application of an electric field or optical excitation) has been a significant driving force behind a recent boom in research on these charge-transfer materials (43-50). Nevertheless, there is much controversy surrounding the novel properties of these materials due to a lack of understanding of the underlying mechanisms at work (45). A limiting factor with many of these materials is that their structures are yet to be elucidated, primarily since there is no appropriate technique for characterizing the TCNQ compounds *in situ*. As mentioned in the Introduction, *ex situ* studies are prone to error since the action of removing the sample from the solvent to air or vacuum environments may result in changes in the morphology of the synthesized crystals. Metal TCNQ systems are no exception (46).

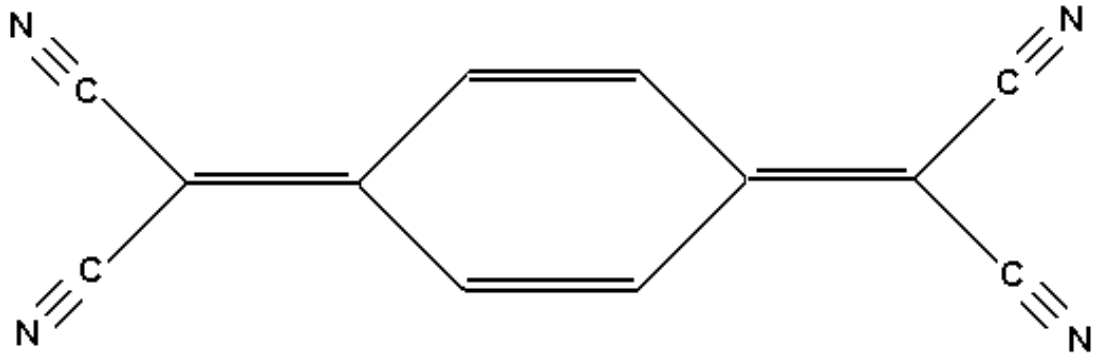

Figure 1-7 *Tetracyanoquinodimethane (TCNQ) complex investigated in this research.*

Although a variety of methods are available for the synthesis of metal TCNQ compounds (48, 49, 51-55), an electrocrystallization approach (40, 41, 44, 45, 50) is very appealing for several obvious reasons. Aside from the relative ease of synthesis associated with a metal TCNQ material when

electrodeposited, the prospect of having an electrochemically controllable deposit is an invaluable tool in future applications (44, 56). Inevitably, the ability to control the reaction by managing the electrochemical deposition parameters allows for a greater control of the resulting physical (e.g. morphology) and chemical (e.g. phase, structure, purity) properties of the prevailing material. Such factors are vitally important for progression of this technology since it is theorized that the phase, morphology and stoichiometry of the materials play a substantial role in determining their electronic and conducting properties (41). Accordingly, the purpose of this research has been in the design and implementation of an appropriate method for the synthesis and *in situ* structural characterization of these materials. Such a method will be applied to two uncharacterized $M^{x+}[TCNQ]_x^-$ systems, namely zinc and cadmium based TCNQ systems.

A Nanocharacterization Scheme for Metal – TCNQ Molecules

In the last few decades, advanced synchrotron sources have offered the possibility of probing *in situ* the buried interface of electrochemical systems. As opposed to conventional laboratory based X-ray sources, the highly intense nature of synchrotron radiation aligns itself perfectly to studying electrodes beneath an electrode layer. Essentially, powerful synchrotron X-ray sources allow beam penetration through the electrolyte - a feat which conventional X-ray sources struggle to achieve - and allows *in situ* structural characterization of the interphase (4). In particular, the emergence of third generation synchrotron X-ray sources have provided higher energy X-rays, and this can be used to penetrate electrolytes at thicknesses of up to several millimetres. As a result of these improvements, electrochemists have been able to characterize materials surrounded by an electrolyte without a significant loss in beam intensity. In the context of the present research, the phase chemistry of electrodeposited metal TCNQ can be investigated using a synchrotron source without the need of removing the electrode from its natural electrochemical environment.

Synchrotron radiation / grazing-incidence X-ray diffraction (SR / GIXRD) is an ideal method for characterizing the crystal structure of electrocrystallized films. ***Figure 1-8*** shows a simplified schematic of the experimental setup used in SR / GIXRD measurements. Essentially SR / GIXRD offers all of the benefits of conventional X-ray diffraction while allowing surface diffraction measurements for the externally reflected beam that skims across the surface. In general, diffraction techniques are based on the elastic scattering of X-rays from structures with long range order. As a result they provide detailed information on the crystal structures, grain sizes and preferred orientations of the electrocrystallized materials with relative ease. Accordingly, as demonstrated in ***Chapters 8*** and ***9***, SR / GIXRD is an ideal method for investigating the phase and structural chemistry of electrocrystallized metal TCNQ compounds.

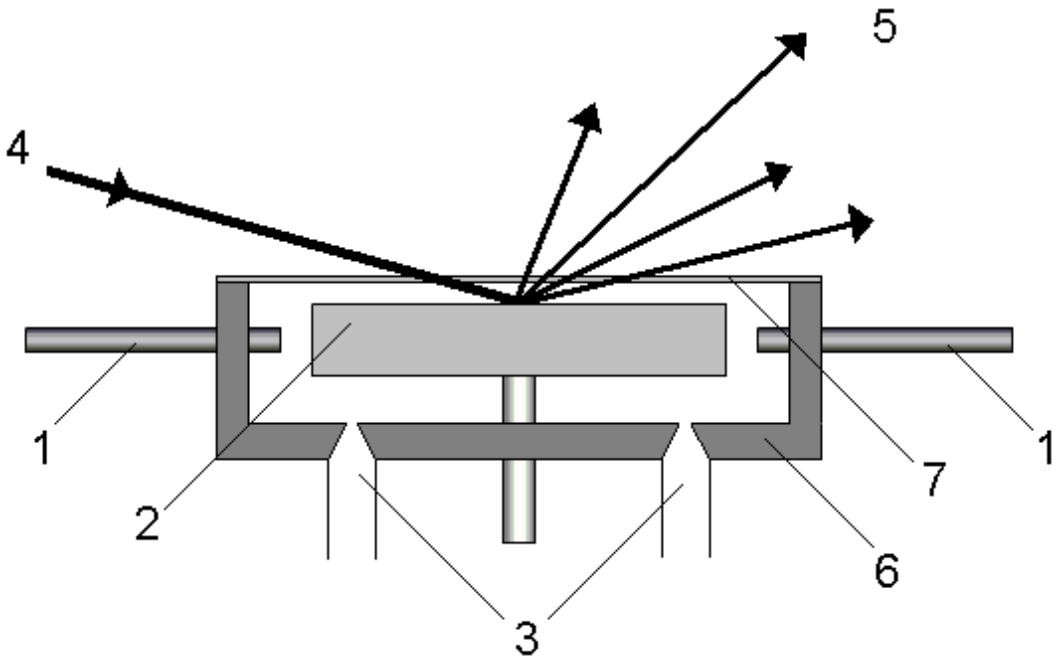

Figure 1-8 *Simplified schematic of the experimental set-up of a GIXRD experiment applied to in situ studies of electrochemically generated thin films. 1) Auxiliary and reference electrodes, 2) working electrode, 3) electrolyte reservoir inlet / outlet, 4) incident X-ray beam at small angles, 5) diffracted X-ray beam, 6) cell body, 7) X-ray transparent window.*

In addition to SR/GIXRD, infrared (IR) spectroscopy and thermogravimetric studies were carried out to provide complementary information on the compositions and structures of the electrocrystallized materials, i.e. to determine if the hydrated metal-TCNQ compound was formed. On the other hand, scanning electron microscopy (SEM) studies were undertaken to study the morphology of the electrocrystallized material on the eletrode surface[1].

[1] The concept of IR spectroscopy has already been introduced in this chapter (and explained in more detail in ***Appendix I***). On the other hand, thermogravimetry and SEM are already well established and widely understood techniques. In the context of studying metal TCNQ systems, these techniques merely serve the purpose of ensuring the reliability of GIXRD. As a result, further discussions of these techniques are not warranted in this section.

References

1. Nagy Z, You H. Applications of surface X-ray scattering to electrochemistry problems. Electrochim Acta. 2002;47(19):3037-55.

2. Lucas CA, Markovic NM. In-situ X-ray Diffraction Studies of the Electrode/Solution Interface. In: Alkire RC, Kolb DM, Lipkowski J, Ross PN, editors. Advances in Electrochemical Science and Engineering. Weinheim: Wiley; 2006.

3. Dowsett MG, Adriaens A. Cell for Simultaneous Synchrotron Radiation X-ray and Electrochemical Corrosion Measurements on Cultural Heritage Metals and Other Materials. Anal Chem. 2006;78(10):3360-5.

4. Renner FU, Grunder Y, Zegenhagen J. Portable chamber for the study of UHV prepared electrochemical interfaces by hard x-ray diffraction. Rev Sci Instrum. 2007;78(3):1-8.

5. Bakker E, Buhlmann P, Pretsch E. Polymer membrane ion-selective electrodes. What are the limits? Electroanal. 1999;11(13):915-33.

6. Bakker E, Diamond D, Lewenstam A, Pretsch E. Ion sensors: current limits and new trends. Anal Chim Acta. 1999;393(1-3):11-8.

7. Michalska A. Optimizing the analytical performance and construction of ion-selective electrodes with conducting polymer-based ion-to-electron transducers. Anal Bioanal Chem. 2006;384(2):391-406.

8. Bakker E, Pretsch E. A New Wave of Ion Selective Electrodes. Anal Chem. 2002;74(15):420A-6A.

9. Bakker E, Pretsch E. Potentiometry at trace levels. Trends Anal Chem. 2001;20(1):11-9.

10. Bakker E. Electrochemical Sensors. Anal Chem. 2004;76(12):3285-98.

11. Lewenstam A, Maj-Zurawska M, Hulanicki A. Application of ion-selective electrodes in clinical analysis. Electroanal. 1991;3(8):727-34.

12. Konopka A, Sokalski T, Michalska A, Lewenstam A, Maj-Zurawska M. Factors Affecting the Potentiometric Response of All-Solid-State Solvent Polymeric Membrane Calcium-Selective Electrode for Low-Level Measurements. Anal Chem. 2004;76(21):6410-8.

13. Goldberg HD, Brown RB, Liu DP, Meyerhoff ME. Screen printing: a technology for the batch fabrication of integrated chemical-sensor arrays. Sens Actuators, B. 1994;B21(3):171-83.

14. Gyurcsanyi RE, Nyback A-S, Toth K, Nagy G, Ivaska A. Novel polypyrrole based all-solid-state potassium selective microelectrodes. Analyst. 1998;123:1339-44.

15. Morf WE. The Principles of Ion-Selective Electrodes and of Membrane Transport Studies in Analytical Chemistry. New York: Elsevier Scientific Publishing Company; 1981. p. 431.

16. Meyerhoff ME, Opdycke WN. Ion-selective electrodes. In: Speigel HE, editor. Adv Clin Chem. London: Academic Press; 1986.

17. Cattrall RW, Freiser H. Coated wire ion-selective electrodes. Anal Chem. 1971;43(13):1905-6.

18. Buck R. Ion-Selective Electrodes in Analytical Chemistry. Freiser H, editor. New York: Plenum; 1978.

19. Bobacka J. Conducting polymer-based solid-state ion-selective electrodes. Electroanal. 2006;18(1):7-18.

20. Cadogan A, Gao Z, Lewenstam A, Ivaska A, Diamond D. All-solid-state sodium-selective electrode based on a calixarene ionophore in a

poly(vinyl chloride) membrane with a polypyrrole solid contact. Anal Chem. 1992;64(21):2496-501.

21. Nikol'skii BP, Materova EA. Solid contact in membrane ion-selective electrodes. Ion-Sel Electrode Rev. 1985;7(1):3-39.

22. Ammann D, Pretsch E, Simon W. Lipophilic Salts as Membrane Additives and Their Influence on the Properties of Macro- and Micro- Electrodes Based on Neutral Carriers. Anal Chim Acta. 1985;171:119-29.

23. Nagele M, Mi Y, Bakker E, Pretsch E. Influence of Lipophilic Inert Electrolytes on the Selectivity of Polymer Membrane Electrodes. Anal Chem. 1998;70:1686-91.

24. Faridbod F, Ganjali MR, Dinarvand R, Norouzi P. Developments in the Field of Conducting and Non-conducting Polymer Based Potentiometric Membrane Sensors for Ions Over the Past Decade. Sensors. 2008;8(4):2331-412.

25. Bakker E, Nagele M, Schaller U, Pretsch E. Applicability of the phase boundary potential model to the mechanistic understanding of solvent membrane-based ion-selective electrodes. Electroanal. 1995;7(9):817.

26. Moody GJ, Oke RB, Thomas JDR. Calcium-selective electrode based on a liquid ion exchanger in a poly(vinyl chloride) matrix. Analyst. 1970;95(1136):910-8.

27. Qin Y, Peper S, Bakker E. Plasticiser-Free Polymer Membrane Ion-Selective Electrodes Containing a Methacrylic Copolymer Matrix. Electroanal. 2002;14(19-20):1375-81.

28. Heng LY, Hall EAH. Methacrylic-acrylic polymers in ion-selective membranes: acheiving the right polymer recipe. Anal Chim Acta. 2000;403(1-2):77-89.

29. Johnson RD, Bachas LD. Ionophore-based ion-selective potentiometric and optical sensors. Anal Bioanal Chem. 2003;376:328-41.

30. Karpfen FM, Randles JEB. Ionic equilibria and phase-boundary potentials in oil-water systems. Trans Faraday Soc. 1953;49:823-32.

31. Bakker E, Chumbimuni-Torres KY. Modern Directions for Potentiometric Sensors. J Braz Chem Soc. 2008;19(4):621-9.

32. Bakker E, Pretsch E. Potentiometric sensors for trace-level analysis. Trends Anal Chem. 2005;24(3):199-207.

33. Lindner E, Gyurcsanyi RE. Quality control criteria for solid-contact, solvent polymeric membrane ion-selective electrodes. J Solid State Electrochem. 2009;13(1):51-68.

34. De Marco R, Veder J-P, Clarke G, Nelson A, Prince K, Pretsch E, et al. Evidence of a water layer in solid-contact polymeric ion sensors. Phys Chem Chem Phys. 2008;10:73-6.

35. Fibbioli M, Morf WE, Badertscher M, De Rooij NF, Pretsch E. Potential drifts of solid-contacted ion-selective electrodes due to zero-current ion fluxes through the sensor membrane. Electroanal. 2000;12(16):1286-92.

36. Brett CMA. Electrochemical Impedance Spectroscopy for Characterisation of Electrochemical Sensors and Biosensors. ECS Trans. 2008;13(13):67-80.

37. Gerold V, Kostorz G. Small-Angle Scattering Applications to Materials Science. J Appl Crystallogr 1978;11:376-404.

38. King SM. Small Angle Neutron Scattering. 2003 [cited 2010]; Available from: www.isis.rl.ac.uk/archive/largescale/loq/documents/sans.htm.

39. Zhao H, Heintz R, Ouyang X, Dunbar KR. Spectroscopic, Thermal, and Magnetic Properties of Metal/TCNQ Network Polymers with Extensive Supramolecular Interactions between Layers. Chem Mater. 1999;11:736-46.

40. Nafady A, O'Mullane AP, Bond AM, Neufeld AK. Morphology Changes and Mechanistic Aspects of the Electrochemically-Induced Reversible Solid-Solid Transformation of Microcrystalline TCNQ into $Co[TCNQ]_2$-Based Materials (TCNQ=7,7,8,8-tetracyanoquinodimethane). Chem Mater. 2006;18:4375-84.

41. Nafady A, Bond AM, Bilyk A, Harris AR, Bhatt AI, O'Mullane AP, et al. Tuning the Electrocrystallization Parameters of Semiconducting $Co[TCNQ]_2$-Based Materials to Yield either Single Nanowires or Crystalline Thin Films. J Am Chem Soc. 2007;129(8):2370-82.

42. Zhao H, Heintz R, Ouyang X, Grandinetti G, Cowen J, Dunbar KR. Insight into the behaviour of $M(TCNQ)_n$ (n=1, 2) crystalline solids and films: x-ray, magnetic and conducting properties. Veciana J, editor. Dordrecht: Kluwer; 1999.

43. Liu Y, Li H, Tu D, Ji Z, Wang C, Tang Q, et al. Controlling the Growth of Single Crystalline Nanoribbons of Copper Tetracyanoquinodimethane for the Fabrication of Devices and Device Arrays. J Am Chem Soc. 2006;128:12917-22.

44. Neufeld AK, O'Mullane AP, Bond AM. Control of Localized Nanorod Formation and Patterns of Semiconducting CuTCNQ Phase I Crystals by Scanning Electrochemical Microscopy. J Am Chem Soc. 2005;127:13846-53.

45. O'Mullane AP, Neufeld AK, Bond AM. Distinction of the Two Phases of CuTCNQ by Scanning Electrochemical Microscopy. Anal Chem. 2005;77:5447-52.

46. Qu X, Nafady A, Mechler A, Zhang J, Harris AR, O'Mullane AP, et al. AFM study of morphological changes associated with electrochemical solid-solid transformation of three dimensional crystals of TCNQ to metal derivatives (metal=Cu, Ni; TCNQ=tetracyanoquinodimethane). J Solid State Electrochem. 2008;12:739-46.

47. Cao G, Ye C, Fang F, Xing X, Xu H-H, Sun D, et al. Scanning electron microscopy investigation of Cu-TCNQ micro/nanostructures synthesized via vapor-induced reaction method. Micron. 2005;36:267-70.

48. Gu N, Yang X-M, Sheng H-Y, Lu W, Wei Y. Electrical switching properties of CuTCNQ organic crystals with nanometer feature size. Synth Met. 1995;71:2221-2.

49. Liu S-G, Liu Y-Q, Zhu D-B. Amorphous somiconducting film containing nanometer particles of CuTCNQ: preparation, characterisation and electrical switching properties. Thin Solid Films. 1996;280(1-2):271-7.

50. Potember R, Poehler T, Cowan D. Electrical Switching and memory phenomena in copper-TCNQ thin films. Appl Phys Lett. 1979;34(6):405-7.

51. Hoagland JJ, Wang XD, Hipps KW. Characterization of Cu-CuTCNQ-M devices using scanning electron microscopy and scanning tunneling microscopy. Chem Mater. 1993;5(1):54-60.

52. Gu N, Zhang H-Q, Wei Y, Shen H-Y, Zhang L. Rectifying phenomenon of Cu-TCNQ organometallic crystallite device. Supramol Sci. 1998;5:691-3.

53. Sun S, Xu X, Wu P, Zhu D. Characterization and electrical switching properties of Cu-tetracyanoquinodimethane films formed under different conditions. J Mater Sci Lett. 1998;17(9):719-21.

54. Liu S-G, Liu Y-Q, Wu P-J, Zhu D-B. Multifaceted Study of CuTCNQ Thin-Film Materials. Fabrication, Morphology, and Spectral and Electrical Switching Properties. Chem Mater. 1996;8(12):2779-87.

55. Heintz RA, Zhao H, Ouyang X, Grinetti G, Cowen J, Dunbar KR. New Insight into the Nature of Cu(TCNQ): Solution Routes to Two Distinct Polymorphs and Their Relationship to Crystalline Films That Display Bistable Switching Behavior. Inorg Chem. 1999;38(1):144-56.

56. Nafady A, Bond AM, Bilyk A. Controllable Synthesis and Fabrication of Semiconducting Nanorod.Nanowire Bundles of $Fe[TCNQ]_2(H_2O)_2$ via Electrochemically Induced Solid-Solid Phase Transformation of TCNQ Microcystals. J Phys Chem C. 2008;112:6700-9.

Chapter Two

2 *In Situ* Structural Characterization of Electrochemical Systems Using Synchrotron - Radiation Techniques

Roland De Marco and Jean-Pierre Veder

Trends in Analytical Chemistry **29**, 528-537 (2010).

Abstract – In recent times, *in situ* synchrotron-radiation techniques have been used extensively in studies of scientifically and technologically important electrochemical systems. In this review, we showcase the power of electrochemical measurements, either active or passive, in combination with *in situ* synchrotron-radiation techniques, using research reported on battery systems, corroding metals, ion-selective electrodes and fuel cells. Moreover, we review the specialized electrochemical cells and general design principles utilized by electrochemical synchrotron researchers.

Introduction

Electrochemical systems are complex in nature and difficult to understand. This is primarily due to the transfer of charge between electrically and ionically conducting phases, whereby these complex processes occur at the boundary or the interface separating two phases (i.e. electrode and electrolyte). Often, these charge-transfer processes occur over a depth scale of several

hundred Ångstroms (Å) on either side of the electrode surface, and the molecular structure of the interphase region can differ considerably from the bulk structures (1). Consequently, surface-analysis tools are crucial in the field of electrochemical science and technology.

Generally, *ex situ* surface studies of electrochemical systems provide valuable insights into certain properties of different systems, but there always remains a doubt about whether the removal of an electrode from its natural electrochemical environment may affect deleteriously the composition of the electrode (2-4). For example, exposure of surfaces to ambient air, containing not only oxygen but also other reactive components (e.g., carbon dioxide) may result in an uncontrollable structural change of the surface (4). To exacerbate this problem, many electrochemical surfaces are inclined to undergo transformations in the absence of the applied electric field in the native electrochemical environment. Accordingly, the “holy grail” of modern electrochemical surface analysis involves *in situ* characterization of electrochemical systems, and this is a major imperative for contemporary electrochemistry research.

In this context, it is necessary to use a probe that can penetrate the electrode / electrolyte systems, so as to enable reliable measurements without a significant loss of intensity from the excitation source (1). Due to these stringent conditions, many techniques are deemed unsuitable for *in situ* characterization of complex electrochemical systems.

Recently, the introduction of highly-advanced synchrotron sources has offered the means and the capability for probing *in situ* the complex buried interface of electrochemical systems. Specifically, synchrotron-light sources are instruments that accelerate electrons or positrons in very large orbits approaching the speed of light. Deflections of the charged particles through magnetic fields will create extremely bright light, in directions tangential to the

electron orbit. Essentially, this bright light is commonly referred to as synchrotron radiation (SR). Further insertion devices (e.g., multi-pole wigglers and undulators) are installed into the synchrotron with the intention of significantly increasing the intensity of the light. The basic principle behind the use of insertion devices is to make the charged particles undergo sharp serpentine motions, thereby adding further flux to the already bright light source (5). The net result of this process is a highly intense, collimated and polarized beam that has the added advantage of tunability across the entire wavelength range of the electromagnetic spectrum (from infrared to X-rays). A full description of synchrotron science is beyond the scope of this review, but further information on contemporary synchrotron sources can be found in a comprehensive review by Bilderback et.al. (6).

By contrast to conventional laboratory-based X-ray sources, the highly intense nature of SR, as previously described, aligns itself perfectly to applications in electrochemical science and technology. Essentially, powerful SR X-ray sources offer the possibility of penetrating matter (e.g., electrodes and electrolytes) with relative ease - a feat that conventional X-ray sources struggle to achieve - and they allow *in situ* studies of structural parameters of the electrochemical system (4). In particular, the emergence of third generation SR X-ray sources has seen higher beam energies that can penetrate electrodes and electrolyte solutions at depths of up to several millimetres, and sophisticated detectors may be used in time-resolved studies of the electrochemical reactivity. Furthermore, the highly-collimated SR beam allows high-resolution spectroscopic imaging of electrodes, while the substantial boost in light flux of the SR beam also allows a substantial enhancement of the signal-to-noise ratio of conventional structural characterization techniques, thereby yielding data of the highest quality. Last but not least, there is the advantage of tunability of the source enabling the experimentor to optimize the beam energy, thereby yielding high-quality data (e.g., X-ray diffraction [XRD] data in the presence of negligible levels of fluorescence, X-ray photoelectron spectroscopy [XPS] data with vastly

enhanced detection limits, and beam penetration at high energy to allow transmission through a thin electrode cell), or by allowing the conduct of X-ray absorption spectroscopy (XAS) experiments requiring a scan of the beam energy around the absorption edge of the test element.

In summary, the present review describes a series of applications of SR techniques in contemporary electrochemistry. It must be stressed that the scope of this review is not to provide a comprehensive treatise on *in situ* SR techniques but rather to demonstrate the power of combined *in situ* SR and electrochemical studies of scientifically important systems. In this context, the review has been organised so as to provide an overview of *in situ* electrochemical cells, followed by a review of exciting recent literature on *in situ* studies of electrochemical systems using SR techniques.

In Situ Cell Designs

Typically, the use of SR in the characterization of electrochemical systems requires the design of a specific flow cell to carry out electrochemistry whilst also allowing the appropriate X-ray measurements to be made. A primary assessment of literature on this topic reveals many electrochemical-cell designs, each of which can carry out a wide variety of *in situ* synchrotron studies. The field of *in situ* electrochemical X-ray analysis is so mature that the evolution of *in situ* cells has been reviewed previously for specific applications (i.e. cells used to study battery materials by XRD (1, 5, 7, 8)). As a general trend, each reported cell design differs slightly from the earliest reported designs (9-12) in order to extend the cell to new SR experiments and / or provide enhanced electrochemistry. Nevertheless, each cell is intrinsically based on one of two specific designs which correspond to two different measurement geometries (i.e. reflection and transmission modes of measurement).

Reflection cells generally comprise an X-ray transparent window (usually Kapton or Mylar) that is situated parallel (9, 10, 12-14), or sometimes perpendicular (as with thick layer reflection cells) (4, 15-20), to the working-electrode interface, noting that this configuration is only utilized in surface analyses of substrates. This window is responsible for containing the electrolyte whilst not severely attenuating the X-ray beam itself.

Transmission cells (21-29), otherwise known as thin layer cells, are arranged such that the X-ray beam passes through the entire cell that incorporates a thin deposit of the electrode material under examination. Often, the contribution to the absorbance by electrolyte solution is minimized by using layers of filter paper or alike soaked in electrolyte as a separator between the working electrode and the counter electrode. ***Figure 2-1*** shows each experimental configuration associated with reflection and transmission geometries.

It is widely acknowledged that each of these geometries comes with associated advantages and disadvantages, but the appropriate choice of *in situ* cell requires careful consideration of the configuration of the synchrotron beamline to be used, as well as the nature of the electrochemical system under scrutiny. Nagy et al. (19) discussed further comparisons between thick-layer and conventional reflectance cells in an early, but informative, review of the two configurations.

In the past, transmission cells have been used typically for a variety of measurements ranging from XRD to XAS. In many cases the electrode material has the form of a powder that is pressed into a thin pellet, and a filter paper that is moistened by electrolyte. Notably, several groups included ionically transferring membranes (22, 24, 27, 30) in place of the electrolyte-soaked filter paper to enhance electrochemical attributes. Morcrette et al. (8) and Russell et

al. (7) critically reviewed a variety of cells similar in nature to those outlined above, so no further comments are warranted.

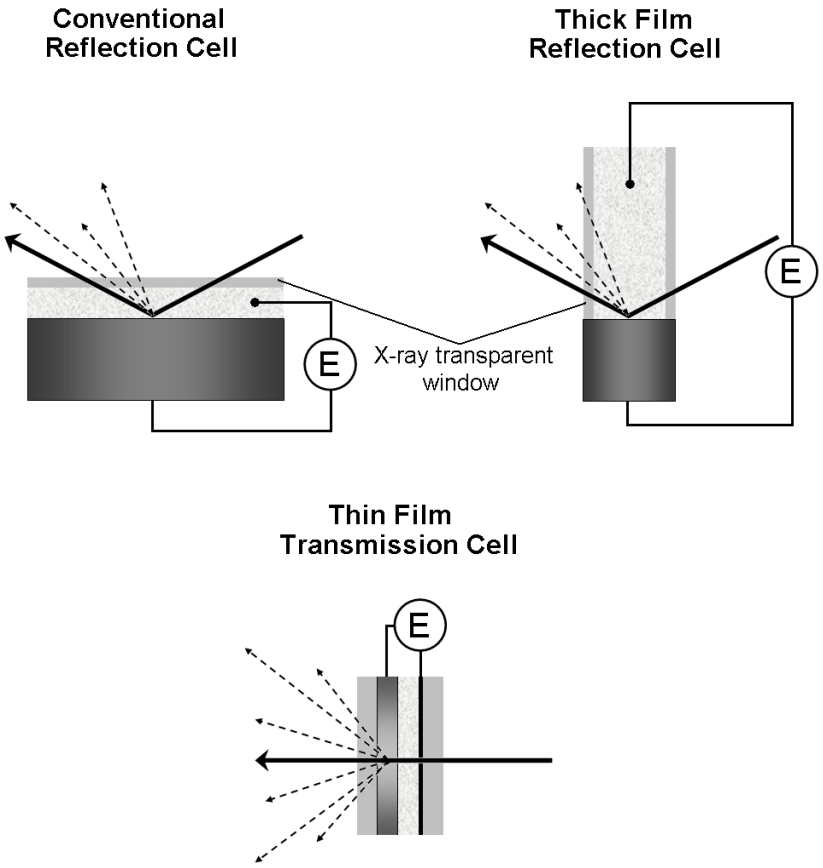

Figure 2-1 *Differing cell configurations in transmission and reflection geometries. The thick black arrow shows the path of the X-ray beam whilst the dashed arrows show the scattered beam (Adapted from Nagy et al. (1)).*

Despite the numerous options available for cell geometries, in many instances, the experimenter will be limited by the type of cell that may be implemented on the beamline available for X-ray analysis. In simple terms, electrochemical cells must be designed and implemented with respect to the sample holders, the detectors and the experimental set-ups at the host beamlines. Consequently, Morcrette et al. proposed (8) that there is no ideal design for an *in situ* X-ray electrochemical cell, and the design of cell is left to the imagination and creativity of the SR user.

X-ray Diffraction and Synchrotron Radiation / Grazing Incidence X-ray Diffraction

Synchrotron radiation / grazing incidence X-ray diffraction (SR / GIXRD) or surface XRD aligns the collimated SR beam at low angles of incidence and the technique is surface sensitive. Since the introduction of SR / GIXRD in the late 1970's to early 1980's (31, 32), it has been used to study many systems concerned primarily with surfaces and thin layers. Below the critical angle at a given wavelength of radiation, SR / GIXRD accomplishes its surface sensitivity by restricting the depth of penetration of the externally-reflected X-ray beam and the concomitant sampling depth to the order of Å. Importantly, buried interface structures below the surface can be studied with relative ease by altering the penetration depth of the SR beam by varying the angle of incidence. We do not set out to provide a comprehensive description of basic XRD methods, so, for detailed explanations on XRD and GIXRD, we refer readers to the excellent review by Robinson and Tweet (33).

In this section, we will showcase *in situ* SR / XRD and SR / GIXRD using examples in the fields of batteries, supercapacitors, corrosion and ion-selective electrodes (ISEs).

Battery-Electrode Materials

One of the biggest areas of research combining *in situ* electrochemistry with SR-XRD is associated with energy storage in batteries. This elevated interest stems from the increasing use of consumer products requiring reliable, powerful secondary batteries (i.e. mobile phones and laptop computers), not to mention the emergence of hybrid electric vehicles and the gradual depletion of conventional energy supplies (e.g. oil and gas). *In situ* SR / XRD provides an excellent method for studying the structural changes during electrochemical

cycling of batteries, whilst also avoiding exposure of battery materials to air and humidity that might lead to a degradation in the battery material.

Most recently, Bramnik and co-workers (34) took advantage of a favourable characterization strategy and applied it to the study of delithiation of metallophosphates. They revealed that electrochemical delithiation occurred to the extent of ~ 50% Li extraction, and that two phases are evident for the Co^{2+} / Co^{3+} and M^{2+} / M^{3+} couples in the mixed-metallophosphate cathode. Further delithiation saw the formation of a complete solid-solution where the unit cell volume changed continuously upon further discharge. In the case of the systems in which M = Mn or Fe, the higher degrees of delithiation caused the emergence of another phase and the concomitant loss of the solid-solution domains. A similar investigation was also undertaken on a related metallophosphate system of $LiCoPO_4$ (35).

In situ SR-XRD has also been used to investigate the structure of electrode materials in Li-ion batteries. Most notably, the $LiCoO_2$ system tends to attract the majority interest because it is arguably the most important, widely-used cathode material in commercial Li-ion batteries. Using *in situ* SR / XRD, Rosciano and co-workers (28) went to great effort to show that potentiodynamic charging induced an enlargement of the c-axis of the rhombohedral unit cell of $LiCoO_2$, as evidenced by progressive shifting to lower angles of the (003) rhombohedral peak.

Renner et al. (36) focused their attention on a study of anodes utilizing gold prepared with different methods (i.e. Au nanoparticles on highly orientated pyrolytic graphite and Au(111) single crystals). Notably, in the nanoparticulate system, the charging cycle resulted in an Au-Li alloy with much the same size and orientation as the starting material, while the Au(111) single crystal undergoes severe fracturing and nanocrystallites with a much larger mosaic distribution are observed.

Supercapacitors have also aroused great attention for energy storage. In such systems, charge storage ideally takes place in the electrical double-layer formed near large-surface-area, carbonaceous electrodes (37). Nevertheless, Ruch and co-workers (29) successfully used *in situ* SR / XRD to show that insertion of electrolyte ions into carbon electrodes can also occur in the operating potential range of supercapacitors. By following the intensity of the (002) reflection of graphite, they showed that the intercalation of $(C_2H_5)_4N^+$ from the electrolyte occurs at around 1V vs. Li/Li^+, whilst that of BF_4^- takes place at potentials in excess of 5V vs. Li/Li^+.

Figure 2-2 presents the SR / XRD pattern series for the first and second anodic cycles of graphite in acetonitrile (AN) and propylene carbonate (PC). Notably, there is a gradual splitting, merging and shifting of several peaks in the series of diffraction patterns captured at very short intervals, demonstrating the power of *in situ* SR / XRD in tracking the evolution and the transformation of phases within an electrode whilst under electrochemical polarization.

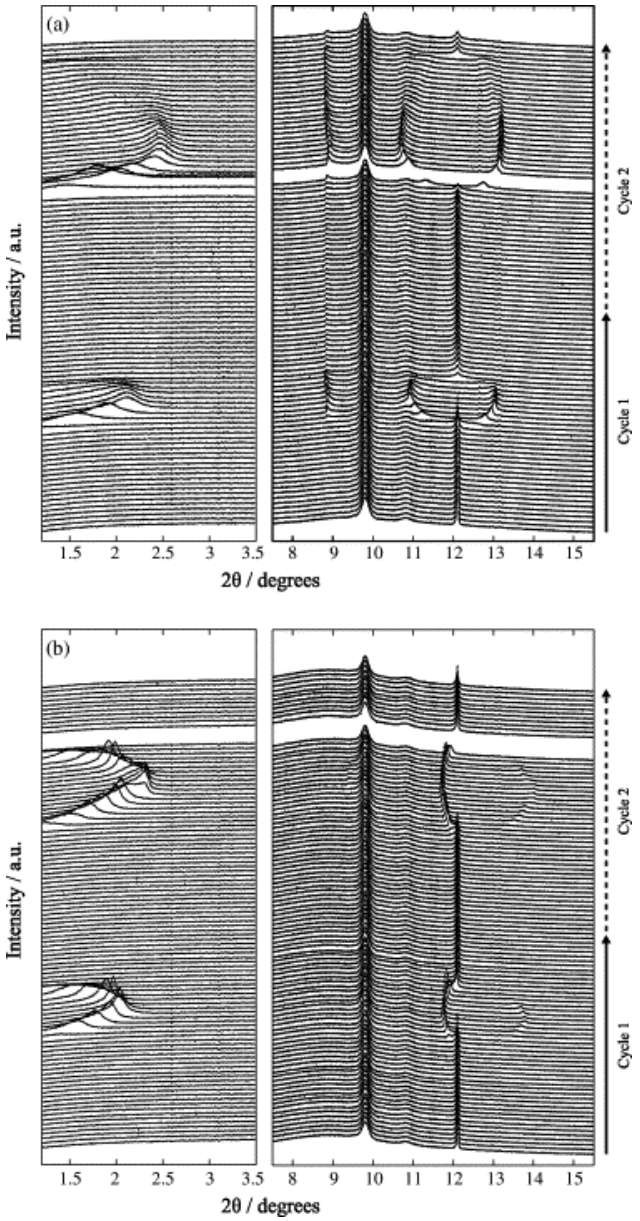

Figure 2-2 *In situ synchrotron-radiation X-ray diffraction patterns for the first and second cycles of graphite in a 1-M solution of $(C_2H_5)_4NBF_4$ in acetonitrile (a) and in propylene carbonate (b) (Reproduced from ref. 29 ©2007 Elsevier).*

Corrosion

An area of research of significant interest to the electrochemical community is the corrosion of metals. Recently, there has been considerable progress on applications of *in situ* SR / XRD, carried out in tandem with

electrochemical measurements, on important systems of cultural, environmental and technological significance, which are highly susceptible to corrosion.

In 2005, De Marco et al. (38) studied the influence of the carbon-dioxide corrosion of mild steel on the corrosion behaviour of pipelines used in the oil and gas industries. SR / GIXRD was employed in conjunction with the long-term monitoring of mixed potentials to examine the surface reactions occurring at the mild-steel working electrode. The study revealed that, during the initial stages of corrosion, $Fe_2O_2CO_3$ was formed due to preferential deposition of the reaction product at the cathodic sites of the electrode induced by the reaction between carbonic acid (formed from the dissolved carbon dioxide content in water) and the poorly crystalline native oxide film on the mild steel [i.e. H_2CO_3 reacting with FeO(OH)]. This reaction step was shown to be followed by the formation of the two reaction products of $Fe_2O_2CO_3$ and $Fe_2(OH)_2CO_3$ at anodic reaction sites over the electrode.

This research was later extended (39) to study the influence of acetate on the carbon-dioxide corrosion of mild steel. It was shown, using SR / GIXRD and simultaneous electrochemical impedance spectroscopy (EIS), that acetate significantly alters the crystallization habit of the corrosion products. As a result of acetate's involvement, corrosion was seen to occur initially in a thin, non-porous film that protected the mild-steel substrate against further carbon-dioxide corrosion of the mild steel.

Similarly, Leyssens and co-workers (40) studied corrosion using *in situ* SR / XRD, but their study was applied to metallic artefacts of cultural heritage. The purpose of the study was to examine the effectiveness of corrosion potential (E_{corr}) measurements as a corrosion-monitoring tool for copper-based artifacts recovered from wet environments. The study involved a copper substrate covered in nantokite (CuCl) and correlated its phase transformation, as evidenced by the SR / XRD and E_{corr} data obtained with this system. It was

revealed that, contrary to popular belief, the E_{corr} data did not correspond completely with the transformations seen on a molecular level, casting doubt over the effectiveness of E_{corr} measurements as an analysis tool for the corrosion of copper.

Ion-Selective Electrodes

The application of ion-selective electrodes (ISEs) in environmental analysis of trace metals is highly desirable, but this research imperative is hindered by a multitude of stumbling blocks, one being the ageing of the electrodes in real samples (e.g., seawater). De Marco and co-workers (41) used SR / GIXRD to study the response mechanism of the mercury(II) chalcogenide ISE in saline media. This study revealed that electrode fouling in synthetic seawater was linked to the formation of poorly crystalline silver chloride. SR-GIXRD also showed that the low level of free mercury in a calibration buffer is able to undergo a metathesis reaction with silver(I) sulphide in the membrane to produce mercury(II) sulphide. Without doubt, the most significant finding of the study suggested that real seawater reduced the effect of silver-chloride fouling due presumably to the peptization of silver chloride by the surfactant-like nature of seawater ligands at pH 8. Notably, this result is of high value to electrochemists dealing with ISEs, because knowledge pertaining to the electrode's interaction with seawater is rudimentary at best.

De Marco and co-workers (42, 43) also investigated the reactivity of the modified surface layer (MSL) of the iron(III)-chalcogenide glass ISE in synthetic and real seawater using SR / GIXRD coupled to mixed potential and EIS measurements. Interestingly, this work revealed that oxidative attack of the membrane MSL yielded erroneous ISE-response data in calibration standards compared to raw seawater, but the adoption of a seawater-ligand mimetic calibration system not only emulated the response of the sensor in seawater but it also replicated nicely the surface chemistry of the electrode in natural

seawater ligands, thereby confirming the mimetic ligand mixture's suitability for adoption in the analysis of seawater.

X-ray Absorption Spectroscopy

XAS is of significant value to electrochemists since it can be used to determine the properties pertaining to the atomic and electronic structure, as well as the composition of electrode materials. Specifically, XAS can provide valuable information (e.g., the oxidation state and local coordination of a central atom in a molecular structure). A typical XAS experiment involves scanning the X-ray energies through the absorption edge of an element in the sample, with subsequent excitation of a core-level electron of the absorbing atom to an unoccupied orbital. This X-ray energy corresponds to an absorption edge of the material. The region that extends to energies of about 50 eV above the absorption edge is known as the X-ray absorption near-edge structure (XANES), where rich information about the electronic and vibrational properties of the material can be obtained. More energetic incident X-ray photons lead to the excitation of a core electron of the absorber into the continuum. This process leads to the emission of a photoelectron that can be represented as a spherical wave. The outgoing wave tends to scatter with surrounding atoms producing in-going, or backscattered, waves. Constructive and destructive interference between the interacting waves results in oscillatory behaviour of the absorption intensity. Such a region corresponds to the extended X-ray absorption fine structure (EXAFS), which can reach to 1000 eV beyond the edge and have a magnitude of typically less than 15% of the edge jump (5). Detailed information on the technique as well as the application of XAS to the study of electrochemical systems prior to 2006 was reviewed by Deb and Cairns (24), Russell and Rose (7), and Long and Kruger (44).

As in the previous section, we will provide examples of *in situ* XAS using literature in the fields of fuel cells, batteries and corrosion.

Fuel Cells

Arruda et al. (45) used XAS to study halide poisoning of fuel cells, but also found that carbon monoxide (CO) was problematic, and this has sparked a considerable amount of interest in the field. CO, commonly introduced into the system as a contaminant of reformed hydrogen, is adsorbed strongly onto the Pt anode - causing blockage of hydrogen adsorption and oxidation, which inevitably leads to significant power losses. Nevertheless, metal-decorated Pt-based catalysts can be used to provide a level of CO tolerance, but the mechanistic reasons for CO tolerance are not widely understood.

Recently, Pereira and co-workers (46) investigated the effectiveness of certain bimetallic Pt-based catalysts supported on carbon (PtRu / C, PtFe / C, PtMo / C and PtW / C) in mitigating the effect of CO poisoning of fuel cells using *in situ* XANES, and found that an increase in the Pt 5d-band vacancies for the bimetallic catalysts led to a weakening of the Pt-CO bond, aiding CO tolerance. This was corroborated by electrochemical data, with the PtRu / C system showing an overpotential loss of only 110 mV at 1 A / cm^2, when compared to a regular Pt / C system.

Scott et al. (47) also used XANES to study the relative adsorbate coverages of CO, OH and H on bimetallic oxide Pt-based anodes (in this instance utilizing RuO_n, MoO_n and SnO_n), showing that Mo and Sn tend to oxidise at low potentials, exerting relatively strong ligand effects at all potentials (i.e. perturbations in the electronic properties of the Pt atoms causing reduction in the Pt-CO bond strength). However, Ru does not exhibit significant ligand interaction effects until larger metallic-like islands of Ru are formed, leading to further oxidation to RuO_n. Essentially the ligand effect was shown to increase in the order $Ru < MoO_n \leq SnO_n < RuO_n$, which corresponds to the strengthening of the Pt-OH bonds (to which CO can migrate to and be oxidized) and the

weakening of the Pt-CO bonds, indicating that the oxidation state of the metal is an important factor on the CO tolerance of a system.

Interesting developments pertaining to the CO poisoning of fuel cells were recently made on two separate occasions by Rose and co-workers (48, 49). In the first study (48), EXAFS was carried out as a function of applied electrode potential to study Ru-modified carbon-supported Pt catalysts. Notably, a better understanding of the chemistry relating to the oxidation of CO occurring at the interface of the PtRu alloy surfaces was obtained through the suggestion that Ru^{3+} and Ru^{4+} co-exist at this boundary for the potential region at which CO oxidation occurs.

Furthermore, the second study (49) used *in situ* EXAFS at the Ru K-edge to examine the Ru-CO bonds of CO absorbed onto a PtRu / C catalyst, showing a CO:metal surface atom ratio of greater than 1:1, which suggested that the electrochemically-active surface area of the catalyst, determined from both CO chemisorption and CO stripping voltammograms, may represent significant over-estimations of the surface chemistry.

Batteries

Just as *in situ* SR / XRD is widely used in the characterization of battery systems (as demonstrated in earlier in the chapter), XAS is often applied to battery materials to provide complimentary information about the complex properties of a system. By contrast to SR / XRD, which provides information pertaining to the crystal structure of the system, XAS can provide information about the electronic properties of the battery material. Moreover, the oxidation states of certain species on the electrochemical charge / discharge cycling of the cell may provide information that is of great interest to the electrochemistry community.

Cho and co-workers (50) studied the synthesis and characterization of $Li[Ni_{0.41}Li_{0.08}Mn_{0.51}]O_2$ nanoplates for use as an Li-ion battery cathode. The specific use of XAS demonstrated that, upon charge / discharge cycling, the electrode operated primarily with the Ni^{2+} / Ni^{4+} redox couple between 4.8 V and 2 V. Alternatively, the oxidation state of Mn remained constant at 4+ indicating that this was the predominant chemical state of Mn (51), while Mn was found to be electrochemically inactive in the system of $Li_{1.05}Ni_{0.35}Co_{0.25}Mn_{0.4}O_2$, as shown by Deb et al. (52). In this investigation, the oxidation states of the transition metals in the discharged state were found to be Ni^{2+}, Co^{3+} and Mn^{4+}, which later saw Ni^{2+} oxidized to Ni^{3+} in an intermediate stage and finally to Ni^{4+}. Cobalt was found to be in an oxidation state of 3.89+ in its fully-charged condition. The superior cycling characteristics of this system were linked to the preservation of its symmetry and structural short-range order, as defined in the XAS experiments. The electrochemical dormancy of Mn does not hold true for all systems, but a recent *in situ* study (53) of $Li_{0.33}MnO_2$ showed that Mn changes its oxidation state from 4+ to 3+ upon lithium intercalation into the cathode.

Miscellaneous *In Situ* Synchrotron Studies of Electrode Surfaces

In the previous discussion, this review has focused primarily on the situ techniques of SR / XRD, SR / GIXRD and XAS due to the popularity of these techniques in *in situ* studies of electrochemical systems. Nevertheless, there are reports on *in situ* electrochemical studies using alternative SR techniques that are just as powerful as the X-ray techniques mentioned above. Some of these SR techniques are in an early stage of development and show immense promise, whilst other *in situ* SR techniques have already been utilized extensively and effectively to characterize technologically-important electrochemical systems.

This section seeks to provide an overview of the alternative techniques, albeit not as extensively as *in situ* SR / XRD, SR / GIXRD and XAS studies.

Ambient-Pressure X-ray Photoelectron Spectroscopy

Ambient-pressure X-ray photoelectron spectroscopy (AP-XPS) is a unique SR probe designed to study systems *in situ* without the need for ultra-high vacuum, as is traditionally the case with conventional XPS. XPS involves the photoionization of the atoms in the sample via the Einstein photoelectric effect, and the photoelectrons (with a narrow escape depth / sampling depth of Å) are analysed for their kinetic energy. Furthermore, XPS provides high-quality quantitative information on the elemental-surface composition of the sample, as well as chemical shifts in the peak positions consistent with changes in the oxidation state associated with the electrochemical reactivity of the substrate.

Recently, McDaniel and co-workers (54) used AP-XPS in electrochemical studies of a well-known solid oxide fuel cell (SOFC) system utilizing a Ni working electrode and a Pt counter and reference electrode on Y_2O_3-stabilized ZrO_2 (YSZ). Notably, the study revealed that sulfur was present as a contaminant on the Ni-electrode surface, which could be driven off the by anodic polarization. Nevertheless, the sulfur content returns on subsequent reduction. More significantly, it was shown using AP-XPS, and later confirmed by post-mortem microscopy, that the Ni-working-electrode film became porous after electrode polarization. These results revealed the emergence of a Zr 3d core-level peak, indicative of the YSZ substrate, after polarization of the Ni electrode (see ***Figure 2-3***).

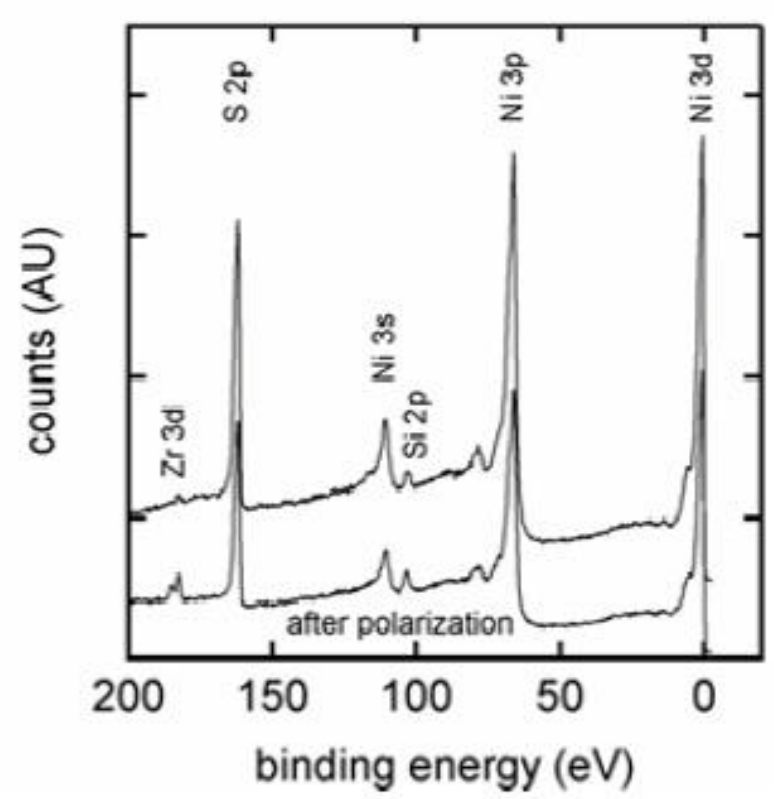

Figure 2-3 AP-XPS survey scan taken at photon energy of 490 eV prior to (upper trace) and following (lower trace) polarization (Reproduced from ref. 54 ©2009 The Electrochemical Society).

Soft X-ray Microscopy

A significant innovation in studies of the buried interface of electrochemical systems *in situ* has been the pioneering work of Bozzini and co-workers on the use of *in situ* soft X-ray microscopy (SXM) (55), in which Ni electrodeposition from ammonium and chloride solutions was monitored as a function of the electrochemical polarization applied. The study revealed that electrodeposition of Ni from the ammonium-based electrolyte led to the formation of a homogenous film of dendrites at different positions on the cathode based on the current-density distribution and the local concentrations of $[Ni(NH_3)_6]^{2+}$. However, electrodeposition from the chloride-containing system showed the formation of humps, blisters and islands growing progressively at

the Au / electrolyte interface, based again on the current-density distribution of the system.

Small Angle X-ray Scattering

The application of small-angle X-ray scattering (SAXS) can provide valuable information about the structure of disordered structures on a nanoscale. The power of this approach in studies of small structures is made possible through its ability to resolve scatterers ranging in size from 1 nm to fractions of a μm. Conventionally, SAXS can be considered as diffuse scattering that occurs between the angle of the specular beam and the half angle of the first Bragg reflex (27). Recently, Smith and co-workers (56) observed the nature of Pt-catalyst nanoparticles as a function of continual potential cycling. This investigation led to the realization that, depending on the Pt loading on the carbon-nanoparticle support, the particle size increases significantly, in some cases rapidly, from the initial dimensions of the nanoparticles (demonstrated in ***Figure 2-4***). This is an extremely important result for the future of fuel cells because it suggests that the lifetime of the fuel cell is dictated by the coarsening of the Pt-electrocatalyst nanoparticles, which provides a concomitant loss in the electrochemical active material's surface area.

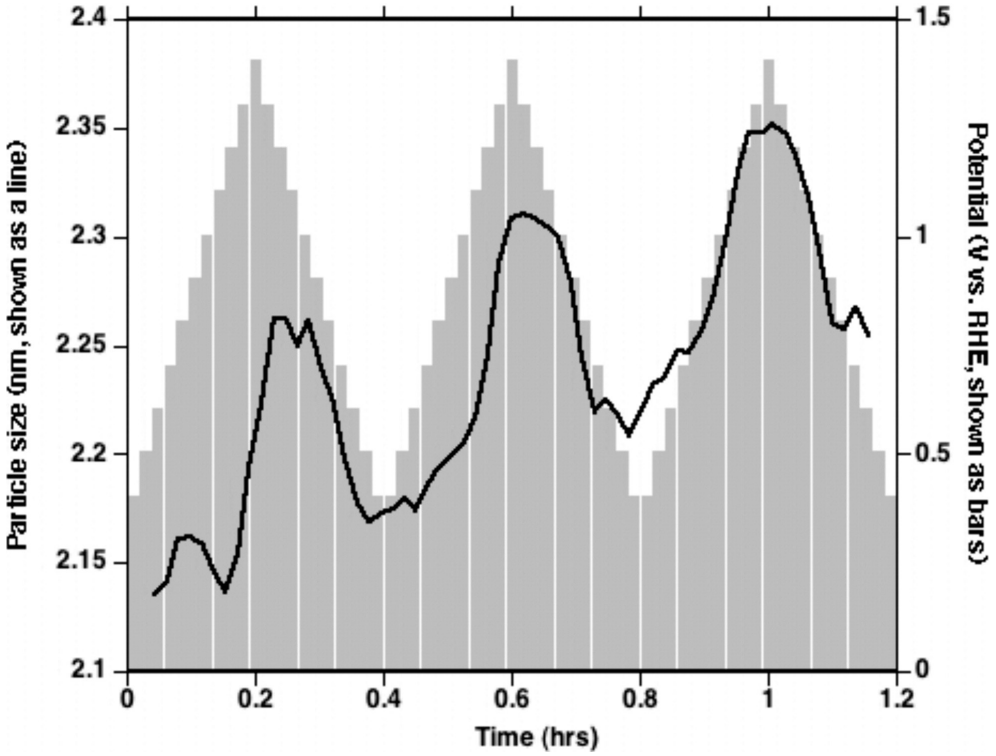

Figure 2-4 *Recorded catalyst size as determined from in situ synchrotron SAXS compared against corresponding cycle potentials (Reproduced from ref. 56 ©2008 American Chemical Society).*

Synchrotron Radiation / Fourier-Transform-Infrared Microspectroscopy

So far, we have focused primarily on the benefits of SR X-ray techniques, but Fourier transform-infrared microspectroscopy (FT-IRM) also offers significant advantages (e.g., enhanced IR spectral signal-to-noise ratio and augmented spatial resolution of the imaging technique). The utility of FT-IRM was demonstrated in 2007 by Hahn and co-workers (57), who carried out spectroscopic measurements in the mid-IR and far-IR regions to characterize, *in situ*, layers of copper oxide on corroded copper. The technique was surface sensitive by measuring the IR spectra using a grazing-angle FT-IR attachment. Significantly, Hahn et al. (57) studied the copper electrode at potentials in the range -1.4 - 0 V versus an Hg / Hg_2SO_4 reference electrode using only 1 nL of active solution, finding that the surface film on copper comprised mainly CuO, with possible traces of $Cu(OH)_2$ also present at 0 V.

Conclusions

Although we have described the application of in-situ SR techniques to a variety of electrochemical systems (e.g., batteries, corrosion research, fuel cells and ISEs), it is obvious that applications of these techniques are boundless. Accordingly, we anticipate that, with the emergence of the newer *in situ* methodologies (e.g., SXM, SAXS and AP-XPS), there will be many studies of electrochemical systems using these exciting new techniques.

Due to the powerful nature of SR and its ability to probe electrode materials *in situ*, the structural characteristics and concomitant mechanistic aspects of electrochemical systems may be derived, so there is an excellent chance for widespread adoption of these techniques by the electrochemistry community. However, It is important to note that, whilst SR techniques are powerful enough to be used solely with associated electrochemistry instrumentation, undoubtedly the most successful research carried out in this field will always use a combination of complementary techniques for surface and materials characterization to obtain an integrated picture of the system.

Most significantly, we have illustrated how *in situ* surface and materials characterization of electrode materials can glean important insights into the mechanistic chemistry of batteries, fuel cells, corroding metals and ISEs. Moreover, the fundamental research on these applied electrochemical systems has allowed the development of innovative approaches to extending battery durability, the electrochemical efficiency of fuel cells, corrosion-mitigation strategies, and reliable analytical methodologies to handle ISEs. Last but not least, the ability to couple measurements of electrode structure to electrochemical-polarization events enables the exciting option of linking electrode-reaction products to the observed electrode kinetic data, and this makes it a formidable characterization tool in electrochemistry.

References

1. Nagy Z, You H. Applications of surface X-ray scattering to electrochemistry problems. Electrochim Acta. 2002;47(19):3037-55.

2. Lucas CA, Markovic NM. In-situ X-ray Diffraction Studies of the Electrode/Solution Interface. In: Alkire RC, Kolb DM, Lipkowski J, Ross PN, editors. Advances in Electrochemical Science and Engineering. Weinheim: Wiley; 2006.

3. Dowsett MG, Adriaens A. Cell for Simultaneous Synchrotron Radiation X-ray and Electrochemical Corrosion Measurements on Cultural Heritage Metals and Other Materials. Anal Chem. 2006;78(10):3360-5.

4. Renner FU, Grunder Y, Zegenhagen J. Portable chamber for the study of UHV prepared electrochemical interfaces by hard x-ray diffraction. Rev Sci Instrum. 2007;78(3):1-8.

5. Abruna HD, White JH, Albaralli MJ, Bommarito GM, Bedzyk MJ, McMillian M. Is There Any Beam Yet? Uses of Synchrotron Radiation in the in Situ Study of Electrochemical Interfaces. J Phys Chem. 1988;92:7045-52.

6. Bilderback DH, Elleaume P, Weckert E. Review of third and next generation synchrotron light source. J Phys B: Atomic, Molecular and Optical Physics. 2005;38:S773-S97.

7. Russell AE, Rose A. X-ray Absorption Spectroscopy of Low Temperature Fuel Cell Catalysts. Chem Rev. 2004;104(10):4613-35.

8. Morcrette M, Chabre Y, Vaughan G, Amatucci G, Leriche J-B, Patoux S, et al. In situ X-ray diffraction techniques as a powerful tool to study battery electrode materials. Electrochim Acta. 2002;47:3137-49.

9. Fleischmann M, Hendra PJ, Robinson J. X-ray diffraction from adsorbed iodine on graphite. Nature. 1980;288:152-4.

10. Fleischmann M, Oliver A, Robinson J. In situ X-ray diffraction studies of electrode solution interfaces. Electrochim Acta. 1986;31(8):899-906.

11. Dahn JR, Haering RR. Anomalous Bragg Peak Widths in Li_xTiS_2. Solid State Commun. 1981;40:245-8.

12. Chianelli RR, Scanlon JC, Rao BML. Dynamic X-Ray Diffraction. J Electrochem Soc. 1978;125:1563-6.

13. Veder J-P, Nafady A, Clarke G, Williams RP, De Marco R, Bond AM. A Flow Cell for Transient Voltammetry and its Application to In Situ Grazing Incidence X-ray Diffraction Characterization of Electrocrystallised $Cd(TCNQ)_2$. Electrochim Acta. 2010;Submitted.

14. Kautek W, Mirwald S, Sahre M, Nauer GE. In-situ grazing incidence X-ray diffractometry of polycrystalline copper in alkaline chloride and sulphate electrolytes. Electrochim Acta. 1998;43:2979-84.

15. Ingham B, Illy BN, Toney MF, Howdyshell ML, Ryan MP. In Situ Synchrotron X-ray Diffraction Experiments on Electrochemically Deposited ZnO Nanostructures. J Phys Chem C. 2008;112:14863-6.

16. Brossard F, Etgens VH, Tadjeddine A. In situ surface X-ray diffraction using a new electrochemical cell optimised for third generation synchrotron light sources. Nucl Instrum Methods Phys Res B. 1997;129:419-22.

17. Felici R, Bertalot L, DeNinno A, LaBarbera A, Violante V. In situ measurements of the deuterium (hydrogen) charging of a palladium electrode during electrolysis by energy dispersive x-ray diffraction. Rev Sci Instrum. 1995;66(5):3344-8.

18. Robinson KM, O'Grady WE. A transmission geometry electrochemical cell for in situ x-ray diffraction Rev Sci Instrum. 1993;64(4):1061-5.

19. Nagy Z, You H, Yonco RM, Melendres CA, Yun W, Maroni VA. Cell design for in-situ x-ray scattering study of electrodes in the transmission geometry. Electrochim Acta. 1991;36(1):209-12.

20. Nagy Z, You H, Yonco RM. Cell design for in situ x-ray scattering studies of metal/solution interfaces under electrochemical control. Rev Sci Instrum. 1994;65(7):2199-205.

21. Knapp M, Carsten B, Ehrenberg H, Fuess H. The synchrotron powder diffractometer at beamline B2 at HasYLAB/DESY: status and capabilities. J Synch Rad. 2004;11:328-34.

22. Wiltshire RJK, King CR, Rose A, Wells PP, Hogarth MP, Thompsett D, et al. A PEM fuel cell for in situ XAS studies. Electrochim Acta. 2005;50:5208-17.

23. Nikolowski K, Baehtz C, Bramnik NN, Ehrenberg H. A Swagelok-type in situ cell for battery investigations using synchrotron radiation. J Appl Crystallogr. 2005;38:851-3.

24. Deb A, Cairns EJ. In situ X-ray absorption spectroscopy - A probe of cathode materials for Li-ion cells. Fluid Phase Equilibria. 2006;241:4-19.

25. Maniguet S, Mathew RJ, Russell AE. EXAFS of Carbon Monoxide Oxidation on Supported Pt Fuel Cell Electrocatalysts. J Phys Chem B. 2000;104:1998-2004.

26. Herron ME, Doyle SE, Pizzini S, Roberts KJ, Robinson J, Hards G, et al. In situ studies of a dispersed platinum on carbon electrode using x-ray absorption spectroscopy. Electroanal Chem. 1992;324:243-58.

27. Braun A, Shrout S, Fowlks AC, Osaisai BA, Seifert S, Granlund E, et al. Electrochemical in situ reaction cell for X-ray scattering, diffraction and spectroscopy. J Synch Rad. 2003;10:320-5.

28. Rosciano F, Holzapfel M, Kaiser H, Scheifele W, Ruch PW, Hahn M, et al. A multi-sample automatic system for in situ electrochemical x-ray diffraction synchrotron measurements. J Synch Rad. 2007;14:487-91.

29. Ruch PW, Hahn M, Rosciano F, Holzapfel M, Kaiser H, Scheifele W, et al. In situ X-ray diffraction of the intercalation of $(C_2H_5)_4N^+$ and BF_4^- into graphite from acetonitrile and propylene carbonate based supercapacitor electrolytes. Electrochim Acta. 2007;53:1074-82.

30. Mukerjee S, Srinivasan S, Soriaga MP. Role of Structural and Electronic Properties of Pt and Pt Alloys on Electrocatalysis of Oxygen Reduction. J Electrochem Soc. 1995;142:1409-22.

31. Marra WC, Eisenberger P, Cho AY. X-ray total-external-reflection-Bragg diffraction: A structural study of the GaAs-Al interface. J Appl Phys. 1979;50(11):6927-33.

32. Eisenberger P, Marra WC. X-ray Diffraction Study of the Ge(001) Reconstructed Surface. Phys Rev Lett. 1981;46(16):1081-4.

33. Robinson IK, Tweet DJ. Surface x-ray diffraction. Rep Prog Phys. 1992;55:599-651.

34. Bramnik NN, Trots DM, Hofmann HJ, Ehrenberg H. Mixed $LiCo_{0.6}M_{0.4}PO_4$ (M = Mn, Fe, Ni) phosphates: cycling mechanism and thermal stability. Phys Chem Chem Phys. 2009;11:3271-7.

35. Bramnik NN, Nikolowski K, Baehtz C, Bramnik KG, Ehrenberg H. Phase Transitions Occuring upon Lithium Insertion-Extraction of $LiCoPO_4$. Chem Mater. 2007;19:908-15.

36. Renner FU, Kageyama H, Siroma Z, Shikano M, Schoder S, Grunder Y, et al. Gold model anodes for Li-ion batteries: Single crystalline systems studied by in situ X-ray diffraction. Electrochim Acta. 2008;53:6064-9.

37. Kotz R, Carlen M. Principles and applications of electrochemical capacitors. Electrochim Acta. 2000;45:2483-98.

38. De Marco R, Jiang Z-T, Pejcic B, Poinen E. An In Situ Synchrotron Radiation Grazing Incidence X-Ray Diffraction Study of Carbon Dioxide Corrosion. J Electrochem Soc. 2005;152(10):B389-B92.

39. De Marco R, Jiang Z-T, John D, Sercombe M, Kinsella B. An in situ electrochemical impedance spectroscopy / synchrotron radiation grazing incidence X-ray diffraction study of the influence of acetate on the carbon dioxide corrosion of mild steel. Electrochim Acta. 2007;52:3746-50.

40. Leyssens K, Adriaens A, Dowsett MG, Schotte B, Oloff I, Pantos E, et al. Simultaneous in situ time resolved SR-XRD and corrosion potential analyses to monitor the corrosion on copper. Electrochem Commun. 2005;7:1265-70.

41. De Marco R, Pejcic B, Prince K, van Riessen A. A multi-technique surface study of the mercury(II) chalcogenide ion-selective electrode in saline media. Analyst. 2003;128(6):742-9.

42. De Marco R, Jiang Z-T, Pejcic B, Van Riessen A. In situ synchrotron radiation grazing incidence X-ray diffraction - A powerful technique for the characterization of solid-state ion-selective electrode surfaces. Electochim Acta. 2006;51:4886-91.

43. De Marco R, Jiang Z-T, Martizano J, Lowe A, Pejcic B, Van Riessen A. In situ electrochemical impedance spectroscopy / synchrotron radiation grazing incidence X-ray diffraction - A powerful new technique for the

characterization of electrochemical surfaces and interfaces. Electochim Acta. 2006;51:5920-5.

44. Long GG, Kruger J. Surface X-ray Absorption Spectroscopy, EXAFS and NEXAFS, for the in Situ and ex Situ Study of Electrodes. In: Varma R, Selman JR, editors. Techniques for Characterization of Electrodes and Electrochemical Processes. New York: John Wiley and Sons, Inc.; 1991.

45. Arruda TM, Shyam B, Ziegelbauer JM, Mukerjee S, Ramaker DE. Investigation into the Competitive and Site-Specific Nature of Anion Adsorption on Pt Using In Situ X-ray Absorption Spectroscopy. J Phys Chem C. 2008;112:18087-97.

46. Pereira LGS, Paganin VA, Ticianelli EA. Investigation of the CO tolerance mechanism at several Pt-based bimetallic anode electrocatalysts in a PEM fuel cell. Electrochim Acta. 2009;54:1992-8.

47. Scott FJ, Mukerjee S, Ramaker DE. Contrast in Metal-Ligand Effects on Pt_nM Electrocatalysts with M Equal Ru vs Mo and Sn exhibited by in situ XANES and EXAFS Measurements in Methanol. J Phys Chem C. 2010;114:442.

48. Rose A, Bilsborrow R, King CR, Ravikumar MK, Qian Y, Wiltshire RJK, et al. In situ Ru K-edge EXAFS of CO adsorption on a Ru modified Pt/C fuel cell catalyst. Electrochim Acta. 2009;54(22):5262-6.

49. Rose A, Crabb EM, Qian Y, Ravikumar MK, Wells PP, Wiltshire RJK, et al. Potential dependance of segregation and surface alloy formation of a Ru modified carbon supported Pt catalyst. Electrochim Acta. 2007;52:5556-64.

50. Cho J, Kim Y, Kim MG. Synthesis and Characterization of $Li[Ni_{0.41}Li_{0.08}Mn_{0.51}]O_2$ Nanoplates for Li Battery Cathode Material. J Phys Chem C. 2007;111:3192-6.

51. Bard AJ, Faulkner LR. Electrochemical Methods: Fundamentals and Applications. second ed. Harris D, Swan E, Aiello E, editors. New York: John Wiley and Sons, Inc.; 2001.

52. Deb A, Bergmann U, Cramer SP, Cairns EJ. In Situ X-ray Absorption Spectroscopic Study of $Li_{1.05}Ni_{0.35}Co_{0.25}Mn_{0.4}O_2$ Cathode Material Coated with $LiCoO_2$. J Electrochem Soc. 2007;154(6):A534-A41.

53. Wei YJ, Ehrenberg H, Kim KB, Park CW, Huang ZF, Baehtz C. Characterisation on the structural and electronic properties of thermal lithiated $Li_{0.33}MnO_2$. J Alloys Compd. 2009;470:273-7.

54. McDaniel AH, El Gabaly F, Akhadov E, Farrow RL, McCarty KF, Linne MA, et al. In-situ Investigation of SOFC patterned Electrodes Using Ambient-Pressure X-ray Photoelectron Spectroscopy. ECS Trans. 2009;25(2):335-43.

55. Bozzini B, D'Urzo L, Gianoncelli A, Kaulich B, Prasciolu M, Tondo ISE, et al. An in Situ Synchrotron-Based Soft X-ray Microscopy Investigation on Ni Electrodeposition in a Thin-Layer Cell. J Phys Chem C. 2009;113:9783-7.

56. Smith MC, Gilbert JA, Mawdsley JR, Seifert S, Myers DJ. In Situ Small-Angle X-ray Scattering Observation of Pt Catalyst Particle Growth During Potential Cycling. J Am Chem Soc. 2008;130:8112-3.

57. Hahn F, Mathis Y-L, Bonnefont A, Maillard F, Melendres CA. In situ synchrotron far-infrared spectromicroscopy of a copper electrode at grazing incidence angle. J Synch Rad. 2007;14:446-8.

The chapters 3 and 4 have been removed due to copyright restrictions

Chapter Five

5 Water Uptake in the Hydrophilic Solid-Contact of Polymeric Ion-Selective Electrodes

Jean-Pierre Veder, Roland De Marco, Benjamin Connell, Robert Dalgliesh, Ernö Pretsch and Eric Bakker

The Analyst, **In Preparation** (2010).

Abstract – Solid-contact (SC) ion-selective electrodes (ISEs) utilizing thin films of poly(3,4-ethylenedioxythiophene):poly(styrenesulfonate) (PEDOT:PSS) and plasticized poly(vinylchloride) (PVC) have been produced using a spin casting procedure. This study was carried out with a view to characterizing this popular and well known SC ISE using a series of complementary and powerful surface analysis methods. The study revealed that PEDOT:PSS prevents the separation of an undesirable water layer at the buried interface of this SC ISE due to the high miscibility of water in the hydrophilic PEDOT:PSS layer. The lack of a clearly defined and molecularly sharp buried interface prohibits the formation of a water layer presumably by eliminating sites which promote water accumulation. This outcome is important to the chemical sensor community since it provides further insights into the compatibility of sensor components in SC ISEs.

Introduction

The choice of an appropriate solid-contact (SC) in ion-selective electrodes (ISEs) is not a straightforward task due to the extensive amount of research that has been devoted to the development of new materials. The emergence of each new material is often accompanied by suggestions of enhanced performance with respect to existing technologies. In general, SCs comprise conducting or redox polymers, high surface area solid electron conductors or ion-conducting sensing membranes incorporating a redox couple loaded into the membrane (1). Within this family of materials, several SCs have attracted considerable attention in recent times, especially, hydrophobic self-assembled monolayers with redox active moieties (2-6) and high capacitance materials such as three dimensionally ordered macroporous carbon (7) or single-walled carbon nanotubes (8, 9). Despite the excitement surrounding these new materials, arguably the most widely used and accepted form of solid-contact is that of conducting polymers, such as poly(3-octylthiophene) (POT), polypyrrole (PPy) and poly(3,4-ethylenedioxythiophene) doped with poly(styrenesulfonate) (PEDOT:PSS). Specifically, PEDOT:PSS has proven to be a favoured option due to its superior performance, such as reduced sensitivity to interference from O_2 and CO_2 compared to PPy (10-12) and faster ion diffusion kinetics compared to other conducting polymers (13, 14). Moreover, PEDOT:PSS has been used in novel applications such as all-plastic, disposable ISEs, as reported by Michalska et.al. (15), whereby detection limits as low as 5×10^{-9} M were reported for calcium-selective sensors.

It was shown in ***Chapter 4*** that the ideal system for inhibition of undesirable water layers is the combination of a hydrophobic sensing membrane in conjunction with a hydrophobic conducting polymer SC (16). On the other hand, given the extensive use of the hydrophilic PEDOT:PSS SC, the authors have focussed their attention onto this popular SC. The purpose of the following study is to ascertain if there is an uptake of water into the PEDOT:PSS SC when

a hydrophobic ion-selective membrane is coupled with this hydrophilic SC. In this context we used the same surface analysis scheme described in ***Chapters 3*** and ***4*** but also utilized synchrotron radiation / Fourier transform-infrared microspectroscopy (SR / FT-IRM) as a complementary research tool for studying water accumulation at the SC / ISE membrane buried interface.

Experimental

Materials

The following Selectophore Fluka reagents were used in this research: high molecular weight poly(vinylchloride) (PVC), bis(2-ethylhexyl) sebecate (DOS), ETH 500, calcium ionophore IV and sodium tetrakis [3,5-bis(triflouromethyl)phenyl]borate (NaTFPB). High conductivity grade poly(3,4-ethylenedioxythiophene):poly(styrenesulfonate) (PEDOT:PSS) and analytical grade sodium perchlorate were obtained from Sigma-Aldrich, along with inhibitor free tetrahydrofuran (THF) (99.8%). Analytical grade sulfuric acid and hydrogen peroxide used for piranha etching solutions, along with anhydrous calcium chloride and sodium chloride were obtained from the Ajax Chemical Co. Laboratory grade dichloromethane and xylene were obtained from Chem-Supply. The highly polished silicon wafers (8 cm x 4 cm x 2 cm) used in NR measurements comprised conductive boron doped electrodes that were purchased from Crystran Ltd. Gold (111) mirrors used in the FTIR studies were obtained from Arrandee^{TM}. The gold used in the SIMS experiment was obtained as a sheet from Precious Metals Engineering W.A., cut to size and ground and polished manually using Struers polishing materials (viz., SiC paper [grit 800 – 4000] and DP-Nap polishing cloth). Milli-Q water was used to prepare all aqueous solutions.

Combined Neutron Reflectometry / Electrochemical Impedance Spectroscopy

NR measurements were carried out on the CRISP reflectometer at the ISIS facility of the Rutherford Appleton Laboratory (Oxfordshire, UK). A brief theory and summary of experimental conditions have been reported previously (16-18), however, the ISIS reflectometer utilizes a spallation neutron source and "time-of-flight" mode of measurements. Effectively, the energies of the reflected neutrons are determined by their flight time from the source of the polychromatic beam to the detector. In this study three incident angles were used per reflectometry measurement (0.35^{o}, 0.8^{o} and 1.5^{o}) to cover a relatively wide Q-range. In the majority of cases, the incoherent background reflectivity became dominant above a Q value of $0.25 Å^{-1}$, and each NR measurement took 2-4 hours.

The polished silicon wafers were thoroughly cleaned by applying a xylene rinse followed by a piranha etch (3 parts conc. H_2SO_4 : 1 part 30% v/v H_2O_2) for 10-20 minutes. A similar procedure to this has been reported previously (16); however, in this instance, the wafers were not cleaned at elevated temperatures. The clean wafers were thoroughly rinsed prior to spin coating at a rate of 2000 rpm for 2 minutes with a dilute aqueous suspension of PEDOT:PSS (1 part PEDOT:PSS : 3 parts H_2O). Subsequently, the coated wafers were annealed overnight in an inert atmosphere of nitrogen gas at $175^{o}C$. The PEDOT:PSS-coated wafer was subsequently spin-coated with an ion-selective polymer matrix of plasticized PVC at a spinning rate of 2000 rpm for 2 minutes. The PVC matrix comprised of 30 wt% PVC, 60 wt% DOS and 10 wt% ETH500 in an appropriate amount of THF (0.3% w/v). The resultant bi-layer coated wafer was subsequently annealed overnight at $60^{o}C$ in a nitrogen saturated atmosphere.

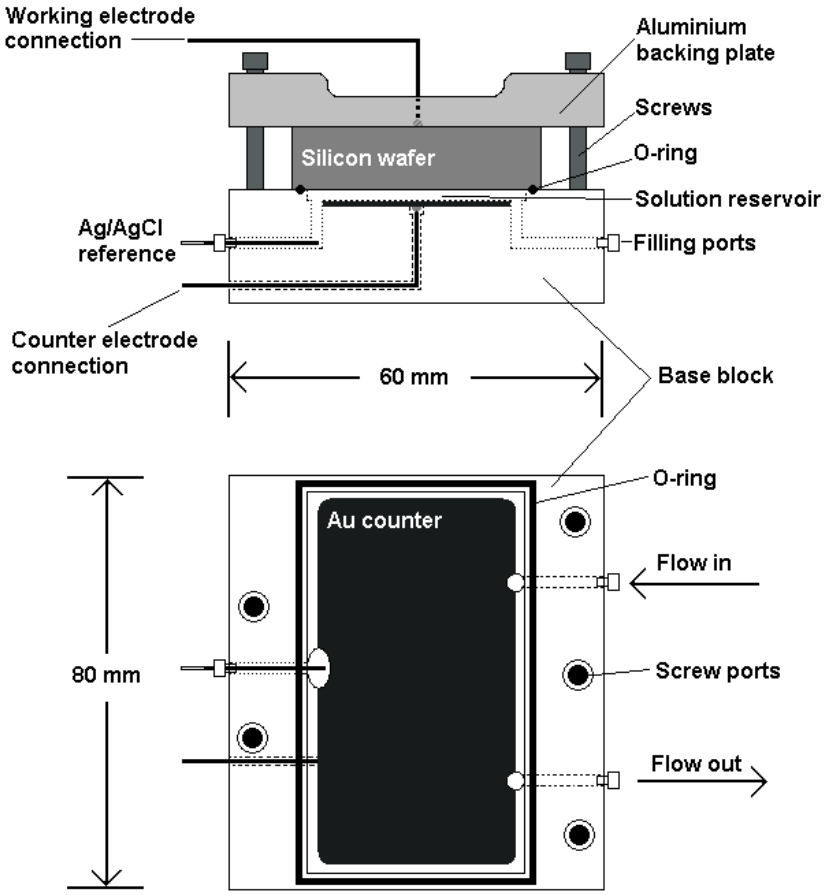

Figure 5-1 *Cell diagram for in situ neutron reflectometry / electrochemical impedance spectroscopy measurements. Upper diagram shows the front view of the NR cell, while the lower diagram presents a top view of the base block without the silicon and aluminium backing plate in place.*

The PEDOT / PVC-coated silicon wafers were housed in a neutron reflectometry cell (16, 18, 19) which was specially adapted for simultaneous *in situ* EIS / NR studies. A solid state Ag / AgCl reference wire electrode was located in the solution reservoir of the cell through an electrode port bored into the base of the cell (see ***Figure 5-1***). A large gold sheet counter electrode (electrically contacted through the base of the cell) was positioned within the base of the cell so that the face of the silicon working electrode was parallel to and facing the gold counter electrode. This arrangement ensured a uniform electric field between the counter and working electrodes. The cell was filled

with a D_2O solution of 1 M sodium perchlorate. Several NR measurements were performed prior to switching to a 1 M sodium perchlorate solution in H_2O.

Subsequent to sample alignment in the beam, the electrodes were connected to a Princeton Applied Research Parstat 2263 portable potentiostat. All EIS spectra were collected using an excitation potential of 10 mV rms and a frequency range of 100 kHz to 10 mHz. Time resolved NR studies were undertaken by carrying out 7 measurements in the D_2O electrolyte, and only one in the H_2O contrast. The measurement in the H_2O contrast was performed solely for the purpose of uncovering any information that may have been obscured due to a possible contrast matching of any components in the D_2O electrolyte. EIS measurements were undertaken concurrently with all the NR measurements.

Synchrotron Radiation / Fourier-Transform Infrared Spectroscopy

SR / FT-IR was carried out on calcium ISEs utilizing gold (111) mirror substrates. The ion-selective PVC membranes were prepared by combining PVC (32.5 wt%), DOS (65.9 wt%), NaTFPB (0.5 wt%) and calcium ionophore IV (1.1 wt%) with 2 mL of THF and cast onto the 11 x 11 mm mirrors in a volume of 15.4 µL. The concentration and volume of the cast solution was carefully chosen so as to achieve coatings thin enough to minimize the IR absorption cross-section of the material. PEDOT:PSS sub-layer coatings were also applied on some of the samples at a spin rate of 2000 rpm for 2 minutes. The ISEs coated in PEDOT:PSS were annealed under nitrogen for 2 hours at 200^{o}C while those which had a sole or subsequent coating of PVC were further annealed overnight at 60^{o}C in a nitrogen atmosphere. The resultant SC ISEs were bathed in a 0.1M calcium chloride solution for 3 days. Prior to measurement, the ISEs were rinsed in water and dried in a stream of nitrogen to remove excess surface water. To minimize membrane dehydration, measurements were performed immediately after the samples had been removed from solution. The results obtained from those bathed in solution were compared to identical samples that had not been exposed to solution.

All SR / FT-IRM measurements were carried out at the IR beamline of the Australian Synchrotron, Melbourne, Australia. The spectra were recorded with an FTIR spectrometer (Vertex V80v) coupled with an IR microscope (Bruker Hyperion 2000) and a mercury cadmium telluride (MCT) detector cooled with liquid nitrogen. The microscope and spectrometer were controlled using the Bruker Opus software version 6.5. The general ranges of measurements were from 3800 to 700 cm^{-1} and measured with a beam aperture of 5 × 5 µm. Spectral collection was performed in the reflection mode using 16 scan data averaging. IR imaging of substrates was performed in the mapping mode (refer to ***Appendix I*** for further details on mapping mode measurements), and all spectral maps were displayed using the OPUS 6.5 software.

Secondary Ion Mass Spectrometry

Gold coupons (5 x 10 x 0.5 mm) were used as ISE substrates, and polymer cocktails were cast directly onto the coupon after a thorough cleaning and polishing procedure, as reported previously (16). Identical polymer cocktails to those used in SR-FTIR analyses were employed; however, the cocktails were diluted 10-fold and cast onto the gold coupon in a volume of 44.3 µL so that the approximate film thickness was 8 µm. This thickness ensured the transportation of water over a period of only 48 hours thereby allowing for water layer formation at the buried interface. One of two PEDOT:PSS / PVC ISEs was bathed in 0.1 M NaCl, while the other was submerged into 0.1 M $CaCl_2$ solution for 48 hours. The treated ISEs were removed from solution and rinsed in Milli-Q water. The PVC film was peeled carefully from the ISE to reveal the PEDOT:PSS layer, and depth profiles were carried out on the buried PEDOT:PSS layer.

All SIMS data were collected on a Cameca IMS 5f dynamic SIMS instrument. A 10 keV Cs^+ primary ion source, with a beam current of 0.3 nA, was used to analyze for a number of species including ^{23}Na, ^{40}Ca and ^{35}Cl. The data collected from the treated ISEs were compared to data collected from a gold

control sample that had not been bathed in solution. Spectral intensities taken from SIMS were normalized against the $^{133}Cs^{+}$ signal for each sample.

Results and Discussion

Figure 5-2 (a) and ***5-2 (c)*** show NR reflectivity curves for consecutive measurements in the D_2O electrolyte as well as the H_2O electrolyte, respectively. A close examination of the data in D_2O shows that there are very few Kiessig fringes resulting from the difference in path length of reflected neutron waves. Such an effect is usually indicative of a roughened interface causing diffuse scattering. Notably, the one major Kiessig fringe in the NR spectra for D_2O that occurs at a Q value of approximately $0.026Å^{-1}$ (see ***Figure 5-2 (b)*** for an expanded view of ***Figure 5-2 (a)***) is seen to gradually shift to smaller Q values. This suggests that the polymer film is swelling and expanding upon exposure to the electrolyte. These observations are verified using the customized NR modelling software, IGOR Pro – Motofit (20). The modelled data (see ***Table 5-1***) revealed a clear and definitive alteration of the polymer's physical dimensions and condition from its original state. As expected, the polymeric bi-layer swelled to a considerable extent with the PVC showing only an overall increase in thickness of 15 Å while the PEDOT:PSS showed a significant increase of 33 Å from initial thicknesses of 262 Å and 160 Å, respectively.

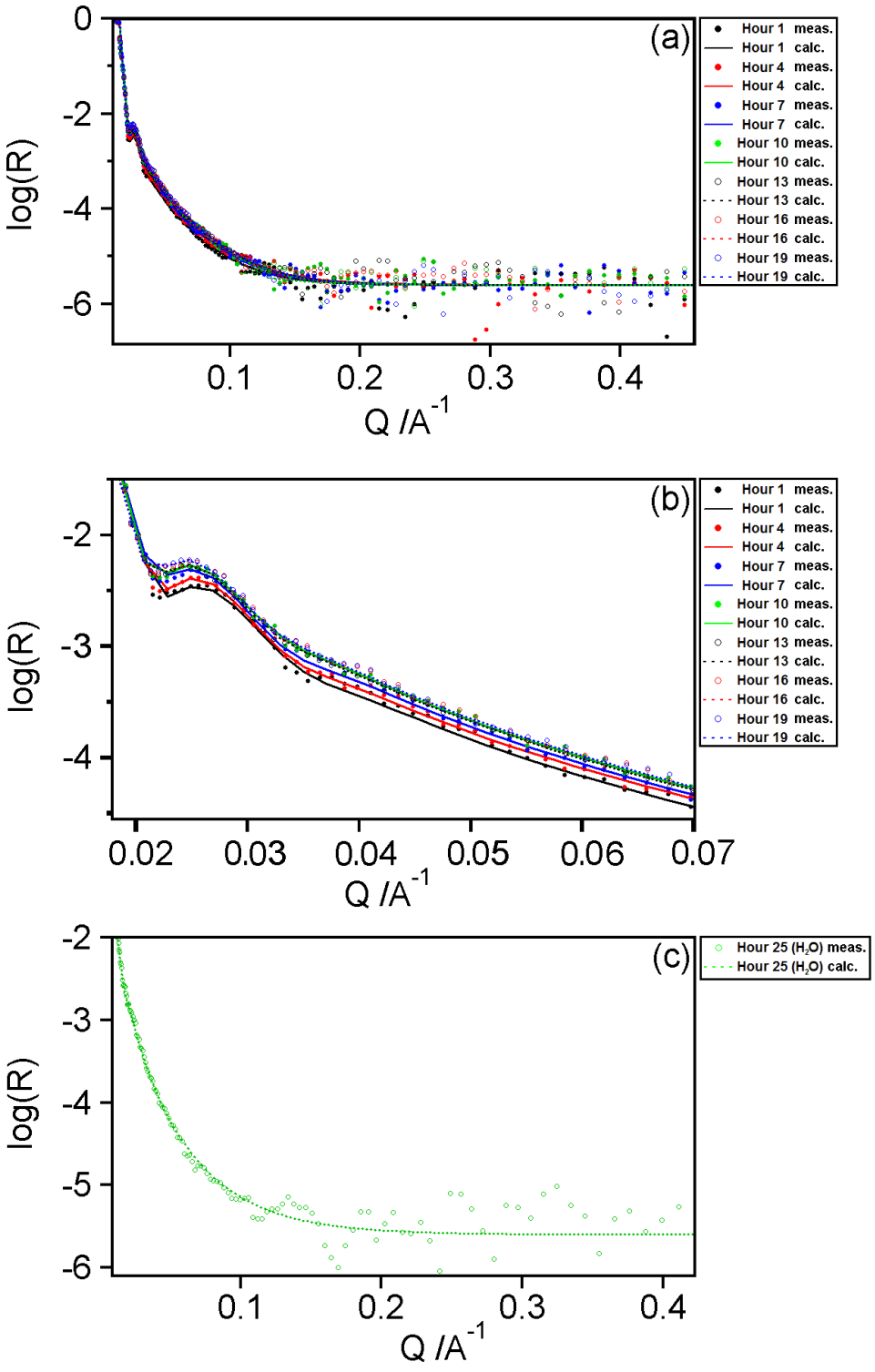

Figure 5-2 *NR reflectivity curves for the PEDOT / PVC solid-contact ISE system: (a) NR data in D_2O as a function of time; (b) Expanded view of the major Kiessig fringes evident in (a); (c) NR data in the H_2O electrolyte.*

For PEDOT:PSS SC, the increase in film thickness came as no surprise since this polymer system is hydrophilic and has a tendency to soak up water transported to the buried interface. This is evidenced by the concomitant increase in neutron scattering length density (SLD) of the PEDOT:PSS film from 4.464 x 10^{-6} Å^{-2} to 5.075 x 10^{-6} Å^{-2} after exposure to the D_2O electrolyte. Such an increase corresponds to a gradual matching of contrast to that of the supporting D_2O electrolyte (6.36 x 10^{-6} Å^{-2}), which arises from solvent penetration into the PEDOT:PSS film. Furthermore, the SLD of the PEDOT:PSS film in air is much lower (2.16 x 10^{-6} Å^{-2}), which is indicative of considerable solvent penetration in the initial 2-4 hour time span. Nevertheless, it is important to note that although the PEDOT:PSS blend is hydrophilic, the PEDOT component is actually hydrophobic (21). When PEDOT is made into an aqueous suspension, it is surrounded by a hydrated "shell" of PSS which is dried during annealing of the film. In the present study, the PSS portion of the polymer lacks contrast from the neutron SLD of the PEDOT so it is not possible to distinguish between the layers of PEDOT and PSS. Nevertheless, this lack of contrast was previously circumvented by Higgins et.al. (22, 23) who used deuterated PSS to show that a surface-rich layer forms as a result of the spin coating process. Herein, the surface rich layer of PSS was non-identifiable when the polymer was exposed to heavy water due presumably to insufficient contrast in neutron SLDs, or heterogeneous swelling or film roughening, etc. Accordingly the PEDOT:PSS layer reported herein is a single layer.

Table 5-1 *Neutron reflectivity parameters for the two layer model of PEDOT:PSS / PVC.*

Hour	PVC Thickness (Å) ± 4 %	SLD (10^{-6} Å^{-2})	Roughness (Å) ± 7 %	PEDOT Thickness (Å) ± 16 %	SLD (10^{-6} Å^{-2})	Roughness (Å) ± 11 %
1 (D_2O)	262	0.484	83	160	4.464	77
4 (D_2O)	262	0.484	82	169	4.598	79
7 (D_2O)	264	0.484	83	174	4.790	80
10 (D_2O)	270	0.484	85	174	4.976	95
13 (D_2O)	271	0.484	85	174	4.977	94
16 (D_2O)	274	0.484	85	174	5.074	97
19 (D_2O)	274	0.484	85	174	5.075	97
25 (H_2O)	277	0.464	88	193	0.297	98

Evidently the conductive polymer is hydrated to an extent of approximately 55% from its original state on continuous exposure to the D_2O electrolyte. Notably, the relative constancy in neutron SLDs at the end of the D_2O electrolyte runs (Hour 13-19) show that the polymer bi-layer film has acquired equilibrium. As a corroboration of this finding, the neutron SLD drops to 0.297×10^{-6} Å^{-2} as a result of H_2O (with SLD of -0.559×10^{-6} Å^{-2}) substitution of D_2O in the films.

The swelling of the PVC ion-selective membrane reported previously (16, 18), is attributable to small quantities of miscible and freezable water that have been transported into the membrane. Nevertheless, the swelling of the PVC membrane is about half of that noted in the PEDOT layer. Similarly, only a slight shift is observed in the SLD of PVC from 0.484×10^{-6} Å^{-2} to 0.464×10^{-6} Å^{-2} on switching from the D_2O to H_2O electrolyte.

An unexpected outcome in these NR measurements was the roughness of the PVC and PEDOT:PSS films. Initially, each layer had a roughness of about 80 Å. The roughness in the PVC layer is probably attributable to the highly volatile THF casting solvent producing somewhat roughened films. It is also probable that the inherent roughness of the PVC film is exacerbated by the rough, globular nature of the PEDOT:PSS sub-layer. Nevertheless, the roughness of the PVC layer changed negligibly throughout the investigation, while the PEDOT:PSS layer changed from 78 Å to 98 Å. At first glance the significant roughness of the PEDOT:PSS layer is somewhat puzzling as unpublished AFM studies showed that the mean roughness of PEDOT:PSS deposited under identical conditions was about 25 Å. A possible explanation is a surface rich layer of PSS within the PEDOT:PSS layer (22) which is instead reflected as a surface roughness. This is an artefact of NR measurements and arises due to the lack of contrast between the PSS and PEDOT components which the modelling software interprets as a large roughness. Higgins et.al. (22) reported that the process of annealing accentuates the surface segregation of

PSS to a depth of as much as 10 nm. The slow increase in surface roughness with time can be attributed to the progressive ingression of water into the hydrophilic component (PSS layer). Equally possible is the scenario where the two polymers are slightly miscible, resulting in a broad interface between the two polymers. In this instance, the increasing surface roughness could result from thermally excited capillary waves (24) which are known to cause interfacial broadening between two slightly miscible polymers over time. In any case, the lack of a clearly defined, molecularly sharp interface between the PVC and PEDOT:PSS layers may aid in the prevention of water layer formation by eliminating sites at which water can condense and accumulate.

Table 5-2 *EIS equivalent circuit fitted parameters for the PEDOT / PVC solid-contact ISE.*

Bathing time (min)	R_s (Ω)	Q_B ($\mu\Omega^{-1}$ s^n)	n_1	R_B (kΩ)	Q_{IT} ($\mu\Omega^{-1}$ s^n)	n_2	R_{IT} (kΩ)
75	14.22	4.28	0.8	4.62	8.27	0.84	107
275	16.05	4.72	0.8	5.56	9.21	0.85	114
1300	18.71	4.80	0.8	10.00	9.82	0.85	138
1550	19.87	4.61	0.8	8.02	9.00	0.82	119
1800	20.33	4.28	0.8	8.53	9.30	0.80	120

Importantly, the NR results fit well to a two-layer model (i.e. PEDOT:PSS sublayer and PVC overlayer) rather than a complex three-layer system incorporating a water layer. This correlates well with EIS data which showed no evidence of a water layer for the time span of the NR measurements. The EIS data were modelled using ZSimpWin Version 2.00 software (25) with a previously reported equivalent circuit (16). As seen in ***Table 5-2***, the bulk membrane resistance, which corresponds to the small set of semi-circles in the Nyquist plots (***Figure 5-3 (a)*** and ***5-3 (b)***), very gradually increases from 4.6 kΩ to 10.0 kΩ over a period of 1300 minutes in a similar manner to that reported elsewhere (26-28). Importantly, the bulk membrane resistance is a convoluted value that also reflects the contact resistances at each of the buried interfaces that exist in the ISE system. The resistance of the membrane continues to

increase until the membrane has equilibrated with water. Any separation of water into a well defined film would act as a low resistance shunt at the PVC / PEDOT interface, and cause a dramatic reduction in the bulk membrane-contact resistance. In a conventional thick film PVC ISE without the use of an SC, it was shown (***Chapter 3***) that a water layer forms when the electrode is exposed to water for anywhere from 3 to 20 hours (18). With a molecularly thin layer like the present one, the accompanying decrease in bulk membrane resistance would occur rapidly as noted in previous studies (16, 18). The lack of a statistically significant decrease in R_B during approximately 20 hours (i.e. >10-20 %RSD which is the reproducibility of EIS) of exposure to D_2O solution infers that there is no water layer. Following this, the decrease in R_B from 10 to 8 kΩ at about 1500 minutes (switch from D_2O to H_2O) is due to H_2O providing higher mobility H^+ ions compared to the bulkier D^+ ions in D_2O. A comparison study by Orient (29) of the mobility of H^+ and D^+ ions in neon gas revealed that the mobility of D^+ ions were 72 ± 2 % of the mobility of H^+ ions. Although the current study is concerned with the mobility of H^+ and D^+ ions in a condensed polymer phase, it is expected that the same trend will exist.

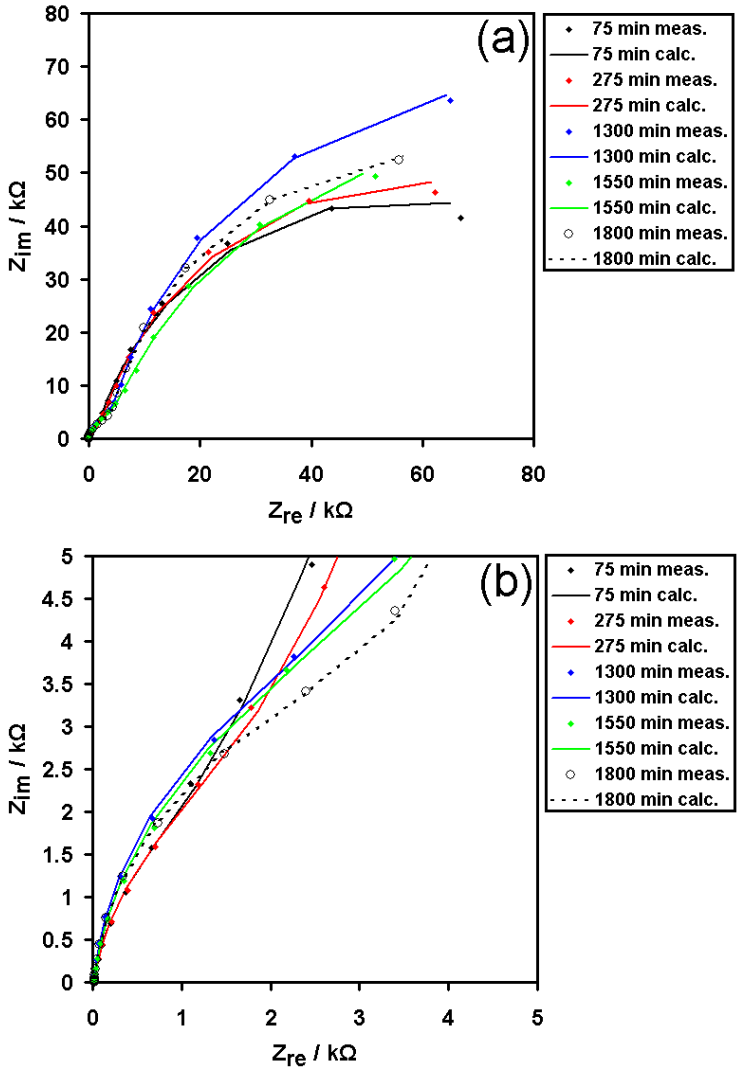

Figure 5-3 *EIS Nyquist plots for the thin film PEDOT / PVC SC ISE system. Dots denote the measured signal whilst the continuous lines show the equivalent circuit fitted outcomes. The last two measurements shown in the plots were measured in an H_2O electrolyte instead of the previous D_2O electrolyte. (a) EIS data over full frequency range. (b) Enlarged view of the high frequency bulk membrane resistance.*

Further credence for the lack of a water layer is provided by the Bode phase plots presented in ***Figure 5-4***. Importantly, the plots only show two distinct time constants which would comprise a further intermediate frequency time constant if there is an intermediate water layer. Furthermore, the NR data

does not show evidence for a dramatic change in the nature of the deposited film (see ***Figure 5-5*** for the combined SLD profile and physical model for the PEDOT solid-contact system).

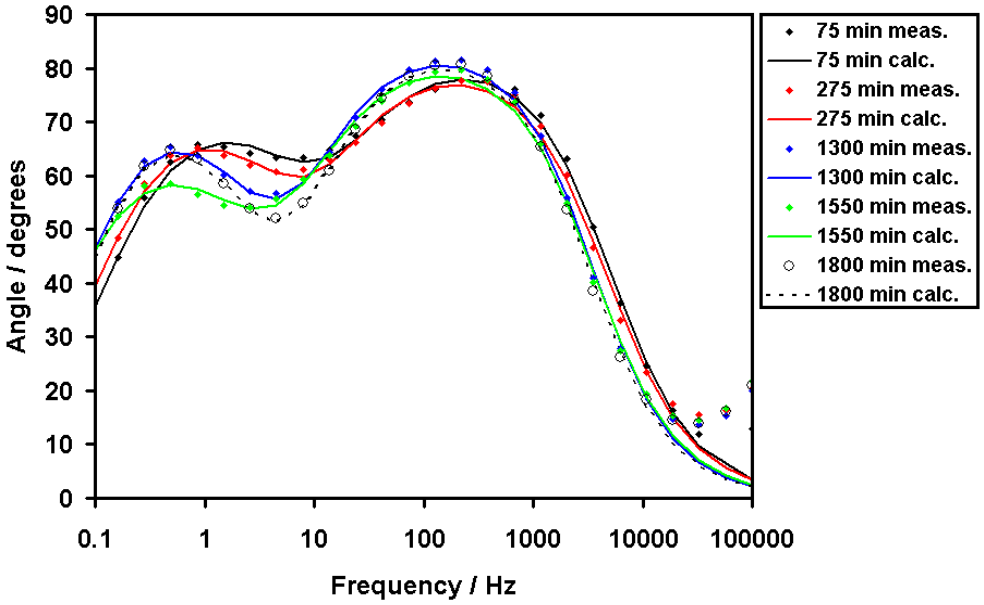

Figure 5-4 *Bode phase plots for all EIS measurements shown in* ***Figure 5-2****.*

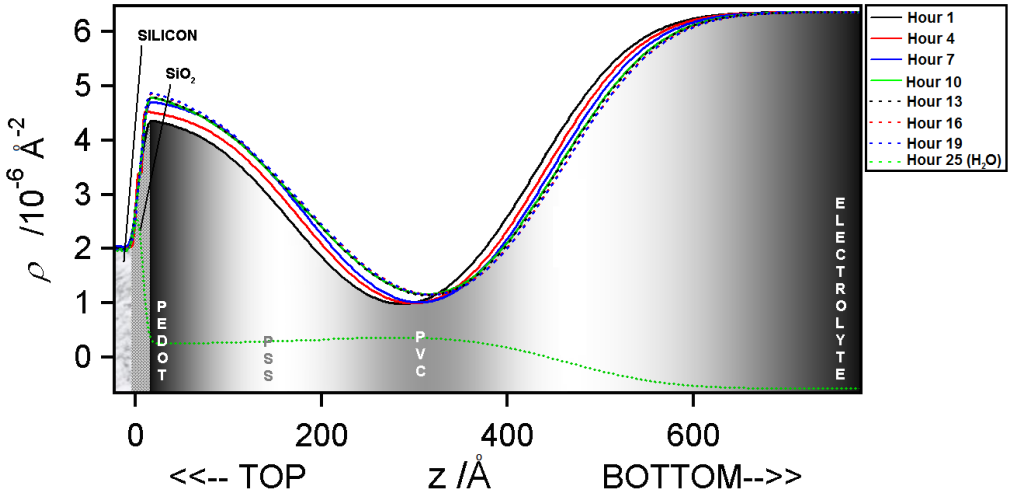

Figure 5-5 *Scattering length density profile of PEDOT / PVC solid-contact system. The illustrated portion of the profile presents the physical model for the system.*

SR-FT-IRM measurements carried out on gold (111) mirrors coated with a single layer of PVC further validates earlier work with the material (18) and unequivocally confirms that the transportation of water through the ion-selective PVC membrane does occur to a significant extent. ***Figure 5-6*** shows the IR spectrum for a region of interest on the unbathed and bathed PVC ISEs. It is evident that the bathed sample contains a sharp peak at 1645 cm^{-1} which is indicative of the OH bending mode of water. This peak is not evident in the unbathed sample. As water passes through the PVC matrix it is well established that inhomogeneities are formed and it is often the case that water accumulates in droplet form within the membrane (26). Evidence for this phenomenon was also shown in a previous publication by the authors (***Chapter 3***) (18). An SR / FT-IRM map, as presented in ***Figure 5-7***, shows a "hot spot" of water corresponding to a distinctive defect in the PVC membrane (i.e. either at the buried interface or within the membrane). Notably, the so-called dry or control sample shows some evidence of H_2O, probably due to molecular H_2O (shifted to higher wavenumbers) rather than condensed water. Presumably, this molecular H_2O originates from latent humidity.

Unfortunately, since water accumulates within the PVC membrane, as well as at the interface, this study cannot be extended to the system incorporating the PEDOT:PSS SC. This is because it would be impossible to discriminate between water formed within the PVC membrane and water which penetrates to the PEDOT:PSS interface.

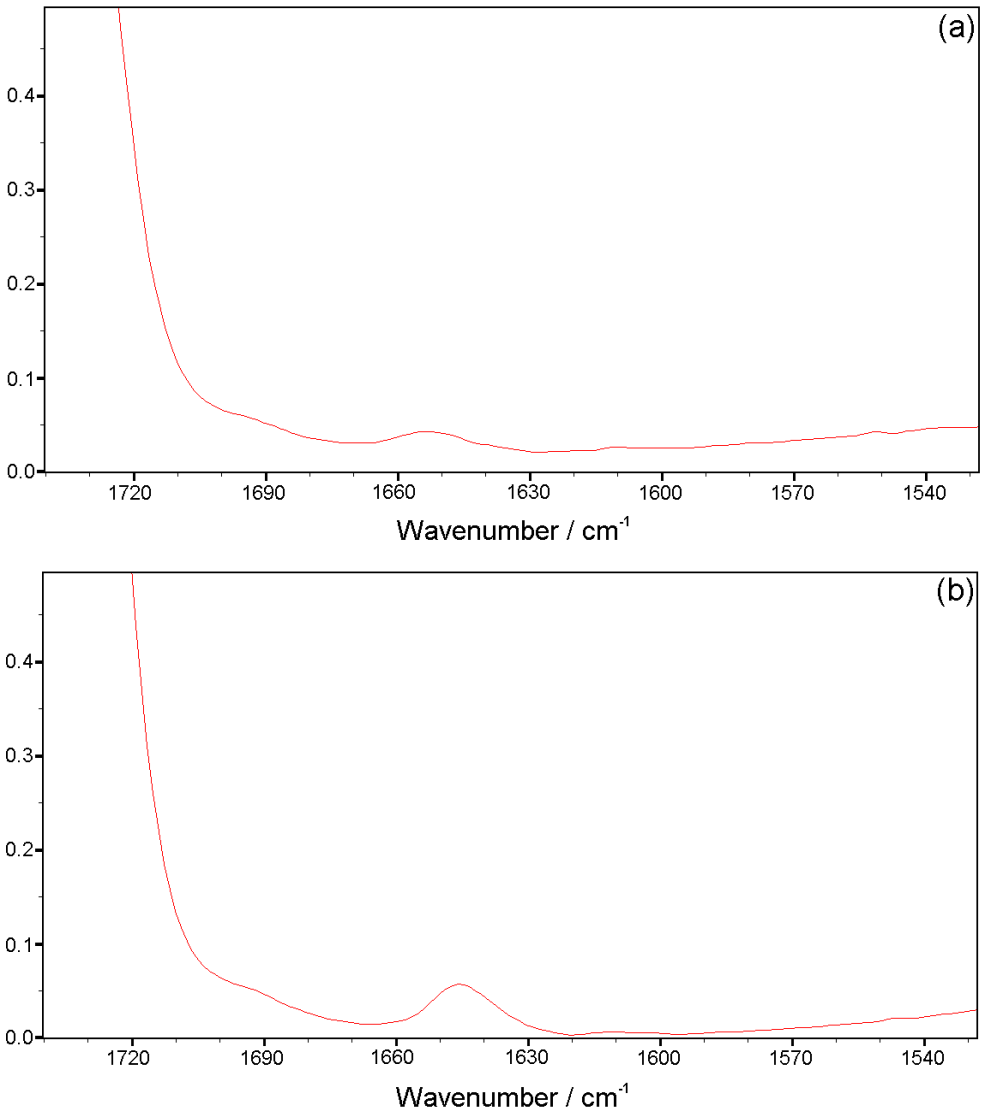

Figure 5-6 *SR/FT-IRM spectra of PVC ion-selective electrode in the region of 1740 – 1530 cm^{-1}. The upper spectrum relates to a dry PVC membrane and the lower spectrum is for a membrane bathed in an electrolyte solution for three days.*

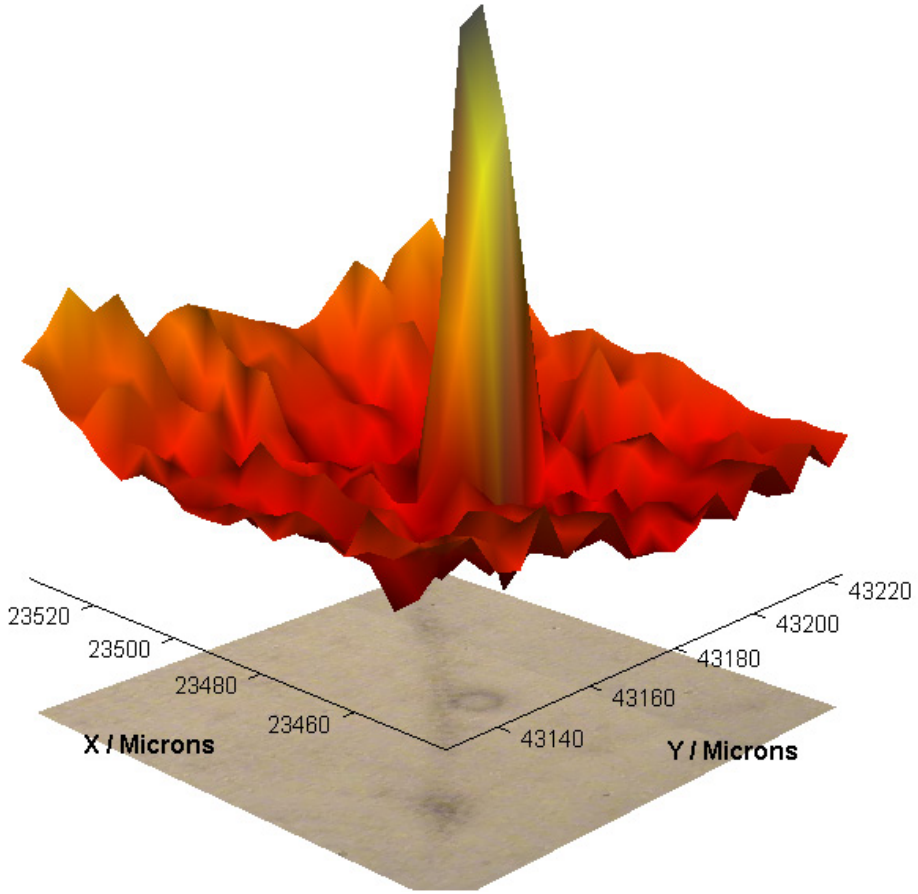

Figure 5-7 *Microscope image of a position of interest on the substrate of the PVC / Au ISE accompanied by the corresponding intensity map of the integrated OH bending peak at 1645 cm^{-1}.*

SIMS surface analysis provided an interesting outcome for the PEDOT:PSS system (see ***Table 5-3***). The data obtained by SIMS suggested that although it was known that water had been transported through the PVC membrane as noted in the NR and SR / FT-IRM results, there were no ion surpluses. Theoretically, as transported water and ions permeate through the membrane, it would be expected that a surplus of ions would be observed wherever there was an accumulation of water. Accordingly, ions were either not transported through to the conducting polymer, or are distributed evenly throughout the PEDOT:PSS “water-sponge” portion of the ISE. This scenario would result in low concentrations of ions that would avoid detection by SIMS.

Table 5-3 *SIMS spectral intensities for $^{133}Cs^{N}M^{+}$ species sputtered from the Au / PEDOT:PSS substrate (normalized against the $^{133}Cs^{+}$ signal for each sample) for PEDOT:PSS / PVC sensors subjected to various pre-treatments. Five replicates were performed in each case, and the relative standard deviations (% RSD) are provided in parentheses.*

Sample	$^{133}Cs^{23}Na^{+}$	$^{133}Cs^{35}Cl^{+}$	$^{133}Cs^{40}Ca^{2+}$
Au/PEDOT:PSS (control)	202,000 (59)	6,620 (27)	269,000 (54)
Au/PEDOT:PSS (0.1M $CaCl_2$)	----------	2,780 (25)	85,100 (8)
Au/PEDOT:PSS (0.1M NaCl)	108,000 (44)	3,450 (55)	----------

The results of this study are interesting for research into SC ISEs. Although the PEDOT:PSS SC does not form a well-defined water layer, it appears that there is a significant uptake of miscible water in the PEDOT:PSS SC, and this film will behave similar to a hydrogel. Obviously, when used for long-term applications, such a hydrogel PEDOT:PSS layer comprising water and co-transported ions, albeit at low concentrations, is expected to yield spurious transmembrane fluxes. These fluxes would inevitably yield a degradation in the lower limit of Nernstian response and the selectivity of the ISE (30).

Conclusion

This study presented the first direct experimental evidence that PEDOT:PSS is capable of preventing the formation of a detrimental water layer. The hydrophilic polymer effectively discourages the separation of miscible water from the polymer membrane through the “soaking” action of the polymer, akin to the behaviour of a sponge or hydrogel when exposed to water. Accordingly, this eliminates possible sites for water to accumulate at the PEDOT:PSS / PVC interface. These results were further confirmed using EIS, which displayed remarkable stability and gave no evidence for the formation of a water layer. This outcome will be invaluable in the exploration of new polymer solid-contacts

by allowing an enhanced understanding of the physical state of the polymer layers in SC ISEs upon exposure to solution.

References

1. Lindner E, Gyurcsanyi RE. Quality control criteria for solid-contact, solvent polymeric membrane ion-selective electrodes. J Solid State Electrochem. 2009;13(1):51-68.

2. Fibbioli M, Bandyopadhyay K, Liu S-G, Echegoyen L, Enger O, Diederich F, et al. Redox-Active Self-Assembled Monolayers for Solid-Contact Polymeric Membrane Ion-Selective Electrodes. Chem Mater. 2002;14:1721-9.

3. Grygolowicz-Pawlak E, Palys B, Biesiada K, Olszyna AR, Malinowska E. Covalent binding of sensor phases - a recipe for stable potentials of solid-state ion selective sensors. Anal Chim Acta. 2008;625:137-44.

4. Grygolowicz-Pawlak E, Plachecka K, Zbigniew B, Malinowska E. Further studies on the role of redox-active monolayer as intermediate phase of solid-state sensors. Sens Actuators B: Chem. 2007;123:480-7.

5. Grygolowicz-Pawlak E, Wygladacz K, Sek S, Bilewicz R, Brzozka Z, Malinowska E. Studies on ferrocene organothiol monolayer as an intermediate phase of potentiometric sensors with gold inner contact. Sens Actuators B. 2005;111-112:310-6.

6. Sek S, Bilewicz R, Grygolowicz-Pawlak E, Grudzien I, Brzozka Z, Malinowska E. Design of ferrocene organothiol monolayer as intermediate phase for miniaturized electrochemical sensors with gold contact. Polish J Chem. 2004;78(9):1655-65.

7. Lai C-Z, Fierke MA, Stein A, Buehlmann P. Ion-Selective Electrodes with Three-Dimensionally Ordered Macroporous Carbon as the Solid Contact. Anal Chem. 2007;79(12):4621-6.

8. Crespo GA, Macho S, Bobacka J, Rius FX. Transduction mechanism of carbon nanotubes in solid-contact ion-selective electrodes. Anal Chem. 2009;81:676-81.

9. Crespo GA, Macho S, Rius FX. Ion-selective electrodes using carbon nanotubes as ion-to-electron transducers. Anal Chem. 2008;80:1316-22.

10. Bobacka J. Conducting polymer-based solid-state ion-selective electrodes. Electroanal. 2006;18(1):7-18.

11. Vazquez M, Bobacka J, Ivaska A, Lewenstam A. Influence of oxygen and carbon dioxide on the electrochemical stability of poly(3,4-ethylenedioxythiophene) used as ion-to-electron transducer in all-solid-state ion-selective electrodes. Sens Actuators B. 2002;82:7-13.

12. Bobacka J. Potential Stability of All-Solid-State Ion-Selective Electrodes Using Conducting Polymers as Ion-to-Electron Transducers. Anal Chem. 1999;71(21):4932-7.

13. Bobacka J, Lewenstam A, Ivaska A. Electrochemical impedance spectroscopy of oxidised poly(3,4-ethylenedioxythiophene) film electrodes in aqueous solutions. J Electroanal Chem. 2000;489:17-27.

14. Gustafsson JC, Liedberg B, Inganas O. In situ spectroscopic investigations of electrochromism and ion transport in a poly(3,4-ethylenedioxythiophene) electrode in a solid state electrochemical cell. Solid State Ionics. 1994;69:145-52.

15. Michalska A, Maksymiuk K. All-plastic, disposable, low detection limit ion-selective electrodes. Anal Chim Acta. 2004;523:97-105.

16. Veder J-P, De Marco R, Clarke G, Chester R, Nelson A, Prince K, et al. Elimination of Undesirable Water Layers in Solid-Contact Polymeric Ion-Selective Electrodes. Anal Chem. 2008;80(17):6731-40.

17. Richardson RM, Dalgliesh RM, Brennan T, Lovell MR, Barnes AC. A neutron reflection study of the effect of water on the surface of float glass. J Non-Crystalline Solids. 2001;292:93-107.

18. De Marco R, Veder J-P, Clarke G, Nelson A, Prince K, Pretsch E, et al. Evidence of a water layer in solid-contact polymeric ion sensors. Phys Chem Chem Phys. 2008;10:73-6.

19. James M, Nelson A, Schulz JC, Jones MJ, Studer AJ, Hathaway P. A new neutron reflectometer at Australia's HIFAR research reactor. Nucl Instrum Methods Phys Res, Sect A. 2005;536(1-2):165-75.

20. Nelson A. Co-refinement of multiple contrast neutron / X-ray reflectivity data using MOTOFIT. J Appl Crystallogr. 2006;39(2):273-6.

21. Groenendaal L, Jonas F, Dieter F, Pielartzik H, Reynolds J. Poly(3,4-ethylenedioxythiophene) and Its Derivatives: Past, Present, and Future. Adv Mater. 2000;12(7):481-94.

22. Higgins AM, Martin SJ, Jukes PC, Goeoghegan M, Jones RAL, Langridge S, et al. Interfacial structure in semiconducting polymer devices. J Mater Chem. 2003;13:2814-8.

23. Jukes PC, Martin SJ, Higgins AM, Geoghegan M, Jones RAL, Langridge S, et al. Controlling the surface composition of poly(3,4-ethylene dioxythiophene)-poly(styrene sulfonate) blends by heat treatment. Adv Mater. 2004;16(9):807-11.

24. Sferrazza M, Heppenstall-Butler M, Cubitt R, Bucknall D, Webster J, Jones RAL. Interfacial Instability Driven by Dispersive Forces: The early stages of Spinodal Dewetting of a Thin Polymer Film on a Polymer Substrate. Phys Rev Lett. 1998;81:5173-6.

25. Yeum B. Equivalent Circuit, Users Manual. EChem Software. 2nd ed 2001.

26. Li Z, Li X, Petrovic S, Harrison DJ. Dual-Sorption Model of Water Uptake in Poly(vinyl chloride)-Based Ion-Selective Membranes: Experimental Water Concentration and Transport Parameters. Anal Chem. 1996;68(10):1717-25.

27. Ye Q, Borbely S, Horvai G. Microstructure of Ion-Selective Plasticized PVC Membranes Studied by Small-Angle Neutron Scattering. Anal Chem. 1999;71(19):4313-20.

28. Chan AD, Harrison DJ. NMR study of the state of water in ion-selective electrode membranes. Anal Chem. 1993;65(1):32-6.

29. Orient OJ. Mobilities of H^+ and D^+ ions in Neon Gas. Journal of Physics d: Applied Physics. 1974;7(16):2266-8.

30. Sundfors F, Bereczki R, Bobacka J, Toth K, Ivaska A, Gyurcsanyi R. Microcavity based solid-contact ion-selective microelectrodes. Electroanal. 2006;18(13-14):1372-8.

Chapter Six

6 An SR / FT-IRM Study of Undesirable Water Inclusions in Polymeric Solid-Contact Ion-Selective Electrodes

Jean-Pierre Veder, Kunal Patel, Graeme Clarke, Ewa Grygolowicz-Pawlak, Debbie S. Silvester, Roland De Marco, Ernö Pretsch and Eric Bakker

Analytical Chemistry **82**, 6203-6207 (2010).

Abstract – This paper reports on three-dimensional synchrotron radiation / Fourier transform-infrared microspectroscopy (SR / FT-IRM) imaging studies of water inclusions at the buried interface of solid-contact ion-selective electrode (SC-ISEs). It is our intention to describe a nondestructive method that may be used in surface studies of the buried interface of materials, especially multilayers of polymers. Herein, we demonstrate the power of SR / FT-IRM for studying water inclusions at the buried interfaces of SC-ISEs. A poly(methylmethacrylate) / poly(decylmethacrylate) (PMMA / PDMA) copolymer revealed the presence of micrometer sized inclusions of water at the gold / membrane interface, while a coupling of a hydrophobic solid-contact of poly(3-octylthiophene-2,5-diyl) (POT) prevented the accumulation of water at the buried interface. A similar study with poly(3,4-ethylenedioxythiophene) / poly(styrenesulfonate) (PEDOT / PSS) solid-contact also revealed an absence of distinct micrometer-sized pools of water; however, there were signs of absorption of water accompanied by swelling of the PEDOT / PSS underlayer, and these membrane zones are enriched with respect to water.

Introduction

Robust miniaturized ion-selective electrodes (ISEs) are of high significance in modern analytical and clinical chemistry (1-3). To achieve the required potential stability, miniaturized hydrogel-based liquid contacts are used between the sensing membrane and the inner electrode (1, 3). This complicated design requires complex manufacturing steps and long conditioning periods in order to rehydrate the inner layer. Consequently, ISEs without such a liquid layer [i.e., with an inner solid-contact (SC)] are highly desirable. Since their inferior potential stability can pose a problem with SC ISEs, a considerable amount of research has been undertaken to characterize the interfacial region of these devices (2, 4-6).

Detrimental to the stability of SC-ISEs is the formation of a water layer at the buried interface of the electrode substrate / ion-selective membrane (7-10). A water film often results in drifting ISE potentials by acting as a reservoir for electrochemically active or pH altering species such as H_2O, O_2 and CO_2 along with ionic species transported across the membrane (2, 7, 11). In a previous study, a combination of surface analysis tools was used in the elucidation (7) (***Chapter 3***) and elimination (4) (***Chapter 4***) of the detrimental water layer in SC-ISEs. These studies demonstrated that a system incorporating a poly(vinylchloride) (PVC) ion-sensing membrane in direct contact with an inert metal was susceptible to the formation of a continuous water layer (7). Likewise, a water-repellent poly(methylmethacrylate) / poly(decylmethacrylate) (PMMA / PDMA) copolymer ion-sensing membrane resulted in water “pooling” at the buried interface on the inert metal substrate, most likely in areas surrounding physical imperfections(4). Most significantly, the adoption of a PMMA / PDMA copolymer together with a hydrophobic poly(3-octylthiophene-2,5-diyl) (POT) solid-contact as the ion-to-electron-transducer provided an excellent strategy for eliminating the detrimental water layer (4, 12, 13).

Previous studies (4, 7) used surface analysis techniques such as neutron reflectometry (NR), scanning electron microscopy (SEM) and secondary ion mass spectrometry (SIMS) to identify localized zones of water at the PMMA / PDMA / metal interface; however, this evidence is inferred through the apparent interfacial roughening in the NR data, along with the fact that the SEM and SIMS studies were conducted on metal coupons after scraping the strongly adhered PMMA / PDMA film away from the electrode substrate, which in all likelihood destroyed the buried interface. Consequently, a direct and nondestructive surface analysis method that identifies water at the buried interface is required for the reliable characterization of this system.

This paper introduces synchrotron radiation / Fourier transform-infrared microspectroscopy (SR / FT-IRM) as a method for visualizing the existence of localized water at the buried interface of PMMA / PDMA SC ISEs. IRM is a microanalytical and imaging technique which achieves analytical contrast via the intramolecular vibrational modes (14). Highly focussed SR in the IR region of the electromagnetic spectrum is about 1000 times brighter than a conventional laboratory source and is capable of providing considerably enhanced signal-to-noise ratios (14), as well as an enhanced spatial resolution when considering micrometer-sized fluid inclusions (15). The study of inclusions via SR / FT-IRM is a well established technique that is often applied to studies of fluid inclusions in minerals, particularly as a means of identifying rock samples as potential oil sources (14, 15). Hence, previous research was performed with great success providing both structural information and unequivocal evidence for the existence of fluid inclusions (15) using this nondestructive method. On this basis, SR / FT-IRM has been chosen for this study since it is a powerful technique for the location of chemical and physical heterogeneities in materials, as well as determinations of their association with localized inclusions. Hence, this study should have important implications in the field of materials science. Since SR / FT-IRM has the potential to glean important insights into the water distribution of hydrogels and new gel-based materials, it will allow the location of

organic inclusions such as proteins in natural biomaterials as a means to understanding the physical and mechanical properties of these unique materials. Accordingly, it is anticipated that SR / FT-IRM will be an excellent method for identifying localized zones of water at the buried interface of SC ISEs, as well as any localized differences in the IR spectra accompanying the polymer and / or metallic substrate.

Experimental Details

Herein, a similar study to the previous ex situ SIMS experiment on PMMA / PDMA (4) entailing exposure to solution for an extended period of time (500 h) was performed on ISE membranes; with the exception that a much thinner membrane (10 μm) was used to enable faster water transportation, this polymer film was not peeled to reveal the buried interface, with reflectance SR / FT-IRM measurements undertaken on the unperturbed thin film immediately following exposure to solution. All measurements were performed after blotting the treated membranes on tissue to remove excess surface water, or dry the membranes. Importantly, the gold surfaces were prepared using standard methods for the fabrication of conventional SC ISEs. As compared to the previous ex situ SIMS study, SR / FT-IRM allows a study of the ISE buried interface without inducing physical damage in both the membrane as well as the interfacial region between the membrane and the electrode substrate.

Reagents

Calcium ionophore IV or N,Ndicyclohexyl-N',N'-dioctadecyl-3-oxapentanediamide, sodium tetrakis [3,5-bis(triflouro-methyl)phenyl]borate (NaTFPB) (Selectophore), and regioregular poly(3-octylthiophene-2,5-diyl) (POT) as well as high conductivity grade poly (3,4-ethylenedioxythiophene): poly(styrenesulfonate) (PEDOT:PSS) were obtained from Sigma-Aldrich, Australia. Analytical grade reagent chloroform was sourced from Selby, while

laboratory grade dichloromethane was from Chem. Supply. The washing solvents of acetone and ethanol were laboratory grade and were obtained from APS chemicals and CSR Distilleries, respectively. Analytical grade nitric acid used in electrode washings was sourced from the Ajax Chemical Co. Analytical grade $CaCl_2$ was from Merck. The monomers, methyl methacrylate, 99.5%, (MMA) and n-decyl methacrylate (DMA), 99%, were obtained from Polysciences, Inc. The polymerization initiator 2,2'-azobis(isobutyronitrile) (AIBN), 98%, was obtained from Sigma-Aldrich. Ethyl acetate and 1,4-dioxane used in the copolymer synthesis were reagent grade as sourced from Chem. Supply. Milli-Q water was used to prepare all aqueous solutions unless otherwise specified.

Gold Substrate Electrodes

Solid gold coupons (5 x 10 x 0.5 mm), obtained from Precious Metals Engineering Western Australia, were polished using alumina nanoparticles (0.1 μm in diameter) and copious quantities of water in conjunction with a rotating polishing pad. Polishing pads and alumina nanoparticles were all obtained from Metrohm^{TM}. After polishing, the electrodes were rinsed with vast quantities of Milli-Q water and bathed for 5 minutes at a time, under sonication, in acetone, nitric acid (10^{-4}M), Milli-Q water, and finally dichloromethane. The electrodes were thoroughly rinsed with Milli-Q water and completely air-dried after each cleaning step. A hydrogen flame was used to anneal the gold surfaces, which were subsequently cooled in Milli-Q water.

Ion-Selective Electrode (ISE) Membrane and Solid-Contact Preparation and Deposition

Synthesis of the PMMA / PDMA copolymer was carried out using the method of Qin et al (16). A calcium-selective copolymer cocktail was prepared by dissolving the PMMA / PDMA copolymer (97.7 wt%), calcium ionophore IV (1.7 wt%) and NaTFPB (0.6 wt%) together in dichloromethane (1% w/v). The

casting solution for POT was prepared by dissolving the polymer in chloroform (0.005 % w/v). The commercially available PEDOT:PSS polymer was obtained as an aqueous suspension and used as supplied.

Electrodes coated with a sole layer of PMMA / PDMA copolymer were prepared by casting the copolymer cocktail onto a gold substrate using a cocktail volume of 63 µL [this lower volume gave a thinner film (10 µm) that enabled mass transportation of water to the buried interface in the time frame of these experiments]. Following membrane deposition, the ISEs were annealed overnight at 80^{o}C in a nitrogen saturated environment. All electrodes utilizing conductive polymer underlayers in combination with the copolymer membrane were treated in the same manner, however, under varied casting and annealing conditions, as described below. For the system utilizing POT as a solid-contact, the electrode was coated 6 times with the POT solution using a total volume of 6.3 µL. The electrodes were subsequently annealed in an inert environment at 80^{o}C overnight. The PEDOT:PSS solid-contact system required spin coating of the aqueous PEDOT:PSS suspension at 3000 rpm for 2 minutes followed by annealing for 2 hours at 200^{o}C under an inert atmosphere prior to membrane deposition.

Synchrotron Radiation / Fourier Transform-Infrared Microspectroscopy (SR / FT-IRM)

ISEs were bathed in a 0.1 M calcium chloride solution for approximately 3 days. Following bathing, the ISEs were briefly rinsed in a jet of ultrahigh purity water and quickly blown dry with nitrogen to remove any excess surface water. Measurements were made immediately after the samples had been removed from the electrolyte to ensure that all measurements were made prior to the membranes drying out. The results obtained from those bathed in solution were also compared to identical samples that had not been exposed to solution.

All SR / FT-IRM measurements were carried out at the IR beamline (2BM1) of the Australian synchrotron, Melbourne, Australia. The spectra were recorded with a Bruker Vertex V80 vacuum FT-IR spectrometer and Bruker Hyperion 2000 IR microscope (Bruker Optik GmbH, Ettlingen, Germany) in conjunction with a mercury cadmium telluride (MCT) detector cooled with liquid nitrogen and IR radiation emitted from a bending magnet of the synchrotron storage ring. The microscope and spectrometer were controlled through the Bruker Opus software, version 6.5. The general range of measurements was from 3800 to 700 cm^{-1} at a spectral resolution of 8 cm^{-1}. The spectra were measured with a beam aperture of 10 × 10 µm in place. Spectral collections were made in reflection mode with 16 scan data averaging statistics. The measurements were all made in the mapping mode, which consisted of running individual measurements in a pre-specified grid size (9 x 9 scan positions) in a region of interest on the sample (***Supplementary Figure 6-1***). Certain bands of interest in the IR spectra were later chosen for integration, and an intensity map was generated showing the intensity of the integrated band correlated back to its position in the measured grid.

Results and Discussion

The IRM instrument at the Australian Synchrotron is a conventional and commercially available instrument that may be utilized in either reflectance or transmission mode. Either way, IRM spectra are representative of bulk chemical compositions of small irradiated volumes of the sample during high resolution chemical mapping, noting that the reflected beam experiences a double pass through the polymer film (once for the incoming and once for the outgoing beams), while the transmission mode involves a single pass through the bulk material. In the present study, IRM is performed in the reflectance mode since the polished gold substrates are highly reflective and nontransparent to infrared radiation. The primary advantage of using SR from the bending magnet beamline at the Australian Synchrotron is that the highly collimated and

polarized beam provides a superior spatial resolution of several micrometers and a 100-fold enhancement in beam intensity, as compared to a conventional laboratory globar light source. These important features of SR enable high resolution and high quality infrared microspectroscopy imaging of materials.

Most significantly, since the PMMA / PDMA copolymer is known to be water repellent and unsuitable for water sorption at measurable levels in the bulk membrane (4), the detection (or nondetection) of water by reflectance SR / FT-IRM is symbolic of the presence (or absence) of localized zones of water at the buried interface of a solid-contact ISE employing PMMA / PDMA as the sensing membrane.

Figure 6-1 presents the optical micrograph of an area of interest taken from a Ca^{2+}-selective copolymer membrane coated onto a gold coupon (5 x 10 x 0.5 mm) after exposure to solution, along with the corresponding 3-D intensity map of the integrated OH bending mode of water [δ(OH) $\approx$ 1645 cm^{-1}]. The data reveals a region on the sample, corresponding to the blurred region in the microscopic image of the membrane, where there is a significant increase in the intensity of the integrated δ(OH) peak. This region is indicative of a high amount of interfacial water, which is due to localized or droplet-like inclusions of water at the buried interface. When compared to all measured sites on a dry sample, the integrated peak intensity in the bathed sample at 1645 cm^{-1}, corresponding to the OH bending mode of water, was absent from the IR spectrum of any of the regions on the dry sample.

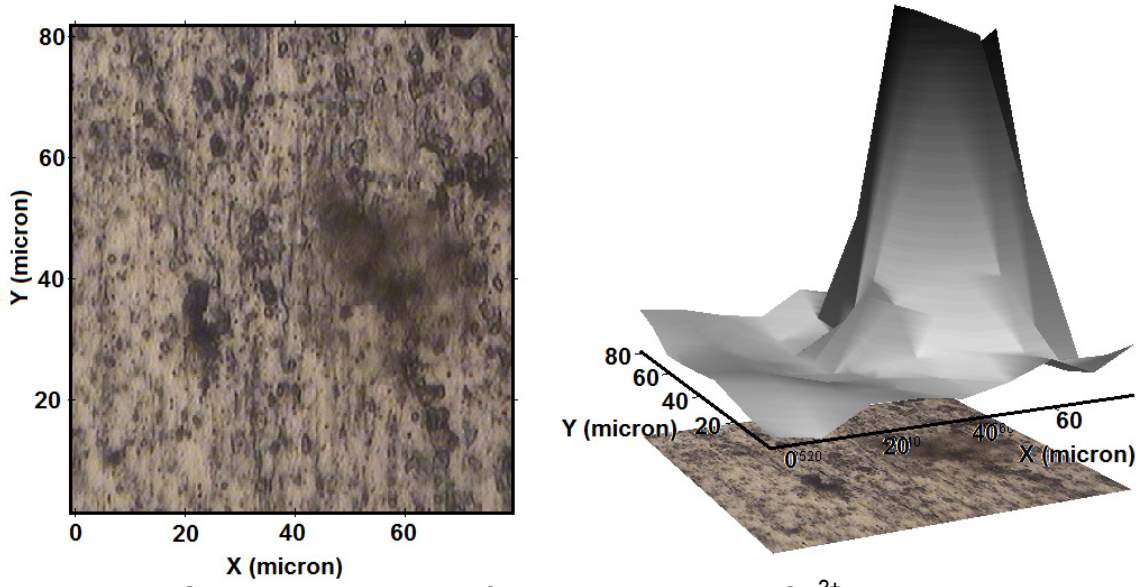

Figure 6-1 *Optical micrograph of a PMMA / PDMA Ca^{2+}-selective membrane coated onto gold and exposed to solution (left), as well as the corresponding three-dimensional intensity map of the integrated OH bending mode of water (right).*

Interestingly, the image of the ISE shown in ***Figure 6-1*** reveals a degree of surface roughness that is only evident on a microscopic level. Apparently, the corresponding 3-D map shows that the water is accumulating in a region on the sample which is ascribable to physical (e.g., microscopic surface roughness, poor adhesion, etc.) and / or chemical imperfections (e.g. ionic impurities) at the substrate / membrane interface. Either scenario would generate sites at which water could accumulate.

Further credence for the above-mentioned interpretation is the previous and complementary small angle neutron scattering (SANS) (4) study of water sorption in the PMMA / PDMA copolymer membrane, which showed negligible levels of neutron scattering from nanosized scatterers in the membrane such as water nanodroplets; highlighting that water was not taken up by the bulk membrane, so the water inclusions must be formed at the buried interface.

The present study on PMMA / PDMA has been extended to a system also incorporating a POT solid-contact. A comparable SR / FT-IRM study of a system incorporating POT as a conductive polymer SC (image and map not shown) showed an absence of water in the numerous randomly sampled regions of over 100 spot analyses. This result is not unexpected since the hydrophobic POT film inhibits the accumulation of water at the buried interface by providing an effective barrier of a hydrophobic substrate over the metal electrode surface that prevents water deposition at chemical and / or physical imperfections. Significantly, this result validates previous surface studies (4) showing that a POT / PMMA / PDMA copolymer ISE eliminates water pools at the buried interface of the ISE.

In this study, the authors have used the sharp water δ(OH) band at 1645 cm^{-1} over the broad and more intense water ν(OH) band at 3500 cm^{-1} since the presence of broad reflectance interference fringes in the background spectra of the dry and wet samples made it very difficult to decipher the membrane signal from the background while examining the broad ν(OH) band. Furthermore, the IRM maps of the δ(OH) data for the dry samples or treated sample that is free of water inclusions (e.g., POT / PMMA / PDMA) (not shown) revealed featureless maps, actually comprising noise spikes on the low background signals. Accordingly, we have demonstrated a relative absence of water in dry samples, as well as the treated POT / PMMA / PDMA sample, by showing representative overlay spectra fro the δ(OH) band in ***Supplementary Figure 6-2*** to ***6-4*** in the Supplementary Information section.

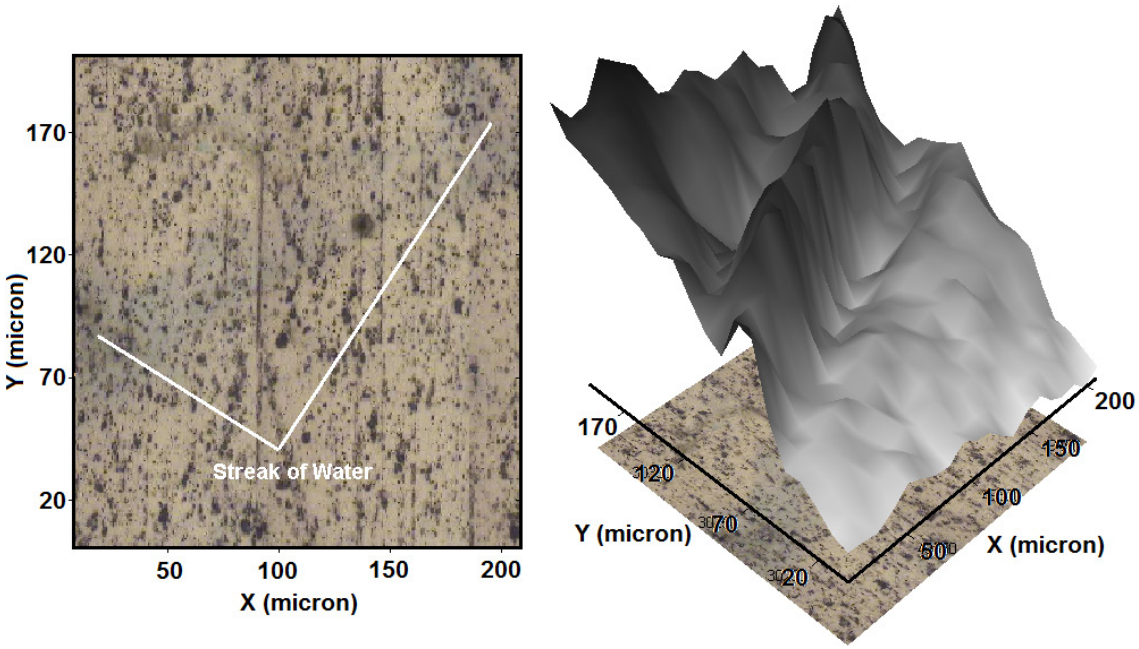

Figure 6-2 *Optical micrograph of a region of interest for a solid-contact ISE system comprising PMMA / PDMA calcium selective membrane coated on a PEDOT:PSS conductive polymer layer on a gold substrate after exposure to solution (left), as well as three-dimensional intensity map of the integrated OH bending mode of water (right).*

Since a combination of a hydrophobic ion-selective membrane (e.g., PMMA / PDMA copolymer) with a hydrophobic solid contact (e.g., POT) displayed an ability to eliminate water inclusions, we decided to carry out a comparable study of the hydrophobic ion-selective copolymer membrane in conjunction with the relatively hydrophilic SC of PEDOT:PSS, so as to gauge if this system may also be used in the production of SC ISEs that are devoid of deleterious water layers. ***Figure 6-2*** presents an optical micrograph of an interesting region on a PEDOT:PSS / copolymer ISE after exposure to solution, along with the corresponding 3-D intensity map of the integrated OH bending mode of water (1645 cm^{-1}). Notably, a distinct trail of water (marked) is visible in the 3D intensity map, which is evident as a grey and hazy streak in the optical micrograph. Indeed, this outcome suggests a swelling and roughening of the PEDOT:PSS / copolymer interface, especially when a hydrophobic membrane is

coupled with the hydrophilic SC. In this context, water transported through the membrane probably exists in a miscible form within the PEDOT:PSS and does not separate into droplets, with the dark streak in the optical micrograph corresponding to areas where water has been transported to the ion-selective membrane / PEDOT:PSS interface and is absorbed relatively evenly into the hydrophilic PEDOT:PSS layer in much the same way as water is absorbed into a sponge. Accordingly, it is likely that PEDOT will behave analogously to a hydrogel and will provide a transient transmembrane flux of ions, and a concomitant degradation in the sensitivity and selectivity of the PEDOT SC-ISE. Significantly, such a thick hydrogel is unable to display a sensitivity in water layer testing, but will still display degraded potentiometric response characteristics, noting that both of these outcomes were observed elsewhere by Sundfors et al. (17).

Conclusion

The results of this study demonstrate the power, as well as simplicity, of SR / FT-IRM as a research tool for studying the buried interface of multilayered materials. The use of high-resolution 3-dimensional mapping enables a visual depiction of the location and nature of fluid inclusions at interfaces, in this case, demonstrated by a study of water in polymeric ISEs.

Specifically, this work has confirmed unequivocally that PMMA / PDMA copolymer is susceptible to the pooling of water droplets at the buried interface of the electrode. Additionally, the use of a hydrophobic conducting polymer SC such as POT inhibits the deposition of water by removing possible sites for water accumulation. Different results are evident when a hydrophilic conducting polymer SC such as PEDOT:PSS is used in conjunction with a hydrophobic PMMA / PDMA copolymer membrane. Evidently, the PEDOT:PSS SC leads to the formation of water in a miscible state within the PEDOT:PSS underlayer, akin to a hydrogel, instead of a separate and thin water layer.

Most significantly, SR / FT-IRM is suitable for studies of other polymeric ISEs such as silicone rubbers, polyurethanes, polyvinyl chlorides, etc. on alternate electrode substrates such as nanostructured carbons, doped silicon, platinum, etc. and may be used in the elucidation of novel mechanistic information about these important electrochemical sensors.

The aforementioned outcomes present valuable insights into the physical behavior of technologically important materials such as ISE membranes exposed to fluid media for prolonged periods. Parallels between the physicochemical information obtained via SR / FT-IRM and the chemical behavior of the functional material can undoubtedly be drawn to achieve an enhanced understanding of the materials systems under consideration.

References

1. Bakker E, Diamond D, Lewenstam A, Pretsch E. Ion sensors: current limits and new trends. Anal Chim Acta. 1999;393(1-3):11-8.

2. Lindner E, Gyurcsanyi RE. Quality control criteria for solid-contact, solvent polymeric membrane ion-selective electrodes. J Solid State Electrochem. 2009;13(1):51-68.

3. D'Orazio P. Biosensors in clinical chemistry. Clin Chim Acta. 2003;334(1-2):41-69.

4. Veder J-P, De Marco R, Clarke G, Chester R, Nelson A, Prince K, et al. Elimination of Undesirable Water Layers in Solid-Contact Polymeric Ion-Selective Electrodes. Anal Chem. 2008;80(17):6731-40.

5. Al-Shatti LA, Marafie HM, Shoukry AF. Surface analysis of new chlorpromazinium plastic membrane electrodes. J Pharm Biomed Anal. 2008;46(2):328-34.

6. Sundfors F, Bobacka J. EIS study of the redox reaction of Fe(CN)63-/4- at poly(3,4-ethylenedioxythiophene) electrodes: influence of dc potential and cOx:cRed ratio. J Electroanal Chem. 2004;572(2):309-16.

7. De Marco R, Veder J-P, Clarke G, Nelson A, Prince K, Pretsch E, et al. Evidence of a water layer in solid-contact polymeric ion sensors. Phys Chem Chem Phys. 2008;10:73-6.

8. Fibbioli M, Morf WE, Badertscher M, De Rooij NF, Pretsch E. Potential drifts of solid-contacted ion-selective electrodes due to zero-current ion fluxes through the sensor membrane. Electroanal. 2000;12(16):1286-92.

9. Grygolowicz-Pawlak E, Plachecka K, Zbigniew B, Malinowska E. Further studies on the role of redox-active monolayer as intermediate phase of solid-state sensors. Sens Actuators B: Chem. 2007;123:480-7.

10. Cha GS, Liu DP, Meyerhoff ME, Cantor HC, Midgley AR, Goldberg HD, et al. Electrochemical Performance, Biocompatibility, and Adhesion of New Polymer Matrices for Solid-State Ion Sensors. Anal Chem. 1991;63:1666-72.

11. Bobacka J. Conducting polymer-based solid-state ion-selective electrodes. Electroanal. 2006;18(1):7-18.

12. Sutter J, Lindner E, Gyurcsanyi RE, Pretsch E. A polypyrrole-based solid-contact Pb^{2+}-selective PVC-membrane electrode with a nonomolar detection limit. Anal Bioanal Chem. 2004;380(1):7-14.

13. Sutter J, Radu A, Peper S, Bakker E, Pretsch E. Solid-contact polymeric membrane electrodes with detection limits in the subnanomolar range. Anal Chim Acta. 2004;523:53-9.

14. Sham T-K, editor. Chemical Applications of Synchrotron Radiation. Singapore: World Scientific Publishing Co. Ltd,; 2002.

15. Guilhaumou N, Dumas P, Carr GL, Williams GP. Synchrotron Infrared Microspectrometry Applied to Petrography in Micrometer-Scale Range: Fluid Chemical Analysis and Mapping. Appl Spect. 1998;52:1029-34.

16. Qin Y, Peper S, Bakker E. Plasticiser-Free Polymer Membrane Ion-Selective Electrodes Containing a Methacrylic Copolymer Matrix. Electroanal. 2002;14(19-20):1375-81.

17. Sundfors F, Bereczki R, Bobacka J, Toth K, Ivaska A, Gyurcsanyi R. Microcavity based solid-contact ion-selective microelectrodes. Electroanal. 2006;18(13-14):1372-8.

Supplementary Information

SR / FT-IRM Mapping of Surfaces

During SR / FT-IRM mapping of the surface, individual spectra were recorded in a pre-specified grid (9 x 9 scan positions) around a region of interest on the sample, as shown in Figure S1.

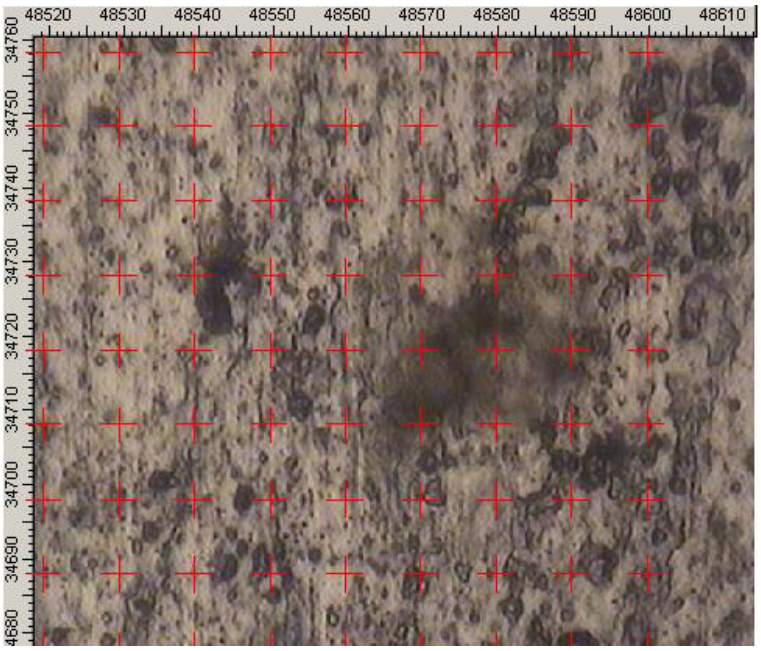

Supplementary Figure 6-1 *Image showing a region of interest for the copolymer / Au ISE accompanied by crosshairs representing the corresponding locations at which measurements were made and subsequently mapped.*

Comparative Spectra of Dry and Wet Samples at δ(OH) Peak

Figures S2-S4 present spectra of the δ(OH) peak of interest at 1645 cm^{-1} for PMMA / PDMA on gold, PMMA / PDMA /PEDOT:PSS on gold and PMMA / PDMA / POT on gold, respectively, noting that the broken line represents the dry or control spectrum and the continuous line depicts the wet or treated specimen. All spectra were converted to absorbance and subsequently "mapped" using an integration of the δ(OH) peak using the OPUS 6.5 software.

Background signals were subtracted from all spectra by comparison against a clean gold control coupon.

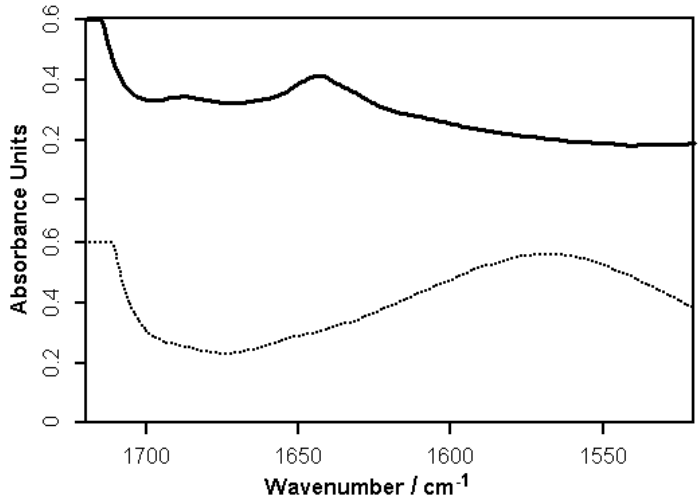

Supplementary Figure 6-2 *Spectra for the δ(OH) band for dry or control PMMA / PDMA sample (broken line) and the wet PMMA / PDMA sample showing a water pool (continuous line).*

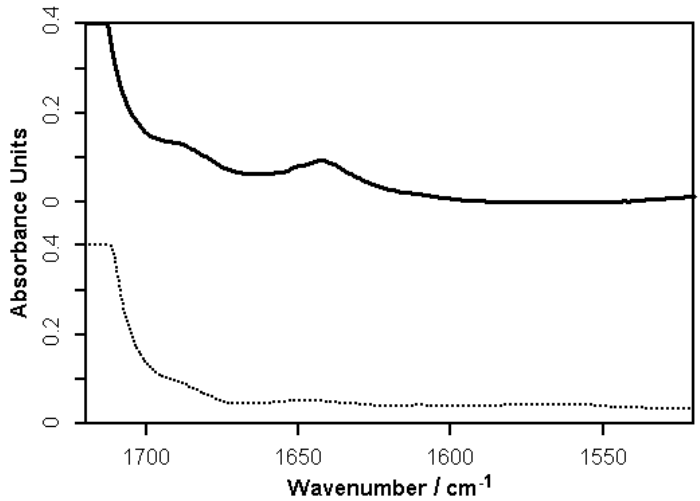

Supplementary Figure 6-3 *Spectra for the δ(OH) band for dry or control PMMA / PDMA / PEDOT:PSS sample (broken line) and the wet PMMA / PDMA / PEDOT:PSS sample showing the water streak (continuous line).*

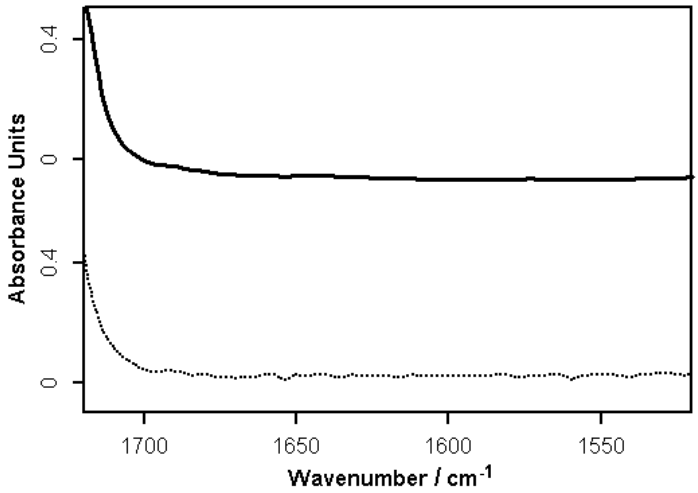

Supplementary Figure 6-4 *Spectra for the δ(OH) band for dry or control PMMA / PDMA / POT sample (broken line) and the wet PMMA / PDMA / POT sample (continuous line).*

Chapter Seven

7 Studying the Depth of Ion-to-Electron Transduction in Solid-Contact Ion-Selective Electrodes

Jean-Pierre Veder, Roland De Marco, Kunal Patel, Pengchao Si, Ewa Grygolowicz-Pawlak, Ernö Pretsch, and Eric Bakker.

In Preparation, (2010).

Abstract – Synchrotron radiation X-ray photoelectron spectroscopy (SR / XPS) and neutron reflectometry (NR) were carried out on doped poly(3-octylthiophene-2,5-diyl) (POT) solid-contacts (SCs) to study ion-to-electron transduction in solid-state ion-selective electrodes (ISEs). The study was performed with the intention of determining the minimum thickness of POT required in order to function optimally as a SC. Using [3,5-bis(triflouromethyl)phenyl]borate ($TFPB^-$) as the electroactive polymer dopant, SR / XPS and NR were only able to detect $TFPB^-$ in the upper 14 Å of SC material. This result demonstrates that charge-transfer events, which might be expected to prevail throughout the entire underlying SC layer, are surface confined processes.

Introduction

Shortly after the emergence of coated-wire electrodes (1) (CWEs) in the early 1970s, it became apparent that, although providing a significant advance

for the prospect of miniaturization, these electrodes lacked long-term potential stability (2, 3). This was later attributed to poorly defined charge-transfer processes at the blocked interface between the ion-selective membrane and the electrically conductive substrate (4). Furthermore, the gradual formation of water layers at the buried interface (5, 6) also interfered with the intended sensor response which was detrimental to the technological advancement of these sensors. The implementation of solid-contact (SC) intermediate layers to provide an electrochemically well-defined buried interface (7) was a major advancement in the field of solid-contact sensors (8, 9). Ever since the discovery of SC sensors, they have generally comprised thick (i.e. several microns) electroactive polymers that exhibit both electronic and ionic conductivity so as to provide a well-defined ion-to-electron transduction mechanism at the interface buried between the SC and ion-sensing membrane. However, research into SCs over recent years has led to the introduction of new materials, which seemingly challenge previous notions of how SCs function to improve the potential stability. Notably, redox-active self assembled monolayers (7, 10-14) (SAMs) have shown success in their application as SCs, as well as high surface area carbonaceous materials (15-17). A disconnect now exists as to what characteristics are required for a material to function effectively as an SC. Our goal is to therefore aid in addressing questions that currently present a dilemma for the sensor community such as: "*Is there really a requirement for the SC material to exceed a certain thickness given the success observed with SAMs?"* and also *"How can some materials work well as SCs (i.e. carbon nanotubes and macroporous carbon) despite the lack of an obvious ion-to-electron transduction mechanism?"*

This study focused on electroactive polymers, particularly poly(3-octylthiophene-2,5-diyl) (POT), so as to scrutinise the ion-to-electron transduction processes of these materials. Significantly, since POT is a proven SC, as evidenced by previous work (8) (***Chapter 4***), obviating the formation of detrimental water layers at the buried interface due to its hydrophobicity, it was chosen for this fundamental study of ion-to-electron transduction without fear of

any side reactions from a spontaneous water layer. Furthermore, it has been reported that systems incorporating POT as an SC have yielded nanomolar detection limits (18), as well as providing highly stable ion-to-electron transduction processes (19). In consideration of the aforementioned factors, POT is an ideal material for a study of charge-transfer processes occurring between the ion-selective membrane and the underlying SC.

The mechanism for ion-to-electron transduction is understood to occur via a three phase process as summarised by Si et al. (20). In this work, the conducting polymer is oxidized from POT to POT^+. This process triggers the redistribution of the [3,5-bis(triflouromethyl)phenyl]borate ($TFPB^-$) anionic species of the lipophilic ion-exchanger from the outer membrane phase to the conducting polymer layer. Accordingly, it follows that the presence of $TFPB^-$ throughout the POT SC is indicative of charge-transfer processes that occur in the SC ISE. This study utilized synchrotron radiation X-ray photoelectron spectroscopy (SR / XPS) and neutron reflectometry (NR) to track the electrochemically driven ingression of $TFPB^-$ into the POT SC. XPS and NR (refer to ***Appendix I*** for detailed descriptions) are extremely useful surface analysis tools that can easily scrutinize the chemical and physical properties of the POT SC with excellent spatial and chemical resolution.

Experimental

Materials

High molecular weight poly(vinylchloride) (PVC), N,N-dicyclohexyl-N′,N′-dioctadecyl-3-oxapentanediamide (calcium ionophore IV), potassium and sodium tetrakis (KTFPB and NaTFPB), tridodecylmethylammonium chloride (TDMACl, 97%) and bis(2-ethylhexyl)-sebacate (DOS) were Selectophore® Fluka reagents obtained from Sigma-Aldrich (Castle Hill, New South Wales, Australia). Anhydrous lithium perchlorate (99.99%), 3-octylthiophene-2,5-diyl,

regioregular POT (99.99%), anhydrous acetonitrile (99.8%), anhydrous N,N-dimethyl-formamide (DMF, 99.8%) and inhibitor free tetrahydrofuran (THF, 99.8%) were also obtained from Sigma-Aldrich (Castle Hill, New South Wales, Australia). Analytical grade sulfuric acid and hydrogen peroxide used for piranha etching solutions were obtained from the Ajax Chemical Co. (Taren Point, New South Wales, Australia). Laboratory grade xylene was obtained from Chem-Supply (Gillman, Port Adelaide, South Australia). The highly polished silicon wafers (8 cm x 4 cm x 2 cm) used in NR measurements (boron doped for electrical conductivity) were purchased from Crystran Ltd. (Dorset, United Kingdom). Gold (111) mirrors used in the SR / XPS studies were obtained from Arrandee^{TM} (Werther, Germany) and rinsed with copious quantities of Milli-Q water and acetonitrile prior to use. Milli-Q water was used to prepare all aqueous solutions unless otherwise specified.

Synchrotron Radiation X-ray Photoelectron Spectroscopy

POT was electropolymerized onto 12 mm x 12 mm Au(111) mirror substrates and subsequently oxidized using a specially designed Teflon three-electrode cell described elsewhere (21). In the cell's operating configuration, the Au(111) mirror functioned as a working electrode, a solid-state Ag/AgCl wire was used as a reference electrode and a Pt wire coil acted as a counter electrode. A Princeton Applied Research Parstat 2263 portable potentiostat was used to carry out all electrochemical polarization and oxidation experiments on the Au(111) working electrodes. The cell contained a solution that was 0.1 M 3-octylthiophene and 0.1 M $LiClO_4$ in acetonitrile, which was purged with nitrogen for 15 minutes prior to electropolymerization. POT was subsequently electropolymerized via cyclic voltammetry (30 scans at a rate of 100 mV s^{-1}) in a potential window of 0 – 1.5 V. Following electropolymerization, the POT film was discharged at 0 V for 300 seconds and immersed in pure acetonitrile for 30 minutes to remove residual electrolyte. The POT SCs were allowed to dry in air for 30 minutes.

A plasticized PVC membrane was deposited onto the electrode following the electropolymerization of POT. The PVC membrane was drop cast (60 µL) from a solution containing PVC (32.3 wt%), DOS (64.7 wt%), KTFPB (2.4 wt%) and TDMACl (0.6 wt%) in THF (5% w/v) and allowed to dry for several hours in air. Chronoamperometry was carried out on the resultant ISE in a solution of 0.1 M NaCl in order to oxidize the POT SC. The electrode was held at a potential of 1.3 V for 20 minutes to allow adequate time for $TFPB^-$ to enter the POT SC layer.

After oxidation of the SC, the PVC membrane was peeled from the SC and the electrode was subsequently immersed several times in THF to remove all traces of PVC, thereby exposing the insoluble POT SC underlayer. SR / XPS analysis was carried out by probing the F(1s), C(1s), S(2p) and Au(4f) core orbital energy levels. These analyses were made using a photon energy of 800 eV with a pass energy of 10 eV so as to maximise the weak F(1s) signal originating from the transfer of the $TFPB^-$ anion across the buried interface. All spectral binding energies were calibrated against the C(1s) peak.

Subsequent to each XPS analysis, the electrode was removed from the XPS analysis chamber and transferred to the sample preparation chamber where the exposed POT SC was gradually eroded using an argon ion sputtering gun with 3 kV beam energy focused to 2.4 kV (i.e. 80 % of beam energy). After each increment of argon ion sputtering, the sample was transferred back into the analysis chamber for further SR / XPS measurements. This procedure was repeated several times until there was no evidence of $TFPB^-$ within the POT SC. The sputter rate was determined by calibrating the ion sputtering gun against a POT SC of known thickness as determined by atomic force microscopy (not shown). In this instance, the process of XPS analysis and sputtering were performed simultaneously until a sufficient Au(4f) intensity was measured (originating from the Au(111) substrate), signalling the complete erosion of the

SC layer. Near edge X-ray absorption fine structure (NEXAFS) studies were also carried out on the POT SC upon completion of each SR / XPS analysis.

SR / XPS measurements were carried out at the Soft X-ray Spectroscopy beamline (14ID) of the Australian Synchrotron, Melbourne, Australia. The insertion device for the beamline is an elliptically polarised undulator providing a flux of between 3 x 10^{12} and 5 x 10^{11} photons / s / 200 mA at the sample at 400 eV. The beamline's optimal energy range is 90 – 2000 eV with a resolution ($\Delta E/E$) between 5000 and 10,000 and provides a beam size of 0.6 x 0.6 mm normal to the beam. The data acquisition software used in this study was SPECSlab2. The endstation was constructed by OmniVac and PreVac using a SPECS Phobios 150 hemispherical electron energy analyser in conjunction with photodiode and drain current detectors. An OmniVac UHV-compatible retarding grid analyser operated in partial electron yield mode was utilized for the acquisition of NEXAFS spectra. The vacuum of the analysis chamber was maintained at 2 x 10^{-10} Torr or better and the storage ring was operated in the decay mode.

Neutron reflectometry / Electrochemistry

The NR / electrochemistry measurements utilized a specially designed solid – liquid cell described previously (22) (Chapter 5). Furthermore, the silicon wafer substrates used in the current study were cleaned and prepared using a procedure already described in Chapter 4 (8). An additional step involved cleaning of the substrates using an ozone cleaner (UVO Cleaner® 144AX) for 20 minutes to remove any residual organic contaminants. A solution of POT (0.3% w/v) was filtered (Iso-DiskTM 0.2 μm PTFE Syringe Tip Filter) and deposited onto the silicon wafer and annealed in a vacuum oven for 3 hours at 80°C. The wafer was immediately spun at 2000 rpm for one minute. In total, two spin coating applications of POT were deemed necessary to achieve a desirable thickness. A plasticized PVC cocktail comprising PVC (32.5 wt%), DOS (65.9 wt%), calcium ionophore IV (1 wt%) and NaTFPB (0.6 wt%) in DMF

(1.5% w/v) was subsequently coated onto the SC at a spin rate of 3500 rpm for 1 minute.

NR and EIS were initially carried out on the POT / PVC ISE until no significant changes were observed between successive spectra, i.e. the polymeric ISE was allowed to equilibrate with the D_2O electrolyte. Subsequently, cyclic voltammetry (CV) was used to establish the potential required to oxidize the POT SC layer. Chronoamperometry was subsequently performed to carry out the oxidation at a potential of 1.3 V for 1 hour. EIS and NR measurements were resumed once the POT layer had been oxidized.

All of the NR and electrochemistry reported herein were undertaken at the Australian Nuclear Science and Technology Organization (ANSTO). NR measurements were recorded using the Platypus time-of-flight neutron reflectometer at the OPAL 20MW research reactor (23). A cold neutron spectrum (3.0 Å ≤ λ ≤ 18.0 Å) was used and 23 Hz neutron pulses were generated using a disk chopper system (EADS Astrium GmbH) in a medium resolution ($\Delta\lambda/\lambda$ = 4%). The reflected neutron spectra were recorded on a 2-D helium-3 neutron detector (Denex GmbH) at 0.5° for 30 minutes and 2° for 2.5 hours. The vertical slits were configured for each measurement to maintain a constant footprint (7 cm x 3.5 cm) and direct beam measurements were collected under the same collimation conditions for each measured angle. Data reduction and analysis of the reflectivity profiles were performed using the Motofit reflectometry analysis program (24).

CV and chronoamperometry studies were carried out on a Metrohm Autolab-PGSTAT128N. All EIS measurements were performed using a Princeton Applied Research Parstat 2263 portable potentiostat. EIS spectra were collected using an excitation potential of 10 mV rms and a frequency range of 100 kHz to 10 mHz. CV and chronoamperometry were performed prior to commencing NR measurements, whilst EIS was undertaken concurrently with

the reflectivity studies. The electrolyte used throughout all measurements was a 0.1 M $CaCl_2$ solution in D_2O.

Results and Discussion

SR / XPS was used as a surface sensitive approach to study the ion-to-electron processes in the SC of ISEs. Importantly, XPS provides insights into the influence of the chemical and physical factors that control the behaviour of the SC in polymeric ISEs and has a tremendous ability for structure elucidation in the outermost layers of the sample for elements above 1 atomic percent (25). Lower detection limits are attainable in SR / XPS due to the option of tunability of the beam through the use of beam energies near to the absorption edge where photo-absorption cross sections are increased by 1 – 2 orders of magnitude. In this study, fluorine and sulfur were utilized as tracer elements to track the ion-to-electron process of POT. The ability of XPS to discriminate between different oxidation states of atoms enabled the study of either neutral sulfur originating from the neutral SC, or oxidized sulfur arising from an oxidation of the thiophene functional group of POT. The detection of fluorine in the SC layer further implies the ingression of the $TFPB^-$ as fluorine is only present in the $TFPB^-$ component of the entire ISE. Importantly, XPS studies of a native electropolymerized POT SC surface has been reported previously (25), and the spectra for a control POT sample reported herein compares favourably.

Figure 7-1 presents XPS depth-resolved spectra of the oxidized POT SC. The F(1s) spectra (***Figure 7-1 (a)***) shows a distinct peak prior to sample sputtering, which is severely diminished following ion beam sputtering of the POT SC layer. Actually, the intensity of the fluorine peak falls to background levels after only 1 minute of ion beam sputtering. This corresponds to a sputtering depth of approximately 14 Å, which shows that the incorporation of $TFPB^-$ into the POT SC layer is surface confined. It is important to confirm that fluorine resulted from migration of $TFPB^-$ during electrochemical oxidation of POT rather than residual quantities of the ion-selective PVC membrane

(removed prior to SR / XPS analysis) that may have remained on the SC. The former was justified by the absence of chlorine in XPS survey scans for all SCs after dissolving the PVC membrane, thereby confirming that the overlaying ion-selective membrane was removed in its entirety. Furthermore, a quartz crystal microbalance study of the POT layer following prolonged exposure to THF revealed a lack of dissolution of the underlying POT film.

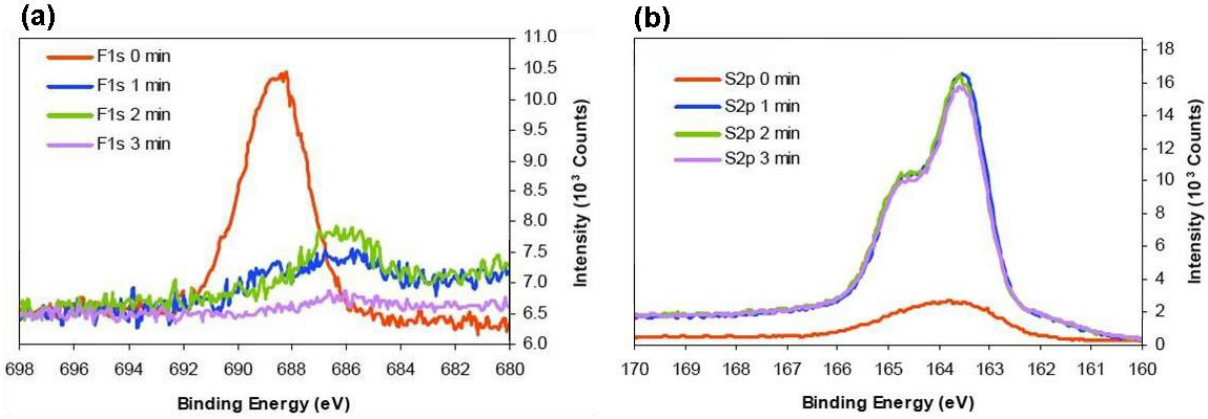

Figure 7-1 *SR / XPS depth-resolved spectra of an oxidized POT SC after argon ion sputtering for various times. (a) Spectrum for the F(1s) core level, whilst (b) presents the S(2p) core level spectrum. All spectral binding energies were calibrated against the C(1s) peak.*

The S(2p) spectra (***Figure 7-1 (b)***) are in accordance with the outcome observed from the F(1s) spectra. At the surface prior to sample sputtering, a broad peak is evident in the S(2p) core level spectrum which results from a convolution of at least two slightly offset spin-orbital-split doublets [$S(2p_{1/2})$ and $S(2p_{3/2})$] from the oxidized and neutral chemical states of sulfur. Whilst it is expected that the $S(2p_{3/2})$ peak for a neutral thiophene unit should occur at a binding energy of about 163.6 eV, a component exhibiting a small positive shift (≤ 1 eV) in the $S(2p_{3/2})$ peak readily suggests that some of the sulfur atoms exist in an oxidized chemical environment. Undoubtedly, this is due to electrochemical oxidation of a portion of the thiophene units and a concomitant ingression of the $TFPB^-$ dopant (26) and the mixture of thiophene species is responsible for the convoluted S(2p) spectrum. Nevertheless, it is evident that

sulfur in thiophene has not been over-oxidized to sulfone or sulfate species since the binding energy shift from the neutral S(2p) peak would be far more significant (25, 27, 28). Instead, it is evident that the oxidized form of sulfur is the positively charged thiophene group, or polaron, associated with $TFPB^-$. After only one minute of sputtering, two partially resolved peaks are present at binding energies of 163.6 and 165 eV, which are indicative of the $S(2p_{3/2})$ and $S(2p_{1/2})$ spin-orbit split components in neutral sulfur (26, 29). The low intensity at the oxidized POT surface is attributable to the high concentration of $TFPB^-$ that occupies much of the surface of the oxidized SC. Essentially, $TFPB^-$ forms on the oxidized POT surface, and this attenuates the photoelectrons from the underlying POT substrate[4].

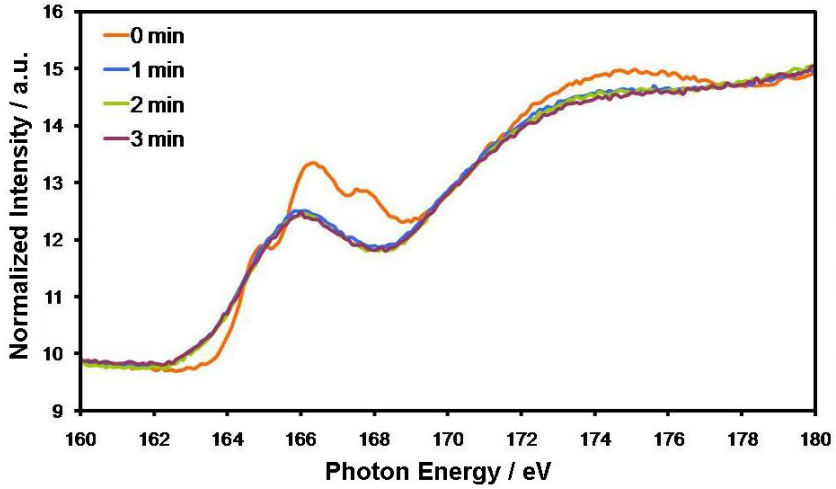

Figure 7-2 *NEXAFS spectra corresponding to the S(2p) core atomic orbital for an oxidized POT SC film.*

NEXAFS studies of the S(2p) absorption edge also pointed to a surface confinement of the ion-to-electron process at the POT SC / ion-selective membrane interface. NEXAFS is a powerful tool for distinguishing between the oxidized and unoxidized states of POT due to its sensitivity to nearest neighbours during constructive and destructive scattering of electrons arising

[4] It is possible to estimate the thickness of the $TFPB^-$ rich overlayer using an approximation of the electron mean free path in addition to the areas of the S(2p) peaks before and after depth profiling. It is anticipated that such an analysis will be performed in future work when the XPS data is modelled.

from photoionization of the S(2p) core orbital. Furthermore, another asset of NEXAFS is its polarization dependence which is very sensitive to state symmetry and molecular orientation (30). The spectra shown in ***Figure 7-2*** show distinct differences between the sample measured before and after sputtering. Importantly, the fact that excitations arise from two initial states separated by approximately 1 eV (i.e. $2p_{1/2}$ and $2p_{3/2}$) makes it somewhat difficult to interpret the sulfur edge since one essentially has two spectra superimposed and shifted by 1 eV (31). Nevertheless, the NEXAFS spectra are comparable to those obtained elsewhere for the S(2p) absorption edge of thiophene functional groups (30, 31). The characteristic multiplet peak in the spectrum obtained prior to sputtering is indicative of one highly orientated chemical form (30). Conversely, the spectra obtained following argon ion sputtering reveals a broad peak which is suggestive of a highly disorientated thiophene species which is present in multiple chemical states. This is not an unexpected outcome since sulfur is well known to exist in many chemical states which would cause considerable overlap in the NEXAFS spectra. The net result of this would be a broad, convoluted peak as seen in the spectra relating to the bulk of the polymer. The fact that the initial layer (i.e., prior to sputtering) is relatively well-defined provides further credence for the fact that the surface layer has become completely oxidized.

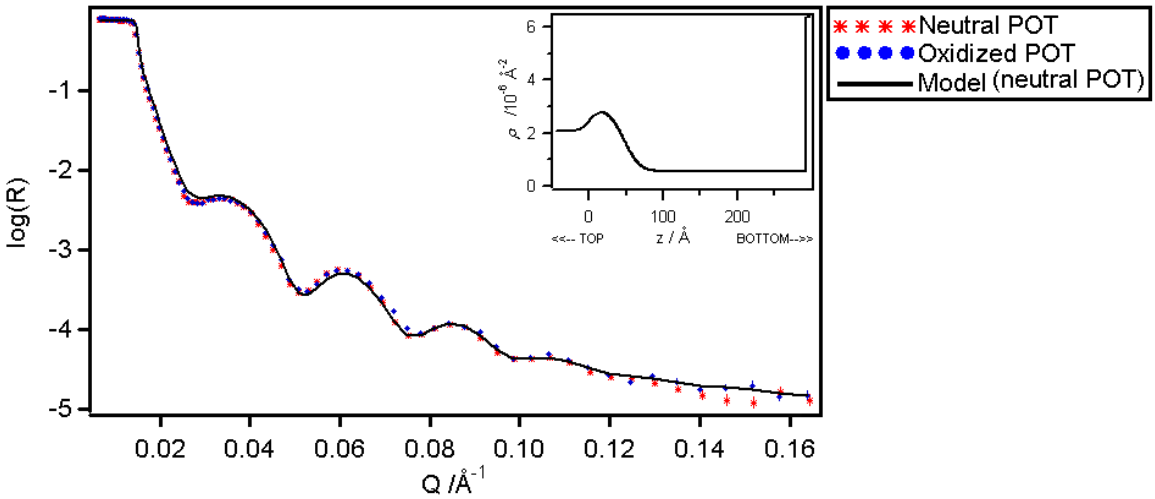

Figure 7-3 *NR spectra of a POT SC prior to and after electrochemical doping with TFPB$^-$. The modelled fit is also included for the neutral POT. The inset pertains to the scattering length density profile of the neutral POT model.*

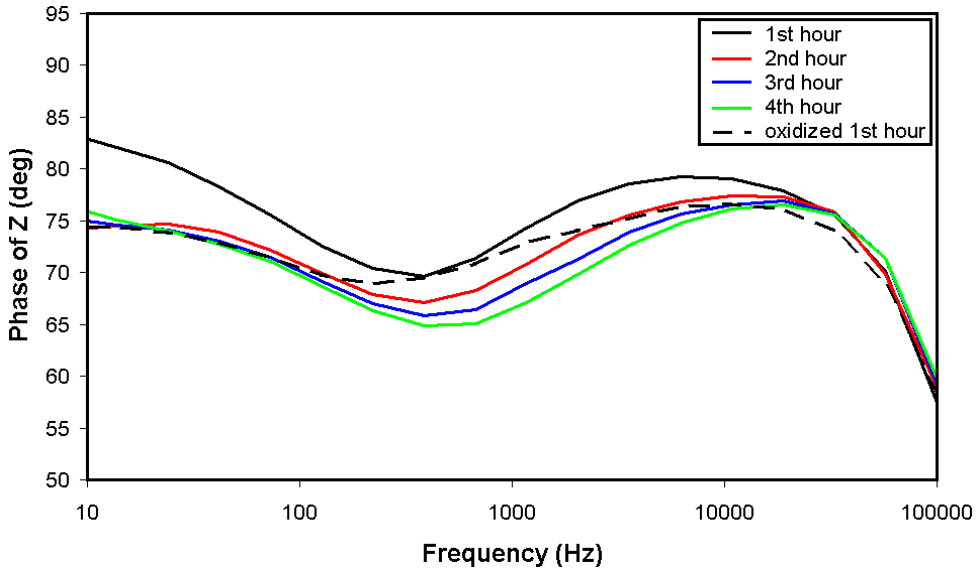

Figure 7-4 *Bode phase data for the SC ISE system whilst bathing in a D_2O electrolyte and also after electrochemical doping with $TFPB^-$.*

In situ NR was carried out on the SC ISE before and after electrochemical oxidation of the POT SC. This was an *in situ* analogue of the aforementioned SR / XPS experiment, thereby providing a corroboration of the SR / XPS experiments. ***Figure 7-3*** presents the NR spectra before and after electrochemical oxidation of the POT SC. A fitted model of the neutral POT is also presented. The model suggests that the thicknesses of the POT and PVC layers are 48 Å and 246 Å, respectively. Furthermore, each of these respective layers have neutron scattering length densities (SLD) of 2.87×10^{-6} $Å^{-2}$ and 0.56×10^{-6} $Å^{-2}$. Oxidation of the underlying POT SC is confirmed through the Bode phase data presented in ***Figure 7-4***, which shows a significant difference in the spectra obtained during equilibration of the ISE with D_2O compared to that after oxidation of the SC. This difference (a broadening of the time constant around 1000 Hz) is indicative of a new time constant, probably ascribable to the formation of an overlayer of POT / $TFPB^-$ polaron, which has been induced by the oxidation of POT. On the other hand, evidence for oxidation of the SC contact is not immediately obvious in the NR data. Importantly, an attempt to fit

a model directly to the oxidized POT based on such small differences would be meaningless. Instead, ***Figure 7-5*** presents two ideal models (not fitted to any data) based on the starting parameters obtained from the fitted model of the neutral POT (as shown in ***Figure 7-3*** and also included in ***Figure 7-5*** for comparative purposes). The models relate to the two different extreme-case scenarios which could occur during the electrochemical oxidation of the POT SC; namely, a surface confined oxidation and a full oxidation of the SC film. Clearly, the former model, which has a neutral POT thickness of 34 Å and an oxidized POT layer[5] of 14 Å thickness, closely resembles the actual dataset obtained in NR for the electrochemically oxidized POT SC. On the other hand, the model of the completely oxidized POT has almost no resemblance to the initial neutral POT model or the actual dataset for the oxidized POT SC system. These outcomes provide strong indirect evidence that the oxidation of POT is surface confined.

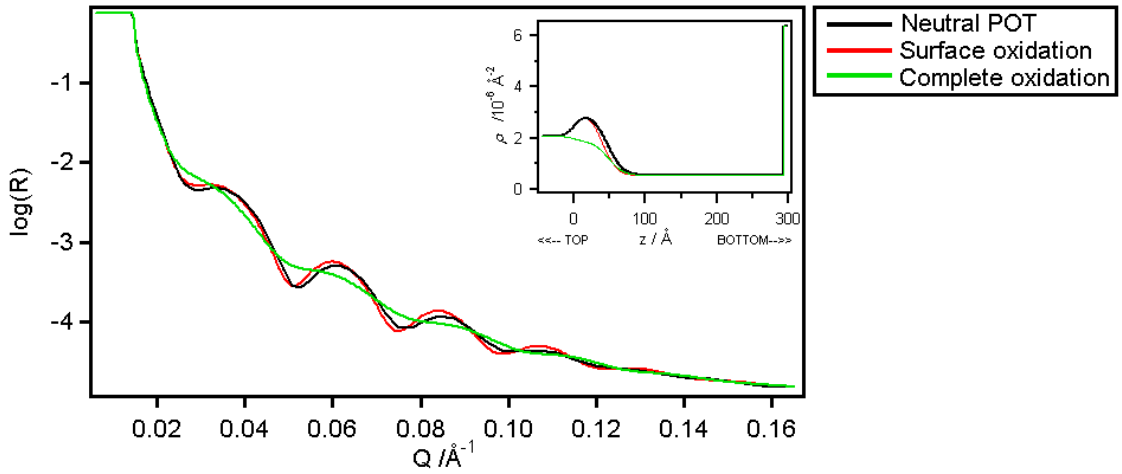

Figure 7-5 *Theoretical models of the surface confined oxidation of POT (not fitted to data) and complete oxidation of the POT SC layer (not fitted to data) for comparative purposes. These models are based on the parameters provided from the model of neutral POT (fitted to neutral POT data in* ***Figure 7-3****). The inset presents the scattering length density profile for all three theoretical models.*

[5] The SLD of the oxidized POT (used in the ideal models) was calculated as 1.88 x 10^{-6} $Å^{-2}$ from the theoretical doping of all oxidized thiophene units with the $TFPB^-$ ion.

The results of this study strongly support the notion that the ion-to-electron process occurring in the SC of ISEs is limited to a very thin surface layer (up to 14 Å) of the conducting polymer. Nevertheless, it is important to note that the diffusion time of the bulky $TFPB^-$ ion could have limited the electrochemically driven process. The chronopotentiogram obtained from the oxidation of the POT SC revealed that the bulk of the process occurred within approximately 2 minutes, after which point the current changed negligibly. Despite this observation, the potential was held for a further 18 minutes for the SR / XPS experiment and a further 58 minutes for the NR experiment in order to allow adequate time for the process to occur. In both instances, the results pointed to a surface confinement of charge-transfer (i.e. limited to the upper few Ångstroms of material) which suggests that the diffusion time is not the dominant factor with this system. Accordingly, it is highly likely that charge-transfer is playing a dominant role in the ion-to-electron transduction process under electrochemical oxidation conditions.

Importantly, this new knowledge about surface confinement of charge-transfer events at the underlying SC has important ramifications for the sensor community. Subsequent studies have proven that smaller anions (e.g., ClO_4^-, SCN^- and NO_3^-) do not enable deeper ion diffusion, thereby confirming these results as a generalized mechanism for ion-to-electron transduction. Accordingly, it is now obvious that a large amount of conductive polymer is unnecessary in SC fabrication. In fact, only a monolayer of material is required for the SC to function as an effective ion-to-electron transducer. This outcome explains the successful adoption of SAM SC systems (7, 10-14), which have been utilized in recent years. The notion that ion-to-electron transduction is surface confined also explains why the use of various other forms of SC (i.e. three dimensionally ordered macroporous carbon (15), single-walled carbon nanotubes (16, 17), etc.) also function well. Essentially, the fact that the charge-transfer processes are only evident on the surface of the SC shows that the ion-

to-electron transduction process is associated with a high double layer capacitance. Accordingly, a SC material possessing a high double layer capacitance, such as single-walled carbon nanotubes and three dimensionally ordered macroporous carbon reported elsewhere (15, 16), are expected to display excellent properties as SCs. This new understanding should allow sensor researchers to develop new redox active or capacitive SC materials for use in improved SC sensors.

Conclusion

These results demonstrate that ion-to-electron transduction in electroactive polymers, such as POT, occur via a surface confined charge-transfer reaction. In this study, the combined results from SR / XPS and NR strongly suggest that these processes occur in a thickness of up to 14 Å of the SC material. This outcome is significant for the sensor research community because it provides a new insight into the mechanism of ion-to-electron transduction in SCs. We propose that the performance of SCs in solid-state ISEs is not based on the thickness or extent of ion diffusion within the material, but rather the capacitive nature of the material. Furthermore, such a result will inevitably prevent needless wastage of expensive material by demonstrating that SCs only need be used sparingly.

References

1. Cattrall RW, Freiser H. Coated wire ion-selective electrodes. Anal Chem. 1971;43(13):1905-6.

2. Cattrall RW, Drew DM, Hamilton IC. Alkylphosphoric acid esters for use in coated-wire calcium-selective electrodes. I. Response characteristics. Anal Chim Acta. 1975;76(2):269-77.

3. Hauser PC, Chiang DWL, Wright GA. A potassium-ion selective electrode with valinomycin based poly(vinyl chloride) membrane and a poly(vinyl ferrocene) solid contact. Anal Chim Acta. 1995;302:241-8.

4. Buck R. Ion-Selective Electrodes in Analytical Chemistry. Freiser H, editor. New York: Plenum; 1978.

5. De Marco R, Veder J-P, Clarke G, Nelson A, Prince K, Pretsch E, et al. Evidence of a water layer in solid-contact polymeric ion sensors. Phys Chem Chem Phys. 2008;10:73-6.

6. Sutter J, Radu A, Peper S, Bakker E, Pretsch E. Solid-contact polymeric membrane electrodes with detection limits in the subnanomolar range. Anal Chim Acta. 2004;523:53-9.

7. Fibbioli M, Bandyopadhyay K, Liu S-G, Echegoyen L, Enger O, Diederich F, et al. Redox-Active Self-Assembled Monolayers for Solid-Contact Polymeric Membrane Ion-Selective Electrodes. Chem Mater. 2002;14:1721-9.

8. Veder J-P, De Marco R, Clarke G, Chester R, Nelson A, Prince K, et al. Elimination of Undesirable Water Layers in Solid-Contact Polymeric Ion-Selective Electrodes. Anal Chem. 2008;80(17):6731-40.

9. Bobacka J, Ivaska A, Lewenstam A. Potentiometric Ion Sensors. Chem Rev. 2008;108(2):329-51.

10. Grygolowicz-Pawlak E, Wygladacz K, Sek S, Bilewicz R, Brzozka Z, Malinowska E. Studies on ferrocene organothiol monolayer as an intermediate phase of potentiometric sensors with gold inner contact. Sens Actuators B. 2005;111-112:310-6.

11. Grygolowicz-Pawlak E, Plachecka K, Zbigniew B, Malinowska E. Further studies on the role of redox-active monolayer as intermediate phase of solid-state sensors. Sens Actuators B: Chem. 2007;123:480-7.

12. Fibbioli M, Enger O, Diederich F, Pretsch E, Bandyopadhyay K, Liu S-G, et al. Redox-active self-assembled monolayers as novel solid contacts for ion-selective electrodes. Chem Commun. 2000;5:339-40.

13. Sek S, Bilewicz R, Grygolowicz-Pawlak E, Grudzien I, Brzozka Z, Malinowska E. Design of ferrocene organothiol monolayer as intermediate phase for miniaturized electrochemical sensors with gold contact. Polish J Chem. 2004;78(9):1655-65.

14. Grygolowicz-Pawlak E, Palys B, Biesiada K, Olszyna AR, Malinowska E. Covalent binding of sensor phases - a recipe for stable potentials of solid-state ion selective sensors. Anal Chim Acta. 2008;625:137-44.

15. Lai C-Z, Fierke MA, Stein A, Buehlmann P. Ion-Selective Electrodes with Three-Dimensionally Ordered Macroporous Carbon as the Solid Contact. Anal Chem. 2007;79(12):4621-6.

16. Crespo GA, Macho S, Bobacka J, Rius FX. Transduction mechanism of carbon nanotubes in solid-contact ion-selective electrodes. Anal Chem. 2009;81:676-81.

17. Crespo GA, Macho S, Rius FX. Ion-selective electrodes using carbon nanotubes as ion-to-electron transducers. Anal Chem. 2008;80:1316-22.

18. Chumbimuni-Torres KY, Rubinova N, Radu A, Kubota LT, Bakker E. Solid Contact Potentiometric Sensors for Trace Level Measurements. Anal Chem. 2006;78:1318-22.

19. Bobacka J, McCarrick M, Lewenstam A, Ivaska A. All solid-state poly(vinyl chloride) membrane ion-selective electrodes with poly(3-octylthiophene) solid internal contact. Analyst. 1994;119(9):1985-91.

20. Si P, Bakker E. Thin layer electrochemical extraction of non-redoxactive cations with an anion-exchanging conducting polymer overlaid with a selective membrane. Chem Commun. 2009:5260-2.

21. Si P. Nanostructured Chemical Sensors Based on Polythiophene and Its Derivatives. Denmark: Roskilde University Center; 2008.

22. Veder J-P, De Marco R, Connell B, Dalgliesh R, Pretsch E, Bakker E. Water uptake in the hydrophilic solid-contact of polymeric ion-selective electrodes. Analyst. 2010;In Preparation.

23. Schulz JC, James M, Nelson A, Brule A. Platypus: a time-of-flight neutron reflectometer at Australia's new research reactor. Neutron Res. 2006;14(2):91-108.

24. Nelson A. Co-refinement of multiple contrast neutron / X-ray reflectivity data using MOTOFIT. J Appl Crystallogr. 2006;39(2):273-6.

25. De Marco R, Jee E, Prince K, Pretsch E, Bakker E. Synthesis and characterization of high-integrity solid-contact polymeric ion sensors. Solid State Electrochem. 2008;13:137-48.

26. Kang ET, Neoh KG, Tan KL. X-ray photoelectron spectroscopy studies of poly(2,2'-bithiophene) and its complexes. Phys Rev B. 1991;44(19):10461-9.

27. Kang ET, Neoh KG, Tan KL. Surface modifications of poly(3-alkylthiophene) films by graft copolymerization. Macromolecules. 1992;25:6842-8.

28. Kaul A, Udipi K. Electron Spectroscopy for Chemical Analysis Study of the Surface Oxidation of Poly(phenylene sulfide) Powder by Heterogeneous Reactions. Macromolecules. 1989;22(3):1201-7.

29. Riga J, Snauwaert A, De Pryck R, Lazzaroni R, Boutique JP, Verbist JJ, et al. Electronic structure of sulphur-containing conducting polymers. Synth Met. 1987;21:223-8.

30. Hitchcock AP, Horsley JA, Stohr J. Inner shell excitation of thiophene and thlolane: Gas, solid, and monolayer states. J Chem Phys. 1986;85(9):4835-48.

31. Tourillon G, Mahatsekake C, Andrieu C, Williams GP, Garret RF, Braun W. Electronic structure and orientation studies of undoped pol-3-alkyl thiophenes electrochemically deposited on Pt as studied by NEXAFS. Surf Sci. 1988;201:171-84.

Chapter Eight

8 A Flow Cell for Transient Voltammetry and its Application to *In Situ* GIXRD Characterization of Electrocrystallized $Cd(TCNQ)_2$

Jean-Pierre Veder, Ayman Nafady, Graeme Clarke, Ross P. Williams, Roland De Marco and Alan Bond.

Electrochimica Acta, **56**, 1546-1553 (2010).

Abstract – An easy to fabricate and versatile cell that can be used with a variety of electrochemical techniques also meeting the stringent requirement for undertaking cyclic voltammetry under transient conditions in *in situ* electrocrystallization studies and total external reflection X-ray analysis has been developed. Application is demonstrated through an *in situ* synchrotron radiation / grazing incidence X-ray diffraction (SR / GIXRD) study of the electrocrystallized cadmium (II) tetracyanoquinodimethane (TCNQ) material, $Cd(TCNQ)_2$, from acetonitrile (0.1 M $[NBu_4][PF_6]$). Importantly , this versatile cell design makes SR / GIXRD suitable for almost any combination of total external reflection X-ray analysis (e.g., GIXRF, GISAXS, GIXRD, etc.) and electrochemical perturbation, also allowing its application in acidic, basic, aqueous, non-aqueous, low and high flow pressure conditions.

Introduction

Currently, there is a large body of literature on electrochemical cell designs for use in *in situ* transmission and total external reflection X-ray analysis. It also has been well established that synchrotron light sources may be utilized advantageously in such studies (1), thereby allowing characterization of electrode materials surrounded by an electrolyte solution without a significant loss in intensity due to photon absorption or scattering by the electrolyte solution (2). In many cases, the cells have been applied to the characterization of scientifically and technologically important systems (3-9). Importantly, the cells have all of the essential features needed for *in situ* transmission and total external reflection X-ray analysis. However, commonly the cells are limited to studies of the bulk properties of porous electrode substrates, and also with respect to the combination of electrochemical and X-ray measurements that can be performed. Commonly, the electrochemical cells are only capable of measurements in aqueous electrolytes, and they often possess inherently high ohmic resistances due to a confined solution electrolyte volume. To exacerbate this problem, the designs can lead to a substantially uneven IR (ohmic) drop on the electrode surface, thereby leading to inhomogeneity in electrochemically generated materials. Thus, there is a need for a versatile electrochemical cell that is applicable to electrochemical interrogation by a wide range of techniques (e.g. impedance spectroscopy, potentiometry, cyclic voltammetry, chrono-potentiometry, chronoamperometry, and pulsed voltammetry), followed by *in situ* surface studies using a variety of total external reflection X-ray characterization methods (i.e., grazing incidence X-ray diffraction (GIXRD), grazing incidence X-ray fluorescence (GIXRF), grazing incidence small angle X-ray scattering (GISAXS), etc.)].

A survey of the recent literature on the employment of *in situ* transmission synchrotron X-ray analysis of electrochemically deposited materials revealed a plethora of reports related to porous electrodes and lithium ion intercalators (10-15) using XRD, porous proton exchange membrane fuel cells (16) using X-ray

absorption spectroscopy (XAS) and porous battery electrodes undergoing charge / discharge cycling (17) along with supercapacitor electrodes (18) using XRD. Furthermore, there have been recent papers on *in situ* transmission (19-20) and frontside fluorescence (21-22) synchrotron studies of fuel cell electrocatalysts using extended X-ray absorption fine structure (EXAFS), as well important studies using X-ray absorption near-edge spectroscopy (XANES) study of ZnO nanostructures (23) and SAXS measurements of the growth of Pt catalysts during potentiodynamic cycling (24). In this sense, the application of *in situ* transmission synchrotron X-ray analysis is a mature field, and has been reviewed in 2004 in an excellent contribution by the Russell Group (25).

Reports on electrochemical cell designs for open circuit potential or electrochemical impedance spectroscopy in conjunction with *in situ* total external reflection X-ray analysis are less common (4-5, 26-30), and have mostly been applied to aqueous electrolytes under mild conditions (i.e., room temperature and non-corrosive environments). In electrocrystallization studies, it is common to employ cyclic voltammetry under dynamic fast scan rate conditions to provide mechanistic information as a precursor to controlled potential approaches to deposit bulk amount of crystalline material adhered to the electrode surface. Existing cells do not allow this approach to be used in conjunction with *in situ* external reflection X-ray analysis to characterize the electrocrystallized material. We have now developed a cell that allows transient voltammetric conditions to be achieved as well as many other methods in a very versatile arrangement. Davenport and co-workers (29-30) reported a cell design similar to the present one and another cell design has been reported for *in situ* synchrotron radiation (SR) / GIXRD (31), in a study of the electrocrystallization of ZnO nanoparticles. However, both cell designs (29-31) only allow use of very slow scan rate voltammetric studies because of the high IR_u (I = current, R_u = uncompensated resistance). Cell design (31) utilized a capillary electrolyte solution housing that enhanced R_u, with the shape of the cell also restricting the minimum and maximum angles of incidence that may be used in the depth profiling of the

electrochemically prepared thin film by SR / GIXRD. Cell design (29-30) also used an electrode that is placed at an elevated position with respect to the base of the cell and can give rise to significant IR_u drop so that transient voltammetry is difficult in high resistance organic solvents with this configuration, although precursors in low resistance organic media maybe tractable.

In this paper, we report a versatile electrochemical cell design for *in situ* SR / GIXRD studies of electrochemically prepared thin films that is based on knowledge gained in studies with earlier designs (27-28, 32). In particular, a range of significant improvements has been introduced to specifically meet the aforementioned stringent requirements for the transient form of voltammetry and *in situ* X-ray characterization using a total external reflection X-ray analysis technique. The combined focus of the research is a demonstration of the utility of the new electrochemical cell by an *in situ* SR / GIXRD study of the electrocrystallization of $Cd(TCNQ)_2$ (TCNQ = 7,7,8,8-tetracyanoquinodimethane) from a non-aqueous acetonitrile electrolyte solution, noting that this metal-TCNQ material is a hitherto structurally uncharacterized charge transfer compound that is different from the $[Cd_2(TCNQ)_3]^{2-}$ coordination polymer, which contains the more highly reduced $TCNQ^{2-}$ dianion (33). In addition, metal-organic materials containing the monoanion, $TCNQ^-$, are expected to appeal to many electrochemists and material scientists as this class of compounds have the potential to be utilized in magnetic, sensor, and electrical switching devices (34-37).

Experimental

Materials and Reagents

Analytical reagent grade $Cd(NO_3)_2$ was obtained from BDH Laboratory Reagents, whilst TCNQ (98%) and $[NBu_4][ClO_4]$ were purchased from Aldrich.

Acetonitrile, which was used as the solvent was HPLC grade and sourced from Omnisolv. All reagents were used as received from the suppliers.

Flow Cell Design

The electrochemical / SR-GIXRD cell presented in ***Figure 8-1*** was constructed from the polymer Ketron® PEEK, which is resistant to thermal, electrical and chemical degradation (viz., in acids, alkalis as well as organic solvents). A polycrystalline platinum substrate was used as the working electrode with dimensions of 20 mm x 10 mm. It was connected to a mild steel stub using a conductive silver epoxy contact, and was mounted in an epoxy resin. The working electrode was placed in a circular disk that is 30 mm in diameter and 5 mm in thickness allowing exposure of the top face of the 20 mm x 10 mm platinum substrate. The disk was subsequently pushed firmly into the inner recess of the cell (of similar dimensions to the epoxy mounted electrode) and sealed tightly against an embedded rubber O-ring ensuring that there is no leaking of electrolyte solution onto electrical contacts. The electrode was positioned 160 μm below the top plane of the cell, with this design feature ensuring that during suctioning of the electrolyte solution, either in a stop-flow mode or during reverse pumping of the electrolyte solution, a thin layer of electrolyte solution (i.e., << 160 μm) is always in contact with the electrode so that the incident X-ray beam is not significantly attenuated. Large filling compartments, which allow an unobstructed flow of solvent past all of the electrodes, were located on either side of the working electrode, where the reference and counter electrodes were situated. The filling ports were subsequently positioned in the centre of each compartment and the inlet / outlet were positioned at the underside of the cell.

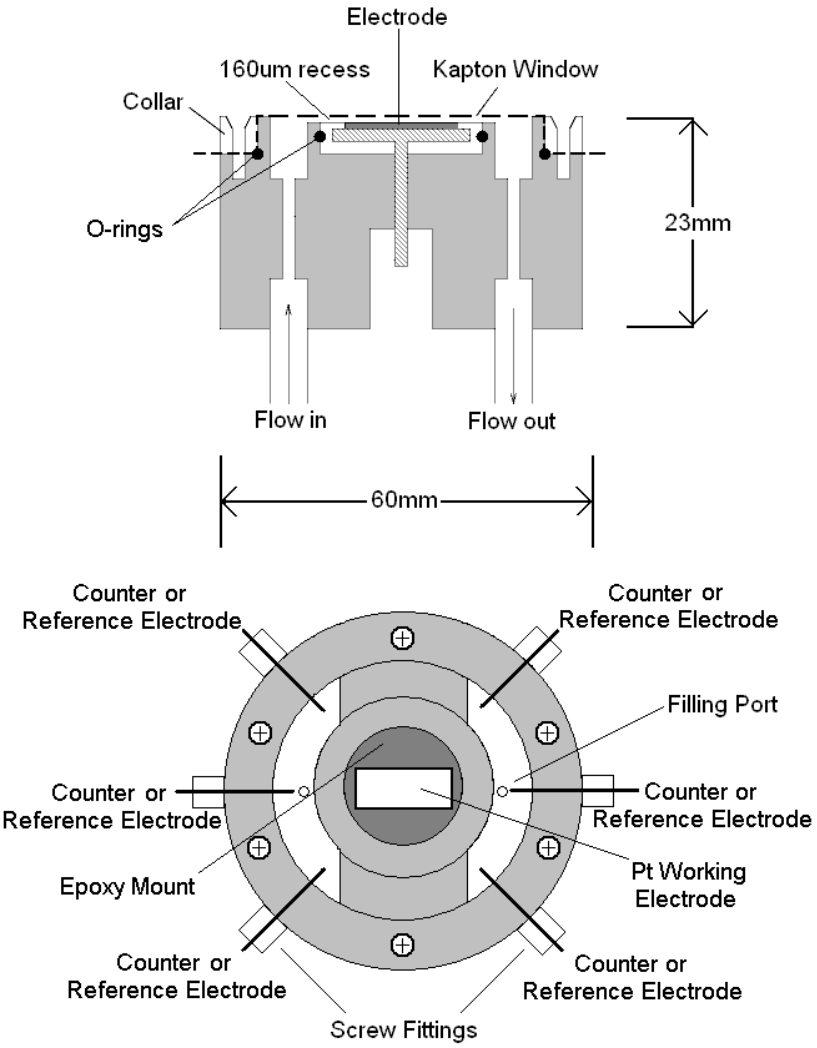

Figure 8-1 *Schematic diagram of the electrochemical cell utilized in electrochemical studies combined with in situ X-ray analyses. The upper diagram shows a side profile of the cell, while the lower diagram presents a top profile of the cell. An O-ring is situated between the epoxy mounted electrode and central cell body to provide a leak-free cell, and the working electrode (2 cm x 1 cm) area is 2 cm^2, while the 5 counter electrodes (1.5 mm in diameter protruding 3 mm into the flow cell) yield a combined area of 0.795 cm^2.*

Four platinum wire counter electrodes and two silver wire quasi-reference electrodes (all wires were 1.5 mm in diameter and protruded 3 mm into the flow channels) were inserted into a set of six small-drilled holes at an even

separation. However, permutations of the number and distribution of the quasi-reference and counter electrodes are possible. The combination of two reference and four counter electrodes led to the best defined voltammetry. Each electrode was firmly fixed to the wires by use of plastic ferrules that were crimped tightly to the wire electrodes by the pressure exerted, whilst screwing the electrodes tightly into the cell. A collar surrounding the entire working electrode and cell filling ports, which sat flush with the top of the cell, was also fabricated to enable the sealing of a 20 μm thick Kapton window over the flow system by pressing the Kapton firmly against a large embedded rubber O-ring in a sandwich type arrangement. As a consequence of the design, the cell could easily be assembled and dismantled to replace used components, e.g., Kapton window, working electrode, etc., or damaged components such as the swelled O-ring surrounding the large epoxy mounted working electrode. Other cell designs that resemble the one reported in this paper do not utilize a counter electrode that enshrouds the working electrode (38), nor do they provide a reference electrode within the cell housing (39-40) (i.e., the reference electrode is situated in the external solution reservoir). They may be susceptible to leaking at the connection point between the working electrode and the external electrical contact (41), and they do not permit transient voltametric studies by reversing the pump flow to ensure suctioning and a concomitant thin layer of electrolyte solution between the recesses electrode and collapsed window that are separated by <<160 μm as in the present cell design (26-28). Furthermore, the present leak-proof cell design permits successful experimentation on a variety of electrodes in a single visit to a synchrotron facility, as pre-fabricated epoxy mounted electrodes of the correct dimension may be popped in into and out of the cell, and new electrodes with new O-ring seals may be inserted for further SR / GIXRD analysis. Previous research has shown that temporal electrochemical or voltametric studies are possible with the present and past cell designs (29-30), as long as steps are taken (viz, sufficient suctioning, or low pumping rates are used (5, 41)) to ensure that the electrolyte solution layer thickness is restricted to a few microns, as has been demonstrated previously in

the pitting corrosion of copper in chloride solution (5), as well as the reconstruction of Au(001) in alkaline and acidic electrolyte solutions (41).

The present design has evolved from passive electrochemical experiments involving SR / GIXRD studies of solid-state ion-selective electrodes in saline media (28) as well as the carbon dioxide corrosion of mild steel in carbonated brine (27). In order to be used under dynamic voltametric conditions and achieve uniformity of the electrodeposited material, two connected quasi-reference electrodes were used and inserted in close proximity to the working electrode in the flow outlet of the cell and the perimeter of the working electrode is shrouded by four separate platinum wire counter electrodes that were short-circuited into a single electrode array. To illustrate the relevance, we focus for the first time on the electrocrystallization of the Cd-TCNQ material from acetonitrile. The product is highly crystalline and amenable to XRD studies, but the method is generically applicable to many scenarios encountered in the electrodeposition of solid materials.

Description of GIXRD

As described in ***Appendix I***, below the critical angle for a given wavelength of radiation, GIXRD accomplishes its surface sensitivity by restricting the depth of penetration of the externally reflected X-ray beam and the concomitant sampling depth of the technique to tens to hundreds of Angstroms (4-5).

In this study, the critical angle (α_c) for $Cd(TCNQ)_2$ has been estimated at 0.124 degrees using the expression provided by Vineyard (42):

$$\alpha_c = \left[\frac{r_e}{\pi} \left(\frac{hc}{E} \right)^2 \frac{\rho n_e}{m} \right]^{1/2} \qquad \textbf{Equation 8-1}$$

where r_e is the classical electron radius (2.871940 x 10^{-15} m), h is the Planck constant (6.62606896 x 10^{-34} Js), c is the speed of light (2.99792458 x 10^{8} m s^{-1}), E is the photon energy (1.98645 x 10^{-15} J at λ = 1.000 Å), ρ = mass density of $Cd(TCNQ)_2$ (1769 kg m^{-3}), n_e is the number of electrons in $Cd(TCNQ)_2$ (256), m is the molar mass of $Cd(TCNQ)_2$ (8.64812 x 10^{-25} kg). Clearly, for the angles of incidence utilized in this study (i.e., 0.25 to 2.00 degrees), the system does not experience total external reflection, and the surface sensitivity is substantially decreased.

Nevertheless, Vineyard (42) has shown that, under conditions near to the critical angle, or at low angles of incidence, severe X-ray absorption by the substrate at angles somewhat above the critical angle is analogous to the condition provided by total external reflection, allowing surface diffraction measurements. In fact, it is possible to estimate the depth of analysis, d, using the equation:

$$d = \frac{2\alpha}{\mu}$$ **Equation 8-2**

where α = angle of incidence in radians, and μ = linear attenuation coefficient (noting that μ = 28.03 cm^{-1} for $Cd(TCNQ)_2$ [formula is $CdC_{24}H_8N_8$ and ρ is 1.769 g cm^{-3}] at 0.1000 nm or 12.4 keV as calculated at http://physics.nist.gov/PhysRefData/FFast/html/form.html and interpolation of the linear relationship for calculated μ vs E (μ = -7.38E + 119.49; R^2 = 0.9947) in the range of 11 to 13 keV, yielding a sampling depth of 3.1 to 24.7 μm at α = 0.25 to 2.00 degrees.

Instrumentation

All in situ voltametric and SR / GIXRD measurements were undertaken on Beamline 20B at the Photon Factory in Tsukuba, Japan, using the “BIGDIFF” diffractometer, noting that the design of the flow cell is amenable to any

synchrotron source around the world and can even be adapted to laboratory-based instrumentation.

After undertaking voltammetric experiments needed to determine the potential to achieve bulk electrocrystallization of the Cd-TCNQ material in the SR-GIXRD configuration, the cell was dismantled, the working electrode was polished and the Kapton film was replaced. All components of the cell were rinsed thoroughly with clean acetonitrile prior to reassembly of the SR / GIXRD cell. The array of four platinum wire counter electrodes and the two AgTCNQ coated silver reference electrodes allowed a relatively even "film" of Cd-TCNQ-based material to be electrocrystallized from acetonitrile (0.1 M $[NBu_4][ClO_4]$) containing high concentrations of TCNQ (10 mM), and $Cd(ClO_4)_2$ (5 mM) onto the entire surface of the platinum working electrode (see *Figure 8-2*) after applying a potential that is more negative than the second reduction process (E_{appl} = -0.38 V vs Ag / AgCl (3 M KCl)) for designated periods of time. Subsequently, the electrosynthesized material was subjected to *in situ* SR / GIXRD analysis and data obtained compared to the *ex situ* powder diffraction pattern of an authentic sample of $Cd(TCNQ)_2$ obtained via reductive bulk electrolysis using a H-type three compartment cell and an indium tin oxide (ITO, area = 0.06 to 0.1 cm^2) working electrode.

For the *in* situ SR / GIXRD measurements, the electrolyte solution was pumped at an extremely high flow rate (415 mL min^{-1}) using a Masterflex peristaltic pump to purposely induce a significant distension in the Kapton window, and acetonitrile resistant Masterflex Norprene® tubing was used in the flow circuit. Note that prior to electrocrystallization, the distension of the Kapton film (bulging of the window to several millimeters in thickness) yielded reproducible cyclic voltammograms (CV) comprising well-defined reduction and oxidation components. After electrodeposition of the solid material of interest using controlled potential electrolysis at -0.38 V for up to 30 minutes, the flow rate of the electrolyte solution was gradually reduced to minimize disturbances

in the uniformity of the electrodeposited solid caused by a sudden fluctuation in the electrolyte solution flow. Finally, the peristaltic pump was switched off, which caused suctioning of the electrolyte solution (obvious to eye and by the detection of diffraction peaks from the electrode substrate). The associated thin layer of electrolyte solution (i.e., << 160 μm) does not attenuate significantly the incident X-ray beam, thereby allowing the acquisition of excellent X-ray diffraction patterns at α > 0.75 degrees.

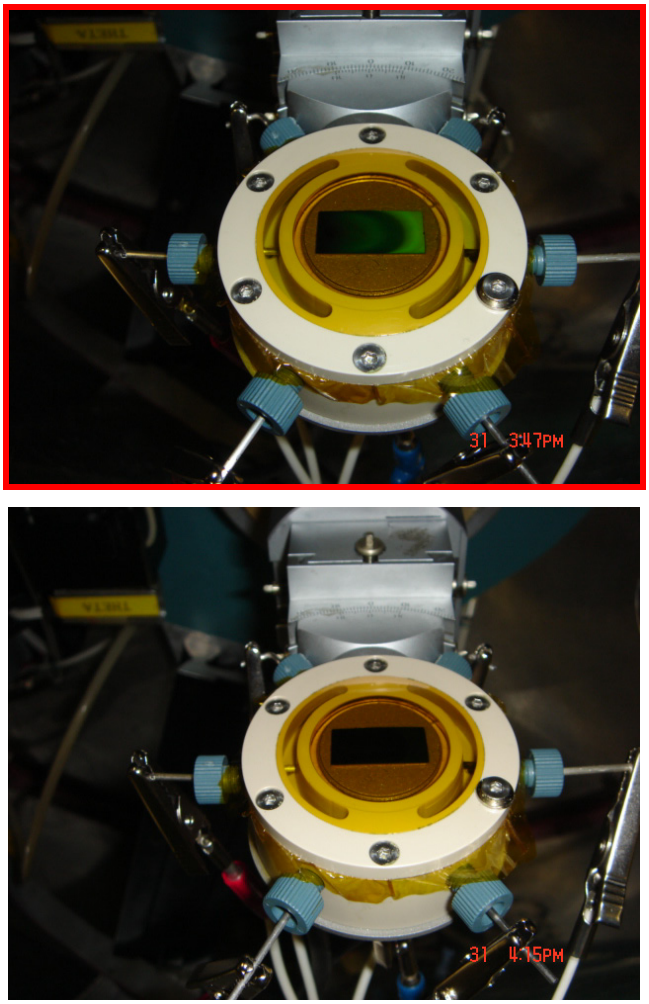

Figure 8-2 *Images of the in situ SR-GIXRD electrochemical cell showing the electrodeposition of blue $Cd(TCNQ)_2$ material on the Pt working electrode from a mixture of 10 mM TCNQ and 5 mM $Cd(ClO_4)_2$ in acetonitrile (0.1 M $[Bu_4N][ClO_4]$) at E_{app} = -0.38 V for 2 mins (top image, light blue) and 28 mins (bottom image, dark blue).*

Electrochemical experiments were carried out on the voltametric / GIXRD cell using a commercially available portable Princeton Applied Research PARSTAT 2263 potentiostat. Beamline 20B at the Photon Factory in Tsukuba, Japan, employs a Si(111) channel cut monochromator which was set to deliver a wavelength of 1.000 Å, so as to minimize the attenuation of the incident X-ray beam by air and the electrolyte solution. Parallel beam optics were also used to provide an incident beam that was 100 μm and 2 mm in the vertical and horizontal directions at α = 0.25 degrees, respectively. All GIXRD measurements were taken at angles between 0.25° and 2° (beam sampling depth of 3.1 to 24.9 μm in this incident angle range) using an exposure time of 20 minutes onto Fuji imaging plates that yield an indicative resolution in 2-theta of 0.01 degrees (observed experimentally) based on the design of the "BIGDIFF" detector under the conditions used herein, noting that the height of the beam in the vertical direction was adjusted to provide a constant beam footprint at all angles of incidence. The platinum electrode diffraction pattern was used as an internal standard for calibration of the synchrotron beam wavelength, yielding an actual value of 0.9962 Å.

The XRD experiments utilized a beam footprint of 11.4 mm in length and 2 mm in width, which only probes parts of the 20 x 10 mm electrode sheet, noting that this design enabled an easy alignment of the cell. Scanning electron microscopy (SEM) studies of the film deposited across the entire electrode surface with Cd-TCNQ (evidenced later in ***Figure 8-6***) suggested a film thickness of about 20 - 30 microns. Studies related with a Zn-TCNQ material (43) (***Chapter 9***) established potential dependant morphologies that can be probed in the present cell.

Powder diffraction patterns were recorded in a 0.3 mm glass capillary tube at a beam wavelength of 1.5084 Å. For purposes of a uniform presentation of the SR / XRD and SR / GIXRD data, the GIXRD data have been normalized

to a 2-theta scale of λ = 1.5418 Å for Cu Kα radiation. The powder diffraction data for $Cd(TCNQ)_2$ was refined using a Pawley refinement employing the TOPAS 4.2 software. Although the powder comprised a major and minor phase, the pattern of the major phase ($Cd(TCNQ)_2$) could be refined using a Pawley refinement of the tetragonal unit cell with a P4 space group and the lattice parameters for $Mn(TCNQ)_2$ as the starting point.

Due to the instant deposition of AgTCNQ material on the silver wires on exposure to TCNQ solution, the practical reference electrode used in this study was Ag / AgTCNQ. In a control experiment to evaluate the potential versus the Ag / AgCl (3M KCl) reference, electrodeposition of $Cd(TCNQ)_2$ - based material was performed at (293 ± 2) K in a N_2 atmosphere using a standard three-electrode electrochemical cell configuration containing an Ag / AgCl (3M KCl) reference electrode, separated from the test solution by a salt bridge, a platinum mesh counter electrode, and both 1.6 mm diameter platinum disk (Bioanalytical systems) and 20 mm x 10 mm platinum sheet as working electrodes. Conversion of the potential measured via the Ag / AgTCNQ reference electrode under our experimental conditions to the aqueous Ag / AgCl (3 M KCl) scale is achieved by the addition of 0.32 V, noting that no correction was made for the junction potential.

In order to establish the importance of IR drop and the applied potential on the electrocrystallization of the Cd-TCNQ material onto Pt, cyclic voltammograms in an acetonitrile solution containing 5 mM TCNQ, 2.5mM $Cd(ClO_4)_2$ (2:1 ratio) and 0.1 M $[NBu_4][ClO_4]$ supporting electrolyte were measured in both conventional and SR / GIXRD flow cells.

Characterization using Physical Measurements

Infrared spectroscopy (IR), scanning electron microscopy (SEM), energy-dispersive X-ray (EDAX) and thermogravimetric analysis were carried out as previously described (32).

Ex situ reflectance microscopy infrared analysis was undertaken on a $Cd(TCNQ)_2$ film that was electrocrystallized from 3.33 mM TCNQ, 1.67 mM $Cd(NO_3)_2$ and 0.1 M $[NBu_4][ClO_4]$ in acetonitrile at an applied potential of -0.38 V vs. aqueous Ag / AgCl (3 M KCl) reference electrode for 30 minutes using the PARSTAT 2263 potentiostat. This instrument utilized a Bruker A590 optical microscope operated at a spot size of 100 mm, and the Bruker IFS66 spectrometer encompassing an MCT detector at 77 K operated using 256 scans at a resolution of 4 cm^{-1}.

Results and Discussion

Metal-TCNQ-based compounds that are of interest in materials science are often coordination polymers that are inherently difficult to characterize by single crystal X-ray diffraction. This difficulty in structural analysis has hampered advances in the field (44). Moreover, these systems are also not readily characterized *in situ* by X-ray powder pattern measurements within an electrochemical environment due to the attenuation of the incident X-ray by the electrolyte solution, whilst *ex situ* methods are susceptible to recrystallization and / or degradation upon removal of the electrode from the electrolyte solution. Herein, we show how the method described by Nafady et.al. (32) for electrochemical synthesis of $Co(TCNQ)_2(H_2O)_2$ can be used to prepare and characterize the related Cd-TCNQ material on the basis of *in situ* SR / GIXRD analysis. This method is based upon electrochemical reduction of TCNQ to $TCNQ^-$ in acetonitrile in the presence of $Cd^{2+}_{(MeCN)}$ ions.

The voltammetric responses obtained with the SR / GIXRD flow-cell (***Figure 8-3 (a)***) exhibit similar features to those observed when the same large area electrode was used in a conventional electrochemical cell (***Figure 8-3 (b)***), and data are compared to those found when a much smaller Pt disk electrode (1.6 mm in diameter) is utilized in normal laboratory based experiments (***Figure***

8-3 (c)). The shift in potential of the reduction and oxidation peaks, found with the large area Pt electrode relative to the 1.6 mm Pt disk, predominantly represents the IR_u drop in the SR / GIXRD cell. Voltammograms obtained in the flowing solution also contain a minor hydrodynamic contribution. However, cyclic voltammograms in the SR / GIXRD cell still allow the voltammetric features associated with the electrocrystallization process to be ascertained. In essence, the main reduction process noted in ***Figure 8-3 (a)*** at E_p^{red} ~ -0.08 V vs. The aqueous Ag / AgCl (3 M KCl) corresponds to the one-electron reduction of TCNQ to $TCNQ^-$ (**Equation 8-1**) followed by rapid precipitation of the Cd-TCNQ material (**Equation 8-2**) via a nucleation-growth process. The oxidation peak at E_p^{ox} = 0.72 V vs. Ag / AgCl (3 M KCl) is then related to removal or stripping of Cd-TCNQ from the electrode surface (**Equation 8-3**).

$$TCNQ_{(MeCN)} + e^- \leftrightarrow [TCNQ]^{\bullet -}_{(MeCN)} \qquad \textbf{Equation 8-3}$$

$$2[TCNQ]^{\bullet -}_{(MeCN)} + Cd^{2+}_{(MeCN)} \xrightarrow{\text{deposition}} Cd[TCNQ]_{2(solid)} \qquad \textbf{Equation 8-4}$$

$$Cd[TCNQ]_{2(solid)} \xrightarrow{\text{stripping}} 2[TCNQ]_{(MeCN)} + Cd^{2+}_{(MeCN)} + 2e^- \qquad \textbf{Equation 8-5}$$

In spite of the significant IR_u drop encountered in the SR / GIXRD cell, a second reduction process at more negative potential (E_P^{red} ~ -0.17 V vs. Ag / AgCl (3 M KCl)) is also found, as in the case of $Co[TCNQ]_2(H_2O)_2$ electrodeposition (32). Thus, two potential dependent pathways for electrocrystallization that give rise to the same product also are available in the $Cd(TCNQ)_2$ system, but with different morphologies. Further details of the electrocrystallization process will be discussed in a future publication. Importantly, since the IR_u drop in the thin layer type SR / GIXRD cell is inversely proportional to the volume of electrolyte solution separating the reference and working electrodes, a distension of the Kapton window and concomitant increase in electrolyte solution layer thickness lessens the influence of IR_u drop in the region of X-ray analysis.

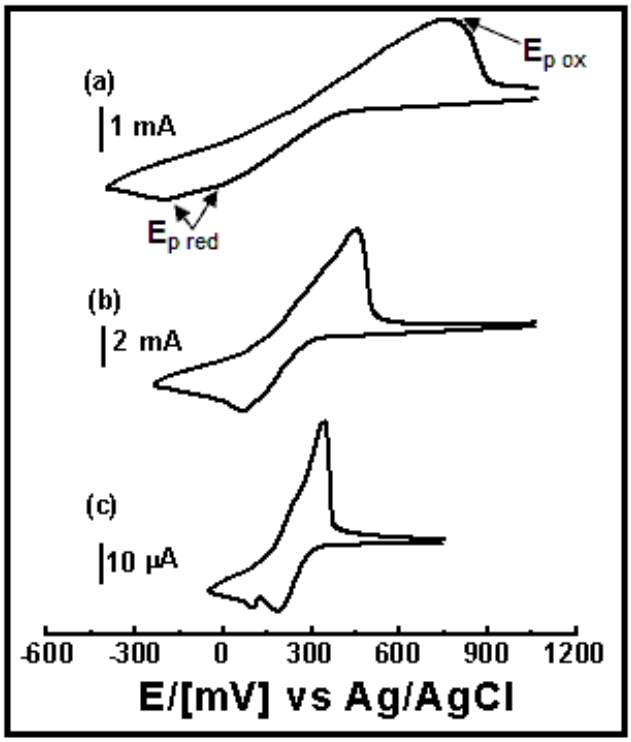

Figure 8-3 *Cyclic voltammograms obtained at a scan rate of 100 mV s^{-1} (295 K) for a mixture of 5.0 mM TCNQ and 2.50 mM $Cd(ClO_4)_2$ in acetonitrile (0.1M $[NBu_4][ClO_4]$) with (a) the large polycrystalline platinum working electrode (area = 2 cm^2) in the SR / GIXRD electrochemical cell and (b) a conventional electrochemical cell. (c) is obtained under the same conditions as (b), but with 1.6 mm diameter Pt disk electrode (area = 0.020 cm^2). Differences in shapes and peak potentials are mainly attributable to IR_u drop.*

Well-defined diffraction patterns are evident for both *in situ* and *ex situ* samples as shown in ***Figure 8-4***. Both solids are attributed to electro-crystallization of $Cd(TCNQ)_2$, as evidenced by the strong correlation of the XRD patterns with those reported for anhydrous $M(TCNQ)_2$ (M = Mn^{2+}, Fe^{2+}, Co^{2+}, Ni^{2+}) materials prepared by chemical methods (44). An additional weak peak, possibly due to small residual amounts of co-precipitated electrolyte (32) was noted in the powder diffraction pattern, as well as preferred orientations in the *in situ* SR-GIXRD patterns at higher angles of incidence. Significantly, ***Figure 8-4***

shows that the majority of Bragg diffraction peaks in the *ex situ* powder XRD pattern are also evident in the *in situ* SR-GIXRD pattern, although several peaks are weaker in the latter case. Last but not least, the relatively large crystallite sizes of the electrodeposited Cd-TCNQ phase compared to the Pt substrate crystallites are inferred by the comparative broadness of the Bragg reflections of the individual phases.

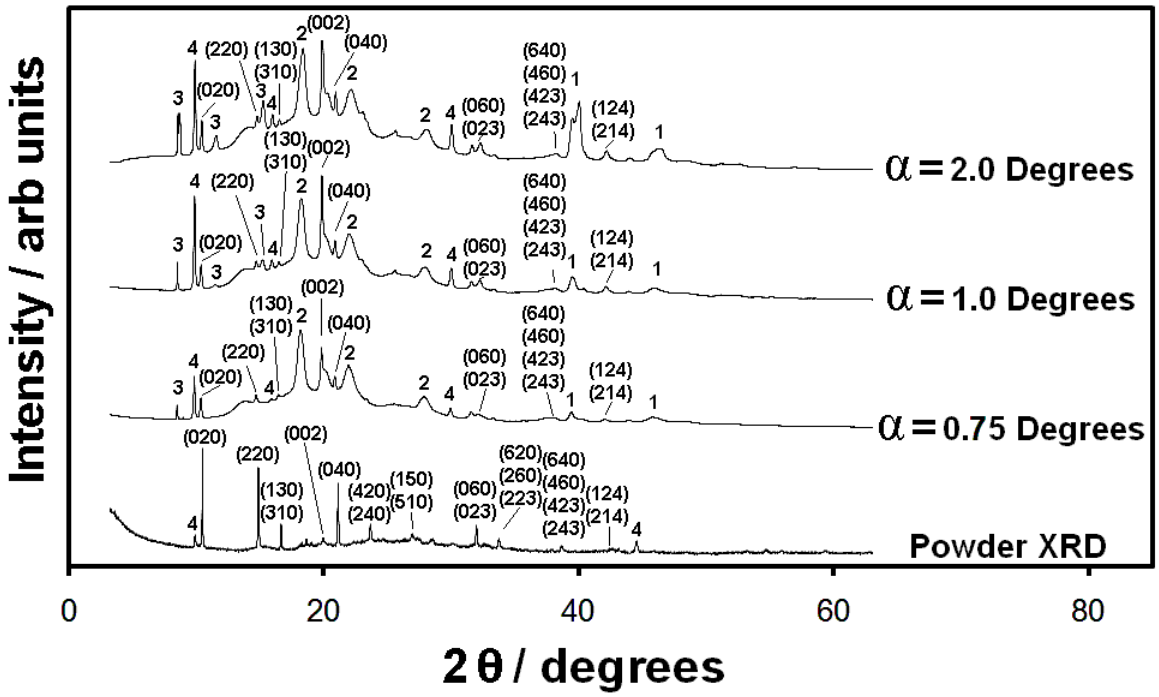

Figure 8-4 *X-ray diffraction plots for in situ SR / GIXRD (upper traces) and conventional powder diffraction (lower trace) of electrochemically synthesized* $Cd(TCNQ)_2$*. All SR / GIXRD 2-theta data are normalized to* $\lambda = 1.5418$ *Å representative of Cu Kα radiation. The diffraction peak assignments are as follows: 1) platinum substrate; 2) Kapton window; 3) small residual amounts of* $[NBu_4][ClO_4]$ *due to occlusion / adsorption of the electrolyte; 4) unidentified peaks.*

An inability to rotate the sample in the beam due to the cable connections to the electrochemical cell facilitates preferred orientation effects in the SR / GIXRD data (17). This is the principal reason for differences between the *ex situ*

and *in situ* SR / GIXRD diffraction patterns, but the diminished signals at α = 0.75 degrees (and to a lesser extent at α = 1 and 2 degrees) are indicative of a high degree of X-ray absorption, scattering and diffraction by the Kapton window and electrolyte solution layer where the pathlength, l, of the beam through the electrolyte solution is high at this low angle of incidence (about 1.222 cm calculated using l = 0.016 / sin α for a 160 μm thick electrolyte solution layer). It is possible to calculate the X-ray transmittance under these conditions using the Beer-Lambert law for light absorption with $\mu(CH_3CN) = 1.081\ cm^{-1}$ yeilding a transmittance of 4.8% at an electrolyte solution thickness of 160 μm, but the absorbance is considerably lower (probably < 10-fold) due to suctioning of the electrolyte solution during stop-flow with the peristaltic pump (obvious to eye and by the detection of diffraction from the electrode substrate) yielding a transmittance of over 73.8%. In any event, the observation of reasonably intense diffraction peaks for $Cd(TCNQ)_2$ and Pt substrate peaks at α = 0.75 and 1.00 degrees reveal that the beam is transmitted sufficiently through the electrolyte solution layer, yielding strong diffraction peaks from the electrode sample (actually not that much different for Pt as compared to a control diffraction pattern [not shown] for a dry and polished Pt electrode in air in the cell that is fitted with a Kapton window prior to any electrolyte solution flow). Note that the powder diffraction data for the Cd-TCNQ based material was refined by using a Pawley refinement of the tetragonal unit cell using a P4 space group and published lattice parameters of $Mn(TCNQ)_2$ (45) as the starting point in the iterative refinement. This led to indexation of the pattern and the following unit cell parameters, a = 16.781 Å and c = 8.829 Å, noting that these values compare favourably with previously published unit cell parameters for $Mn(TCNQ)_2$, $Fe(TCNQ)_2$, $Co(TCNQ)_2$ and $Ni(TCNQ)_2$ (45). Thus, the combined *in situ* and *ex situ* XRD data support the formation of a non-solvated phase of the Cd-TCNQ based material, which is expected to be isostructural with the anhydrous $M(TCNQ)_2$ materials. Furthermore, strong evidence for the presence of the $TCNQ^-$ radical anion and the absence of coordinated water molecules in the electrocrystallized Cd-TCNQ based material was obtained using *ex situ*

FTIR reflection spectroscopy (see ***Figure 8-5***) and thermogravimetric analysis (TGA) on solids generated via reductive bulk electrolysis under similar conditions to those used in the XRD experiments. Thus, the three characteristic IR regions in the spectra of the $M(TCNQ)_2$-based materials, namely the ν(C≡N) (2188(s), 2121(s), 2058(s) cm^{-1}), ν(C=C) (1508 cm^{-1}), and the δ (C-H) band at 823 cm^{-1} are expected for the presence of the $TCNQ^-$ anion radical, not the $[TCNQ]^{2-}$ dianion or neutral TCNQ (45). Note that there was no ClO_4^- band at 933 cm^{-1} indicating that the film was free of significant contamination by the electrolyte. Finally, the absence ν(OH) and δ(OH) bands at about 3400-3300 cm^{-1} and 1640 cm^{-1}, along with the observation of no mass loss up to 220°C in thermogravimetric analysis is unequivocal evidence for anhydrous $Cd(TCNQ)_2$ rather than $Cd(TCNQ)_2(H_2O)_2$.

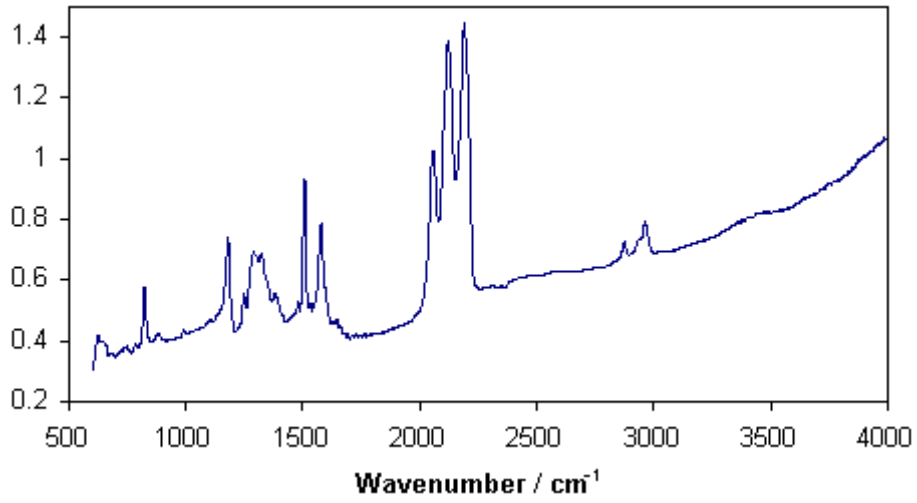

Figure 8-5 *Ex situ reflectance IR spectrum for electrocrystallized $Cd(TCNQ)_2$.*

In summary, it is clear that *in situ* electrochemical-SR / GIXRD measurements can be performed on a material electrocrystallized onto the surface under electrochemical conditions. In the case of electrocrystallized $Cd(TCNQ)_2$ the X-ray data provide high quality information relating to the structure of the generated solids. ***Figure 8-6 (a) - (d)*** present SEM micrographs showing the morphologies of electrocrystallized $Cd(TCNQ)_2$ on the Pt electrode under identical conditions to those utilized in the SR / GIXRD experiments.

Clearly, there is variation in the morphology of the electrocrystallized material in the central and outer regions, associated with the two pathways for electrocrystallization (see *Figure 8-2*). Importantly, around 70% of the electrode-surface area is coated by low-density spherical aggregates (see ***Figure 8-6 (a)***) which represents the area examined in the SR / GIXRD measurements and corresponds to the formation of $Cd(TCNQ)_2$ by ***Equation 8-3*** and ***8-4***. Moreover, measurements of aggregate diameters in the central region of the electrode gave a mean and standard deviation of 32.9 ± 5.6 μm. The observed morphologies and particles sizes produced from repetitive experiments are reproducible within the bounds of experimental uncertainty. Finally, it is noted that the high resolution SEM of the spherical particles [see ***Figure 8-6 (b)***] appears to comprise aggregates of needle-like crystals, similar to the ones observed in the outer region of the electrode [cf. ***Figure 8-6 (d)***]. Accordingly, it is not surprising that the electrocrystallized material observed in the SR / GIXRD cell is crystallographically similar to the powder measured in *ex situ* diffraction studies since the randomly orientated particles in the spherical aggregates are not expected to be highly prone to preferred orientation effects.

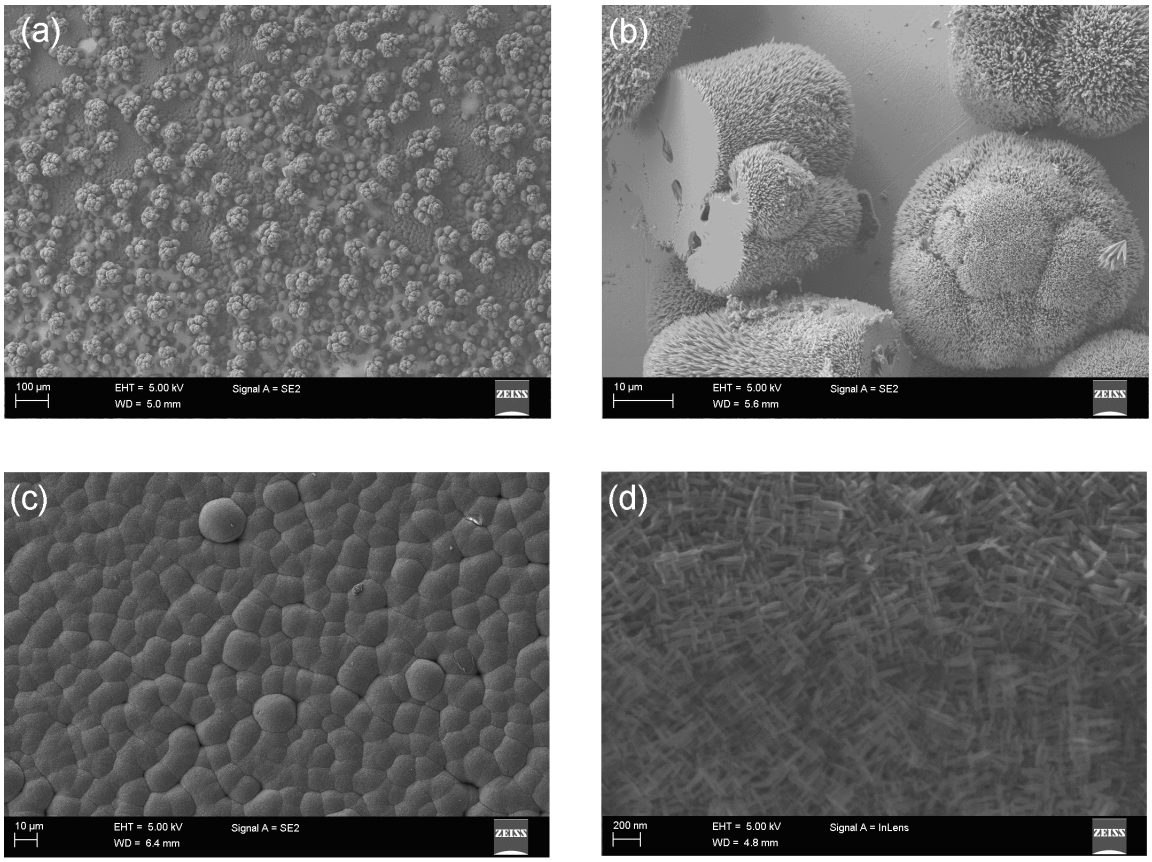

Figure 8-6 *SEM secondary electron micrographs of electrocrystallized $Cd(TCNQ)_2$ in the outer and inner regions of the Pt electrode in the SR / GIXRD cell: (a) low magnification image showing spherical aggregates in the central region; (b) high magnification image of several spherical aggregates showing needle-like agglomerations in the central region; (c) low magnification image of the dense deposit in the outer region; (d) high magnification image showing an intricate network of needle-like crystals for the dense deposit in the outer region.*

Conclusions

A versatile electrochemical cell design has been developed that is capable of simultaneous electrochemical *in situ* SR / GIXRD, or total external reflection X-ray measurements under a variety of experimental conditions. The utility of this cell has been demonstrated in a transient voltammetric study followed by *in situ* SR / GIXRD study of the electrocrystallization of $Cd(TCNQ)_2$

from acetonitrile. Most importantly, this versatile design makes SR / GIXRD suitable for almost any combination of total external reflection X-ray analysis (e.g., GIXRF, GISAXS, GIXRD, etc.) and electrochemical perturbation, also allowing its application acidic, basic, aqueous, non-aqueous, low and high flow pressure conditions.

References

1. Fleischmann M, Oliver A, Robinson J. In situ X-ray diffraction studies of electrode solution interfaces. Electrochim Acta. 1986;31(8):899-906.

2. Brossard F, Etgens VH, Tadjeddine A. In situ surface X-ray diffraction using a new electrochemical cell optimised for third generation synchrotron light sources. Nucl Instrum Methods Phys Res B. 1997;129:419-22.

3. Ball MJ, Lucas CA, Markovic NM, Stamenkovic V, Ross PN. From sub-monolayer to multilayer- an in situ X-ray diffraction study of the growth of Pd films on Pt(111). Surf Sci. 2002;518:201-9.

4. Sathiyanarayanan S, Sahre M, Kautek W. In-situ grazing incidence X-ray diffractometry investigation of phase change processes at the silver / aqueous - halogenide interface. Electrochim Acta. 1998;43:2985-9.

5. Sathiyanarayanan S, Sahre M, Kautek W. In-situ grazing incidence X-ray diffractometry observation of pitting corrosion of copper in chloride solutions. Corros Sci. 1999;41:1899-909.

6. Levi E, Levi MD, Salitra G, Aurbach D, Oesten R, Heider U, et al. Electrochemical and in-situ XRD characterization of $LiNiO_2$ and $LiCo_{0.2}Ni_{0.8}O_2$ electrodes for rechargeable lithium cells. Solid State Ionics. 1999;126:97-108.

7. Johnson CS, Vaughey JT, Thackeray MM, Sarakonsri T, Hackney SA, Fransson L, et al. Electrochemistry and in-situ X-ray diffraction of InSb in lithium batteries. Electrochem Commun. 2000;2:595-600.

8. Rose A, Maniguet S, Mathew RJ, Slater C, Yao J, Russell AE. Hydride phase formation in carbon supported palladium nanoparticle electrodes investigated using in situ EXAFS and XRD. Phys Chem Chem Phys. 2003;5:3220-5.

9. Li J, Herrero E, Abruna HD. The effects of anions on the underpotential deposition of Hg on Au(111) An electrochemical and in situ surface X-ray diffraction study. Colloids and Surf A. 1998;134:113-31.

10. Bramnik NN, Trots DM, Hofmann HJ, Ehrenberg H. Mixed $LiCo_{0.6}M_{0.4}PO_4$ (M = Mn, Fe, Ni) phosphates: cycling mechanism and thermal stability. Phys Chem Chem Phys. 2009;11:3271-7.

11. Bramnik NN, Nikolowski K, Baehtz C, Bramnik KG, Ehrenberg H. Phase Transitions Occuring upon Lithium Insertion-Extraction of $LiCoPO_4$. Chem Mater. 2007;19:908-15.

12. Renner FU, Kageyama H, Siroma Z, Shikano M, Schoder S, Grunder Y, et al. Gold model anodes for Li-ion batteries: Single crystalline systems studied by in situ X-ray diffraction. Electrochim Acta. 2008;53:6064-9.

13. Chang H-H, Chang C-C, Wu H-C, Yang M-H, Sheu H-S, Wu N-L. Study on dynamics of structural transformation during charge/discharge of $LiFePO_4$ cathode. Electrochem Commun. 2008;10:335-9.

14. Kuo S-L, Wu N-L. Electrochemical Capacitor of $MnFe_2O_4$ with Organic Li-Ion Electrolyte. Electrochem and Solid State Lett. 2007;10(7):A171-A5.

15. Rosciano F, Holzapfel M, Kaiser H, Scheifele W, Ruch PW, Hahn M, et al. A multi-sample automatic system for in situ electrochemical x-ray diffraction synchrotron measurements. J Synch Rad. 2007;14:487-91.

16. Wiltshire RJK, King CR, Rose A, Wells PP, Hogarth MP, Thompsett D, et al. A PEM fuel cell for in situ XAS studies. Electrochim Acta. 2005;50:5208-17.

17. Knapp M, Carsten B, Ehrenberg H, Fuess H. The synchrotron powder diffractometer at beamline B2 at HasYLAB/DESY: status and capabilities. J Synch Rad. 2004;11:328-34.

18. Ruch PW, Hahn M, Rosciano F, Holzapfel M, Kaiser H, Scheifele W, et al. In situ X-ray diffraction of the intercalation of $(C_2H_5)_4N^+$ and BF_4^- into graphite from acetonitrile and propylene carbonate based supercapacitor electrolytes. Electrochim Acta. 2007;53:1074-82.

19. Russell AE, Maniguet S, Mathew RJ, Yao J, Roberts MA, Thompsett D. In situ X-ray absorption spectroscopy and X-ray diffraction of fuel cell electrocatalysts. J Power Sources. 2001;96:226-32.

20. Lampitt RA, Carrette LPL, Hogarth MP, Russell AE. In situ and model EXAFS studies on electrocatalysts for methanol oxidation. J Electroanal Chem. 1999;460:80-7.

21. Rose A, Crabb EM, Qian Y, Ravikumar MK, Wells PP, Wiltshire RJK, et al. Potential dependance of segregation and surface alloy formation of a Ru modified carbon supported Pt catalyst. Electrochim Acta. 2007;52:5556-64.

22. Rose A, Bilsborrow R, King CR, Ravikumar MK, Qian Y, Wiltshire RJK, et al. In situ Ru K-edge EXAFS of CO adsorption on a Ru modified Pt/C fuel cell catalyst. Electrochim Acta. 2009;54(22):5262-6.

23. Ingham B, Illy BN, Ryan MP. Direct Observation of Distinct Nucleation and Growth Processes in Electrochemically Deposited ZnO Nanostructures Using in Situ XANES. J Phys Chem C. 2008;112:2820-4.

24. Smith MC, Gilbert JA, Mawdsley JR, Seifert S, Myers DJ. In Situ Small-Angle X-ray Scattering Observation of Pt Catalyst Particle Growth During Potential Cycling. J Am Chem Soc. 2008;130:8112-3.

25. Russell AE, Rose A. X-ray Absorption Spectroscopy of Low Temperature Fuel Cell Catalysts. Chem Rev. 2004;104(10):4613-35.

26. De Marco R, Jiang Z-T, John D, Sercombe M, Kinsella B. An in situ electrochemical impedance spectroscopy / synchrotron radiation grazing

incidence X-ray diffraction study of the influence of acetate on the carbon dioxide corrosion of mild steel. Electrochim Acta. 2007;52:3746-50.

27. De Marco R, Jiang Z-T, Pejcic B, Poinen E. An In Situ Synchrotron Radiation Grazing Incidence X-Ray Diffraction Study of Carbon Dioxide Corrosion. J Electrochem Soc. 2005;152(10):B389-B92.

28. De Marco R, Pejcic B, Prince K, van Riessen A. A multi-technique surface study of the mercury(II) chalcogenide ion-selective electrode in saline media. Analyst. 2003;128(6):742-9.

29. Ocko BM, Wang J. *In Situ* X-Ray Reflectivity and Diffraction Studies of the Au(001) Reconstruction in an Electrochemical Cell. Phys Rev Lett. 1990;65(12):1466-9.

30. Davenport AJ, Oblonsky LJ, Ryan MP. The structure of the passive film that forms on iron in aqueous environments. J Electrochem Soc. 2000;147:2162-73.

31. Ingham B, Illy BN, Toney MF, Howdyshell ML, Ryan MP. In Situ Synchrotron X-ray Diffraction Experiments on Electrochemically Deposited ZnO Nanostructures. J Phys Chem C. 2008;112:14863-6.

32. Nafady A, Bond AM, Bilyk A, Harris AR, Bhatt AI, O'Mullane AP, et al. Tuning the Electrocrystallization Parameters of Semiconducting $Co[TCNQ]_2$-Based Materials to Yield either Single Nanowires or Crystalline Thin Films. J Am Chem Soc. 2007;129(8):2370-82.

33. Hudson TA, Robson R. A New Class of TCNQ Derivatives Easily Generated from $TCNQH_2$ Containing Discrete $TCNQ^{2-}$ Anions and Noncoordinating Cations. Cryst Growth Des. 2009;9(4):1658-62.

34. Arena A, Mezzasalma AM, Patane S, Saitta G. Investigation of the novel charge transfer complex Cd-TCNQ. J Mater Res. 1997;12(7):1693-7.

35. Miyasaka H, Motokawa N, Matsunaga S, Yamashita M, Sugimoto K, Mori T, et al. Control of Charge Transfer in a Series of $Ru_2^{II,II}$/TCNQ Two-Dimensional Networks by Tuning the Electron Affinity of TCNQ Units: A Route to Synergistic Magnetic/Conducting Materials. J Am Chem Soc. 2010;132:1532-44.

36. Wakida S-i, Ujihira Y. Chemically Modified Copper Hybrid Ion Sensor with 7,7,8,8-Tetracyanoquinodimethane. Jpn J Appl Phys. 1988;27:1314-6.

37. Zhou W, Ren L, Lin F, Jiao L, Xue T, Xian X, et al. An electrical switch based on Ag-tetracyanoquinodimethane sandwiched by crossed carbon nanotube electrodes. Appl Phys Lett. 2008;93(12):123115/1-/3.

38. Zegenhagen J, Renner FU, Reitzle A, Lee TL, Warren S, Stierle A, et al. In situ X-ray analysis of solid/electrolyte interfaces: electrodeposition of Cu and Co on Si(111): H and GaAs(001) and corrosion of Cu_3Au(111). Surf Sci. 2004;573:67-9.

39. Herron ME, Doyle SE, Roberts KJ, Robinson IK, Walsh FC. Instrumentation and cell design for *in situ* studies of electrode surfaces using x-ray synchrotron radiation. Rev Sci Instrum. 1992;63:950-5.

40. Barlow N, Brennan C, Doyle SE, Greaves GN, Miller M, Nahle AH, et al. Instrumentation and data acquisition for *in situ* electrochemistry at the Daresbury SRS. Rev Sci Instrum. 1989;60(7):2386-9.

41. Tidswell IM, Markovic NM, Lucas CA, Ross PN. *In situ* x-ray-scattering study of the Au(001) reconstruction in alkaline and acidic electrolytes. Phys Rev B. 1993;47(24):16542-53.

42. Vineyard GH. Grazing-incidence diffraction and the distorted-wave approximation for the study of surfaces. Phys Rev B. 1982;26(8):4146-59.

43. Veder J-P, Nafady A, De Marco R, Bond AM. A Combined Voltammetric/Synchrotron Radiation-Grazing Incidence X-ray Diffraction

Study of the Electrocrystallization of Zinc Tetracyanoquinodimethane. 2010:In Preparation.

44. Zhao H, Heintz R, Ouyang X, Dunbar KR. Spectroscopic, Thermal, and Magnetic Properties of Metal/TCNQ Network Polymers with Extensive Supramolecular Interactions between Layers. Chem Mater. 1999;11:736-46.

45. Clerac R, O'Kane S, Cowen J, Ouyang X, Heintz R, Zhao H, et al. Glassy Magnets Composed of Metals Coordinated to 7,7,8,8-tetracyanoquinodimethane: $M(TCNQ)_2$ (M=Mn, Fe, Co, Ni). Chem Mater. 2003;15:1840-50.

Chapter Nine

9 A Combined Voltammetric / GIXRD Study of the Electrocrystallization of Zinc Tetra-cyanoquinodimethane

Jean-Pierre Veder, Ayman Nafady, Graeme Clarke, Roland De Marco and Alan Bond.

Physical Chemistry Chemical Physics, **In Preperation** (2010).

Abstract – A new approach for exploring *in situ* the electrocrystallization of zinc tetracyanoquinodimethane (TCNQ) is presented in this qualitative study, where a potential dependent synchrotron radiation / grazing incidence X-ray diffraction (SR / GIXRD) study was performed at several applied potentials in the vicinity of and at the observed cyclic voltammetry (CV) peak for reduction of TCNQ to $TCNQ^{-}$ and subsequent electrodeposition of the Zn-TCNQ material.

Introduction

Tetracyanoquinodimethane (TCNQ) materials incorporating zinc as the electron acceptor have been previously reported as exhibiting interesting electrical switching properties(1), which have far reaching implications in the field of nanotechnology; namely, the fabrication of micro-and-nanoelectronic devices. Despite the novel characteristics observed in these materials, Zn-TCNQ materials have received very little attention, in terms of their structural characterisation. Accordingly, the structure of the $Zn(TCNQ)_2$ material is hitherto

unresolved. Clearly, there is a need for an enhanced understanding of the $Zn(TCNQ)_2$ system, so as to properly exploit the unique properties of this material.

In this communication, we have used a previously developed electrochemical cell (2) (***Chapter 8***), with a capability of carrying out in situ SR / GIXRD measurements, and implemented it in a qualitative study of a "potential map" of the peak reduction potential for the electrocrystallization of the Zn(TCNQ)2 material. This study is not only carried out with the intention of demonstrating the capability of the newly developed electrochemical cell (i.e. proof of concept), but also with a view of elucidating factors that affect the electrodeposition process for metal-TCNQ materials using a general method that is applicable to any electrodeposited material.

Results and Discussion

Figure 9-1 (a) presents a cyclic voltammogram for the reduction of 5mM TCNQ in the presence of 2.5mM $Zn(NO_3)_2$ in acetonitrile (0.1M $[NBu_4][ClO_4]$) at a platinum electrode in the SR / GIXRD electrochemical cell[6]. Also included for comparison is the cyclic voltammogram obtained in the same electrolyte, but using a conventional three electrode electrochemical cell [see ***Figure 9-1 (b)***]. It can be seen that the shapes of the features in the two voltammograms are quite similar, however, the thin electrolyte layer in the *in situ* SR-GIXRD cell displays an offset in the reduction and oxidation waves. Nevertheless, despite the ohmic

[6] Prior to electrocrystallisation, acetonitrile solution containing 0.1M tetrabutylammonium perchlorate, 5 mM TCNQ and 2.5 mM zinc nitrate was passed through the cell by use of a peristaltic pump and organic resistant tubing, at a high flow rate so as to allow a significant distension of the Kapton film and hence avoid excessive ohmic (IR) drop otherwise encountered with the electrolyte thickness of less than 160 micron under static conditions. After electrodeposition of the Zn-TCNQ material utilizing a portable Princetone Applied Research PARSTAT 263 potentiostat to undertake chronoamperometry at the selected potential for 10 minutes, the flow rate of the electrolyte was gradually reduced so as to minimize disturbances in the uniformity of the electrodeposited solid caused by a sudden fluctuation in the electrolyte flow. Finally, the peristaltic pump was switched off, which caused a slight suctioning of solution. The very thin layer of electrolyte condition (i.e. ≤ 160 micron) now present does not significantly attenuate the incident in situ X-ray beam, thereby yeilding excellent X-ray diffraction patterns.

(IR) drop at the electrode, there are certainly discernable voltammetric features, as has been noted elsewhere (2) (***Chapter 8***). It is clearly evident in both of the voltammetric traces that there is a well defined peak occurring at negative potentials indicative of the electrochemical reduction of TCNQ to $TCNQ^-$ with subsequent precipitation of the $Zn(TCNQ)_2$ material. On the reverse scan at more positive potentials, $TCNQ^-$ is oxidised back to TCNQ which is accompanied by the dissolution of $Zn(TCNQ)_2$ (3). Clearly, the reduction wave was the peak of interest for the electrocrystallization of the $Zn(TCNQ)_2$ material. More specifically, the cyclic voltammogram in ***Figure 9-1 (a)***[7] shows a voltammetric reduction peak at -0.4V against the *in built* solid-state Ag / AgTCNQ reference electrode[8], and this prompted the present chronoamperometric study of the electrocrystallization of $Zn(TCNQ)_2$ material at three applied potentials, viz., -0.3 V (voltage more positive than the peak reduction potential), -0.4 V (voltage at the peak reduction potential) and -0.5 V (voltage more negative than the peak reduction potential).

[7] Because the CV curves are obtained in high flow rate solutions in the GIXRD cell, a small hydrodynamic contribution is evident in the voltammogram. Such a hydrodynamic contribution is unavoidable due to the fact that the solution IR drop is dominant if low flow rates are instead used and, as a result, it would not be possible to observe well-defined reduction and oxidation processes in such an instance.

[8] As mentioned in ***Chapter 8***, due to the instant deposition of AgTCNQ material on the silver wires on exposure to TCNQ solution, the practical reference electrode used in this study is actually Ag/AgTCNQ.

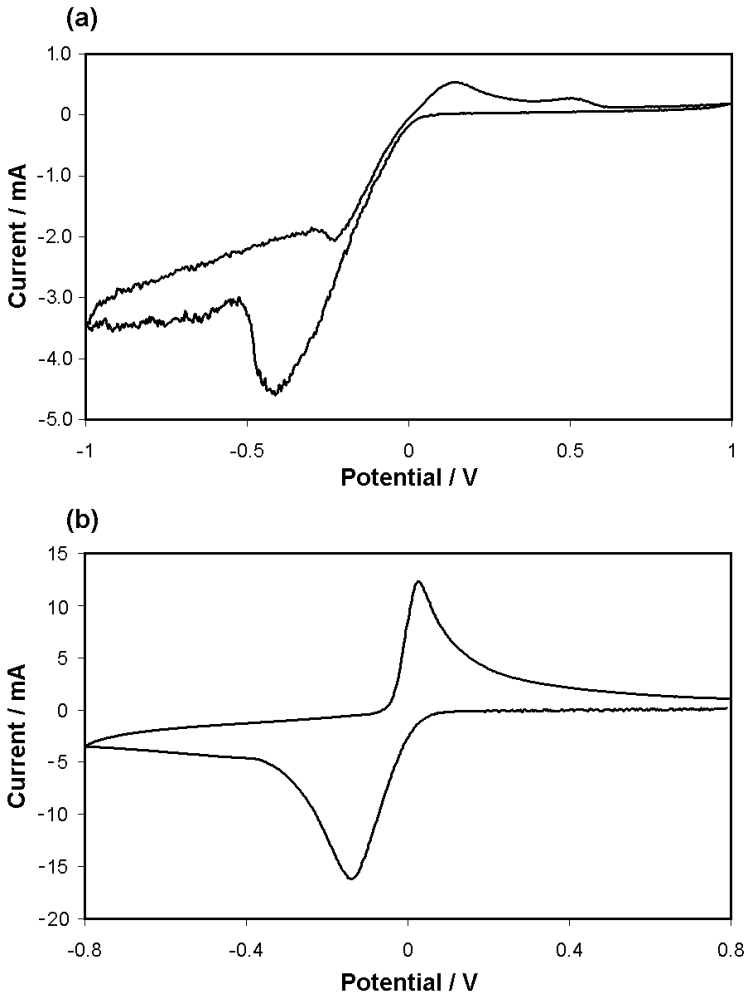

Figure 9-1 *Cyclic voltammograms (CVs) for the formation of $Zn(TCNQ)_2$ from an acetonitrile electrolyte comprising 5 mM TCNQ and 2.5 mM $Zn(NO_3)_2$ in acetonitrile (0.1 M $[NBu_4][ClO_4]$): (a) as measured in the SR / GIXRD electrochemical cell and (b) as measured in a conventional 3 electrode laboratory cell. Both of the measurements were carried out against a Ag/AgTCNQ reference electrode.*

SR / GIXRD depth profiles for electrocrystallized Zn-TCNQ at the aforementioned applied potentials are presented in ***Figure 9-2***, whereby the angle of incidence of the SR was altered from the starting angle of 0.5 degrees, so as to probe the electrocrystallized material at different sampling depths. Each variation in the angle of incidence was accompanied by a systematic alteration in the vertical slit aperture of the beam, so as to ensure that the same volume of

sample was irradiated by the incident X-ray beam utilizing a constant beam footprint on the sample. Such an analysis was carried out so as to examine the crystallographic properties of the elctrocrystallized material at differring depths as opposed to just the bulk specimen. Accordingly, it is possible to estimate the film thicknesses using the linear attenuation coefficient of the X-rays passing through the metal-TCNQ material, as shown in **Equation 9-1**. At the angles of incidence, *α*, utilized in this study, the depth of penentration, *d*, of the externally reflected beam can be calculated using the expression (4):

$$d = \frac{2\alpha}{\mu}$$ **Equation 9-1**

where μ is the linear attenuation coefficient of the beam by the sample, viz., d = 8.7, 13.0, 17.4, 26.0 and 34.7 μm at angles of incidence of 0.50, 0.75, 1.00, 1.50 and 2.00 degrees given that m for Zn-TCNQ material is estimated to be 20.12 cm^{-1} based on a previous calculation for $Co(TCNQ)_2$ (5).

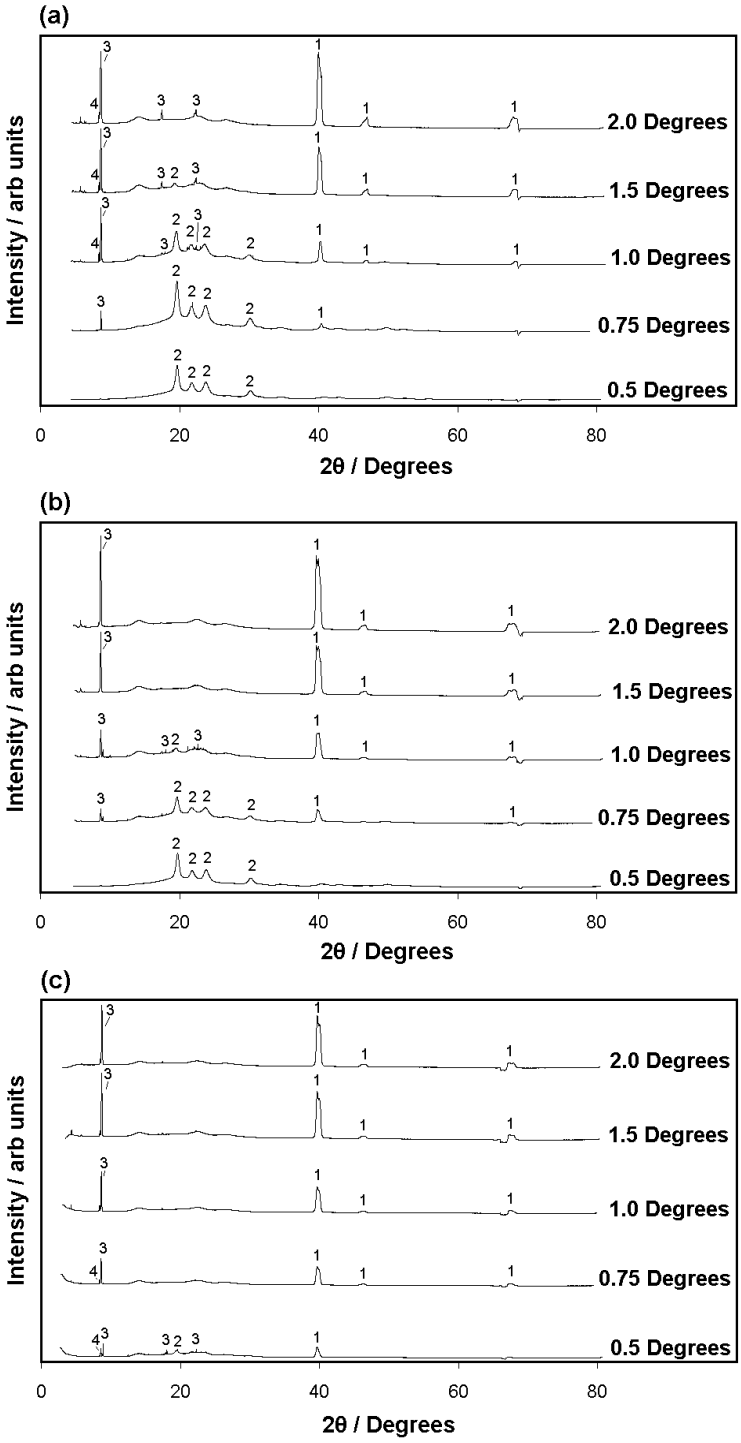

Figure 9-2 *SR / GIXRD depth profiles of the electrocrystallized $Zn(TCNQ)_2$ at reduction potentials of (a) -0.3 V, (b) -0.4 V and (c) -0.5 V. Peaks are labelled as follows: 1) Pt substrate; 2) polymer crystalline phases; 3) $Zn(TCNQ)_2$; 4) unidentified peaks. All diffraction patterns were normalized to the wavelength for Cu Kα radiation (i.e., λ = 1.5418 Å).*

For all diffraction patterns presented in ***Figure 9-2***, the diffraction peaks for the $Zn(TCNQ)_2$ material compare favourably with other M(II)-TCNQ (where M = Mn, Ni, Fe, & Co) phases; these compounds are isostructural (6). Nevertheless, the differences in relative intensities of the observed diffraction peaks for the electrocrystallized Zn-TCNQ material, as compared to the literature diffraction patterns of the isostructural M(II)-TCNQ phases (6), is indicative of a strong preference for electrocrystallization along certain crystallographic planes. This outcome is not unexpected since crystal growth via electrochemical methods is known to occur in harmony with the electrical field lines in the system, as reported in the electrocrystallization of other metal-TCNQ materials (5, 7).

Interestingly, the results shown in the SR / GIXRD depth profiles suggest the formation of a dual layer of electrocrystallized material, whereby the composition consists of an amorphous overlayer and a highly crystalline underlayer. This is evidenced by the appearance of many sharp diffraction peaks associated with the Zn-TCNQ material (8.7 μm < d ≤ 13.0 μm for $0.50^o \leq \alpha \leq 0.75^o$) at -0.3V, while the distinctive diffraction peaks occur earlier in the depth profile for the electrocrystallized Zn-TCNQ material at an overpotential of -0.5V. Furthermore, since the platinum peaks are not evident at $\alpha = 0.5^o$ (d = 8.7 μm) for applied potentials of -0.3 and -0.4 V, this infers a diffuse, thick and amorphous surface layer that prevents the X-ray beam from penetrating to the underlying platinum substrate also comprising the crystalline electrodeposited $Zn(TCNQ)_2$ sublayer. Essentially, the poorly crystalline over-layer would not be detectable using the SR / GIXRD technique. The electrocrystallized Zn-TCNQ diffraction peaks only become apparent at deeper sampling depths (i.e. $0.50^o < \alpha < 0.75^o$ and 8.7 μm < d < 13.0 μm), which is indicative of a crystalline underlayer that presumably grows at nucleation sites beneath the amorphous electrocrystallized Zn-TCNQ material. This outcome has not been witnessed in previous studies of metal-TCNQ phases. However, it should be noted that other

reports on the structural characterization of M-TCNQ materials via SEM, TEM, XRD, etc., are carried out *ex situ*. Accordingly, removal of the M-TCNQ electrocrystallized material from the electrolyte in these *ex situ* studies is probably the reason for these disparate results. It is likely that withdrawal of the M-TCNQ material from its native environment embodying electrolyte and the applied electric field will lead to further crystallization (8), which is seeded to growth by the amorphous or nanocrystalline overlayer. Also possible is a phase transformation of the amorphous or nanocrystalline material into a highly crystalline hydrated material when brought into contact with high vacuum and probing beams during *ex situ* surface analysis (9). The present findings may account for the initially inexplicable crystalline nature of many M-TCNQ materials when analysed via other forms of ex situ structural analysis; a characteristic which was unexpected due to their rapid precipitation (6). At increased depths, especially with the electrocrystallized $Zn(TCNQ)_2$ material at -0.4 and -0.5V, the disappearance of some of the $Zn(TCNQ)_2$ diffraction peaks is indicative of preferred orientation in regions away from the surface boundaries of the electrodeposited material.

As for the film electrocrystallized at the overpotential of -0.5V, the immediate appearance of several distinctive peaks associated with the $Zn(TCNQ)_2$ material at $\alpha = 0.5^{o}$ (d = 8.7 μm) as well as the appearance of Pt substrate peaks, signifies the preferential transformation of the amorphous overlayer into a dense and thin crystalline layer of the $Zn(TCNQ)_2$ material. Here, it is hypothesized that the amorphous overlayer has a tendency to undergo a solid-phase transformation yielding a thinner and tightly packed film of nanocrystallites, or a thin highly crystalline film. Significantly, this theory is supported by voltammetric data (Nafady, personal communication) which revealed an additional electrochemical process (solid-phase transformation) just above the peak reduction potential, as well as scanning electron microscopy evidence (Nafady, personal communication) of a topography and morphology for a denser and tightly packed electrocrystallized material generated under these

conditions.

Conclusions

The results of this study are significant in demonstrating the complementarity of SR / GIXRD measurements and electrochemical techniques. Since the electrocrystallized material can be examined in its natural electrochemical environment, SR / GIXRD can be used to detect subtle differences in the crystallization pattern of electrocrystallized materials at different reduction potentials. The two-phase electrocrystallization of the Zn-TCNQ material (i.e. the amorphous surface layer and the crystalline sublayer) is a significant finding for electrochemically controlled growth and synthesis of Zn-TCNQ materials, where it is evident that the potential employed in the electrocrystallization process can be used to control the morphology of the material due to the nature of the amorphous nucleation layer. This important finding, which is not solely applicable to the M-TCNQ materials, but other electrocrystallized phases, could be a major factor in determining the suitability of electrocrystallized materials for various applications at different applied potentials.

References

1. Ding G, Cheng Y, Dalin Y, Renyuan Q. Electrical switching effect in some TCNQ-ion-radical salt powder compaction. Yingyong Kexue Xuebao. 1987;5(2):159-63.

2. Veder J-P, Nafady A, Clarke G, Williams RP, De Marco R, Bond AM. A Flow Cell for Transient Voltammetry and its Application to In Situ Grazing Incidence X-ray Diffraction Characterization of Electrocrystallised $Cd(TCNQ)_2$. Electrochim Acta. 2010;Submitted.

3. Nafady A, O'Mullane AP, Bond AM, Neufeld AK. Morphology Changes and Mechanistic Aspects of the Electrochemically-Induced Reversible Solid-Solid Transformation of Microcrystalline TCNQ into $Co[TCNQ]_2$-Based Materials (TCNQ=7,7,8,8-tetracyanoquinodimethane). Chem Mater. 2006;18:4375-84.

4. Vineyard GH. Grazing-incidence diffraction and the distorted-wave approximation for the study of surfaces. Phys Rev B. 1982;26(8):4146-59.

5. Nafady A, Bond AM, Bilyk A, Harris AR, Bhatt AI, O'Mullane AP, et al. Tuning the Electrocrystallization Parameters of Semiconducting $Co[TCNQ]_2$-Based Materials to Yield either Single Nanowires or Crystalline Thin Films. J Am Chem Soc. 2007;129(8):2370-82.

6. Clerac R, O'Kane S, Cowen J, Ouyang X, Heintz R, Zhao H, et al. Glassy Magnets Composed of Metals Coordinated to 7,7,8,8-tetracyanoquinodimethane: $M(TCNQ)_2$ (M=Mn, Fe, Co, Ni). Chem Mater. 2003;15:1840-50.

7. Qu X, Nafady A, Mechler A, Zhang J, Harris AR, O'Mullane AP, et al. AFM study of morphological changes associated with electrochemical solid-solid transformation of three dimensional crystals of TCNQ to metal

derivatives (metal=Cu, Ni; TCNQ=tetracyanoquinodimethane). J Solid State Electrochem. 2008;12:739-46.

8. O'Mullane AP, Neufeld AK, Harris AR, Bond AM. Electrocrystallization of Phase I, CuTCNQ (TCNQ = 7,7,8,8-Tetracyanoquinodimethane), on Indium Tin Oxide and Boron-Doped Diamond Electrodes. Langmuir. 2006;22:10499-505.

9. Zhao H, Heintz R, Ouyang X, Dunbar KR. Spectroscopic, Thermal, and Magnetic Properties of Metal/TCNQ Network Polymers with Extensive Supramolecular Interactions between Layers. Chem Mater. 1999;11:736-46.

Supplementary Information

Reagents

Analytical reagent grade $Zn(NO_3)_2$ was obtained from BDH Laboratory Reagents, whilst TCNQ (98%) and $[NBu_4][ClO_4]$ were purchased from Aldrich. Acetonitrile, which was used as the electrolyte solvent was HPLC grade and sourced from Omnisolv. All reagents were used as received from the suppliers.

Instrumentation

All *in situ* voltametric and SR / GIXRD measurements were undertaken on Beamline 20B at the Photon Factory in Tsukuba, Japan, using the "BIGDIFF" diffractometer. This instrument employs a Si(111) channel cut monochromator which was set to deliver a wavelength of 1.000 Å, so as to minimize the attenuation of the incident X-ray beam by air and the electrolyte. Parallel beam optics were also used to provide an incident beam that was 100 μm and 2 mm in the vertical and horizontal directions, respectively. The vertical dimension of the beam was systematically altered prior to each change in angle of incidence so as to provide a constant beam footprint. All GIXRD measurements were taken at angles between 0.1° and 2° using an exposure time of 20 minutes onto Fuji imaging plates. The platinum electrode diffraction pattern was used as an internal standard for calibration of the synchrotron beam wavelength, yielding an actual value of 0.9962 Å. All SR / GIXRD data has been normalized to a 2-theta scale of λ = 1.5418 Å for Cu Ka radiation.

Electrochemical experiments were carried out on the voltametric / GIXRD cell (1) (detailed in ***Chapter 8***) using a commercially available portable Princeton Applied Research PARSTAT 2263 potentiostat. The electrolyte was pumped at extremely high flow rates (415 mL min^{-1}) using a Masterflex peristaltic pump to purposely induce a distension in the Kapton window, and acetonitrile resistant Masterflex Norprene® tubing was used in the flow circuit.

References for Supplementary Information

1. Veder J-P, Nafady A, Clarke G, Williams RP, De Marco R, Bond AM. A Flow Cell for Transient Voltammetry and its Application to In Situ Grazing Incidence X-ray Diffraction Characterization of Electrocrystallised $Cd(TCNQ)_2$. Electrochim Acta. 2010;Submitted.

Chapter Ten

10 Conclusions

The techniques, methods and results presented in this thesis are of significant value to electrochemists because they not only contribute to current knowledge pertaining to water uptake and ion-to-electron transduction in solid-contact ion-selective electrodes (SC ISEs), as well as structure elucidation of metal-tetracyanoquinodimethane (TCNQ) materials, but they also provide electrochemists with a powerful set of surface characterization techniques for investigation of other complex electrochemical systems. The following sections present concise chapter-by-chapter conclusions of the results obtained and the methods employed in the research carried out in this thesis.

Electrochemistry and Synchrotron Radiation: A Review

A review of the compatibility of synchrotron radiation (SR) and electrochemistry was provided in ***Chapter 2***. This review was prepared and published in response to an invitation to the authors to contribute to a special issue of *Trends in Analytical Chemistry* on SR. The concepts associated with combining SR with electrochemistry were discussed and the most recent applications of characterization approaches were presented.

Undesirable Water Layers in Coated Wire Electrodes (CWEs)

Prior to undertaking this research, the undesirable formation of water at the buried interfaces of solid-contact ion-selective electrodes (SC ISEs) was a theorized phenomenon and, as such, there was no direct evidence to provide

confirmation of water layer formation, let alone the extent to which SC-ISEs were affected. The side-effects associated with such a phenomenon had long plagued analytical chemists utilizing SC-ISEs for long-term applications, however, very little research had been undertaken to characterize the water layer. This was mainly due to the lack of an appropriate methodology, not to mention the immense difficulties associated with the characterization of such a problem.

The research undertaken in ***Chapter 3*** was carried out on a SC-ISE system which is widely acknowledged as having instability problems associated with water layers. The system in question was that of CWEs coated with ion-selective plasticized poly(vinylchloride) (PVC) membranes. Using a combination of techniques, namely neutron reflectometry (NR), electrochemical impedance spectroscopy (EIS) and secondary ion mass spectrometry (SIMS), the research was able to provide unequivocal evidence for the formation of a well defined water layer at the ion-selective / conductive substrate interface. The use of EIS was ultimately able to provide a cheap and effective means of signaling the emergence of a water layer at the buried interface through a diminution in the contact resistance of the ion-selective membrane to the electrically conducting substrate. The formation of water at the interface was evident after as little as 3 hours of constant bathing in solution. No distinct changes in the EIS spectra after 20 hours indicated that the penetration of water had acquired an equilibrium. The formation of a water layer was also confirmed through NR which showed that the water had penetrated the membrane to form a 100 - 120Å thick water layer within a 20 hour timeframe of the measurements. A discrepancy between the neutron scattering length densities of the electrolyte and the water layer at the buried interface was consistent with the leaching of plasticizer from the ion-selective membrane into the electrolyte and the undesirably formed water layer. Finally, the application of SIMS in the *ex situ* study of the buried interface revealed surpluses of ionic species, which is indicative of the transportation of water and ions across the membrane.

Using Hydrophobic Polymer Components to Eliminate Undesirable Water Layers in SC-ISEs

In order to combat the major problem associated with the formation of water layers at the buried interfaces of SC-ISEs, it was logical to explore the effect that highly hydrophobic polymer components would have on combating the problem. ***Chapter 4*** introduced the concept of using a hydrophobic poly(methylmethacrylate) / poly(decylmethacrylate) (PMMA / PDMA) copolymer as the ion-selective membrane support in the hope of preventing the diffusion of water through to the interface. EIS studies of a PMMA / PDMA copolymer CWE established that water was indeed able to penetrate through to the buried interface, however at a significantly lower rate when compared to plasticized PVC CWEs. Essentially the ingression of water at the buried interface of a regular CWE took place over a time frame 20 times greater than that of plasticized PVC. This was also validated through the extremely powerful combination of tandem EIS and in situ NR measurements, which was able to provide an indication of the development of water at the buried interface. Such an indication was provided through a reduction in membrane contact resistance, as evidenced through EIS, and a severe roughening of the buried interface, as demonstrated by NR. Although NR was able to provide such an indication, it was unable to establish direct and unequivocal evidence for the presence of water at the interface since the water was unable to accumulate into a well defined water layer under these conditions. Small angle neutron scattering (SANS) was subsequently used to determine the internal nature of the ion-selective membrane and to establish if water was present as nanoinclusions within the membrane. Interestingly, SANS revealed the presence of inhomogeneities within the conventional plasticized PVC ion-selective membranes which corresponded to areas in which water and plasticizer had accumulated in a freezable form. In contrast, the copolymer ion-selective membrane showed no evidence of inhomogeneities within the membrane.

Finally, an *ex situ* SIMS study was undertaken to explore the presence of salt residues from evaporated electrolyte at a buried interface that had been recently exposed for analysis. Whilst a depth profile failed to reveal any excess of ionic species at the buried interface, SIMS imaging was able to reveal “hot spots” at which trace amounts of salt residue existed in detectable quantities. SIMS depth profiles were unable to reveal ion surpluses, while SIMS imaging could due to the scarcity of localized regions of water over the surface. Accordingly, it was suggested that this effect is the result of the formation of small water droplets at the interface rather than a continuous water layer.

In this study no technique was able to detect or indicate the presence of traces of water at the buried interfaces when a hydrophobic underlayer of poly(3-octylthiophene-2,5-diyl) (POT) was used as the ion-to-electron transducer despite the extensive lengths of time at which the SC ISEs were exposed to water. It was established that the hydrophobic POT underlayer was not only essential in converting ionic flow into electrical flow and hence providing a stable response, but it also prevented the formation of a water layer by eliminating sites at which water can accumulate (i.e. imperfections in the ion-selective polymer coating). Additionally, POT proved to be a further deterrent to water due to its hydrophobic nature.

Using Hydrophilic Solid-Contacts as a Means of Preventing Water Layer Formation

The popular use of poly(3,4-ethylenedioxythiophene) doped with poly(styrenesulfonate) (PEDOT:PSS) as an ion-to-electron transducing solid-contact warranted a study to reveal if such a system would be susceptible to the formation of an undesirable water layer. Although PEDOT is hydrophobic in nature, PSS is added as a charge balancing polymer to allow PEDOT’s suspension in water and, as such, the PEDOT:PSS system is often classified as hydrophilic. ***Chapter 5*** sought to investigate if PEDOT:PSS was suitable for use

as a solid-contact in long-term sensor applications through the use of a previously utilized methodology combining NR, EIS and SIMS to study if water was formed at the buried interface. Additionally, synchrotron radiation / Fourier transform-infrared microspectroscopy (SR / FT-IRM) was used to provide a visual depiction of water formed at the buried interface of a PVC CWE. Essentially, the combination of NR and EIS was able to establish that water was indeed transported through the PVC membrane (as expected from earlier studies with PVC CWEs); however, water was not found to accumulate in a freezable form at the buried interfaces. Instead, the continual increase in neutron scattering length density of the PEDOT:PSS solid-contact, in conjunction with an associated gradual increase in thickness, signalled the absorption of water into the PEDOT:PSS sub-layer. In essence, the PEDOT:PSS acted like a sponge and scavenged any traces of water. This was further validated through the associated EIS findings that showed no reduction in the membrane contact resistance which would have been indicative of a separate phase of water inducing a diminution in the contact resistance between the SC and membrane. *Ex situ* SIMS studies of the buried interface showed no evidence of surplus ionic species from any electrolyte salts at the interface, which is due to the fact that ions are dispersed evenly throughout the PEDOT:PSS solid-contact resulting in uniformly low concentrations of ions that are undetectable by SIMS. Finally, SR / FT-IRM was performed in the mapping mode across several areas of interest on a PVC CWE. An intensity map was generated from the integrated OH bending mode of water that was evident in several samples. The intensity maps revealed significant deposits of water at the buried interface, which is further evidence that water is transported through PVC membranes and, as a result, accumulates in locations that allow for the presence of water.

The investigation detailed in ***Chapter 5*** also led to a modified cell design for more versatile *in situ* EIS and NR measurements than the primitive EIS / NR *in situ* cell introduced in ***Chapter 4***.

Investigating Water Inclusions in Copolymer SC ISEs using SR / FT-IRM

Given the success of the previous SR / FT-IRM study in locating minute water inclusions in plasticized PVC CWEs, it was decided that a similar study was warranted on the hydrophobic copolymer SC-ISE system, in order to corroborate the findings of water uptake in SC-ISEs. In this instance, SR / FT-IRM presents itself as an ideal technique to study copolymer SC-ISEs due to the fact that water is known to accumulate in “pockets and pools” as opposed to continuous water layers. ***Chapter 6*** presented research on copolymer CWEs, POT / copolymer SC-ISEs and PEDOT:PSS / copolymer SC-ISEs. Importantly, the FT-IRM research aimed to validate the findings obtained from the previous research on the copolymer system and prove, unequivocally, that water does pass through the copolymer ion-selective membrane through to the buried interface resulting in the formation of water droplets at the interface. As expected, small inclusions of water were found at the buried interface of copolymer CWEs, whilst no traces of water were found in the POT / copolymer SC-ISE system. Interestingly, the PEDOT:PSS / copolymer SC-ISE showed evidence of water sorption; however, this water sorption was located at a region of the microscopic image that resembled a thick or swelled region of PEDOT:PSS. Indeed, this is an expected outcome due to the fact that previous NR data on the PEDOT:PSS system in conjunction with a PVC overlayer revealed that water contacting the PEDOT:PSS layer caused it to swell considerably. In essence, the inhomogeneous swelling of the thin PEDOT:PSS coating allowed certain water-affected regions to become visible when viewed under the optical microscope of the FT-IRM instrument.

Examining the Extent of Ion-to-Electron Transduction in SC ISEs

Despite the widespread use of SCs in solid-state ISEs, particularly POT, there has not been a comprehensive surface study of ion-to-electron transduction in these materials.

Synchrotron radiation / X-ray photoelectron spectroscopy (SR / XPS) and NR were used to study the extent of ion-to-electron transduction in ISEs utilizing electroactive polymers as the SC. Particularly, POT was chosen as an appropriate SC to study such processes due to its superior physical properties that prevent the formation of undesirable water layers. Tetrakis anions (from the lipophilic ion exchanger within the ion-selective membrane) were electrochemically driven into the SC and NR and SR / XPS was used to track the anion ingression into the membrane. Interestingly, it was found that charge-transfer events in electroactive polymeric SCs are limited to the surface of the material. In fact, the results of this study strongly suggested that these processes occur in the upper 14 Å of the SC material. This result is significant to the sensor community since it will inevitably prevent needless wastage of expensive material by demonstrating that SCs function even if deposited as molecularly thin films.

The Design of a Voltametric Cell for Use in Powerful Synchrotron Studies

Although SC ISEs are important electrochemical systems in modern-day science, they are by no means representative of all electrochemical systems. Accordingly, it was deemed necessary to design a new methodology for systems that have entirely different properties, and also require different problems to be resolved. ***Chapter 8*** introduced a novel electrochemical flow cell designed with the intention of use with various synchrotron techniques. In the context of this research, the technique in question was synchrotron radiation / grazing incidence X-ray diffraction (SR / GIXRD). SR / GIXRD was successfully applied to a study of the structure of a cadmium based tetracyanoquino-

dimethane (TCNQ) charge-transfer compound and compared with *ex situ* X-ray powder diffraction data. Although the structure obtained from X-ray powder diffraction data was very similar to that witnessed through *in situ* SR / GIXRD, subtle differences were evident between each dataset corresponding to the preferential crystallization of $Cd(TCNQ)_2$ material in certain crystallographic orientations. Moreover, it was seen that the major phase synthesized and analyzed *in situ* corresponded to the non-hydrated species of $Cd(TCNQ)_2$. Nevertheless, the success of such a technique in determining the structure and phases present *in situ* would inevitably be of great significance in other systems that show more marked alterations in structure when removed from the native electrochemical environment. In any case, the major phase of anhydrous $Cd(TCNQ)_2$ present in the *in situ* formed material was found to have a tetragonal unit cell with cell parameters: a = 16.781 Å and c = 8.829 Å.

Of equal importance to the SR / GIXRD measurements, it was demonstrated that the cell was capable of carrying out effective and meaningful voltammetric and amperometric studies (i.e. cyclic voltammetry and chronoamperometry) which was the motivation behind the final investigation of this thesis.

Demonstrating the Utility of the SR / GIXRD Flow Cell in a Potential Dependent Study of $Zn(TCNQ)_2$ Materials

The research carried out in ***Chapter 9*** was undertaken with the intention of further demonstrating the utility of the new flow cell. In this case, the objective of the research was not to perform a quantitative elucidation of the structure of the $Zn(TCNQ)_2$ material, but rather to compare and contrast the diffraction patterns obtained from depth profiles of $Zn(TCNQ)_2$ materials electrocrystallized at different potentials. As such, the potentials of interest were those in and around the reduction peak corresponding to the electrodeposition of $Zn(TCNQ)_2$ (viz. prior to the peak potential, at the peak potential and after the peak potential

for reduction of TCNQ to $TCNQ^-$). Accordingly, this study would set out to clarify and confirm the dependence of morphology on the potential used in the electrocrystallization process. It was found that the films synthesized at either the underpotential or peak potential for reduction of TCNQ to $TCNQ^-$ displayed characteristics in the depth profiles that were consistent with the formation of a dual layer deposit. Essentially, the electrodeposits consisted of a densely packed, highly amorphous layer of $Zn(TCNQ)_2$ material situated on top of a crystalline phase of $Zn(TCNQ)_2$. In the case of the material deposited at an overpotential, it was clear that the amorphous overlayer had undergone a transformation, such that only the crystalline phase was detectable by SR / GIXRD. Such findings had never been witnessed using *ex situ* techniques despite the fact that it is indeed consistent with theory presented throughout literature.

Future Work

Given the power of the methods developed throughout the course of this thesis, it seems logical that future work should encompass further explorations / adaptations on systems other than those studied in this thesis. Most significantly, the newly developed NR / electrochemical cell should be tested using a wider variety of electrochemical techniques, both passive and active. Further refinements in the cell design would inevitably see its use as a common addition to NR beamlines. Additionally, the use of combined NR / EIS measurements should be extended to achieve a comprehensive exploration of the phenomenon first witnessed in ***Appendix II***, i.e. quantum effects in ultra-thin polymer coatings.

Not only would the application of the SR / GIXRD cell to systems other than the one studied in this research be valuable to many electrochemists (e.g. corrosion studies of mild steel in seawater, nucleation and growth studies of scale formation on steel in the Bayer process, studying interfacial phenomena at

the mineral-solution interface in bioleaching systems, etc.), a further refinement and adaptation to beamlines other than that of diffractometry would be of significant benefit to the progression of this technology to other scientifically important systems. Additionally, as mentioned in ***Chapter 8***, the incorporation of more counter and reference electrodes shrouding the working electrode would inevitably yield enhanced electrochemical measurements which could be interpreted with ease.

In relation to SC ISEs, the tested materials that exhibited excellent performance throughout this thesis (i.e. PMMA / PDMA, POT and PEDOT:PSS), should be assessed in terms of their detection limits and response times after they have been exposed to solutions for extended periods of time. After completion of this work, there should be attempts to duplicate such results on a micro-scale for future applications in the miniaturization of the technology. The Holy Grail for the future of SC ISEs would be their development for use in extremely long term applications, i.e. implanted devices in clinical chemistry, permanent sensors for the monitoring of heavy metals in seawater. Thus, every effort should be made to further explore the suitability of the researched materials in such environments, i.e. blood and seawater.

$Zn(TCNQ)_2$ materials, should be further studied to elucidate the complete structure of the material, as accomplished for the $Cd(TCNQ)_2$ system. Once achieved, subsequent studies on the novel properties of these materials should be carried out so that they can be successfully utilized in new applications.

Bibliography

A

Abruna, H. D., White, J. H., Albaralli, M. J., Bommarito, G. M., Bedzyk, M. J., & McMillian, M. (1988). Is There Any Beam Yet? Uses of Synchrotron Radiation in the in Situ Study of Electrochemical Interfaces. *J. Phys. Chem., 92*, 7045-7052.

Al-Shatti, L. A., Marafie, H. M., & Shoukry, A. F. (2008). Surface analysis of new chlorpromazinium plastic membrane electrodes. *J. Pharm. Biomed. Anal., 46*(2), 328-334.

Ammann, D., Pretsch, E., & Simon, W. (1985). Lipophilic Salts as Membrane Additives and Their Influence on the Properties of Macro- and Micro- Electrodes Based on Neutral Carriers. *Anal. Chim. Acta, 171*, 119-129.

Arena, A., Mezzasalma, A. M., Patane, S., & Saitta, G. (1997). Investigation of the novel charge transfer complex Cd-TCNQ. *J. Mater. Res., 12*(7), 1693-1697.

Arruda, T. M., Shyam, B., Ziegelbauer, J. M., Mukerjee, S., & Ramaker, D. E. (2008). Investigation into the Competitive and Site-Specific Nature of Anion Adsorption on Pt Using In Situ X-ray Absorption Spectroscopy. *J. Phys. Chem. C, 112*, 18087-18097.

B

Bakker, E. (2004). Electrochemical Sensors. *Anal. Chem., 76*(12), 3285-3298.

Bakker, E., Buhlmann, P., & Pretsch, E. (1999). Polymer membrane ion-selective electrodes. What are the limits? *Electroanal., 11*(13), 915-933.

Bakker, E., & Chumbimuni-Torres, K. Y. (2008). Modern Directions for Potentiometric Sensors. *J. Braz. Chem. Soc., 19*(4), 621-629.

Bakker, E., Diamond, D., Lewenstam, A., & Pretsch, E. (1999). Ion sensors: current limits and new trends. *Anal. Chim. Acta, 393*(1-3), 11-18.

Bakker, E., Nagele, M., Schaller, U., & Pretsch, E. (1995). Applicability of the phase boundary potential model to the mechanistic understanding of solvent membrane-based ion-selective electrodes. *Electroanal., 7*(9), 817.

Bakker, E., & Pretsch, E. (2001). Potentiometry at trace levels. *Trends Anal. Chem., 20*(1), 11-19.

Bakker, E., & Pretsch, E. (2002). A New Wave of Ion Selective Electrodes. *Anal. Chem., 74*(15), 420A-426A.

Bakker, E., & Pretsch, E. (2005). Potentiometric sensors for trace-level analysis. *Trends Anal. Chem., 24*(3), 199-207.

Ball, M. J., Lucas, C. A., Markovic, N. M., Stamenkovic, V., & Ross, P. N. (2002). From sub-monolayer to multilayer- an in situ X-ray diffraction study of the growth of Pd films on Pt(111). *Surf. Sci., 518*, 201-209.

Bard, A. J., & Faulkner, L. R. (2001). *Electrochemical Methods: Fundamentals and Applications* (second ed.). New York: John Wiley and Sons, Inc.

Barlow, N., Brennan, C., Doyle, S. E., Greaves, G. N., Miller, M., Nahle, A. H., et al. (1989). Instrumentation and data acquisition for *in situ* electrochemistry at the Daresbury SRS. *Rev. Sci. Instrum., 60*(7), 2386-2389.

Bilderback, D. H., Elleaume, P., & Weckert, E. (2005). Review of third and next generation synchrotron light source. *J. Phys. B: Atomic, Molecular and Optical Physics, 38*, S773-S797.

Blatt, F. J. (1956). *Solid State Physics* (Vol. 4). New York: Academic Press Inc.

Bobacka, J. (1999). Potential Stability of All-Solid-State Ion-Selective Electrodes Using Conducting Polymers as Ion-to-Electron Transducers. *Anal. Chem., 71*(21), 4932-4937.

Bobacka, J. (2006). Conducting polymer-based solid-state ion-selective electrodes. *Electroanal., 18*(1), 7-18.

Bobacka, J., Ivaska, A., & Lewenstam, A. (2003). Potentiometric ion sensors based on conducting polymers. *Electroanal., 15*(5-6), 366-374.

Bobacka, J., Ivaska, A., & Lewenstam, A. (2008). Potentiometric Ion Sensors. *Chem. Rev., 108*(2), 329-351.

Bobacka, J., Lewenstam, A., & Ivaska, A. (2000). Electrochemical impedance spectroscopy of oxidised poly(3,4-ethylenedioxythiophene) film electrodes in aqueous solutions. *J. Electroanal. Chem., 489*, 17-27.

Bobacka, J., Lindfors, T., McCarrick, M., Ivaska, A., & Lewenstam, A. (1995). Single-piece all-solid-state ion-selective electrode. *Anal. Chem., 67*(20), 3819-3823.

Bobacka, J., McCarrick, M., Lewenstam, A., & Ivaska, A. (1994). All solid-state poly(vinyl chloride) membrane ion-selective electrodes with poly(3-octylthiophene) solid internal contact. *Analyst, 119*(9), 1985-1991.

Bozzini, B., D'Urzo, L., Gianoncelli, A., Kaulich, B., Prasciolu, M., Tondo, I. S. E., et al. (2009). An in Situ Synchrotron-Based Soft X-ray Microscopy Investigation on Ni Electrodeposition in a Thin-Layer Cell. *J. Phys. Chem. C, 113*, 9783-9787.

Bramnik, N. N., Nikolowski, K., Baehtz, C., Bramnik, K. G., & Ehrenberg, H. (2007). Phase Transitions Occuring upon Lithium Insertion-Extraction of $LiCoPO_4$. *Chem. Mater., 19*, 908-915.

Bramnik, N. N., Trots, D. M., Hofmann, H. J., & Ehrenberg, H. (2009). Mixed $LiCo_{0.6}M_{0.4}PO_4$ (M = Mn, Fe, Ni) phosphates: cycling mechanism and thermal stability. *Phys. Chem. Chem. Phys., 11*, 3271-3277.

Braun, A., Shrout, S., Fowlks, A. C., Osaisai, B. A., Seifert, S., Granlund, E., et al. (2003). Electrochemical in situ reaction cell for X-ray scattering, diffraction and spectroscopy. *J. Synch. Rad., 10*, 320-325.

Brett, C. M. A. (2008). Electrochemical Impedance Spectroscopy for Characterisation of Electrochemical Sensors and Biosensors. *ECS Trans., 13*(13), 67-80.

Brossard, F., Etgens, V. H., & Tadjeddine, A. (1997). In situ surface X-ray diffraction using a new electrochemical cell optimised for third generation synchrotron light sources. *Nucl. Instrum. Methods Phys. Res. B, 129*, 419-422.

Brown, A. S., Holt, S. A., Saville, P. M., & White, J. W. (1997). Neutron and X-ray reflectometry: solid multilayers and crumpling films. *Aust. J. Phys., 50*(2), 391-405.

Buck, R. (1978). *Ion-Selective Electrodes in Analytical Chemistry* (Vol. 1). New York: Plenum.

C

Cadogan, A., Gao, Z., Lewenstam, A., Ivaska, A., & Diamond, D. (1992). All-solid-state sodium-selective electrode based on a calixarene ionophore in a poly(vinyl chloride) membrane with a polypyrrole solid contact. *Anal. Chem., 64*(21), 2496-2501.

Cao, G., Ye, C., Fang, F., Xing, X., Xu, H.-H., Sun, D., et al. (2005). Scanning electron microscopy investigation of Cu-TCNQ micro/nanostructures synthesized via vapor-induced reaction method. *Micron, 36*, 267-270.

Carim, A. H., Dovek, M. M., Quate, C. F., Sinclair, R., & Vorst, C. (1987). High-resolution electron microscopy and scanning tunneling microscopy of native oxides on silicon. *Science, 237*(4815), 630-633.

Cattrall, R. W., Drew, D. M., & Hamilton, I. C. (1975). Alkylphosphoric acid esters for use in coated-wire calcium-selective electrodes. I. Response characteristics. *Anal. Chim. Acta, 76*(2), 269-277.

Cattrall, R. W., & Freiser, H. (1971). Coated wire ion-selective electrodes. *Anal. Chem., 43*(13), 1905-1906.

Cha, G. S., Liu, D. P., Meyerhoff, M. E., Cantor, H. C., Midgley, A. R., Goldberg, H. D., et al. (1991). Electrochemical Performance, Biocompatibility, and Adhesion of New Polymer Matrices for Solid-State Ion Sensors. *Anal. Chem., 63*, 1666-1672.

Chan, A. D., & Harrison, D. J. (1993). NMR study of the state of water in ion-selective electrode membranes. *Anal. Chem., 65*(1), 32-36.

Chan, A. D., Li, X., & Harrison, D. J. (1992). Evidence for a water-rich surface region in poly(vinyl chloride)-based ion-selective electrode membranes. *Anal. Chem., 64*(21), 2512-2517.

Chang, H.-H., Chang, C.-C., Wu, H.-C., Yang, M.-H., Sheu, H.-S., & Wu, N.-L. (2008). Study on dynamics of structural transformation during charge/discharge of $LiFePO_4$ cathode. *Electrochem. Commun., 10*, 335-339.

Chianelli, R. R., Scanlon, J. C., & Rao, B. M. L. (1978). Dynamic X-Ray Diffraction. *J. Electrochem. Soc., 125*, 1563-1566.

Cho, J., Kim, Y., & Kim, M. G. (2007). Synthesis and Characterization of $Li[Ni_{0.41}Li_{0.08}Mn_{0.51}]O_2$ Nanoplates for Li Battery Cathode Material. *J. Phys. Chem. C, 111*, 3192-3196.

Chopra, K. L. (1969). *Thin Film Phenomena*. New York: McGraw-Hill.

Christmann, K. (1991). *Topics in Physical Chemistry: Introduction to Surface Physical Chemistry*. New York: Springer.

Chumbimuni-Torres, K. Y., Rubinova, N., Radu, A., Kubota, L. T., & Bakker, E. (2006). Solid Contact Potentiometric Sensors for Trace Level Measurements. *Anal. Chem., 78*, 1318-1322.

Clerac, R., O'Kane, S., Cowen, J., Ouyang, X., Heintz, R., Zhao, H., et al. (2003). Glassy Magnets Composed of Metals Coordinated to 7,7,8,8-tetracyanoquinodimethane: $M(TCNQ)_2$ (M=Mn, Fe, Co, Ni). *Chem. Mater., 15*, 1840-1850.

Cooper, J. M., Cubitt, R., Dalgliesh, R., Gadegaard, N., Glidle, A., Hillman, A. R., et al. (2004). *J. Am. Chem. Soc., 126*, 15362-15363.

Crespo, G. A., Macho, S., Bobacka, J., & Rius, F. X. (2009). Transduction mechanism of carbon nanotubes in solid-contact ion-selective electrodes. *Anal. Chem., 81*, 676-681.

Crespo, G. A., Macho, S., & Rius, F. X. (2008). Ion-selective electrodes using carbon nanotubes as ion-to-electron transducers. *Anal. Chem., 80*, 1316-1322.

D

D'Orazio, P. (2003). Biosensors in clinical chemistry. *Clin. Chim. Acta, 334*(1-2), 41-69.

Dahn, J. R., & Haering, R. R. (1981). Anomalous Bragg Peak Widths in Li_xTiS_2. *Solid State Commun., 40*, 245-248.

Davenport, A. J., Oblonsky, L. J., & Ryan, M. P. (2000). The structure of the passive film that forms on iron in aqueous environments. *J. Electrochem. Soc., 147*, 2162-2173.

Davey, J. E., Tiernan, R. J., Pankey, T., & Montgomery, M. D. (1962). The effect of vacuum-evapouration parameters on the structural, electrical and optical properties of thin germanium films. *Solid-State Electronics, 6*, 205-216.

De Marco, R., Jee, E., Prince, K., Pretsch, E., & Bakker, E. (2008). Synthesis and characterization of high-integrity solid-contact polymeric ion sensors. *Solid State Electrochem., 13*, 137-148.

De Marco, R., Jiang, Z.-T., John, D., Sercombe, M., & Kinsella, B. (2007). An in situ electrochemical impedance spectroscopy / synchrotron radiation grazing incidence X-ray diffraction study of the influence of acetate on the carbon dioxide corrosion of mild steel. *Electrochim. Acta, 52*, 3746-3750.

De Marco, R., Jiang, Z.-T., Martizano, J., Lowe, A., Pejcic, B., & Van Riessen, A. (2006). In situ electrochemical impedance spectroscopy / synchrotron radiation grazing incidence X-ray diffraction - A powerful new technique for the characterization of electrochemical surfaces and interfaces. *Electochim. Acta., 51*, 5920-5925.

De Marco, R., Jiang, Z.-T., Pejcic, B., & Poinen, E. (2005). An In Situ Synchrotron Radiation Grazing Incidence X-Ray Diffraction Study of Carbon Dioxide Corrosion. *J. Electrochem. Soc., 152*(10), B389-B392.

De Marco, R., Jiang, Z.-T., Pejcic, B., & Van Riessen, A. (2006). In situ synchrotron radiation grazing incidence X-ray diffraction - A powerful technique for the characterization of solid-state ion-selective electrode surfaces. *Electochim. Acta., 51*, 4886-4891.

De Marco, R., Pejcic, B., Prince, K., & van Riessen, A. (2003). A multi-technique surface study of the mercury(II) chalcogenide ion-selective electrode in saline media. *Analyst, 128*(6), 742-749.

De Marco, R., Veder, J.-P., Clarke, G., Nelson, A., Prince, K., Pretsch, E., et al. (2008). Evidence of a water layer in solid-contact polymeric ion sensors. *Phys. Chem. Chem. Phys., 10*, 73-76.

Deb, A., Bergmann, U., Cramer, S. P., & Cairns, E. J. (2007). In Situ X-ray Absorption Spectroscopic Study of $Li_{1.05}Ni_{0.35}Co_{0.25}Mn_{0.4}O_2$ Cathode Material Coated with $LiCoO_2$. *J. Electrochem. Soc., 154*(6), A534-A541.

Deb, A., & Cairns, E. J. (2006). In situ X-ray absorption spectroscopy - A probe of cathode materials for Li-ion cells. *Fluid Phase Equilibria, 241*, 4-19.

Ding, G., Cheng, Y., Dalin, Y., & Renyuan, Q. (1987). Electrical switching effect in some TCNQ-ion-radical salt powder compaction. *Yingyong Kexue Xuebao, 5*(2), 159-163.

Dowsett, M. G., & Adriaens, A. (2006). Cell for Simultaneous Synchrotron Radiation X-ray and Electrochemical Corrosion Measurements on Cultural Heritage Metals and Other Materials. *Anal. Chem., 78*(10), 3360-3365.

Dutta, P. (2000). Grazing incidence X-ray diffraction. *Current Sci., 78*(12), 1478-1483.

E

Eisenberger, P., & Marra, W. C. (1981). X-ray Diffraction Study of the Ge(001) Reconstructed Surface. *Phys. Rev. Lett., 46*(16), 1081-1084.

F

Faridbod, F., Ganjali, M. R., Dinarvand, R., & Norouzi, P. (2008). Developments in the Field of Conducting and Non-conducting Polymer Based Potentiometric Membrane Sensors for Ions Over the Past Decade. *Sensors, 8*(4), 2331-2412.

Felici, R., Bertalot, L., DeNinno, A., LaBarbera, A., & Violante, V. (1995). In situ measurements of the deuterium (hydrogen) charging of a palladium electrode during electrolysis by energy dispersive x-ray diffraction. *Rev. Sci. Instrum., 66*(5), 3344-3348.

Fibbioli, M., Bandyopadhyay, K., Liu, S.-G., Echegoyen, L., Enger, O., Diederich, F., et al. (2002). Redox-Active Self-Assembled Monolayers for Solid-Contact Polymeric Membrane Ion-Selective Electrodes. *Chem. Mater., 14*, 1721-1729.

Fibbioli, M., Enger, O., Diederich, F., Pretsch, E., Bandyopadhyay, K., Liu, S.-G., et al. (2000). Redox-active self-assembled monolayers as novel solid contacts for ion-selective electrodes. *Chem. Commun., 5*, 339-340.

Fibbioli, M., Morf, W. E., Badertscher, M., De Rooij, N. F., & Pretsch, E. (2000). Potential drifts of solid-contacted ion-selective electrodes due to zero-current ion fluxes through the sensor membrane. *Electroanal., 12*(16), 1286-1292.

Fleischmann, M., Hendra, P. J., & Robinson, J. (1980). X-ray diffraction from adsorbed iodine on graphite. *Nature, 288*, 152-154.

Fleischmann, M., Oliver, A., & Robinson, J. (1986). In situ X-ray diffraction studies of electrode solution interfaces. *Electrochim. Acta, 31*(8), 899-906.

Fogt, E. J., Untereker, D. F., Norenberg, M. S., & Meyerhoff, M. E. (1985). Response of ion-selective field effect transistors to carbon dioxide and organic acids. *Anal. Chem., 57*(9), 1995-1998.

G

Gamry-Instruments. (2006). Electrochemical Impedance Spectroscopy Theory: A Primer. 2010, from http://www.gamry.com/App_Notes/EIS_Primer/EIS_Primer.htm

Gerold, V., & Kostorz, G. (1978). Small-Angle Scattering Applications to Materials Science. *J. Appl. Crystallogr. , 11*, 376-404.

Goldberg, H. D., Brown, R. B., Liu, D. P., & Meyerhoff, M. E. (1994). Screen printing: a technology for the batch fabrication of integrated chemical-sensor arrays. *Sens. Actuators, B, B21*(3), 171-183.

Griffiths, J. (2008). Secondary Ion Mass Spectrometry. *Anal. Chem., 80*, 7194-7197.

Groenendaal, L., Jonas, F., Dieter, F., Pielartzik, H., & Reynolds, J. (2000). Poly(3,4-ethylenedioxythiophene) and Its Derivatives: Past, Present, and Future. *Adv. Mater., 12*(7), 481-494.

Grygolowicz-Pawlak, E., Palys, B., Biesiada, K., Olszyna, A. R., & Malinowska, E. (2008). Covalent binding of sensor phases - a recipe for stable potentials of solid-state ion selective sensors. *Anal. Chim. Acta, 625*, 137-144.

Grygolowicz-Pawlak, E., Plachecka, K., Zbigniew, B., & Malinowska, E. (2007). Further studies on the role of redox-active monolayer as intermediate phase of solid-state sensors. *Sens. Actuators B: Chem, 123*, 480-487.

Grygolowicz-Pawlak, E., Wygladacz, K., Sek, S., Bilewicz, R., Brzozka, Z., & Malinowska, E. (2005). Studies on ferrocene organothiol monolayer as an intermediate phase of potentiometric sensors with gold inner contact. *Sens. Actuators B, 111-112*, 310-316.

Gu, N., Yang, X.-M., Sheng, H.-Y., Lu, W., & Wei, Y. (1995). Electrical switching properties of CuTCNQ organic crystals with nanometer feature size. *Synth. Met., 71*, 2221-2222.

Gu, N., Zhang, H.-Q., Wei, Y., Shen, H.-Y., & Zhang, L. (1998). Rectifying phenomenon of Cu-TCNQ organometallic crystallite device. *Supramol. Sci., 5*, 691-693.

Guilhaumou, N., Dumas, P., Carr, G. L., & Williams, G. P. (1998). Synchrotron Infrared Microspectrometry Applied to Petrography in Micrometer-Scale Range: Fluid Chemical Analysis and Mapping. *Appl. Spect., 52*, 1029-1034.

Gustafsson, J. C., Liedberg, B., & Inganas, O. (1994). In situ spectroscopic investigations of electrochromism and ion transport in a poly(3,4-ethylenedioxythiophene) electrode in a solid state electrochemical cell. *Solid State Ionics, 69*, 145-152.

Gyurcsanyi, R. E., Nyback, A.-S., Toth, K., Nagy, G., & Ivaska, A. (1998). Novel polypyrrole based all-solid-state potassium selective microelectrodes. *Analyst, 123*, 1339-1344.

H

Hahn, F., Mathis, Y.-L., Bonnefont, A., Maillard, F., & Melendres, C. A. (2007). In situ synchrotron far-infrared spectromicroscopy of a copper electrode at grazing incidence angle. *J. Synch. Rad., 14*, 446-448.

Harrison, D., Li, X., & Petrovic, S. (1992). Water and the ion-selective electrode membrane. *ACS Symp. Ser., 487*, 292-300.

Hauser, P. C., Chiang, D. W. L., & Wright, G. A. (1995). A potassium-ion selective electrode with valinomycin based poly(vinyl chloride) membrane and a poly(vinyl ferrocene) solid contact. *Anal. Chim. Acta, 302*, 241-248.

Heintz, R. A., Zhao, H., Ouyang, X., Grinetti, G., Cowen, J., & Dunbar, K. R. (1999). New Insight into the Nature of Cu(TCNQ): Solution Routes to Two Distinct

Polymorphs and Their Relationship to Crystalline Films That Display Bistable Switching Behavior. *Inorg. Chem, 38*(1), 144-156.

Heng, L. Y., & Hall, E. A. H. (2000). Methacrylic-acrylic polymers in ion-selective membranes: acheiving the right polymer recipe. *Anal. Chim. Acta, 403*(1-2), 77-89.

Heng, L. Y., Toth, K., & Hall, E. A. H. (2004). Ion-transport and diffusion coefficients of non-plasticised methacrylic-acrylic ion-selective membranes. *Talanta, 63*, 73-87.

Herron, M. E., Doyle, S. E., Pizzini, S., Roberts, K. J., Robinson, J., Hards, G., et al. (1992). In situ studies of a dispersed platinum on carbon electrode using x-ray absorption spectroscopy. *Electroanal. Chem., 324*, 243-258.

Herron, M. E., Doyle, S. E., Roberts, K. J., Robinson, I. K., & Walsh, F. C. (1992). Instrumentation and cell design for *in situ* studies of electrode surfaces using x-ray synchrotron radiation. *Rev. Sci. Instrum., 63*, 950-955.

Higgins, A. M., Martin, S. J., Jukes, P. C., Goeoghegan, M., Jones, R. A. L., Langridge, S., et al. (2003). Interfacial structure in semiconducting polymer devices. *J. Mater. Chem., 13*, 2814-2818.

Hitchcock, A. P., Horsley, J. A., & Stohr, J. (1986). Inner shell excitation of thiophene and thlolane: Gas, solid, and monolayer states. *J. Chem. Phys., 85*(9), 4835-4848.

Hoagland, J. J., Wang, X. D., & Hipps, K. W. (1993). Characterization of Cu-CuTCNQ-M devices using scanning electron microscopy and scanning tunneling microscopy. *Chem. Mater., 5*(1), 54-60.

Horvai, G., Graf, E., Toth, K., Pungor, E., & Buck, R. (1986). Plasticized poly(vinyl chloride) properties and characteristics of valinomycin electrodes. 1. High-frequency resistances and dielectric properties. *Anal. Chem., 58*(13), 2735-2740.

Horvai, G., Horvath, V., Farkas, A., & Pungor, E. (1988). Inorganic salts trapped in neutral carrier ion-selective electrode membranes form ion-exchange sites. *Anal. Lett., 21*(12), 2165-2175.

Hudson, T. A., & Robson, R. (2009). A New Class of TCNQ Derivatives Easily Generated from $TCNQH_2$ Containing Discrete $TCNQ^{2-}$ Anions and Noncoordinating Cations. *Cryst. Growth Des., 9*(4), 1658-1662.

I

Ingham, B., Illy, B. N., & Ryan, M. P. (2008). Direct Observation of Distinct Nucleation and Growth Processes in Electrochemically Deposited ZnO Nanostructures Using in Situ XANES. *J. Phys. Chem. C, 112*, 2820-2824.

Ingham, B., Illy, B. N., Toney, M. F., Howdyshell, M. L., & Ryan, M. P. (2008). In Situ Synchrotron X-ray Diffraction Experiments on Electrochemically Deposited ZnO Nanostructures. *J. Phys. Chem. C, 112*, 14863-14866.

J

James, M. (2001). Characterisation of Thin-Film Surfaces and Interfaces Using Neutron Reflectometry. *Aust. J. Chem., 54*, 487-491.

James, M., Nelson, A., Schulz, J. C., Jones, M. J., Studer, A. J., & Hathaway, P. (2005). A new neutron reflectometer at Australia's HIFAR research reactor. *Nucl. Instrum. Methods Phys. Res., Sect. A, 536*(1-2), 165-175.

Johnson, C. S., Vaughey, J. T., Thackeray, M. M., Sarakonsri, T., Hackney, S. A., Fransson, L., et al. (2000). Electrochemistry and in-situ X-ray diffraction of InSb in lithium batteries. *Electrochem. Commun., 2*, 595-600.

Johnson, R. D., & Bachas, L. D. (2003). Ionophore-based ion-selective potentiometric and optical sensors. *Anal. Bioanal. Chem., 376*, 328-341.

Jukes, P. C., Martin, S. J., Higgins, A. M., Geoghegan, M., Jones, R. A. L., Langridge, S., et al. (2004). Controlling the surface composition of poly(3,4-ethylene dioxythiophene)-poly(styrene sulfonate) blends by heat treatment. *Adv. Mater., 16*(9), 807-811.

K

Kang, E. T., Neoh, K. G., & Tan, K. L. (1991). X-ray photoelectron spectroscopy studies of poly(2,2'-bithiophene) and its complexes. *Phys. Rev. B, 44*(19), 10461-10469.

Kang, E. T., Neoh, K. G., & Tan, K. L. (1992). Surface modifications of poly(3-alkylthiophene) films by graft copolymerization. *Macromolecules, 25*, 6842-6848.

Karpfen, F. M., & Randles, J. E. B. (1953). Ionic equilibria and phase-boundary potentials in oil-water systems. *Trans. Faraday Soc., 49*, 823-832.

Kaul, A., & Udipi, K. (1989). Electron Spectroscopy for Chemical Analysis Study of the Surface Oxidation of Poly(phenylene sulfide) Powder by Heterogeneous Reactions. *Macromolecules, 22*(3), 1201-1207.

Kautek, W., Mirwald, S., Sahre, M., & Nauer, G. E. (1998). In-situ grazing incidence X-ray diffractometry of polycrystalline copper in alkaline chloride and sulphate electrolytes. *Electrochim. Acta, 43*, 2979-2984.

King, S. M. (2003). Small Angle Neutron Scattering. 2010, from www.isis.rl.ac.uk/archive/largescale/loq/documents/sans.htm

Kline, S. R. (2006). Reduction and Analysis of SANS and USANS Data using Igor Pro. *J. Appl. Crystallogr., 39*(6), 895-900.

Knapp, M., Carsten, B., Ehrenberg, H., & Fuess, H. (2004). The synchrotron powder diffractometer at beamline B2 at HasYLAB/DESY: status and capabilities. *J. Synch. Rad., 11*, 328-334.

Konopka, A., Sokalski, T., Michalska, A., Lewenstam, A., & Maj-Zurawska, M. (2004). Factors Affecting the Potentiometric Response of All-Solid-State Solvent Polymeric Membrane Calcium-Selective Electrode for Low-Level Measurements. *Anal. Chem., 76*(21), 6410-6418.

Kotz, R., & Carlen, M. (2000). Principles and applications of electrochemical capacitors. *Electrochim. Acta, 45*, 2483-2498.

Kuo, S.-L., & Wu, N.-L. (2007). Electrochemical Capacitor of $MnFe_2O_4$ with Organic Li-Ion Electrolyte. *Electrochem. and Solid State Lett., 10*(7), A171-A175.

L

Lai, C.-Z., Fierke, M. A., Stein, A., & Buehlmann, P. (2007). Ion-Selective Electrodes with Three-Dimensionally Ordered Macroporous Carbon as the Solid Contact. *Anal. Chem., 79*(12), 4621-4626.

Lampitt, R. A., Carrette, L. P. L., Hogarth, M. P., & Russell, A. E. (1999). In situ and model EXAFS studies on electrocatalysts for methanol oxidation. *J. Electroanal. Chem., 460*, 80-87.

Levi, E., Levi, M. D., Salitra, G., Aurbach, D., Oesten, R., Heider, U., et al. (1999). Electrochemical and in-situ XRD characterization of $LiNiO_2$ and $LiCo_{0.2}Ni_{0.8}O_2$ electrodes for rechargeable lithium cells. *Solid State Ionics, 126*, 97-108.

Lewenstam, A., Maj-Zurawska, M., & Hulanicki, A. (1991). Application of ion-selective electrodes in clinical analysis. *Electroanal., 3*(8), 727-734.

Leyssens, K., Adriaens, A., Dowsett, M. G., Schotte, B., Oloff, I., Pantos, E., et al. (2005). Simultaneous in situ time resolved SR-XRD and corrosion potential analyses to monitor the corrosion on copper. *Electrochem. Commun., 7*, 1265-1270.

Li, J., Herrero, E., & Abruna, H. D. (1998). The effects of anions on the underpotential deposition of Hg on Au(111) An electrochemical and in situ surface X-ray diffraction study. *Colloids and Surf. A, 134*, 113-131.

Li, X., Petrovic, S., & Harrison, D. J. (1990). A novel spectroscopic method to image H2O distribution in Ion-Selective Membranes. *Sens. Actuators, B, 1*(1-6), 275-280.

Li, Z., Li, X., Petrovic, S., & Harrison, D. J. (1993). Water distribution in poly(vinyl chloride) based ion-selective electrode membranes and the effect of additives. *Anal. Methods Instrum., 1*(1), 30-37.

Li, Z., Li, X., Petrovic, S., & Harrison, D. J. (1996). Dual-Sorption Model of Water Uptake in Poly(vinyl chloride)-Based Ion-Selective Membranes: Experimental Water Concentration and Transport Parameters. *Anal. Chem., 68*(10), 1717-1725.

Li, Z., Li, X., Petrovic, S., & Harrison, D. J. (1996). Dual-sorption model of water uptake in poly(vinyly chloride)-based ion-selective membranes: experimental water concentration and transport parameters. *Anal. Chem., 68*(10), 1717-1725.

Li, Z., Li, X., Rothmaier, M., & Harrison, D. J. (1996). Comparison of Numerical Modeling of Water Uptake in Poly(vinyl chloride)-Based Ion-Selective Membranes with Experiment. *Anal. Chem., 68*(10), 1726-1734.

Lifshitz, I. M., & Kosevich, A. M. (1955). *Izv. Akad. Nauk SSSR, Ser. Fiz., 19*, 395.

Lindner, E., & Gyurcsanyi, R. E. (2009). Quality control criteria for solid-contact, solvent polymeric membrane ion-selective electrodes. *J. Solid State Electrochem., 13*(1), 51-68.

Liu, S.-G., Liu, Y.-Q., Wu, P.-J., & Zhu, D.-B. (1996). Multifaceted Study of CuTCNQ Thin-Film Materials. Fabrication, Morphology, and Spectral and Electrical Switching Properties. *Chem. Mater., 8*(12), 2779-2787.

Liu, S.-G., Liu, Y.-Q., & Zhu, D.-B. (1996). Amorphous somiconducting film containing nanometer particles of CuTCNQ: preparation, characterisation and electrical switching properties. *Thin Solid Films, 280*(1-2), 271-277.

Liu, Y., Li, H., Tu, D., Ji, Z., Wang, C., Tang, Q., et al. (2006). Controlling the Growth of Single Crystalline Nanoribbons of Copper Tetracyanoquinodimethane for the Fabrication of Devices and Device Arrays. *J. Am. Chem. Soc., 128*, 12917-12922.

Long, G. G., & Kruger, J. (1991). Surface X-ray Absorption Spectroscopy, EXAFS and NEXAFS, for the in Situ and ex Situ Study of Electrodes. In R. Varma & J. R. Selman (Eds.), *Techniques for Characterization of Electrodes and Electrochemical Processes*. New York: John Wiley and Sons, Inc.

Lucas, C. A., & Markovic, N. M. (2006). In-situ X-ray Diffraction Studies of the Electrode/Solution Interface. In R. C. Alkire, D. M. Kolb, J. Lipkowski & P. N. Ross (Eds.), *Advances in Electrochemical Science and Engineering* (Vol. 9). Weinheim: Wiley.

M

Macdonald, J. R. (1987). *Impedance Spectroscopy Emphasizing Solids Materials and Systems*. New York: John Wiley & Sons.

Maniguet, S., Mathew, R. J., & Russell, A. E. (2000). EXAFS of Carbon Monoxide Oxidation on Supported Pt Fuel Cell Electrocatalysts. *J. Phys. Chem. B., 104*, 1998-2004.

Marra, W. C., Eisenberger, P., & Cho, A. Y. (1979). X-ray total-external-reflection-Bragg diffraction: A structural study of the GaAs-Al interface. *J. Appl. Phys., 50*(11), 6927-6933.

May, R. P. (2003). Small-Angle Scattering. In A.-J. Dianoux & G. Lander (Eds.), *Neutron Data Booklet*. Grenoble: OCP Science.

McDaniel, A. H., El Gabaly, F., Akhadov, E., Farrow, R. L., McCarty, K. F., Linne, M. A., et al. (2009). In-situ Investigation of SOFC patterned Electrodes Using Ambient-Pressure X-ray Photoelectron Spectroscopy. *ECS Trans., 25*(2), 335-343.

McKelvy, M. L., Britt, T. R., Davis, B. L., Gillie, J. K., Lentz, L. A., Leugers, A., et al. (1996). Infrared Spectroscopy. *Anal. Chem., 68*, 93R-160R.

Melnichenko, Y. B., & Wignall, G. D. (2007). Small-angle neutron scattering in materials science: Recent practical applications. *J. Appl. Phys., 102*(021101), 1-24.

Messadi, D., & Vergnaud, J. M. (1982). Plasticizer transfer from plasticized PVC into ethanol-water mixtures. *J. Appl. Polym. Sci., 27*(10), 3945-3955.

Meyerhoff, M. E., & Opdycke, W. N. (1986). Ion-selective electrodes. In H. E. Speigel (Ed.), *Adv. Clin. Chem.* (Vol. 25). London: Academic Press.

Michalska, A. (2005). Improvement of analytical characteristic of calcium selective electrode with conducting polymer contact. The role of conducting polymer spontaneous charge transfer processes and their galvanostatic compensation. *Electroanal., 17*(5-6), 400-407.

Michalska, A. (2006). Optimizing the analytical performance and construction of ion-selective electrodes with conducting polymer-based ion-to-electron transducers. *Anal. Bioanal. Chem., 384*(2), 391-406.

Michalska, A., Dumanska, J., & Maksymiuk, K. (2003). Lowering the Detection Limit of Ion-Selective Plastic Membrane Electrodes with Conducting Polymer Solid Contact and Conducting Polymer Potentiometric Sensors. *Anal. Chem., 75*(19), 4964-4974.

Michalska, A., & Maksymiuk, K. (2004). All-plastic, disposable, low detection limit ion-selective electrodes. *Anal. Chim. Acta, 523*, 97-105.

Migdalski, J., Blaz, T., & Lewenstam, A. (1996). Conducting polymer-based ion-selective electrodes. *Anal. Chim. Acta, 322*(3), 141-149.

Mikhailov, G. M., Malikov, I. V., Chernykh, A. V., Fomin, L. A., Joyez, P., Pothier, H., et al. (2002). Signatures of ballistic transport in the magnetoresistance of nanostructures made of single-crystalline refractory metals. *Nanotech., 13*, 226-230.

Minami, H., Sato, N., Sugawara, M., & Umezawa, Y. (1991). Comparative study on the potentiometric response between a valinomycin-based bilayer lipid membrane and a solvent polymeric membrane. *Anal. Sci., 7*, 853-862.

Miyasaka, H., Motokawa, N., Matsunaga, S., Yamashita, M., Sugimoto, K., Mori, T., et al. (2010). Control of Charge Transfer in a Series of $Ru_2^{II,II}$/TCNQ Two-Dimensional Networks by Tuning the Electron Affinity of TCNQ Units: A Route to Synergistic Magnetic/Conducting Materials. *J. Am. Chem. Soc., 132*, 1532-1544.

Moody, G. J., Oke, R. B., & Thomas, J. D. R. (1970). Calcium-selective electrode based on a liquid ion exchanger in a poly(vinyl chloride) matrix. *Analyst, 95*(1136), 910-918.

Morcrette, M., Chabre, Y., Vaughan, G., Amatucci, G., Leriche, J.-B., Patoux, S., et al. (2002). In situ X-ray diffraction techniques as a powerful tool to study battery electrode materials. *Electrochim. Acta, 47*, 3137-3149.

Morf, W. E. (1981). The Principles of Ion-Selective Electrodes and of Membrane Transport *Studies in Analytical Chemistry* (Vol. 2, pp. 431). New York: Elsevier Scientific Publishing Company.

Mukerjee, S., Srinivasan, S., & Soriaga, M. P. (1995). Role of Structural and Electronic Properties of Pt and Pt Alloys on Electrocatalysis of Oxygen Reduction. *J. Electrochem. Soc., 142*, 1409-1422.

N

Nafady, A., Bond, A. M., & Bilyk, A. (2008). Controllable Synthesis and Fabrication of Semiconducting Nanorod.Nanowire Bundles of $Fe[TCNQ]_2(H_2O)_2$ via Electrochemically Induced Solid-Solid Phase Transformation of TCNQ Microcystals. *J. Phys. Chem. C, 112*, 6700-6709.

Nafady, A., Bond, A. M., Bilyk, A., Harris, A. R., Bhatt, A. I., O'Mullane, A. P., et al. (2007). Tuning the Electrocrystallization Parameters of Semiconducting

Co[TCNQ]$_2$-Based Materials to Yield either Single Nanowires or Crystalline Thin Films. *J. Am. Chem. Soc., 129*(8), 2370-2382.

Nafady, A., O'Mullane, A. P., Bond, A. M., & Neufeld, A. K. (2006). Morphology Changes and Mechanistic Aspects of the Electrochemically-Induced Reversible Solid-Solid Transformation of Microcrystalline TCNQ into Co[TCNQ]$_2$-Based Materials (TCNQ=7,7,8,8-tetracyanoquinodimethane). *Chem. Mater., 18*, 4375-4384.

Nagele, M., Mi, Y., Bakker, E., & Pretsch, E. (1998). Influence of Lipophilic Inert Electrolytes on the Selectivity of Polymer Membrane Electrodes. *Anal. Chem., 70*, 1686-1691.

Nagy, Z., & You, H. (2002). Applications of surface X-ray scattering to electrochemistry problems. *Electrochim. Acta, 47*(19), 3037-3055.

Nagy, Z., You, H., & Yonco, R. M. (1994). Cell design for in situ x-ray scattering studies of metal/solution interfaces under electrochemical control. *Rev. Sci. Instrum., 65*(7), 2199-2205.

Nagy, Z., You, H., Yonco, R. M., Melendres, C. A., Yun, W., & Maroni, V. A. (1991). Cell design for in-situ x-ray scattering study of electrodes in the transmission geometry. *Electrochim. Acta, 36*(1), 209-212.

Nelson, A. (2006). Co-refinement of multiple contrast neutron / X-ray reflectivity data using MOTOFIT. *Journal of Applied Crystallography, 39*, 273-276.

Nelson, A. (2006). Co-refinement of multiple contrast neutron / X-ray reflectivity data using MOTOFIT. *J. Appl. Crystallogr., 39*(2), 273-276.

Nelson, A., Muir, B., Oldham, J., Fong, C., McLean, K., Hartley, P., et al. (2006). X-ray and neutron reflectometry study of glow-discharge plasma polymer films. *Langmuir, 22*(1), 453-458.

Neufeld, A. K., O'Mullane, A. P., & Bond, A. M. (2005). Control of Localized Nanorod Formation and Patterns of Semiconducting CuTCNQ Phase I Crystals by Scanning Electrochemical Microscopy. *J. Am. Chem. Soc., 127*, 13846-13853.

Ng, L., & Simmons, R. (1999). Infrared Spectroscopy. *Anal. Chem., 71*, 343R-350R.

Nikol'skii, B. P., & Materova, E. A. (1985). Solid contact in membrane ion-selective electrodes. *Ion-Sel. Electrode Rev., 7*(1), 3-39.

Nikolowski, K., Baehtz, C., Bramnik, N. N., & Ehrenberg, H. (2005). A Swagelok-type in situ cell for battery investigations using synchrotron radiation. *J. Appl. Crystallogr., 38*, 851-853.

O

O'Mullane, A. P., Neufeld, A. K., & Bond, A. M. (2005). Distinction of the Two Phases of CuTCNQ by Scanning Electrochemical Microscopy. *Anal. Chem., 77*, 5447-5452.

O'Mullane, A. P., Neufeld, A. K., Harris, A. R., & Bond, A. M. (2006). Electrocrystallization of Phase I, CuTCNQ (TCNQ = 7,7,8,8-Tetracyanoquinodimethane), on Indium Tin Oxide and Boron-Doped Diamond Electrodes. *Langmuir, 22*, 10499-10505.

Ocko, B. M., & Wang, J. (1990). *In Situ* X-Ray Reflectivity and Diffraction Studies of the Au(001) Reconstruction in an Electrochemical Cell. *Phys. Rev. Lett., 65*(12), 1466-1469.

Ogrin, Y. F., Lutskii, V. N., & Elinson, M. I. (1966). *Soviet Phys. JETP Letters, 3*, 71.

Orient, O. J. (1974). Mobilities of H^+ and D^+ ions in Neon Gas. *Journal of Physics D: Applied Physics,* 7(16), 2266-2268.

P

Pereira, L. G. S., Paganin, V. A., & Ticianelli, E. A. (2009). Investigation of the CO tolerance mechanism at several Pt-based bimetallic anode electrocatalysts in a PEM fuel cell. *Electrochim. Acta, 54*, 1992-1998.

Porod, G. (1982). *Small-Angle X-ray Scattering*. London, U.K.: Academic Press.

Potember, R., Poehler, T., & Cowan, D. (1979). Electrical Switching and memory phenomena in copper-TCNQ thin films. *Appl. Phys. Lett., 34*(6), 405-407.

Q

Qin, Y., Peper, S., & Bakker, E. (2002). Plasticiser-Free Polymer Membrane Ion-Selective Electrodes Containing a Methacrylic Copolymer Matrix. *Electroanal., 14*(19-20), 1375-1381.

Qu, X., Nafady, A., Mechler, A., Zhang, J., Harris, A. R., O'Mullane, A. P., et al. (2008). AFM study of morphological changes associated with electrochemical solid-solid transformation of three dimensional crystals of TCNQ to metal derivatives (metal=Cu, Ni; TCNQ=tetracyanoquinodimethane). *J. Solid State Electrochem., 12*, 739-746.

R

Renner, F. U., Grunder, Y., & Zegenhagen, J. (2007). Portable chamber for the study of UHV prepared electrochemical interfaces by hard x-ray diffraction. *Rev. Sci. Instrum., 78*(3), 1-8.

Renner, F. U., Kageyama, H., Siroma, Z., Shikano, M., Schoder, S., Grunder, Y., et al. (2008). Gold model anodes for Li-ion batteries: Single crystalline systems studied by in situ X-ray diffraction. *Electrochim. Acta, 53*, 6064-6069.

Richardson, R. M., Dalgliesh, R. M., Brennan, T., Lovell, M. R., & Barnes, A. C. (2001). A neutron reflection study of the effect of water on the surface of float glass. *J. Non-Crystalline Solids, 292*, 93-107.

Riga, J., Snauwaert, A., De Pryck, R., Lazzaroni, R., Boutique, J. P., Verbist, J. J., et al. (1987). Electronic structure of sulphur-containing conducting polymers. *Synth. Met., 21*, 223-228.

Robinson, I. K., & Tweet, D. J. (1992). Surface x-ray diffraction. *Rep. Prog. Phys., 55*, 599-651.

Robinson, K. M., & O'Grady, W. E. (1993). A transmission geometry electrochemical cell for in situ x-ray diffraction *Rev. Sci. Instrum., 64*(4), 1061-1065.

Rosciano, F., Holzapfel, M., Kaiser, H., Scheifele, W., Ruch, P. W., Hahn, M., et al. (2007). A multi-sample automatic system for in situ electrochemical x-ray diffraction synchrotron measurements. *J. Synch. Rad., 14*, 487-491.

Rose, A., Bilsborrow, R., King, C. R., Ravikumar, M. K., Qian, Y., Wiltshire, R. J. K., et al. (2009). In situ Ru K-edge EXAFS of CO adsorption on a Ru modified Pt/C fuel cell catalyst. *Electrochim. Acta, 54*(22), 5262-5266.

Rose, A., Crabb, E. M., Qian, Y., Ravikumar, M. K., Wells, P. P., Wiltshire, R. J. K., et al. (2007). Potential dependance of segregation and surface alloy formation of a Ru modified carbon supported Pt catalyst. *Electrochim. Acta, 52*, 5556-5564.

Rose, A., Maniguet, S., Mathew, R. J., Slater, C., Yao, J., & Russell, A. E. (2003). Hydride phase formation in carbon supported palladium nanoparticle electrodes investigated using in situ EXAFS and XRD. *Phys. Chem. Chem. Phys., 5*, 3220-3225.

Ruch, P. W., Hahn, M., Rosciano, F., Holzapfel, M., Kaiser, H., Scheifele, W., et al. (2007). In situ X-ray diffraction of the intercalation of $(C_2H_5)_4N^+$ and BF_4^- into graphite from acetonitrile and propylene carbonate based supercapacitor electrolytes. *Electrochim. Acta, 53*, 1074-1082.

Russell, A. E., Maniguet, S., Mathew, R. J., Yao, J., Roberts, M. A., & Thompsett, D. (2001). In situ X-ray absorption spectroscopy and X-ray diffraction of fuel cell electrocatalysts. *J. Power Sources, 96*, 226-232.

Russell, A. E., & Rose, A. (2004). X-ray Absorption Spectroscopy of Low Temperature Fuel Cell Catalysts. *Chem. Rev., 104*(10), 4613-4635.

Russell, T. P. (1990). X-ray and neutron reflectivity for the investigation of polymers. *Mater. Sci. Rep., 5*, 171-181.

S

Sathiyanarayanan, S., Sahre, M., & Kautek, W. (1998). In-situ grazing incidence X-ray diffractometry investigation of phase change processes at the silver / aqueous - halogenide interface. *Electrochim. Acta, 43*, 2985-2989.

Sathiyanarayanan, S., Sahre, M., & Kautek, W. (1999). In-situ grazing incidence X-ray diffractometry observation of pitting corrosion of copper in chloride solutions. *Corros. Sci., 41*, 1899-1909.

Schmidt, H., Huger, E., Chakravarty, S., Stahn, J., Gutberlet, T., Tietze, U., et al. (2009). Neutron Reflectometry: A Tool to Investigate Diffusion Processes in Solids on the Nanometer Scale. *Adv. Eng. Mater., 11*(6), 446-451.

Schulz, J. C., James, M., Nelson, A., & Brule, A. (2006). Platypus: a time-of-flight neutron reflectometer at Australia's new research reactor. *Neutron Res., 14*(2), 91-108.

Scott, F. J., Mukerjee, S., & Ramaker, D. E. (2010). Contrast in Metal-Ligand Effects on Pt_nM Electrocatalysts with M Equal Ru vs Mo and Sn exhibited by in situ XANES and EXAFS Measurements in Methanol. *J. Phys. Chem. C, 114*, 442.

Sek, S., Bilewicz, R., Grygolowicz-Pawlak, E., Grudzien, I., Brzozka, Z., & Malinowska, E. (2004). Design of ferrocene organothiol monolayer as intermediate phase for miniaturized electrochemical sensors with gold contact. *Polish J. Chem., 78*(9), 1655-1665.

Sferrazza, M., Heppenstall-Butler, M., Cubitt, R., Bucknall, D., Webster, J., & Jones, R. A. L. (1998). Interfacial Instability Driven by Dispersive Forces: The early stages of Spinodal Dewetting of a Thin Polymer Film on a Polymer Substrate. *Phys. Rev. Lett., 81*, 5173-5176.

Sham, T.-K. (Ed.). (2002). *Chemical Applications of Synchrotron Radiation* (Vol. 12A). Singapore: World Scientific Publishing Co. Ltd,.

Si, P. (2008). *Nanostructured Chemical Sensors Based on Polythiophene and Its Derivatives.* Roskilde University Center, Denmark.

Si, P., & Bakker, E. (2009). Thin layer electrochemical extraction of non-redoxactive cations with an anion-exchanging conducting polymer overlaid with a selective membrane. *Chem. Commun.*, 5260-5262.

Smith, M. C., Gilbert, J. A., Mawdsley, J. R., Seifert, S., & Myers, D. J. (2008). In Situ Small-Angle X-ray Scattering Observation of Pt Catalyst Particle Growth During Potential Cycling. *J. Am. Chem. Soc., 130*, 8112-8113.

Sun, S., Xu, X., Wu, P., & Zhu, D. (1998). Characterization and electrical switching properties of Cu-tetracyanoquinodimethane films formed under different conditions. *J. Mater. Sci. Lett., 17*(9), 719-721.

Sundfors, F., Bereczki, R., Bobacka, J., Toth, K., Ivaska, A., & Gyurcsanyi, R. (2006). Microcavity based solid-contact ion-selective microelectrodes. *Electroanal., 18*(13-14), 1372-1378.

Sundfors, F., & Bobacka, J. (2004). EIS study of the redox reaction of Fe(CN)63-/4- at poly(3,4-ethylenedioxythiophene) electrodes: influence of dc potential and cOx:cRed ratio. *J. Electroanal. Chem., 572*(2), 309-316.

Sutter, J., Lindner, E., Gyurcsanyi, R. E., & Pretsch, E. (2004). A polypyrrole-based solid-contact Pb^{2+}-selective PVC-membrane electrode with a nonomolar detection limit. *Anal. Bioanal. Chem., 380*(1), 7-14.

Sutter, J., Radu, A., Peper, S., Bakker, E., & Pretsch, E. (2004). Solid-contact polymeric membrane electrodes with detection limits in the subnanomolar range. *Anal. Chim. Acta, 523*, 53-59.

T

Tavger, B. A., & Demikhovskii, V. Y. (1963). *Soviet Phys.-Solid State English Transl., 4*, 469.

Thomas, A., & Muniandy, K. (1987). Absorption and desorption of water in rubbers. *Polymer, 28*(3), 408-415.

Tidswell, I. M., Markovic, N. M., Lucas, C. A., & Ross, P. N. (1993). *In situ* x-ray-scattering study of the Au(001) reconstruction in alkaline and acidic electrolytes. *Phys. Rev. B, 47*(24), 16542-16553.

Tourillon, G., Mahatsekake, C., Andrieu, C., Williams, G. P., Garret, R. F., & Braun, W. (1988). Electronic structure and orientation studies of undoped pol-3-alkyl thiophenes electrochemically deposited on Pt as studied by NEXAFS. *Surf. Sci., 201*, 171-184.

U

V

Vazquez, M., Bobacka, J., Ivaska, A., & Lewenstam, A. (2002). Influence of oxygen and carbon dioxide on the electrochemical stability of poly(3,4-

ethylenedioxythiophene) used as ion-to-electron transducer in all-solid-state ion-selective electrodes. *Sens. Actuators B, 82*, 7-13.

Veder, J.-P., De Marco, R., Clarke, G., Chester, R., Nelson, A., Prince, K., et al. (2008). Elimination of Undesirable Water Layers in Solid-Contact Polymeric Ion-Selective Electrodes. *Anal. Chem., 80*(17), 6731-6740.

Veder, J.-P., De Marco, R., Connell, B., Dalgliesh, R., Pretsch, E., & Bakker, E. (2010). Water uptake in the hydrophilic solid-contact of polymeric ion-selective electrodes. *Analyst, In Preparation*.

Veder, J.-P., Nafady, A., Clarke, G., Williams, R. P., De Marco, R., & Bond, A. M. (2010). A Flow Cell for Transient Voltammetry and its Application to In Situ Grazing Incidence X-ray Diffraction Characterization of Electrocrystallised $Cd(TCNQ)_2$. *Electrochim. Acta, Submitted*.

Veder, J.-P., Nafady, A., De Marco, R., & Bond, A. M. (2010). A Combined Voltammetric/Synchrotron Radiation-Grazing Incidence X-ray Diffraction Study of the Electrocrystallization of Zinc Tetracyanoquinodimethane. In Preparation.

Vineyard, G. H. (1982). Grazing-incidence diffraction and the distorted-wave approximation for the study of surfaces. *Phys. Rev. B, 26*(8), 4146-4159.

W

Wakida, S.-i., & Ujihira, Y. (1988). Chemically Modified Copper Hybrid Ion Sensor with 7,7,8,8-Tetracyanoquinodimethane. *Jpn. J. Appl. Phys., 27*, 1314-1316.

Wei, Y. J., Ehrenberg, H., Kim, K. B., Park, C. W., Huang, Z. F., & Baehtz, C. (2009). Characterisation on the structural and electronic properties of thermal lithiated $Li_{0.33}MnO_2$. *J. Alloys Compd., 470*, 273-277.

Wiltshire, R. J. K., King, C. R., Rose, A., Wells, P. P., Hogarth, M. P., Thompsett, D., et al. (2005). A PEM fuel cell for in situ XAS studies. *Electrochim. Acta, 50*, 5208-5217.

X

Xu, X., Bojkov, H., & Goodman, W. (1994). Electrochemical study of ultrathin silica films supported on a platinum substrate. *Vacuum Science and Technology A, 12*(4), 1882-1885.

Y

Ye, Q., Borbely, S., & Horvai, G. (1999). Microstructure of Ion-Selective Plasticized PVC Membranes Studied by Small-Angle Neutron Scattering. *Anal. Chem., 71*(19), 4313-4320.

Yeum, B. (2001). ZSimpWin Version 2.00 (Version 2nd): EChem Software.

Yeum, B. (2001). Equivalent Circuit, Users Manual (Version 2nd).

Z

Zegenhagen, J., Renner, F. U., Reitzle, A., Lee, T. L., Warren, S., Stierle, A., et al. (2004). In situ X-ray analysis of solid/electrolyte interfaces: electrodeposition of Cu and Co on Si(111): H and GaAs(001) and corrosion of Cu_3Au(111). *Surf. Sci., 573*, 67-69.

Zhao, H., Heintz, R., Ouyang, X., & Dunbar, K. R. (1999). Spectroscopic, Thermal, and Magnetic Properties of Metal/TCNQ Network Polymers with Extensive Supramolecular Interactions between Layers. *Chem. Mater., 11*, 736-746.

Zhao, H., Heintz, R., Ouyang, X., Grandinetti, G., Cowen, J., & Dunbar, K. R. (1999). *Insight into the behaviour of $M(TCNQ)_n$ (n=1, 2) crystalline solids and films: x-ray, magnetic and conducting properties* (Vol. 518). Dordrecht: Kluwer.

Zhou, W., Ren, L., Lin, F., Jiao, L., Xue, T., Xian, X., et al. (2008). An electrical switch based on Ag-tetracyanoquinodimethane sandwiched by crossed carbon nanotube electrodes. *Appl. Phys. Lett., 93*(12), 123115/123111-123115/123113.

Appendix I

Electrochemical Impedance Spectroscopy (EIS)

Essentially, a small sinusoidal AC excitation potential is applied to an electrochemical system. The excitation potential has the form:

$$E(t) = E_o \sin(\omega t) \qquad \textbf{Equation I}$$

where E(t) is the potential at time t, E_o is the amplitude of the signal, and ω is the radial frequency expressed in radians / second. The radial frequency is related to the frequency, f, (in Hertz) by the expression:

$$\omega = 2\pi f \qquad \textbf{Equation II}$$

The measured response to the applied AC potential is an AC current signal containing the excitation frequency and its harmonics as expressed below:

$$I(t) = I_o \cos(\omega t - \phi) \qquad \textbf{Equation III}$$

where I(t) is the current at time t, I_o is the amplitude of the measured signal and ϕ is the phase angle between the perturbation and the response signal (1-2).

With a knowledge of the applied AC potential and measured AC current, the impedance can be calculated using the following derivation of Ohm's law:

$$Z(\omega) = \frac{E(t)}{I(t)} = \frac{E_o \cos(\omega t)}{I_o \cos(\omega t - \phi)} = Z_o \frac{\cos(\omega t)}{\cos(\omega t - \phi)} \qquad \textbf{Equation IV}$$

Accordingly, the impedance is expressed as a function of magnitude (Z_o) and phase shift (ϕ) (1). The expression Z(ω) is composed of real (Z') and

imaginary (Z") components which are often plotted as -Z" vs. Z'. The resultant graph is a Nyquist plot. In the simplest case, the Nyquist plot presents each time constant associated with the electrochemical system as separate semi-circles which begin from high frequencies and finish at low frequencies (see ***Figure I***). These semi-circles can be subsequently modelled to an equivalent circuit which represents the particular system under investigation. The impedance can be represented as a vector of length |Z| and the phase angle, ϕ, is the angle between this vector and the X-axis.

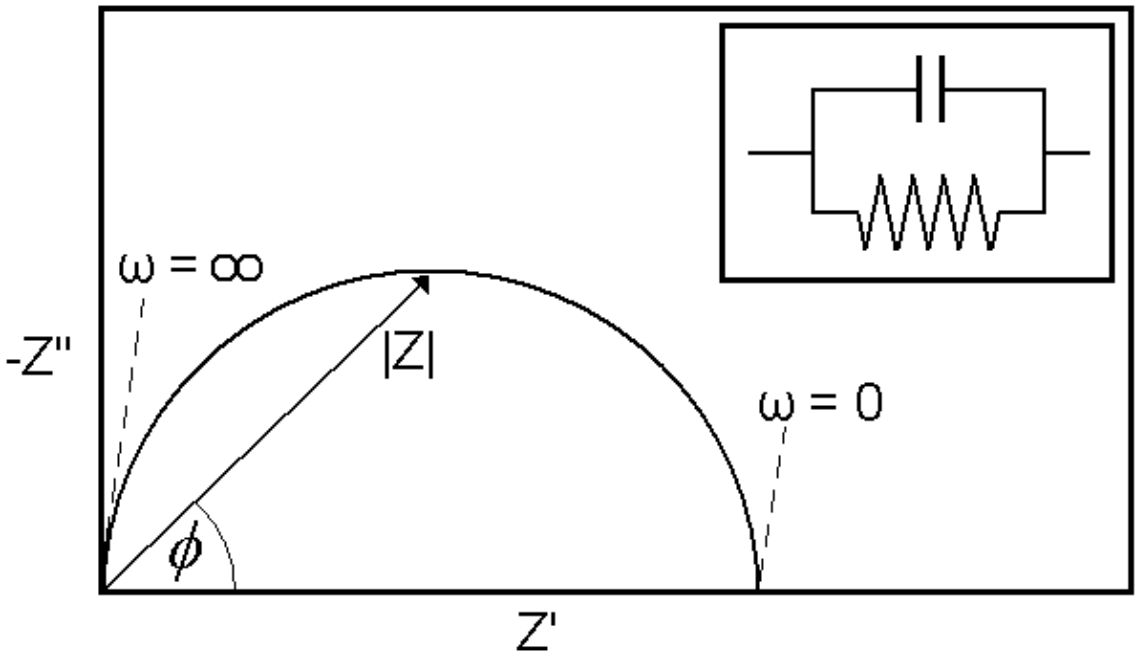

Figure I *A typical Nyquist plot of a simple electrochemical system with only one time constant. The inset presents an equivalent circuit for such a system.*

In practice, real electrochemical systems often contain many time constants which may result in only portions of the semi-circles being resolved. ***Figure II*** presents such a system in which multiple resistive and capacitive elements exist.

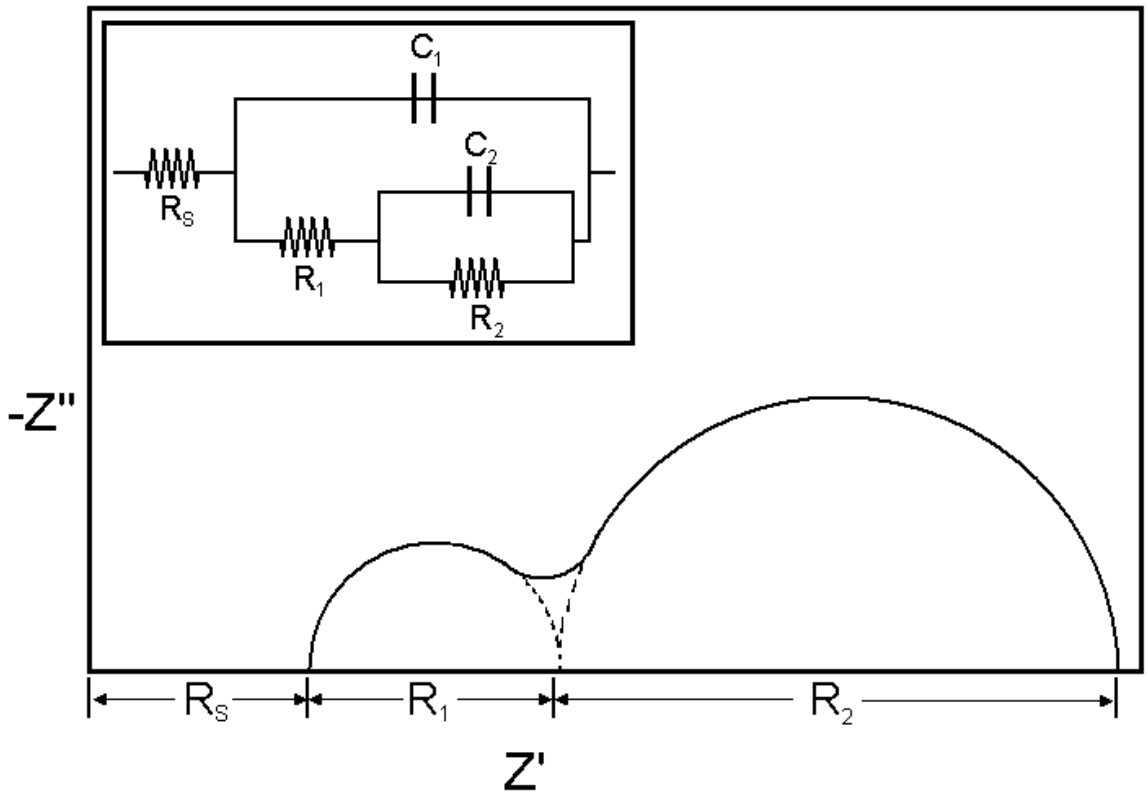

Figure II *An example of a Nyquist plot for a real electrochemical system. The inset shows an equivalent circuit for a system that produces such a Nyquist plot.*

Bode plots are also common features of EIS and are sometimes presented instead of, or together with, Nyquist plots. A Bode plot comes in two forms, either presenting the absolute impedance or phase angle plotted against the log of frequency. In contrast to the Nyquist plot, Bode plots clearly present information related to frequency (1). Examples of typical Bode plots are presented in ***Figure III***.

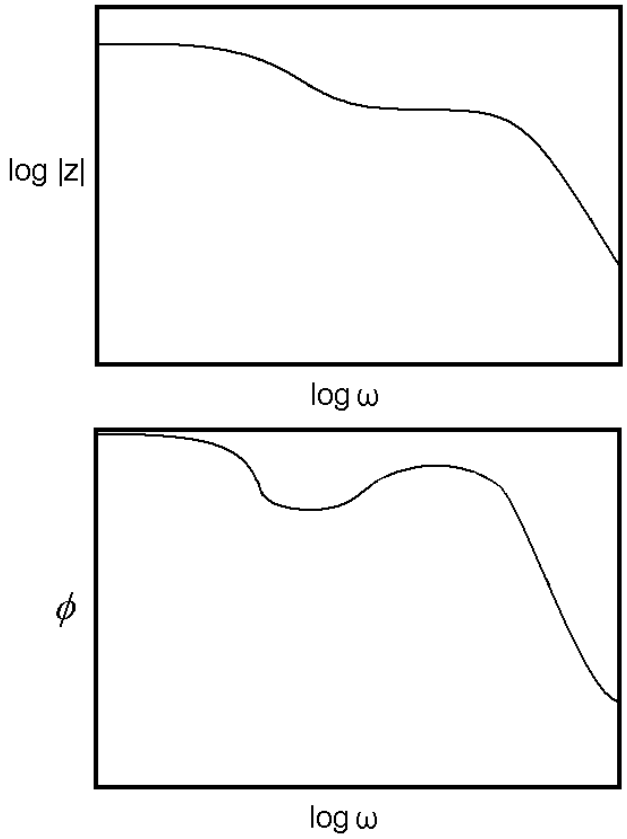

Figure III *Typical Bode plots for a system with an equivalent circuit of the type presented in* ***Figure II****.*

Neutron Reflectometry (NR)

Provided that the refractive indices on either side of an interface are different, a highly collimated beam of neutrons that impinges on an extremely flat surface will undergo reflection and refraction. Beyond the critical angle below which total internal or external reflection occurs, many neutrons get absorbed by the sample, transmitted through the sample and also reflected from the flat interface (3). Neutrons that are reflected from a thin film, such as a spin cast ion-selective membrane, not only originate from the superstrate / thin film interface but also from any underlying interfaces such as the thin film / substrate interface (3) (See ***Figure IV***).

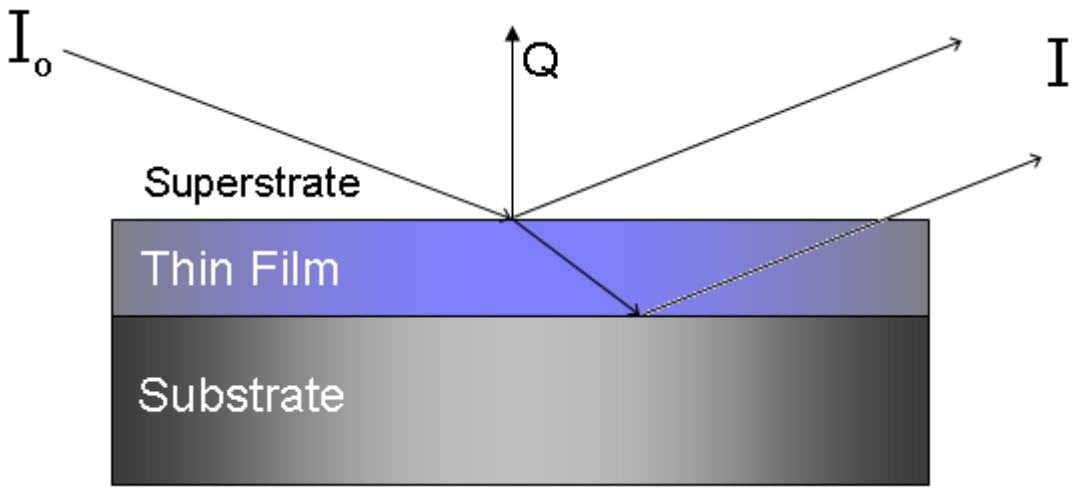

Figure IV *Simplified schematic of a typical reflectometry experiment. I_o and I represent the incident and reflected neutrons or X-rays. Q is the scattering vector which is normal to the thin film surface.*

If the interfaces that neutrons reflect from are sufficiently smooth, the difference in path-lengths of reflected neutrons will result in constructive and deconstructive interference in the reflected intensity (4). The reflectivity of the thin film sample can be measured as follows (5):

$$R = \frac{I}{I_o}$$ **Equation V**

where I is the number of neutrons reflected and I_o is the number of neutrons incident on the thin film.

The reflectivity is often then plotted as a function of the scattering vector, Q, which is given by the expression (5):

$$Q = \frac{4\pi \sin\theta}{\lambda}$$ **Equation VI**

where θ is the angle of incidence of the neutron beam and λ is the neutron wavelength.

Depending on the facility used to provide neutrons for reflectometry, the Q value may be varied by measuring reflected angles with monochromatic neutrons or by measuring the wavelength at a constant angle of incidence in a "time-of-flight" system. In either case, the resultant reflectivity profile presents a series of sharp fringes known as Kiessig fringes (see ***Figure V***). These fringes arise as a result of the constructive and deconstructive interference of reflected neutrons. From this profile, a model can be constructed and refined to replicate the measured reflectivity trace and finally reveal the physical and structural properties of the system.

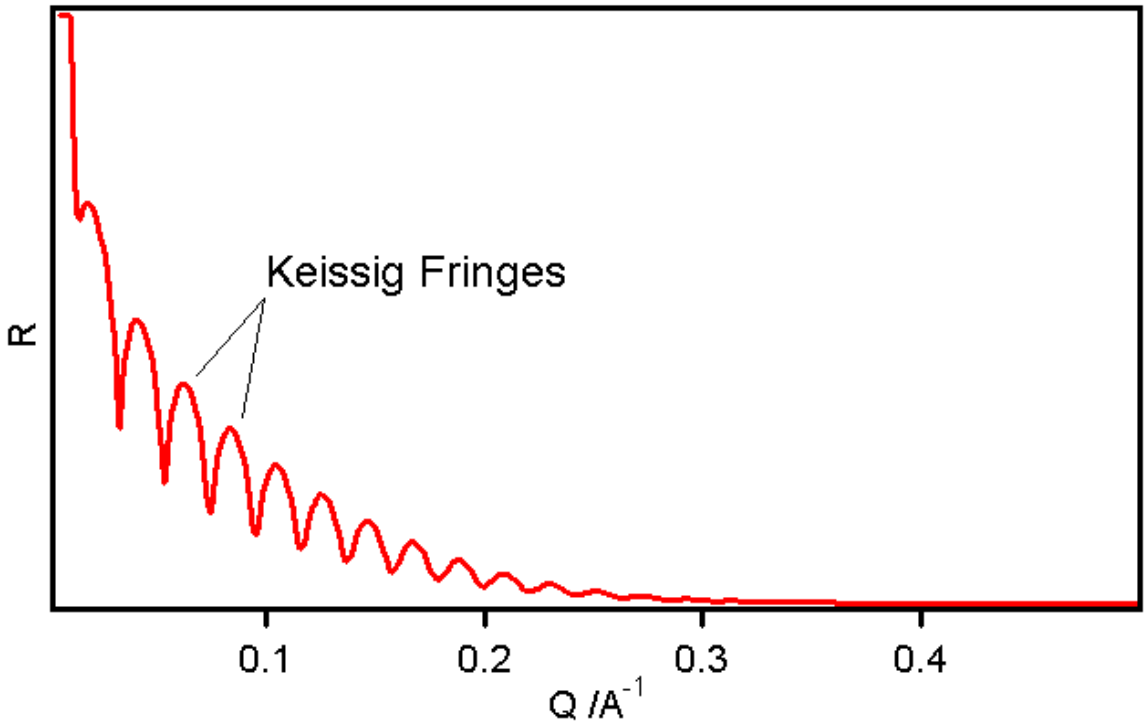

Figure V *A typical neutron reflectivity profile for a thin polymer film (300 Å thickness) on a silicon substrate. The Kiessig fringes evident in the spectrum result from the constructive and destructive interference of the reflected neutron beam.*

In order to construct a model to fit the reflectivity data one may first estimate the film thickness through the inverse relationship of the spacing

between the minima of successive fringes (ΔQ_f) and the film thickness, i.e. $\Delta Q_f = 2\pi / d$. The neutron refractive index, n, of a specimen may then be considered. With samples in which neutron absorption is too small to consider, the refractive index is slightly less than unity and is expressed as follows (3):

$$n = \frac{\lambda^2}{2\pi} N_A \sum_i \frac{\rho_i b_i}{M_i}$$ **Equation VII**

where N_A is Avagadro's constant, λ is the wavelength, b_i is the neutron scattering length of the i^{th} component with density ρ_i and atomic mass M_i. Notably, the terms N_A, b_i and M_i combine to give the scattering length density (SLD) of the material. The reflectivity may then be calculated as follows (3):

$$R(Q) = \frac{16\pi^2}{Q^4} \left|\rho'(Q)\right|$$ **Equation VIII**

where Q is the scattering vector defined in **Equation VI** and $\left|\rho'(Q)\right|$ is the Fourier transform of the SLD. Importantly, local roughness in the sample will alter the specular reflectivity in a manner akin to that of a diffuse interface. A Debye-Waller like factor based on the root mean square surface roughness may be added to account for such a physical characteristic of the sample (3).

A notable feature of neutron studies lies in the random variation of neutron scattering lengths from element to element. This is in stark contrast to X-rays which increase almost linearly with atomic number. Furthermore, isotopes of an element scatter neutrons with different amplitude and sometimes, as in the case of protons and deuterons, with opposite phase (3). Using these properties of neutron scattering, an investigator may achieve contrast variation with various samples by isotopically labelling differing components with hydrogen or deuterium. This is often carried out to provide different perspectives that may aid in revealing certain components which may otherwise have been obscured if only one contrast was used (as illustrated in ***Figure VI***).

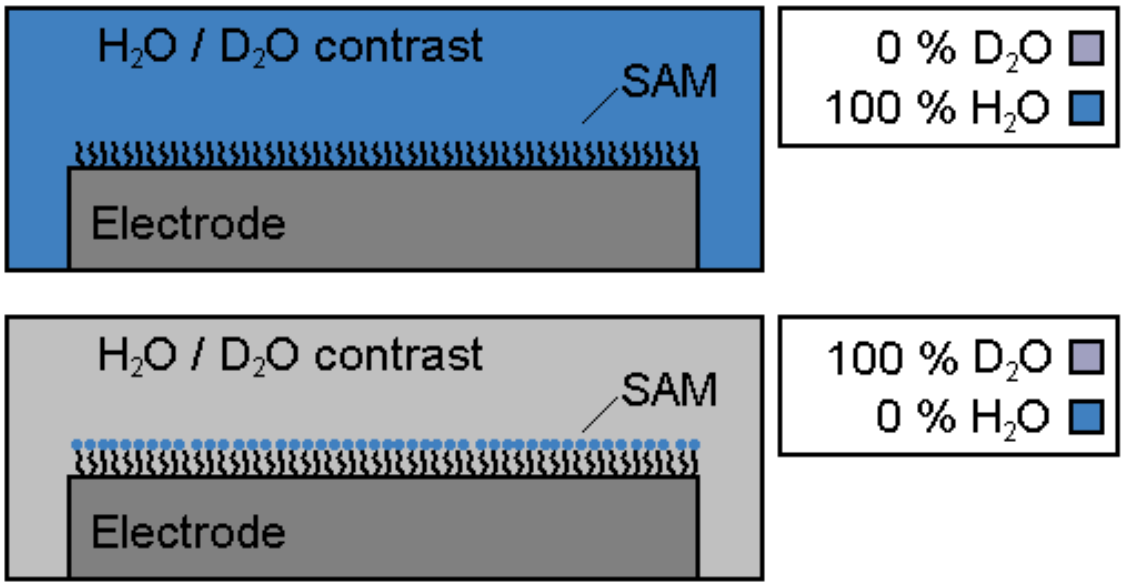

Figure VI *An illustration of contrast variation in a solid / liquid NR experiment for a self-assembled monolayer (SAM) system. Only a tightly packed hydrocarbon film is visible to neutrons when H_2O is used as the solvent. A change in contrast to D_2O reveals a bulky head group on the hydrocarbon chain which would otherwise have been overlooked if only one contrast was used.*

Small Angle Neutron Scattering (SANS)

Many powerful techniques developed to study materials over recent years are rendered inadequate by their very power when applied to materials of the complexity of polymer alloys, colloidal suspensions or microporous media (6). Essentially, these techniques can yield information in such fine detail that the more interesting features of the bulk material are obscured. On the other hand, SANS emerges as a technique in which the microscopic length scale is probed whilst remaining insensitive to much finer or much coarser details.

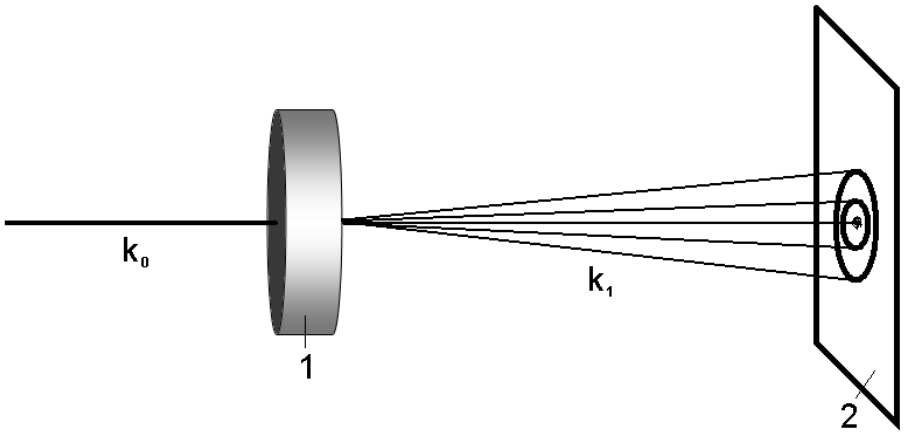

Figure VII *Simplified schematic of a typical SANS experiment. 1) sample, 2) 2-dimensional detector, k_o) incident wave vector, k_1) scattering wave vector.*

Figure VII presents a schematic of a typical SANS experiment. Importantly, the scattering vector, Q, is equal to the scattering vector, k_1, minus the incident wave vector, k_o. Typically, SANS involves a sample that is situated in a beam of collimated neutrons so that a small volume, V, is illuminated such that:

$$V = At_s \qquad \textbf{Equation IX}$$

where A is the cross-sectional area of the beam and t_s is the pathlength of the sample (7).

Similar to NR, incident neutrons are transmitted, absorbed or scattered. A detector records the number of neutrons scattered into a solid-angle element, ΔΩ, at a scattering angle, θ, from the sample as expressed by:

$$I_s(\lambda,\theta) = \Phi_o \Delta\Omega \eta(\lambda) TV \frac{d\sigma}{d\Omega}(Q) \qquad \textbf{Equation X}$$

where Φ_o is the neutron flux on the sample, η is the detector efficiency for a given wavelength, T is the sample transmission and dσ/dΩ is the differential scattering cross section per unit volume (8).

The major objective of a SANS experiment is to determine the differential scattering cross-section of a sample because it is this term that contains all of the information on the shape, size and interactions of the scattering bodies in the sample (7). The differential cross-section is expressed as:

$$\frac{d\sigma}{d\Omega}(Q) = N_p V_p^2 (\Delta\delta)^2 P(Q) S(Q) + B_{inc} \qquad \textbf{Equation XI}$$

where N_p is the number concentration of scattering bodies, V_p is the volume of a scattering body, $(\Delta\delta)^2$ is the square of the difference in neutron scattering length density, P(Q) is a function known as the form or shape factor, S(Q) is the inter-particle structure factor, Q is the modulus of the scattering vector and B_{inc} is the incoherent background signal.

By using the relationship in **Equation XI** one can begin to construct a model to attain all of the necessary information required from the system of interest.

In a similar manner to NR experiments, the use of neutrons in the technique of SANS also allows investigators to exploit contrast variation in samples. Varying the deuterium and hydrogen ratios in samples highlights interesting aspects and hence achieves greater insights into the system under scrutiny.

Secondary Ion Mass Spectrometry (SIMS)

SIMS is an *ex-situ,* destructive technique in which primary ions bombard a sample's surface and dislodge secondary species by the action of sputtering. These ions are analysed by a mass spectrometer (MS) (9). Secondary species are positive, negative or neutral depending on the primary ion's identity. However, only charged species are analysed by the MS (see ***Figure VIII***).

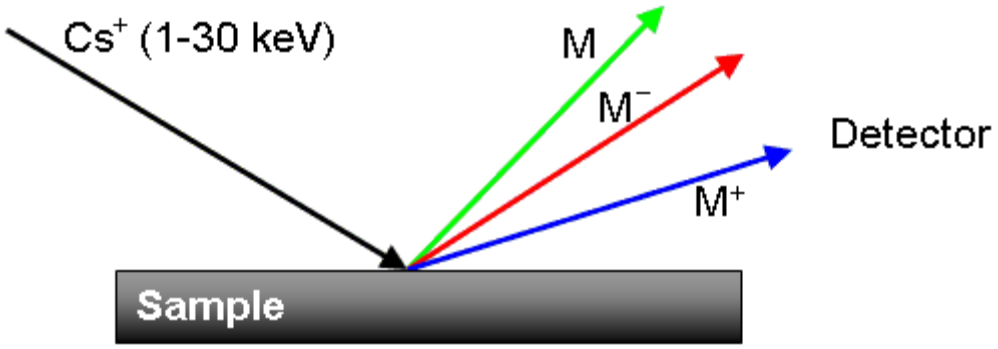

Figure VIII *Schematic of a common SIMS experiment. The sample is bombarded by high energy ions that lead to the ejection of charged and neutral species. Only charged ions are detected by the MS.*

Importantly, a "dynamic SIMS" instrument, as used throughout this research, possesses additional benefits over traditional "static SIMS" instruments. As opposed to static SIMS instruments which only provide sub-monolayer elemental analyses, dynamic SIMS instruments have the added options of imaging and depth profiling capabilities. In order to carry out SIMS in the imaging mode, the incident beam is focused and scanned across the surface to obtain compositional images. On the other hand, depth profiling measurements make use of the destructive nature of the SIMS technique by recording sequential SIMS spectra as the surface is gradually sputtered away by the primary ion beam probe (9). Accordingly, a study of the intensity of secondary ions as a function of time can be correlated to the secondary ion yield as a function of depth.

These capabilities establish SIMS as an ideal characterisation tool for electrochemical systems, particularly those that possess multiple layers and interfaces. The inherent ability of SIMS to provide compositional information as a function of depth is extremely valuable for the prospect of examining the complex buried interface of many electrochemical systems.

Synchrotron Radiation / Fourier Transform - Infrared Microspectroscopy (SR / FT-IRM)

SR / FT-IRM is a mature analytical technique that has been applied to studies of a multitude of complex systems (10). IR spectroscopy measures the absorption of IR radiation by chemical bonds in a material. The absorption occurs as a result of the specific frequencies at which molecules rotate or vibrate corresponding to discrete energy levels, or vibrational modes (refer to ***Figure IX*** for examples of vibrational modes). For a vibrational mode in a molecule to be IR active, there must be a change in the molecule's dipole moment as a result of normal molecular motion (10). The resultant IR spectrum, containing various IR bands of different frequencies and intensities, may be used to identify the presence of particular compounds in a mixture.

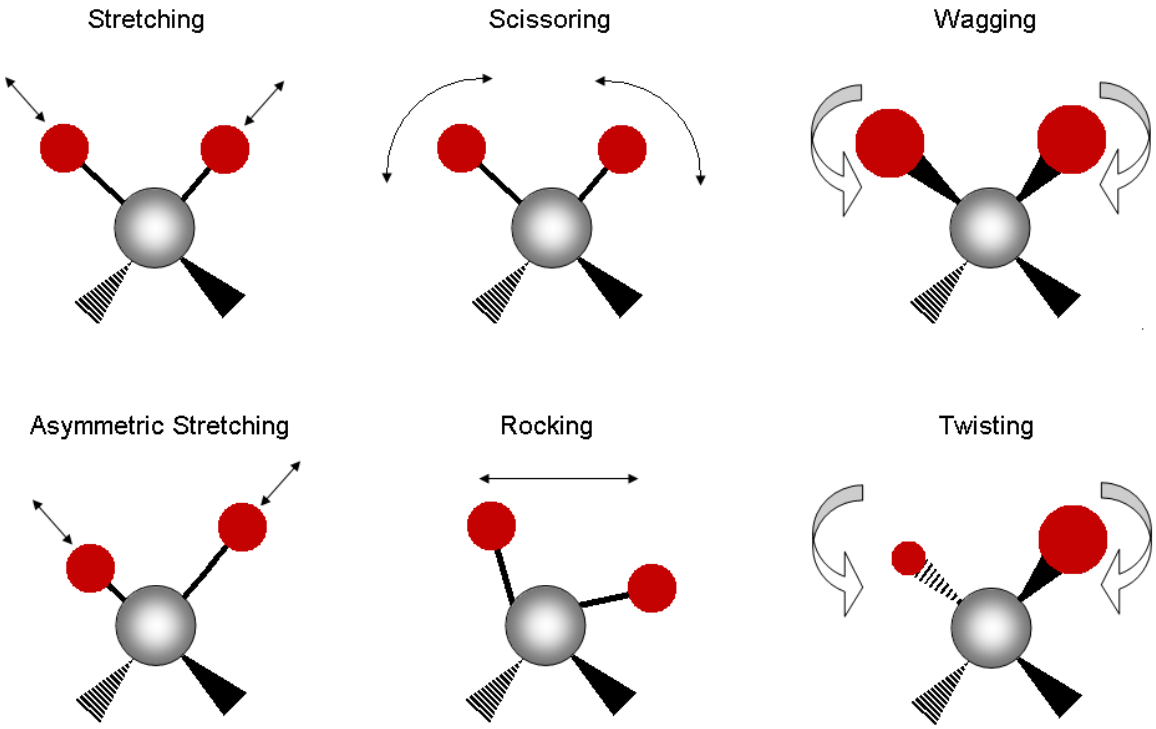

Figure IX *The various vibration modes of a CH_2 group.*

FT-IR spectroscopy, as opposed to IR spectroscopy, is simply a measurement technique for collecting infrared spectra. The technique utilizes an interferometer in place of a monochromator used in conventional (dispersive) IR

spectroscopy. Instead of measuring the amount of energy absorbed whilst the frequency of IR light is varied, an interferogram is measured on which a Fourier transform can be performed to obtain the traditional IR spectra. A major benefit to using FT-IR spectroscopy over the more conventional dispersive IR spectroscopy comes from the speedier acquisition of data which allows multiple spectra to be collected and averaged to improve the signal-to-noise ratio.

Of special interest to this research is the sub-class of IR spectroscopy known as SR / FT-IRM. This technique couples optical microscopy with FT-IR spectroscopy. Notably, the power of SR / FT-IRM is drawn from correlations between the spatial resolution provided by the optical microscope and the identification of subtle differences in chemical components through FT-IR spectroscopy (11).

Without a doubt, the most practical feature of SR / FT-IRM is its ability to undertake mapping measurements and produce 3-dimensional graphics based on the existence of certain chemical species correlated to specific locations on the imaged sample. Essentially, an area of a sample is defined to be analysed using the optical microscope. The use of the high brilliance synchrotron radiation allows for physical apertures to be placed in the beam path so that a well-specified region of the imaged area is sampled. Spectral data are obtained for this region and the sample is subsequently moved so that the apertures are focused on an adjacent portion of the sample. The spectral data are again obtained and the whole process is repeated until the desired sampling area is mapped (11). Once the desired sampling area is mapped, individual IR bands can then be integrated to produce an intensity map based on the previously imaged sample.

Synchrotron Radiation / X-ray Photoelectron Spectroscopy (SR / XPS)

SR / XPS involves a study of electrons that are ejected from a sample into a surrounding vacuum environment when irradiated with monochromatic X-rays. XPS involves a study of the kinetic energies of unscattered electrons. Clearly, the majority of atoms that produce electrons that are unscattered are located sufficiently close to the surface (<20 Å)(12). In this respect, XPS can be considered a surface sensitive technique. The distribution of the unscattered, ejected electrons vs. their kinetic energy is known as the photoelectron spectrum.

The energy, $h\nu$, required for a photon to eject an electron is given by the following expression(12):

$$h\nu = \mathrm{E_b} + \mathrm{E_k} + \mathrm{E_r} + \phi_{\mathrm{sp}} \qquad \textbf{Equation XII}$$

where $\mathrm{E_b}$ is the binding energy, $\mathrm{E_k}$ is the kinetic energy of the electron in the spectrometer, $\mathrm{E_r}$ is the recoil energy at the site of the ejection and ϕ_{sp} is the work function of the spectrometer. The latter two parameters are correction factors and are usually very small. However, they must be taken into account in accurate binding energy assignments. Nevertheless, the terms of most interest to researchers are the kinetic energy of the ejected electron and the energy required to remove the electron from the initial state, i.e, the binding energy. The binding energies are discrete values that are well-defined for different atomic levels in various chemical states. Hence, one can expect discrete kinetic energies corresponding to different atomic levels. The peaks presented in the photoelectron spectra correspond to each atomic level in each chemical state (see ***Figure X***).

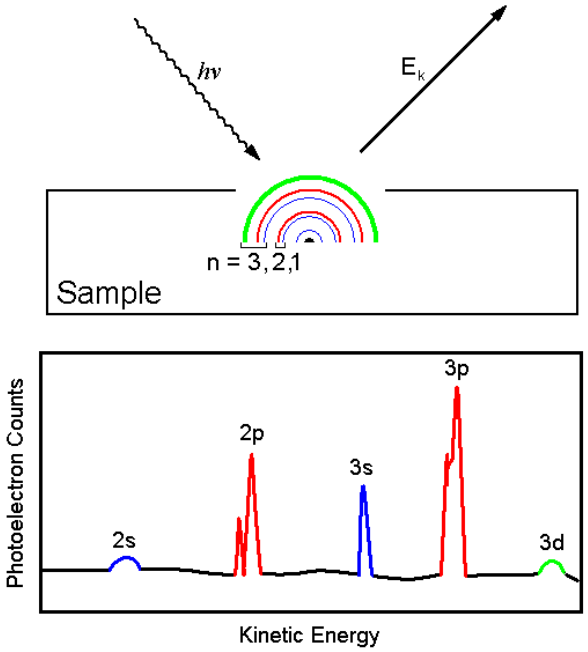

Figure X *Schematic of the electron emission process (upper) and the resulting photoelectron spectrum (lower). The subshells are colour-coded such that blue, red and green represent the "s", "p" and "d" subshells respectively. (Adapted from Bard and Faulkner (12)).*

A significantly useful feature of XPS is its ability to extract information pertaining to the oxidation states of atoms. Such a characteristic of XPS is based on the fact that atomic orbitals exhibit small chemical shifts depending on their chemical environment and bonding status (13). The chemical shifts allow a distinction between various valence or electronic states of atoms.

Synchrotron Radiation / Grazing Incidence X-ray Diffraction (SR / GIXRD)

SR / XRD is a method that is generally used to determine the way in which atoms in a crystal are arranged. Diffraction occurs as a result of the interaction of X-rays with the repeating atomic structure of a crystalline material. A prerequisite of diffraction is that the repeat distance must be approximately the same as the wavelength. Bragg's law of diffraction defines the relationship

between the wavelength, λ, interatomic spacing, d, and the angle of the diffracted beam, θ, as follows:

$$n\lambda = 2d\sin\theta \qquad \textbf{Equation XIII}$$

where n is an integer.

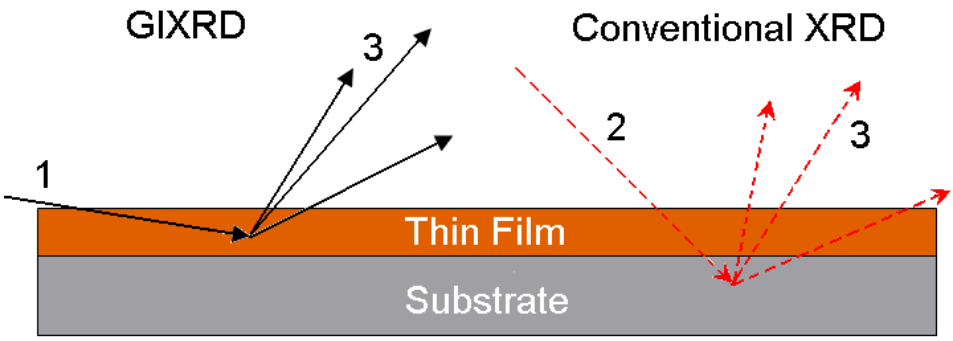

Figure XI *Simplified schematics of grazing-incidence X-ray diffraction (GIXRD) vs. conventional X-ray diffraction (XRD). 1) Incident X-ray beam at small angles for GIXRD, 2) Incident X-ray beam at larger angles in conventional XRD, 3) diffracted X-rays. The direction of X-rays at low angles of incidence allows GIXRD to only sample surfaces or thin films. Conventional XRD, on the other hand, has a larger angle of incidence and hence a larger penetration depth which samples the substrate in addition to the thin film.*

X-rays that impinge on a crystal can diffract into many different directions which can be measured in terms of both intensity and angle. From this data, an accurate picture of the crystalline material's structure, order / disorder, chemical bonds, etc. can be reconstructed with relative ease. **Note:** XRD is a well-established technique that has been reviewed extensively over the past several decades. Accordingly, the principles of conventional XRD will not be discussed in this work. The reader is instead referred to the excellent review by Robinson and Tweet (14) for further information on the theoretical and practical aspects of XRD.

SR / GIXRD, on the other hand, concerns the direction of the collimated beam of X-rays at small incident angles such that diffraction can be made surface sensitive (15-16) (see ***Figure XI***). Below the critical angle for a given wavelength of radiation, SR / GIXRD accomplishes its surface sensitivity by restricting the depth of penetration of the externally reflected X-ray beam and the concomitant sampling depth in the order of angstroms. With X-ray absorption taken into account, surface sensitivity also remains at angles slightly above the critical angle. At X-ray energies, the refractive index for most materials is slightly below 1.0, therefore if the angle of the incident beam is small enough, total external reflection occurs (17). At these angles the beam skims across the sample so that the X-ray intensity is the highest at the surface. The sample is not entirely invisible to X-rays at this point due to an evanescent wave that penetrates the surface. Importantly, the penetration depth of the evanescent wave at such low glancing angles can be purposely varied between tens to thousands of angstroms by making small adjustments to the incident angle of the X-ray beam. When the X-ray beam is incident below the critical angle, any lateral order at the surface will produce diffraction beams at various exit angles (17).

SR was used in the GIXRD studies because of the limitations associated with conventional laboratory-based instruments. Most significantly, at grazing angles, much of the incident X-ray beam is wasted because a significant portion either hits the sides of the sample or passes entirely over the sample (17). Although focusing the incident X-ray beam reduces such an undesirable effect, the converging beam contains a range of incident directions, with many not meeting the prerequisite of falling below the critical angle. The ability of synchrotron sources to provide incident beams that are compact and collimated thus reduces the impact of these undesirable effects.

References

1. Gamry-Instruments. Electrochemical Impedance Spectroscopy Theory: A Primer. 2006 [cited 2010]; Available from: http://www.gamry.com/App_Notes/EIS_Primer/EIS_Primer.htm.

2. Macdonald JR. Impedance Spectroscopy Emphasizing Solids Materials and Systems. New York: John Wiley & Sons; 1987.

3. James M. Characterisation of Thin-Film Surfaces and Interfaces Using Neutron Reflectometry. Aust J Chem. 2001;54:487-91.

4. Schmidt H, Huger E, Chakravarty S, Stahn J, Gutberlet T, Tietze U, et al. Neutron Reflectometry: A Tool to Investigate Diffusion Processes in Solids on the Nanometer Scale. Adv Eng Mater. 2009;11(6):446-51.

5. Russell TP. X-ray and neutron reflectivity for the investigation of polymers. Mater Sci Rep. 1990;5:171-81.

6. Melnichenko YB, Wignall GD. Small-angle neutron scattering in materials science: Recent practical applications. J Appl Phys. 2007;102(021101):1-24.

7. King SM. Small Angle Neutron Scattering. 2003 [cited 2010]; Available from: www.isis.rl.ac.uk/archive/largescale/loq/documents/sans.htm.

8. May RP. Small-Angle Scattering. In: Dianoux A-J, Lander G, editors. Neutron Data Booklet. Grenoble: OCP Science; 2003.

9. Griffiths J. Secondary Ion Mass Spectrometry. Anal Chem. 2008;80:7194-7.

10. McKelvy ML, Britt TR, Davis BL, Gillie JK, Lentz LA, Leugers A, et al. Infrared Spectroscopy. Anal Chem. 1996;68:93R-160R.

11. Ng L, Simmons R. Infrared Spectroscopy. Anal Chem. 1999;71:343R-50R.

12. Bard AJ, Faulkner LR. Electrochemical Methods: Fundamentals and Applications. second ed. Harris D, Swan E, Aiello E, editors. New York: John Wiley and Sons, Inc.; 2001.

13. Christmann K. Topics in Physical Chemistry: Introduction to Surface Physical Chemistry. Baumgartel H, Franck EU, Grunbein W, editors. New York: Springer; 1991.

14. Robinson IK, Tweet DJ. Surface x-ray diffraction. Rep Prog Phys. 1992;55:599-651.

15. Marra WC, Eisenberger P, Cho AY. X-ray total-external-reflection-Bragg diffraction: A structural study of the GaAs-Al interface. J Appl Phys. 1979;50(11):6927-33.

16. Eisenberger P, Marra WC. X-ray Diffraction Study of the Ge(001) Reconstructed Surface. Phys Rev Lett. 1981;46(16):1081-4.

17. Dutta P. Grazing incidence X-ray diffraction. Current Sci. 2000;78(12):1478-83.

Appendix II

The following section presents a preliminary investigation into an interesting observation noted when studying thin film ion-selective electrodes by neutron reflectometry and electrochemical impedance spectroscopy.

Tuning Electrochemical Devices using Quantum Effects

Deviations from the classical theory of resistivity have been observed in an electrochemical sensor system utilizing poly(methylmethacrylate) / poly(decylmethacrylate) (PMMA/PDMA) ultra-thin copolymer films. A significant amount of research has been undertaken on quantum effects in metallic and semiconducting thin films in terms of their optical behaviour and electronic band gaps; however, the resistivity and its dependence on film thickness has received little attention despite an obvious opportunity to utilize this principle in the tunability of practical devices. The most notable contribution to research on the dependence of film thickness on the resistivity of semiconductors was carried out by Davey *et. al. (1)* whereby vacuum-evaporated germanium was deposited onto circular polished quartz plates enabling the electrical resistance of the thin films to be studied as a function of deposition thickness. Furthermore, the only study conducted on an electrochemical system, to the best of our knowledge, was achieved using thin silica films supported on a Pt (111) substrate electrode (2). Clearly, knowledge of the electrical properties of a real electrochemical system employing a thin film device (e.g., a molecularly thin polymer sensor) will be of immense value to electrochemists and materials scientists alike, allowing scope for the tuning of the physical properties and concomitant behaviour of practical electrochemical devices using nanotechnology.

Twelve different films of PMMA / PDMA copolymer doped with a Ag^+ IV ionophore, with molecularly thin layers in the range 40-600 Å (on a doped silicon wafer substrate), as well as 1-100 µm (on a gold substrate) were prepared and investigated using electrochemical impedance spectroscopy (EIS). The ultra-thin films were deposited onto an atomically smooth silicon wafer via a spin coating method using xylene as the casting solvent at a rotation speed of 3500 rpm, whilst the 1-100 µm films were drop cast onto a gold tip electrode using dichloromethane as the solvent. It was established that the ultra-thin films completely covered the silicon substrate, as verified using X-ray reflectometry (XR) (***Figure i***) and EIS (***Figure ii***) of the thin films. Most significantly, the XR data, modelled using Igor Pro-Motofit software (3), suggested that the thin films were of excellent quality with a surface roughness of approximately 4 Å, and the silicon substrate was also shown to be atomically smooth, with a surface roughness of about 5 Å. XR was also used to determine the thicknesses of the ultra-thin films. It is important to note that the EIS Bode phase and Nyquist plots for all electrodes, either the macroelectrode or the molecularly thin film electrodes, suggested that a non-porous film of ion sensing polymer had been deposited onto the electrode substrate, as evidenced by a well-defined high frequency bulk membrane time constant or RC element (see ***Figure ii***). Significantly, if the substrate electrode had not been covered completely by the molecularly thin film of ion sensing polymer then the high frequency bulk membrane time constant would be either severely blurred, or absent totally in the Bode phase plot.

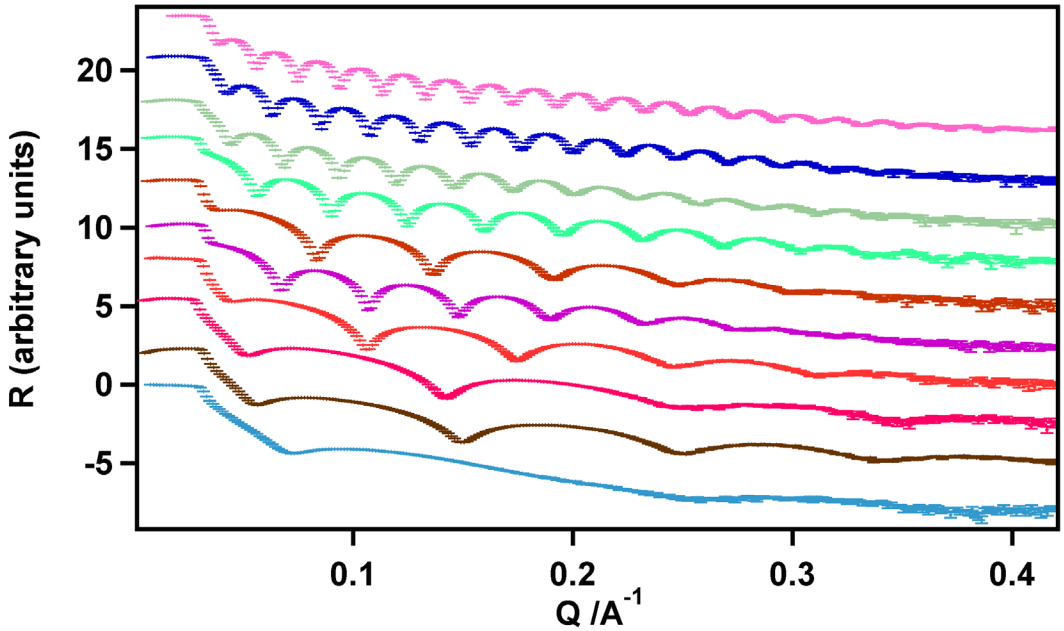

Figure i *Experimental XRR reflectivity curves for various PMMA/PDMA film thicknesses.*

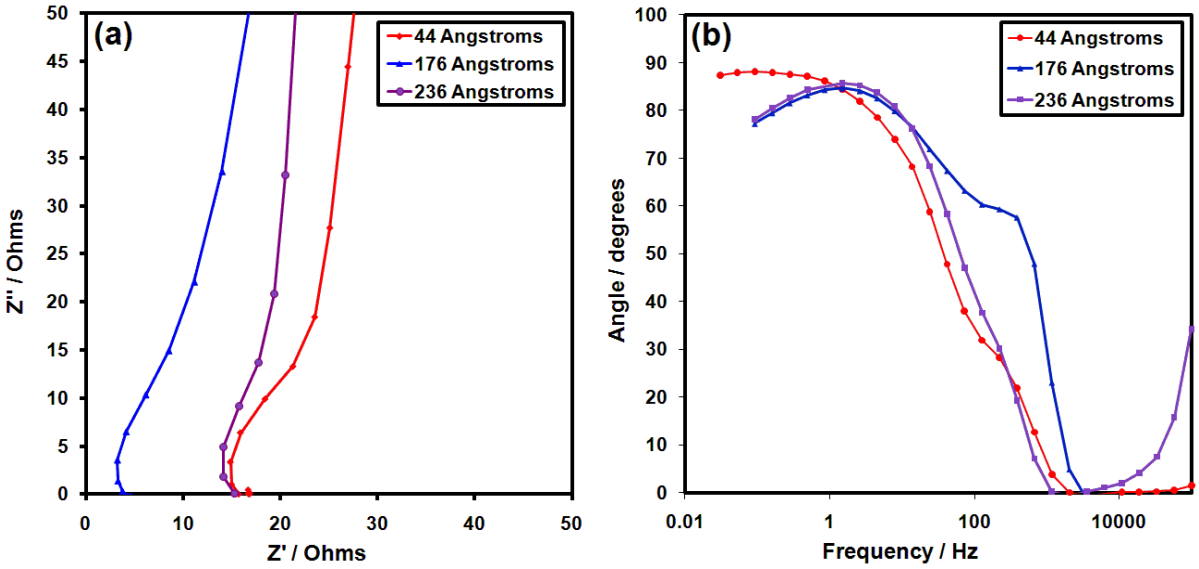

Figure ii *Nyquist (a) and Bode phase plots (b) for a selection of molecularly thin film ISEs.*

The resistances were measured using EIS and modelled in the complex-plane impedance plots using the ZSimpWin software (4). Accordingly, the model

provided the bulk membrane resistivities that are presented in ***Figure iii***. It is very clear that the resistivities of the ultra-thin films deviate markedly from the value for the thick or 1-100 µm films of the PMMA/PDMA copolymer. Although it is not presently possible to draw an unequivocal conclusion about this observation, due to a relative lack of information regarding the physical and chemical properties of the copolymer material, it is nevertheless possible to speculate about the origins of the observed deviations in the bulk membrane resistivity with molecularly thin films.

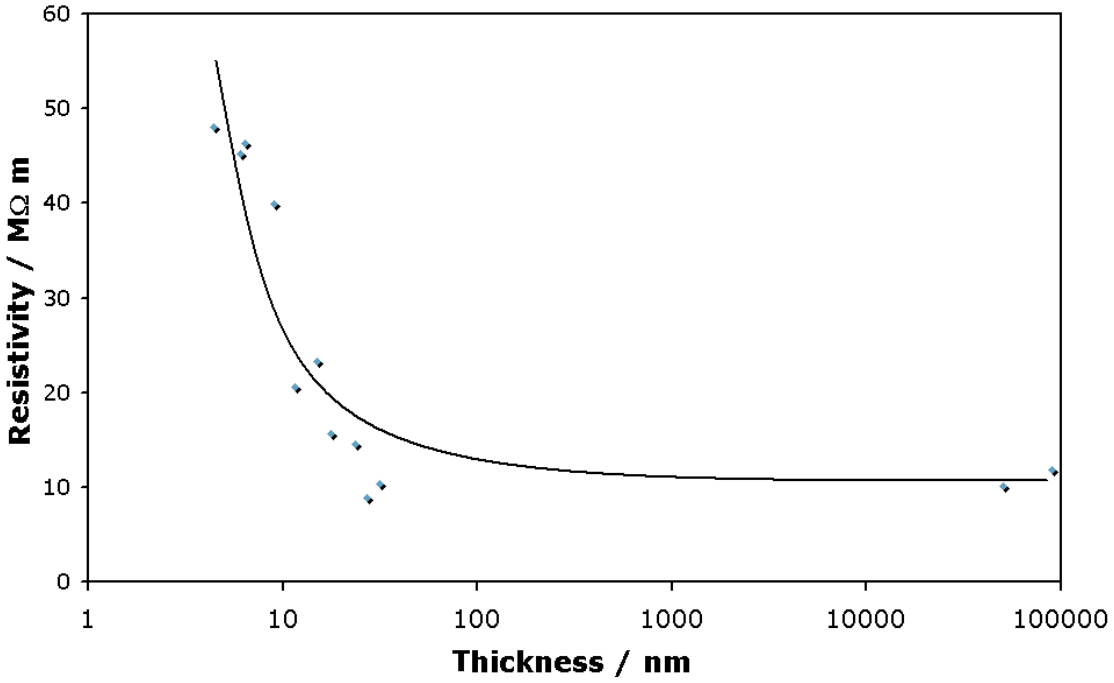

Figure iii *Presents the bulk membrane resistivities measured for ISE films of various thicknesses. A trend line is included to emphasize the deviation from the classical theory of resistivity.*

Note, the authors modelled a scenario based on a constant PMMA / PDMA / Si contact resistance of 21 ohm added to a bulk membrane resistance calculated by a simple linear scaling of the bulk membrane resistivity at 1-100 µm (i.e., 10 MW m on Au) to the ultra-thin films (see ***Supplementary Figure ii***). Even though the model incorporating a constant bias of 21 ohm yielded a very similar trend to the one presented in ***Figure iii***, it was abundantly clear that the

calculated resistivity in the range 30-100 nm was significantly higher than the actual bulk resistivity at 1-100 μm, unlike the observed outcomes for layers at around 30-100 nm whereby the observed resistivity was very similar to the bulk resistivity observed at 1-100 μm. If a constant contact resistance of 21 ohm together with a linear scaling of the bulk membrane resistivity to ultra-thin films was responsible for the observed trend in resistivity then the modelling revealed that the 30-100 nm films should have shown a clear positive bias in resistivity in this range. This anomaly together with the fact that the observed change in resistivity is sharper or more abrupt than the gradual increase predicted by a contact resistance of 21 ohms demonstrate that an alternative explanation (e.g., quantum effects) is responsible for this behaviour. Further credence for this possibility is given by the fact that it is well known that the reciprocal of the charge carrier mobility in the film is ascribable to an additivity of the reciprocals of the intrinsic charge carrier mobility, impurity / imperfection charge carrier mobility and surface scattering mobility (5), so the latter must be manifested at low film thicknesses. Also, the absence of a new EIS time constant for the resistance-capacitance coupling of a contact resistance at the PMMA / PDMA-Si wafer interface, which is expected to prevail with ultra-thin films possessing very low resistances and capacitances, is further evidence of the absence of a significant bias in resistivity due to a constant contact resistance. Last but not least, a consistency in the bulk resistivities of 30-100 nm films on Si, Au and Pt also suggests a negligible contact resistance at the PMMA / PDMA-Si interface, as it is very unlikely that a comparable contact resistance would be present on different electrode substrates.

In summary, the resistivity data reported herein is free of experimental artefacts, and is most probably due to surface scattering phenomena associated with quantum effects.

In this study of PMMA / PDMA molecularly thin films, the observed enhancement in resistivity as a function of film thickness in this nanoscale

domain is self-consistent with the measured behaviour of thin films of germanium deposited onto polished silica (1). Nevertheless, these results are contradictory to those of Xu *et.al.* (2) who noted that the resistivity of a silica thin film was several orders of magnitude less than that of a thick film of silica. Xu *et.al.* (2) rationalized this phenomenon by invoking quantum effects such as electron tunnelling that are linked to highly ordered and structurally aligned hydroxyl functionalities providing conductive defects at the grain boundaries of the silica thin films (2). The phenomenon of quantum tunnelling is highly unlikely in the highly disordered or amorphous films of PMMA / PDMA due to a lack of ionizable functional groups in close proximity, so as to enable electron hopping or tunnelling effects in the material. Nevertheless, quantum effects may provide a rationalization for these unconventional variations in electrical resistivity as a function of film thickness in molecularly thin films. For electrical conductors or semiconductors, it is widely accepted that if the thickness of a semiconducting film is comparable to or smaller than the mean free path and the de Broglie wavelength of the charge carriers in the film, then the film is expected to display quantum effects (5-6). These quantum effects are manifested for all transport properties including the electrical resistivity (6-7). Indeed, this may be the cause of the deviations from the resistivity behaviour of a thick copolymer film, as has also been noted for well-known semiconducting systems such as bismuth where quantum effects can even occur for films as thick as 1 mm at helium temperatures (8). Origin *et.al.* (9) confirmed this behaviour for bismuth films at varying temperatures and film thicknesses.

The low conductivity of the copolymer is akin to but not equal to that of an electrical insulator, although the deviation from the classical theory on the electrical resistivity of molecularly thin films is indicative of a semiconductor material. Chopra (8) proposed theoretically that the dielectric constant of an insulator should be preserved down to a few atomic layers, so that no dependence of the electrical resistivity as a function of thickness is expected for films thicker than 50 Å. Hence, since the observed shifts in resistivity for the bulk

membrane occurred at thicknesses above 50Å, it can be deduced that the copolymer acts more like a semiconductor where surface transport phenomena are well known to significantly influence the electrical properties of the semiconducting material (8). In effect, reducing the thickness of the semiconducting film beyond a certain quantum length ensures that the electronic mean free path is larger than the sample thickness. It is in this region that ballistic transport properties become apparent (10). Essentially, the momentum dissipation of the charge carriers is now dominated by scattering from irregularities at the film boundary, as opposed to scattering that would normally take place within the bulk of the material. This results in a flat-line in the resistance when the film thickness is reduced below the mean free pathlength, as evidenced in ***Figure iv*** which is an alternative representation of the data presented in ***Figure iii***.

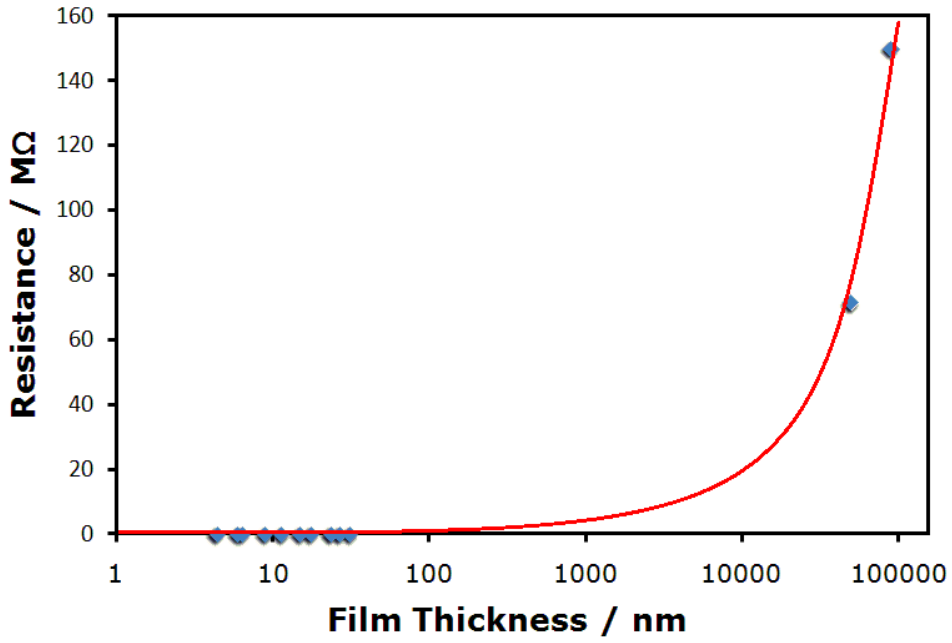

Figure iv *Presents the measured resistances of films of various thicknesses. A trendline is included for clarity.*

Ultimately, the observed behaviour of ultra-thin semiconducting polymer films may prove to be highly advantageous in its practical applications. The

ability to tune the properties of PMMA / PDMA copolymer films using quantum effects has important ramifications in potential electrochemical applications. For example, there is the potential to use molecularly thin films of PMMA / PDMA to tune the properties of ion-selective field effect transistor (ISFET) systems, as well as other areas such as microelectronics and the ever evolving field of nanotechnology. Furthermore, since the thickness of a molecularly thin copolymer film may be affected by variations in external conditions such as humidity, temperature, etc., there is scope to develop novel sensing devices to detect minute changes in atmospheric conditions, whereby a change in humidity or temperature will alter the polymer thickness via sorption and swelling and the concomitant resistivity of the thin film device. Clearly, the extent of possible applications is far reaching, and the possibility of using molecularly thin films in the design of new electrochemical devices is an exciting new perspective.

References

1. Davey JE, Tiernan RJ, Pankey T, Montgomery MD. The effect of vacuum-evapouration parameters on the structural, electrical and optical properties of thin germanium films. Solid-State Electronics. 1962;6:205-16.

2. Xu X, Bojkov H, Goodman W. Electrochemical study of ultrathin silica films supported on a platinum substrate. Vacuum Science and Technology A. 1994;12(4):1882-5.

3. Nelson A. Co-refinement of multiple contrast neutron / X-ray reflectivity data using MOTOFIT. Journal of Applied Crystallography. 2006;39:273-6.

4. Yeum B. ZSimpWin Version 2.00. Equivalent Circuit, Users Manual. 2nd ed: EChem Software; 2001.

5. Blatt FJ. Solid State Physics. New York: Academic Press Inc.; 1956.

6. Lifshitz IM, Kosevich AM. Izv Akad Nauk SSSR, Ser Fiz. 1955;19:395.

7. Tavger BA, Demikhovskii VY. Soviet Phys-Solid State English Transl. 1963;4:469.

8. Chopra KL. Thin Film Phenomena. New York: McGraw-Hill; 1969.

9. Ogrin YF, Lutskii VN, Elinson MI. Soviet Phys JETP Letters. 1966;3:71.

10. Mikhailov GM, Malikov IV, Chernykh AV, Fomin LA, Joyez P, Pothier H, et al. Signatures of ballistic transport in the magnetoresistance of nanostructures made of single-crystalline refractory metals. Nanotech. 2002;13:226-30.

Supplementary Information

Reagents

The following Selectophore Fluka reagents were used in this study: silver ionophore IV and sodium tetrakis [3,5-bis(triflouromethyl)phenyl] borate (NaTFPB). Analytical grade xylene was obtained from Chem-Supply (Port Adelaide, South Australia, Australia). Analytical grade KNO_3 was obtained from Ajax Chemical Co. (Sydney, New South Wales, Australia). Similarly, analytical grade sulfuric acid and hydrogen peroxide used in piranha etching of silicon wafers were obtained from Ajax Chemical Co. The monomers, methylmethacrylate, 99.5%, (MMA) and n-decylmethacrylate (DMA), 99%, were obtained from Polysciences, Inc. (Gymea, New South Wales, Australia). The polymerization initiator 2,2'-azobis(isobutyronitrile) (AIBN), 98%, was obtained from Aldrich. Ethyl acetate and 1,4-dioxane were reagent grade and obtained from Chem-Supply. Milli-Q water was used to prepare all aqueous solutions unless otherwise specified.

Silicon Wafer Substrates

The doped and atomically flat silicon wafers were used as received as the working electrodes since they had been pre-polished to about 1 Å rms roughness [as obtained from Crystran LTD (Poole, Dorset, UK)]. The silicon was initially covered with 5-10 mm of excess xylene and placed on a hotplate at a temperature of 150^{o}C for 10 minutes. The wafer was rinsed with milli-Q water prior to placement in a piranha etching solution for 10 minutes. Following the piranha etching process, a stream of ozone was passed over the silicon wafer surface to oxidize any extraneous organic material. The wafer was attached to the spin coater, and rinsed with Milli-Q water at 3000 rpm. Last, a xylene cocktail of the copolymer membrane was spin cast onto the Si wafer at 3500 rpm.

ISE Membrane Preparation and Deposition

ISE membranes for XRR studies were prepared in a clean room. The piranha-etched wafers were subjected to spin casting, and the thin films were dried in a stream of high purity nitrogen gas prior to XRR measurements.

A PMMA / PDMA film was prepared by spin-coating at 3500 rpm for 2 minutes with a solution of 98 wt.% of PMMA / PDMA copolymer also comprising the silver ionophore (1.5 wt.%) and NaTFPB (0.5 wt.%) dissolved in appropriate quantity of xylene to give the desired film thickness. The PMMA / PDMA-coated wafer was annealed in a vacuum oven at 80 ^{o}C and 1.0 kPa overnight.

Potassium nitrate solutions (1 M) were made up in Milli-Q water, and employed as the electrolyte in EIS studies.

Electrochemical Impedance Spectroscopy (EIS)

An anodised silver / silver chloride solid-state reference electrode was inserted into one of the inlet / outlet ports of the XRR cell, a platinum wire counter electrode was inserted into the other inlet / outlet port, and the silicon wafer working electrode were all connected to a Princeton Applied Research PARSTAT 2263 portable potentiostat. EIS experimental control and data acquisition were performed using a personal computer running the PowerSINE software, and EIS data were collected at the open circuit potential using an A.C. amplitude of $\pm$ 10 mV rms and a frequency range of 100 kHz–10 mHz.

EIS experiments in 1 M KNO_3 were undertaken using a custom-built cell (see ***Supplementary Figure i***).

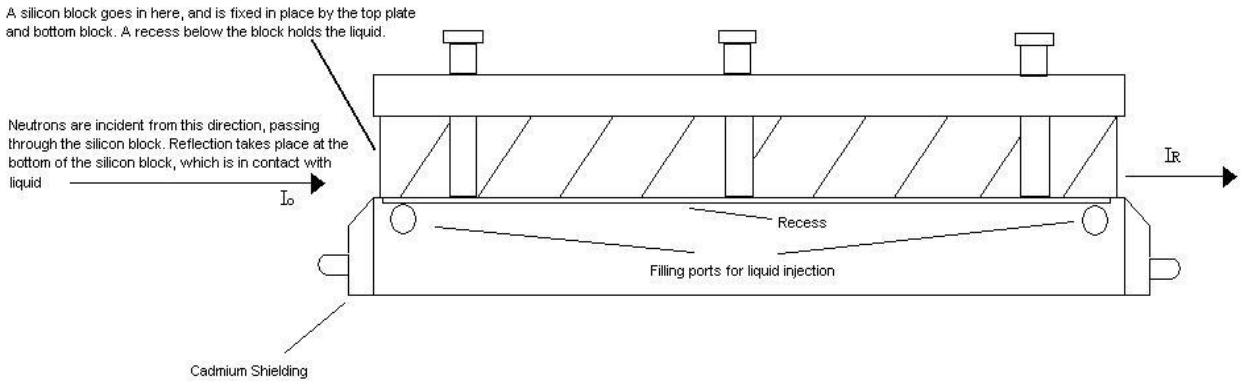

Supplementary Figure i *Schematic diagram of the specialized cell used in the neutron reflectometry experiments.*

X-ray Reflectometry (XRR)

XR was performed on the PMMA/PDMA-coated wafers in air at a wavelength 1.541 Å to ascertain the film thicknesses and roughnesses.

Contact Resistance Considerations

Since the ultra-thin films had a strong tendency to be biased in the positive direction by a constant resistance in the system, especially as the film thickness diminishes, we modelled the impact of a 21 ohm contact resistance at the silicon wafer-PMMA / PDMA interface. In this case, we linearly scaled the resistance (R) for the thin film using a bulk membrane resistivity (ρ) of 11 MW m and the following equation:

$$R = \rho\left(\frac{l}{A}\right) \qquad \textbf{Equation I}$$

where l and A is the thickness and cross-sectional area (πr^2 = 7.854 x 10^{-3} m^2 for a 10 cm diameter silicon wafer) of the wafer.

Henceforth, $R_{apparent}$ is calculated as follows:

$$R_{apparent} = \rho\left(\frac{l}{A}\right) + 21$$ **Equation II**

and $\rho_{apparent}$ is calculated as follows:

$$\rho_{apparent} = R_{apparent}\left(\frac{A}{l}\right)$$ **Equation III**

Supplementary Figure ii presents an overlay of the actual resistivity data together with the apparent resistivity calculated using a constant contact resistance of 21 ohms:

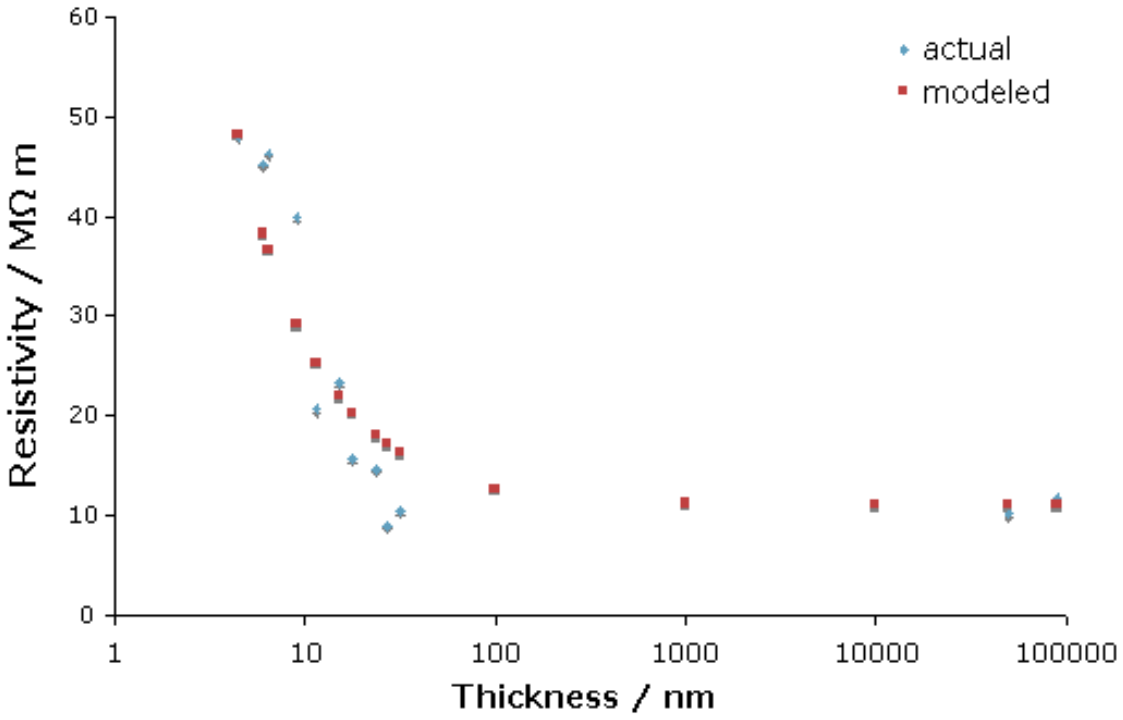

Supplementary Figure ii *An overlay of actual EIS resistivity and calculated resistivity by assuming a constant contact resistance of 21 ohms.*

Clearly, the absence of any deviation at high film thicknesses is expected since the 21 ohm contact resistance cannot affect bulk membrane resistances of tens to hundreds of megaohms. Nevertheless, the trends are very similar, albeit that the actual data displays a sharper or more abrupt change in resistivity, and

the calculated data is generally biased extensively in the negative direction (i.e., a contact resistance cannot explain the results).

Appendix III

The following pages contain documents stating the permission granted from copyright owners to use third party copyright material or published work in which the copyright is held by another party.

Copyright Agreement for Chapter 2

ELSEVIER LICENSE
TERMS AND CONDITIONS

Sep 22, 2010

This is a License Agreement between Jean-Pierre M Veder ("You") and Elsevier ("Elsevier") provided by Copyright Clearance Center ("CCC"). The license consists of your order details, the terms and conditions provided by Elsevier, and the payment terms and conditions.

All payments must be made in full to CCC. For payment instructions, please see information listed at the bottom of this form.

Supplier	Elsevier Limited The Boulevard,Langford Lane Kidlington,Oxford,OX5 1GB,UK
Registered Company Number	1982084
Customer name	Jean-Pierre M Veder
License number	2507401381338
License date	Sep 13, 2010
Licensed content publisher	Elsevier
Licensed content publication	TrAC Trends in Analytical Chemistry
Licensed content title	In situ structural characterization of electrochemical systems using synchrotron-radiation techniques
Licensed content author	Roland De Marco, Jean-Pierre Veder
Licensed content date	June 2010
Licensed content volume number	29
Licensed content issue number	6
Number of pages	10
Type of Use	reuse in a thesis/dissertation
Intended publisher of new work	other
Portion	full article
Format	print
Are you the author of this Elsevier article?	Yes

Will you be translating?	No
Order reference number	
Title of your thesis/dissertation	The Development of a Rigorous Nanocharacterisation Scheme for Electrochemical Systems
Expected completion date	Sep 2010
Estimated size (number of pages)	200
Elsevier VAT number	GB 494 6272 12

Copyright Agreement for Chapter 3

From: CONTRACTS-COPYRIGHT (shared) [Contracts-Copyright@rsc.org]
Sent: Tuesday, 14 September 2010 7:21 PM
To: Veder, Jean-Pierre (CPSE, Clayton)
Subject: RE: Permission Request Form: Jean-Pierre Veder

Dear Mr Veder

The Royal Society of Chemistry (RSC) hereby grants permission for the use of your paper(s) specified below in the printed and microfilm version of your thesis. You may also make available the PDF version of your paper(s) that the RSC sent to the corresponding author(s) of your paper(s) upon publication of the paper(s) in the following ways: in your thesis via any website that your university may have for the deposition of theses, via your university's Intranet or via your own personal website. We are however unable to grant you permission to include the PDF version of the paper(s) on its own in your institutional repository. The Royal Society of Chemistry is a signatory to the STM Guidelines on Permissions (available on request).

Please note that if the material specified below or any part of it appears with credit or acknowledgement to a third party then you must also secure permission from that third party before reproducing that material.

Please ensure that the thesis states the following:

Reproduced by permission of the PCCP Owner Societies

and include a link to the article on the Royal Society of Chemistry's website.

Please ensure that your co-authors are aware that you are including the paper in your thesis.

With future permission requests please specify the journal title.

Regards

Gill Cockhead
Contracts & Copyright Executive

Gill Cockhead (Mrs), Contracts & Copyright Executive
Royal Society of Chemistry, Thomas Graham House
Science Park, Milton Road, Cambridge CB4 0WF, UK
Tel +44 (0) 1223 432134, Fax +44 (0) 1223 423623
http://www.rsc.org

```
-----Original Message-----
From: ved003@csiro.au [mailto:ved003@csiro.au]
Sent: 14 September 2010 03:35
To: CONTRACTS-COPYRIGHT (shared)
Subject: Permission Request Form: Jean-Pierre Veder


Name    : Jean-Pierre Veder
```

Tel : +61400 601 122
Fax :
Email : ved003@csiro.au

I am preparing the following work for publication:

Article/Chapter Title : Evidence of a water layer in solid-contact polymeric ion sensors
Journal/Book Title : PhD Thesis title: The Development of a Rigorous Nanocharacterisation Scheme for Electrochemical Systems
Editor/Author(s) : Jean-Pierre Veder
Publisher : Curtin University

I would very much appreciate your permission to use the following material:

Journal/Book Title : ***Phys. Chem. Chem. Phys.***
Evidence of a water layer in solid-contact polymeric ion sensors
Editor/Author(s) : Roland De Marco, Jean-Pierre Veder, Graeme Clarke, Andrew Nelson, Kathryn Prince, Ernö Pretsch and Eric Bakker
Volume Number : 10
Year of Publication : 2008
Description of Material : Entire article
Page(s) : 73-76

Any Additional Comments :

I kindly wish to request your permission to reproduce an article entitled "Evidence of a water layer in solid-contact polymeric ion sensors." The article, in which I was a main author, is only intended to be used in my PhD thesis which comprises a series of published papers.

Your assistance on this matter will be greatly appreciated.

Kind regards,

Jean-Pierre Veder

Copyright Agreement for Chapter 4

AMERICAN CHEMICAL SOCIETY LICENSE TERMS AND CONDITIONS

Sep 22, 2010

This is a License Agreement between Jean-Pierre M Veder ("You") and American Chemical Society ("American Chemical Society") provided by Copyright Clearance Center ("CCC"). The license consists of your order details, the terms and conditions provided by American Chemical Society, and the payment terms and conditions.

All payments must be made in full to CCC. For payment instructions, please see information listed at the bottom of this form.

License Number	2507400171901
License Date	Sep 13, 2010
Licensed content publisher	American Chemical Society
Licensed content publication	Analytical Chemistry
Licensed content title	Elimination of Undesirable Water Layers in Solid-Contact Polymeric Ion-Selective Electrodes
Licensed content author	Jean-Pierre Veder et al.
Licensed content date	Sep 1, 2008
Volume number	80
Issue number	17
Type of Use	Thesis/Dissertation
Requestor type11	Not specified
Format	Print
Portion	Full article
Author of this ACS article	Yes
Order reference number	
Title of the thesis / dissertation	The Development of a Rigorous Nanocharacterisation Scheme for Electrochemical Systems
Expected completion date	Sep 2010
Estimated size(pages)	200
Billing Type	Invoice
Billing Address	

Customer reference info	
Total	0.00 USD

Copyright Agreement for Chapter 6

AMERICAN CHEMICAL SOCIETY LICENSE TERMS AND CONDITIONS

Sep 22, 2010

This is a License Agreement between Jean-Pierre M Veder ("You") and American Chemical Society ("American Chemical Society") provided by Copyright Clearance Center ("CCC"). The license consists of your order details, the terms and conditions provided by American Chemical Society, and the payment terms and conditions.

All payments must be made in full to CCC. For payment instructions, please see information listed at the bottom of this form.

License Number	2507400253337
License Date	Sep 13, 2010
Licensed content publisher	American Chemical Society
Licensed content publication	Analytical Chemistry
Licensed content title	Synchrotron Radiation/Fourier Transform-Infrared Microspectroscopy Study of Undesirable Water Inclusions in Solid-Contact Polymeric Ion-Selective Electrodes
Licensed content author	Jean-Pierre Veder et al.
Licensed content date	Jul 1, 2010
Volume number	82
Issue number	14
Type of Use	Thesis/Dissertation
Requestor type11	Not specified
Format	Print
Portion	Full article
Author of this ACS article	Yes
Order reference number	
Title of the thesis / dissertation	The Development of a Rigorous Nanocharacterisation Scheme for Electrochemical Systems
Expected completion date	Sep 2010
Estimated size(pages)	200
Billing Type	Invoice
Billing Address	

Customer reference info	
Total	0.00 USD

Copyright Agreement for Chapter 8

ELSEVIER LICENSE
TERMS AND CONDITIONS

Mar 14, 2011

This is a License Agreement between Jean ("You") and Elsevier ("Elsevier") provided by Copyright Clearance Center ("CCC"). The license consists of your order details, the terms and conditions provided by Elsevier, and the payment terms and conditions.

All payments must be made in full to CCC. For payment instructions, please see information listed at the bottom of this form.

Supplier	Elsevier Limited The Boulevard,Langford Lane Kidlington,Oxford,OX5 1GB,UK
Registered Company Number	1982084
Customer name	Jean-Pierre M Veder
License number	2617911035404
License date	Feb 28, 2011
Licensed content publisher	Elsevier
Licensed content publication	Electrochimica Acta
Licensed content title	A flow cell for transient voltammetry and *in situ* grazing incidence X-ray diffraction characterization of electrocrystallized cadmium(II) tetracyanoquinodimethane
Licensed content author	Jean-Pierre Veder, Ayman Nafady, Graeme Clarke, Ross P. Williams, Roland De Marco, Alan M. Bond
Licensed content date	1 January 2011
Licensed content volume number	56
Licensed content issue number	3
Number of pages	8
Start Page	1546
End Page	1553
Type of Use	reuse in a thesis/dissertation
Portion	full article

Format	both print and electronic
Are you the author of this Elsevier article?	Yes
Will you be translating?	No
Order reference number	
Title of your thesis/dissertation	The Development of a Rigorous Nanocharacterization Scheme for Electrochemical Systems
Expected completion date	Mar 2011
Estimated size (number of pages)	290
Elsevier VAT number	GB 494 6272 12
Permissions price	0.00 USD
VAT/Local Sales Tax	0.0 USD / 0.0 GBP
Total	0.00 USD
Terms and Conditions	

Copyright Agreement for Figure 2-2 in Chapter 2

ELSEVIER LICENSE
TERMS AND CONDITIONS

Sep 22, 2010

This is a License Agreement between Jean-Pierre M Veder ("You") and Elsevier ("Elsevier") provided by Copyright Clearance Center ("CCC"). The license consists of your order details, the terms and conditions provided by Elsevier, and the payment terms and conditions.

All payments must be made in full to CCC. For payment instructions, please see information listed at the bottom of this form.

Supplier	Elsevier Limited The Boulevard,Langford Lane Kidlington,Oxford,OX5 1GB,UK
Registered Company Number	1982084
Customer name	Jean-Pierre M Veder
License number	2513500153109
License date	Sep 21, 2010
Licensed content publisher	Elsevier
Licensed content publication	Electrochimica Acta
Licensed content title	*In situ* X-ray diffraction of the intercalation of $(C_2H_5)_4N^+$ and BF_4^-into graphite from acetonitrile and propylene carbonate based supercapacitor electrolytes
Licensed content author	P.W. Ruch, M. Hahn, F. Rosciano, M. Holzapfel, H. Kaiser, W. Scheifele, B. Schmitt, P. Novák, R. Kötz, A. Wokaun
Licensed content date	20 December 2007
Licensed content volume number	53
Licensed content issue number	3
Number of pages	9
Type of Use	reuse in a thesis/dissertation
Intended publisher of new work	other
Portion	figures/tables/illustrations
Number of	1

figures/tables/illustrations	
Format	print
Are you the author of this Elsevier article?	No
Will you be translating?	No
Order reference number	
Title of your thesis/dissertation	The Development of a Rigorous Nanocharacterisation Scheme for Electrochemical Systems
Expected completion date	Sep 2010
Estimated size (number of pages)	200
Elsevier VAT number	GB 494 6272 12

Copyright Agreement for Figure 2-4 in Chapter 2

AMERICAN CHEMICAL SOCIETY LICENSE TERMS AND CONDITIONS

Sep 22, 2010

This is a License Agreement between Jean-Pierre M Veder ("You") and American Chemical Society ("American Chemical Society") provided by Copyright Clearance Center ("CCC"). The license consists of your order details, the terms and conditions provided by American Chemical Society, and the payment terms and conditions.

All payments must be made in full to CCC. For payment instructions, please see information listed at the bottom of this form.

License Number	2513560969765
License Date	Sep 21, 2010
Licensed content publisher	American Chemical Society
Licensed content publication	Journal of the American Chemical Society
Licensed content title	In Situ Small-Angle X-ray Scattering Observation of Pt Catalyst Particle Growth During Potential Cycling
Licensed content author	Matt C. Smith et al.
Licensed content date	Jul 1, 2008
Volume number	130
Issue number	26
Type of Use	Thesis/Dissertation
Requestor type11	Not specified
Format	Print
Portion	Table/Figure/Micrograph
Number of Table/Figure/Micrographs	1
Author of this ACS article	No
Order reference number	
Title of the thesis / dissertation	The Development of a Rigorous Nanocharacterisation Scheme for Electrochemical Systems
Expected completion date	Sep 2010
Estimated size(pages)	200
Billing Type	Invoice
Billing Address	

Customer reference info	
Total	0.00 USD

Copyright Agreement for Figure 2-3 in Chapter 2

Anne Clementson

From: Jean-Pierre Veder [J.Veder@curtin.edu.au]
Sent: Tuesday, November 24, 2009 1:52 AM
To: Copyright
Cc: Roland De Marco
Subject: Figure Reuse Permission
Follow Up Flag: Follow up
Flag Status: Red

Re: Permissions request

I would like to request permission to reproduce, as well as obtain a high quality computer file of a figure shown in ECS Transactions for a review article that is currently being assembled. The details of such a reproduction are as follows:

- **Full bibliographic reference information —**

Journal title: ECS Transactions
Title: In-Situ Investigation of SOFC patterned Electrodes Using Ambient-Pressure X-ray Photoelectron Spectroscopy
Authors: A. H. McDaniel, F. El Gabaly, E. Akhadov, R. L. Farrow, K. F. McCarty, M. A. Linne, S. C. Decaluwe, C. Zhang, B. Eichhorn, G. S. Jackson, Z. Liu, M. Grass, Z. Hussain and H. Bluhm
Issue date: October 4 - October 9 2009
Volume number: 25
Issue Number: 2
Page number: 335 - 343

- **What you intend to use-**

Section to be reproduced: Page 340 - figure 4 only

- **Where it will be reused —**

The figure will be presented in a review article featured in the journal Trends in Analytical Chemistry (TrAC) in a special issue based on "Applications of Synchrotron Radiation in Analytical Chemistry"

- **Contact details -**

Contact: Jean-Pierre Veder
Postal address: Department of Chemistry, Building 500
Curtin University of Technology (Bentley Campus)
Kent Street, Bentley, Perth
Western Australia 6102

12/3/2009

Email: j.veder@curtin.edu.au

- **The deadline by which you need this permission —**

Deadline for permission: 15th December 2009

Your help and cooperation on this matter will be greatly appreciated.

Regards,

Jean-Pierre Veder (B.Sc. Nanotechnology) (Hns.)

Nanochemistry Research Institute
Department of Chemistry
Curtin University
Ph: (08)9266 2180
Mob: 0400601122

Permission is granted to reproduce the above-referenced material. Please acknowledge the author(s) and publication title of the original material, and include the words: "Reproduced by permission of ECS — The Electrochemical Society."

Dec 4, 2009
Date

Ann F. Goedkoop, Director of Publications